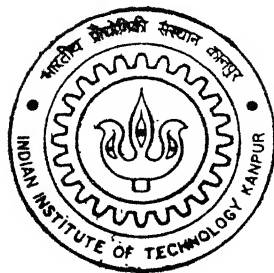


# **ANALYSIS OF SHEET REINFORCEMENT SUBJECTED TO TRANSVERSE FORCE/DISPLACEMENT**

by

**B. Umashankar**



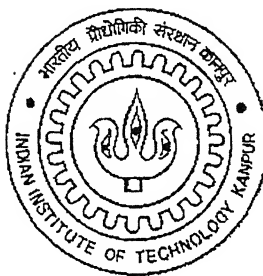
**DEPARTMENT OF CIVIL ENGINEERING**  
**Indian Institute of Technology Kanpur**

**August, 2002**

**ANALYSIS OF SHEET REINFORCEMENT  
SUBJECTED TO  
TRANSVERSE FORCE/DISPLACEMENT**

A Thesis Submitted  
in Partial Fulfillment of the Requirements  
for the Degree of  
**MASTER OF TECHNOLOGY**

by  
**B.UMASHANKAR**



to the  
DEPARTMENT OF CIVIL ENGINEERING  
**INDIAN INSTITUTE OF TECHNOLOGY KANPUR**

August 2002

3 FEB 2003 /CE

पुरुषोत्तम काशीनाथ कैलकर पुस्तकालय

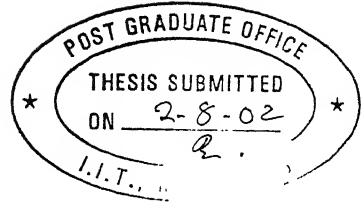
भारतीय त्रैद्योधिकी संस्थान कानपुर

141841

अवाप्ति क्र० A.....



A141841



## CERTIFICATE

It is certified that the work contained in this thesis entitled, "*Analysis of Sheet Reinforcement Subjected to Transverse Force/Displacement*" by B.Umashankar has been carried out under my supervision and the same has not been submitted elsewhere for the award of any degree.

(M.R. Madhav)

Professor

Department of Civil Engineering

I.I.T. Kanpur-208016

August 2002.

## ACKNOWLEDGEMENTS

I take this opportunity to express my gratitude to my supervisor Prof. M.R.Madhav for his involvement, motivation and encouragement throughout this thesis work. I am thankful to him for his amiable attitude towards me. His approach to a research problem, inclination for the subject, time management and untiring energy really impressed me. I shall sincerely try to instill the same in me in my life. His constructive scolding lingers around and makes me get better every time. Above all, his immense patience to sit with me in clarifying a doubt is worth mentioning. He enabled me resolve many problems not only related to this work but also personal matters that I feel would have been difficult to deal with. I consider myself fortunate to have him as my supervisor.

I thank Prof. P.K.Basudhar, Dr. Sarvesh Chandra, Prof. N.S.V. Kameswara Rao and Prof. U.Dayal for enlightening me with many new concepts of Geotechnical Engineering in my course work. I found the Geotechnical faculty very competent during my stay at IIT/K.

I thank all my classmates and friends: Gupta, Dhanu, Keshav, Habib, Ajay, Imran, Avinash, Venkat, M.N. Rao, Manoj and Murali for their cooperation. Thanks to Preti, Mr.S.Das and Mr.Sreenivasulu (Research Scholars) for their good nature.

I convey my best wishes to my other friends Phani, Satish, Prabhakar, Rajini, Swamy, Ramesh and all those who made my stay at IIT/K a memorable one in life.

Special thanks are due to my friends Rajasekhar and Neha for being friendly and helping me in my work towards its end which I can ever forget.

Lastly, I convey my beloved love for my father who toiled to get me to this stage.

**Umashankar. B**

## ABSTRACT

For the last two decades, extensive researches and investigations have been carried out to understand the concept, mechanism and behavior of reinforced soil structure as well as new technologies which resulted in the utilization of a variety of reinforcements and backfill materials. Almost all the available methods for the design of reinforced earth structures incorporate only the axial pullout mechanism and do not consider oblique pull or displacement of the reinforcement. Practically in all the cases, the kinematics of deformation dictates both the force and the displacement to be oblique to the reinforcement element. The response of sheet reinforcement due to an oblique force is a combination of responses due to transverse and axial forces. In this thesis work, a method is proposed for the analysis of reinforcement subjected to transverse force or displacement. Simple mathematical models are proposed to study the responses of inextensible as well as extensible sheet reinforcements subjected to downward transverse displacement/force. The analyses is carried out assuming (i) the full shear resistance to be mobilized along the reinforcement-soil interface and (ii) the shear resistance along reinforcement-soil interface is mobilized as a function of the horizontal displacement of the interface subjected to a maximum value. Firstly, the normal stress-displacement response of the subgrade is assumed to be linear (linear subgrade) and latter a more realistic case of hyperbolic stress-displacement response of the soil is considered. The analysis of both extensible and inextensible sheet reinforcements is carried out for a wide range of soil and soil-reinforcement interface characteristics.

Finally, based on the proposed model, a method for the estimation of the bearing capacity of a two-layered soil with a sheet reinforcement inclusion is presented.

# CONTENTS

**ABSTRACT**

**ACKNOWLEDGEMENT**

**LIST OF FIGURES**

<b>1 INTRODUCTION</b>	<b>1</b>
1.1 General	1
1.2 Objective	4
1.3 Scope and Organization	4
<b>2 LITERATURE REVIEW</b>	<b>6</b>
2.1 General	6
2.2 Soil-Reinforcement Mechanism	6
2.3 Analytical and Experimental Studies on Axial Pullout Response	9
2.4 Studies related to Oblique Force along Reinforcement	11
2.5 Bearing Capacity of Reinforced Soils	13
2.6 Conclusions	17
<b>3 ANALYSIS OF INEXTENSIBLE SHEET REINFORCEMENT SUBJECTED TO A TRANSVERSE FORCE/DISPLACEMENT</b>	<b>18</b>
3.1 General	18
3.2 Problem Statement	18
3.3 Analyses	19
3.3.1 Linear Subgrade – Model I	19
3.3.1.1 The Model	19
3.3.1.2 Analyses	19
3.3.1.3 Numerical Solution	23
3.3.1.4 Characteristics of the Model	24
3.3.1.5 Results and Discussions	24
3.3.2 Non-Linear Subgrade – Model II	37
3.3.2.1 The Model	37
3.3.2.2 Analyses	38
3.3.2.3 Numerical Solution	40
3.3.2.4 Characteristics of the Model	41

3.3.2.5 Results and Discussion	42
3.3.3 Non-Linear Subgrade and Non-Linear Shear Mobilization – Model III	58
3.3.3.1 The Model	59
3.3.3.2 Analyses	60
3.3.3.3 Numerical Solution	64
3.3.3.4 Calculation of Horizontal Displacement along the Length of Reinforcement	65
3.3.3.5 Characteristics of the Model	66
3.3.3.6 Results and Discussion	66
<b>4 ANALYSES FOR EXTENSIBLE REINFORCEMENT SUBJECTED TO TRANSVERSE DOWNWARD FORCE/DISPLACEMENT</b>	93
4.1 General	93
4.2 Problem Statement	93
4.3 Procedure for locating Active Length of Reinforcement	94
4.4 Analyses	96
4.4.1 Linear Subgrade – Model I	96
4.4.1.1 The Model	96
4.4.1.2 Analyses	97
4.4.1.3 Numerical Solution	99
4.4.1.4 Characteristics of the Model	101
4.4.1.5 Results and Discussion	
4.4.2 Non-Linear Subgrade – Model II	114
4.4.1.1 The Model	114
4.4.1.2 Analyses	114
4.4.1.3 Numerical Solution	116
4.4.1.4 Characteristics of the Model	118
4.4.1.5 Results and Discussion	118
<b>5 CONCLUSIONS</b>	129
<b>APPENDIX</b>	133
<b>REFERENCES</b>	149

## NOTATIONS

$D_e$	Embedment depth of reinforcement.
$J$	Stiffness of reinforcement.
$J^*$	Relative stiffness of reinforcement ( $= J/T_{maxp}$ , $T_{maxp} = 2\gamma D_e L \tan \phi_r$ ).
$k_s$	Initial tangent modulus of subgrade reaction.
$k_\tau$	Initial slope of shear stress mobilized vs horizontal displacement of interface.
$L$	Length of reinforcement.
$L_g^l$	Extended length of reinforcement calculated from change in geometry.
$L_g^{l*}$	Extended length due to change in geometry normalized with length of reinforcement.
$L_\epsilon^l$	Extended length of reinforcement calculated from tensions along reinforcement.
$L_\epsilon^{l*}$	Extended length due to strains normalized with length of reinforcement.
$n$	Number of elements the reinforcement is divided.
$P$	Transverse force at front end.
$P^*$	Normalised transverse force ( $= P/\gamma D_e L$ ).
$q$	Normal stress due to transverse displacement.
$q_b$	Stresses acting on bottom surface of reinforcement.
$q_t$	Stresses acting on top surface of reinforcement.
$q_{ult}$	Ultimate bearing resistance of the soil.
$T$	Tension developed in the reinforcement.
$T_{maxp}$	Axial pull out capacity.
$T^*$	Normalised tension developed in the reinforcement ( $= T/T_{maxp}$ , $T_{maxp} = 2\gamma D_e L \tan \phi_r$ ).

$T_{max}^*$	Normalised maximum tension in the reinforcement ( $=T_{max}/T_{maxp}$ )
$u$	Horizontal displacement of interface between soil and interface.
$U$	Horizontal displacement of interface normalized with length of reinforcement ( $=u/L$ ).
$w$	Transverse displacement of reinforcement.
$w_L$	Transverse displacement at front end.
$W$	Transverse displacement of reinforcement normalized with $w_L$ ( $=w/w_L$ ).
$W_L$	Normalised front end displacement ( $=w_L/L$ ).
$W^*$	Transverse displacement of reinforcement normalized with $L$ ( $=w/L$ ).
$X$	Normalized distance ( $=x/L$ ).
$x_o$	Active length of reinforcement.
$X_o$	Active length normalized with length of reinforcement.
$\beta$	a parameter that quantifies the relative initial subgrade modulus with the ultimate bearing resistance of the subgrade ( $=k_s L/q_{ult}$ ).
$\Delta x$	Length of infinitesimal element.
$\Delta X$	Length of infinitesimal element in normalized form.
$\eta$	Relative initial shear stiffness factor for subgrade ( $=k_s L/\gamma D_e$ ).
$\mu$	Relative subgrade stiffness factor ( $=k_s L/\gamma D_e$ ).
$\gamma$	Unit weight of soil.
$\phi_r$	Interface angle of shearing resistance between reinforcement and soil.
$\lambda$	$=k_r/k_s$ .
$\theta$	Inclination of reinforcement.

$\theta_L$	Inclination/slope at front end.
$\tau$	Mobilized shear stress at interface.
$\tau_b$	Shear stresses on bottom surface of reinforcement.
$\tau_t$	Shear stresses on top surface of reinforcement.
$\tau_{max}$	Maximum shear stress that can be mobilized along interface.
$(\tau_{max})_b$	Maximum shear stress that can be mobilized at bottom surface of reinforcement sheet
$(\tau_{max})_t$	Maximum shear stress that can be mobilized at bottom surface of reinforcement sheet

# LIST OF FIGURES

Figure	Caption	Page No.
Fig. 1.1	Common Applications of Reinforced Soil	2
	(a) Reinforced Soil Retaining Walls	
	(b) Reinforced Soil Steep Slopes	
	(c) Reinforced Clay Fill Slopes	
	(d) Reinforced Embankments on Soft Foundation	
	(e) Reinforced Piled Embankments	
	(f) Reinforced Embankments Over Areas Prone to Subsidence	
Fig. 1.2	Typical Reinforced soil mechanism showing two Possible Interaction Mechanisms	3
Fig. 1.3	Kinematics of Reinforcement – Soil Interaction	3
Fig. 1.4	A Typical Pullout Mechanism	4
Fig. 1.5	Outline of the Analyses	5
Fig. 2.1	Two possible interaction Mechanism in Reinforced Soils (Jewell, 1992)	7
Fig. 2.2	Components of direct Shear Resistance for Geogrid reinforcement	7
	(a) Shear Resistance Between Soil and Reinforcement Plane Surface Area	
	(b) Soil to Soil Shear Resistance	
Fig. 2.3	Components of Pullout Resistance for Grid Reinforcement	8
Fig. 2.4	Pullout Bearing Resistance Mechanism	9
	(a) General Bearing Failure Mechanism	
	(b) Punching Shear Failure Mechanism	
Fig. 2.5	Shear Stress-Displacement Curve for the Interface	11
Fig 2.6	Forces considered in the stability Analysis	12
Fig. 2.7	Chain Configuration between Floating Structure and embedded Pile Lug	13
Fig. 2.8	Direct Shear testing of Soil Sample reinforced with a Sheet of Geotextile	14
Fig. 2.9	Assumed Failure Mechanism under a foundation supported by reinforced Earth	16
Fig. 2.10	Effect of Polymernet	
Fig. 3.1	Definition Sketch	19
Fig 3.2	(a) Forces acting on Sheet Reinforcement	20
	(b) Idealization of Soil	

(c) Stress Displacement Response of Soil.

Fig. 3.3 Forces on Infinitesimal Element	20
Fig 3.4 Discretisation of Reinforcement Length into Elements	23
Fig. 3.5 Variation of Normalized Normal Displacement with Normalized Distance	
-Effect of $\mu$ for $w_L/L=0.01$	27
Fig. 3.6 Variation of Normalized Normal Displacement with Normalized Distance	
- Effect of $\mu$ for $w_L/L=0.1$	27
Fig. 3.7 Variation of Normalized Normal Displacement with Normalized Distance	
- Effect of $w_L/L$ for $w_L/L=0.1$	28
Fig. 3.8 Variation of Normalized Tension with Normalized Distance	
Effect of $w_L/L$ for $w_L/L=0.1$	28
Fig. 3.9 Variation of Normalized Tension with Normalized Distance – Effect of $\mu$	29
Fig. 3.10 Variation of Maximum Normalized Tension with $w_L/L$ – Effect of $\mu$	29
Fig. 3.11 Variation of Maximum Horizontal Inclination with $w_L/L$ – Effect of $\mu$	30
Fig. 3.12 Variation of Maximum Normalized Normal Component of Tension with	
$w_L/L$ – Effect of $\mu$	30
Fig. 3.13 Variation of Maximum Normalized Horizontal Component of Tension	
with $w_L/L$ – Effect of $\mu$	32
Fig. 3.14 Variation of Normalized Transverse Force with $w_L/L$ - Effect of $\mu$	32
Fig. 3.15. Variation of Normalized Transverse Force with Interface Friction angle	33
Fig. 3.16a Variation of ‘a’ with $w_L/L$	33
Fig. 3.16b Variation of ‘b’ with $w_L/L$	34
Fig. 3.17 Variation of Maximum Normalized Tension with $\mu$	34
Fig. 3.18 Variation of Maximum Horizontal Inclination with $\mu$	35
Fig. 3.19 Variation of Maximum Normalized Normal Component of Tension with	
$w_L/L$ – Effect of $\mu$	36
Fig. 3.20 Variation of Maximum Normalized Horizontal Component of Tension	
with $w_L/L$ – Effect of $\mu$	36
Fig. 3.21 Variation of Normalized Transverse Force with $\mu$ – Effect of $w_L/L$	37

Fig. 3.22 Hyperbolic Response between stress, $q$ and settlement, $w$	38
Fig. 3.23 Variation of Normalized Displacement with Normalized Distance – Effect of $\mu$	43
Fig. 3.24 Variation of Normalized Displacement with Normalized Distance – Effect of $\beta$	43
Fig. 3.25 Variation of Normalized Tension with Normalized Distance – Effect of $\mu$	44
Fig. 3.26 Variation of Normalized Tension with Normalized Distance – Effect of $\beta$	44
Fig. 3.27 Variation of Maximum Normalized Tension with Normalized Free End Displacement for Different $\mu$	45
Fig. 3.28 Variation of Maximum Inclination of Reinforcement with Horizontal with $w_L/L$ –Effect of $\mu$	46
Fig. 3.29 Variation of Maximum Normalized Normal Tension with Normalized Free End Displacement – Effect of $\mu$	46
Fig. 3.30 Variation of Maximum Normalized Horizontal Component of Tension with Normalized Free End Displacement - Effect of $\mu$	48
Fig. 3.31 Variation of Normalized Transverse Force with Normalized Free End Displacement - Effect of $\mu$	48
Fig. 3.32 Variation of Maximum Normalized Tension with Normalized Free End Displacement – Effect of $\beta$	49
Fig. 3.33 Variation of Maximum Inclination of Reinforcement with Horizontal with $w_L/L$ –Effect of $\beta$	49
Fig. 3.34 Variation of Maximum Normalized Normal Tension with Normalized Free End Displacement for Different $\beta$	50
Fig. 3.35 Variation of Maximum Normalized Normal Tension with Normalized Free End Displacement for Different $\mu$	52
Fig. 3.36 Variation of Normalized Transverse Force with Normalized Free End Displacement - Effect of $\beta$	52

Fig. 3.37 Variation of Normalized Tension with $\mu$ .	53
Fig. 3.38 Variation of Inclination of Reinforcement with $\mu$ .	53
Fig. 3.39 Variation of Normalized Normal Component of Maximum Tension with $\mu$	54
Fig. 3.40 Variation of Normalized Horizontal Component of Tension with $\mu$	54
Fig. 3.41 Variation of Normalized Transverse Force with $\mu$	55
Fig. 3.42 Variation of Maximum Normalized Tension with $\beta$	55
Fig. 3.43 Variation of Inclination of Reinforcement with $\beta$	56
Fig. 3.44 Variation of Normalized Normal Component of Maximum Tension with $\beta$	57
Fig. 3.45 Variation of Normalized Horizontal Component of Maximum Tension with $\beta$	57
Fig. 3.46 Variation of Normalized Transverse Force with $\beta$	58
Fig. 3.47 Shear-Displacement Response of soil (a) Ideal Plastic Response and (b) Elasto-Plastic Response.	58
Fig. 3.48 Hyperbolic Response between Shear Resistance, $\tau$ and Horizontal Displacement.	59
Fig. 3.49 Procedure for Calculation of Horizontal Displacements along the Reinforcement	66
Fig. 3.50 Variation of Normalized Displacement with Normalized Distance – Effect of $\mu$	68
Fig. 3.51 Variation of Normalized Displacement with Normalized Distance – Effect of $\beta$	68
Fig. 3.52 Variation of Normalized Displacement with Normalized Distance – Effect of $\eta$	69
Fig. 3.53 Variation of Horizontal Displacement with Normalized Distance – Effect of $\mu$	69
Fig. 3.54 Variation of Horizontal Displacement with Normalized Distance – Effect of $\mu$	70
Fig. 3.55 Variation of Horizontal Displacement with Normalized Distance – Effect of $\mu$	72
Fig. 3.56 Variation of Normalized Tension with Normalized Distance-	

Effect of $\mu$	72
Fig. 3.57 Variation of Normalized Tension with Normalized Distance-	
Effect of $\beta$	73
Fig. 3.58 Variation of Normalized Tension with Normalized Distance-	
Effect of $\eta$	73
Fig. 3.59 Variation of Normalized Maximum Tension with Normalized Distance-	
Effect of $\mu$	74
Fig. 3.60 Variation of Inclination of Reinforcement at $x=L$ with $w_L/L$ -	
Effect of $\mu$	74
Fig. 3.61 Variation of Maximum Normalized Normal Component of Tension with	
$w_L/L$ – Effect of $\mu$	75
Fig. 3.62 Variation of Normalized Maximum Horizontal Component of Tension with	
$w_L/L$ – Effect of $\mu$	77
Fig. 3.63 Variation of Normalized Transverse Force with $w_L/L$ - Effect of $\mu$	77
Fig. 3.64 Variation of Normalized Maximum Tension with $w_L/L$ - Effect of $\beta$	78
Fig. 3.65 Variation of Inclination of Reinforcement at $x=L$ – Effect of $\beta$	78
Fig. 3.66 Variation of maximum Normalized Normal Component of Tension	
with $w_L/L$ – Effect of $\beta$	79
Fig. 3.67 Variation of Maximum Normalized Horizontal Component of Tension	
with $w_L/L$ – Effect of $\beta$	79
Fig. 3.68 Variation of Normalized Transverse Force with $w_L/L$ - Effect of $\beta$	80
Fig. 3.69 Variation of Normalized maximum Tension with $w_L/L$ - Effect of $\eta$	80
Fig. 3.70 Variation of Inclination of Reinforcement at $x=L$ – Effect of $\eta$	81
Fig. 3.71 Variation of maximum Normalized Normal Component of Tension	
with $w_L/L$ – Effect of $\eta$	81
Fig. 3.72 Variation of Maximum Normalized Horizontal Component of Tension	
with $w_L/L$ – Effect of $\eta$	82
Fig. 3.73 Variation of Normalized Transverse Force with $w_L/L$ - Effect of $\eta$	82
Fig. 3.74 Variation of Normalized Maximum Tension with $\mu$	83
Fig. 3.75 Variation of Inclination of Reinforcement at $x=L$ with $\mu$	83
Fig. 3.76 Variation of Normalized Maximum Normal Component of Tension	
with $\mu$	85

Fig. 3.77 Variation of Normalized Maximum Horizontal Component of Tension with $\mu$	86
Fig. 3.78 Variation of Normalized Transverse Force with $\mu$	86
Fig. 3.79 Variation of Normalized Maximum Tension with $\beta$	87
Fig. 3.80 Variation of Inclination of Reinforcement at $x=L$ with $\beta$	87
Fig. 3.81 Variation of Normalized Maximum Normal Component of Tension with $\beta$ .	
Fig. 3.82 Variation of Normalized Maximum Horizontal Component of Tension with $\beta$	88
Fig. 3.83 Variation of Normalized Transverse Force with $\beta$	89
Fig. 3.84 Variation of Normalized Maximum Tension with $\eta$	89
Fig. 3.85 Variation of Inclination of Reinforcement at $x=L$ with $\eta$	90
Fig. 3.86 Variation of Normalized Maximum Normal Component of Tension with $\eta$	90
Fig. 3.87 Variation of Normalized Maximum Horizontal Component of Tension with $\eta$	91
Fig. 3.88 Variation of Normalized Transverse Force with $\eta$	91
Fig. 3.89 Variation of Normalized shear Resistance with Normalized distance	92
Fig. 4.1 Definition Sketch	94
Fig. 4.2. Deformed Shape and shear Stress Mobilization of Extensible Reinforcement	94
Fig. 4.3 (a) Forces acting on Sheet Reinforcement and (b) Idealization of Soil (c) Stress Displacement Response of Soil.	97
Fig. 4.4 Forces on Infinitesimal Element	98

Fig. 4.5 Discretisation of Reinforcement Length into Elements	100
Fig. 4.6 Variation of Normalized Active Length with $w_L/L$ – Effect of $J^*$ .	103
Fig. 4.7 Variation of Normalized Normal Displacement with Normalized Distance – Effect of $J^*$ .	103
Fig. 4.8 Variation of Normalized Tension with Normalized Distance – Effect of $J^*$	104
Fig. 4.9 Variation of Normalized Maximum Tension with $w_L/L$ – Effect of $J^*$	104
Fig. 4.10 Variation of Maximum Inclination with $w_L/L$ – Effect of $J^*$	106
Fig. 4.11 Variation of Maximum Normalized Normal component of Tension with $w_L/L$ – Effect of $J^*$	106
Fig. 4.12 Variation of Maximum Normalized Horizontal component of Tension with $w_L/L$ – Effect of $J^*$	107
Fig. 4.13 Variation of Normalized Normalized Transverse Force with $w_L/L$ – Effect of $J$	109
Fig. 4.14 Variation of Normalized Active Length with $w_L/L$ – Effect of $J^*$ .	109
Fig. 4.15 Variation of Normalized Normal Displacement with Normalized Distance – Effect of $J^*$	110
Fig. 4.16 Variation of Normalized Tension with Normalized Distance – Effect of $J^*$	110
Fig. 4.17 Variation of Normalized Tension with Normalized Distance – Effect of $J^*$	111
Fig. 4.18 Variation of Maximum Inclination with $w_L/L$ – Effect of $J^*$	111
Fig. 4.19 Variation of Maximum Normalized Normal component of Tension with $w_L/L$ - Effect of $J^*$	112
Fig. 4.20 Variation of Maximum Normalized Horizontal component of Tension with $w_L/L$ – Effect of $J^*$	113
Fig. 4.21 Variation of Normalized Transverse Force with $w_L/L$ – Effect of $J^*$	113
Fig. 4.22 Hyperbolic Response between stress, $q$ , and settlement, $w$	114
Fig. 4.23 Variation of Normalized Active Length with $w_L/L$ – Effect of $J^*$	119
Fig. 4.24 Variation of Normalized Normal Displacement with Normalized Distance - Effect of $J^*$	120
Fig. 4.25 Variation of Normalized Tension with Normalized Distance – - Effect of $J^*$	120
Fig. 4.26 Variation of Maximum Normalized Tension with $w_L/L$ - Effect of $J^*$	121

Fig. 4.27 Variation of Inclination at $x=L$ with $w_L/L$ – Effect of $J^*$	121
Fig. 4.28 Variation of Maximum Normalized Normal Component of Tension with $w_L/L$ -Effect of $J^*$	122
Fig. 4.29 Variation of Maximum Normalized Horizontal Component of Tension with $w_L/L$ -Effect of $J^*$	122
Fig. 4.30 Variation of Normalized Transverse Force with $w_L/L$ – Effect of $J^*$	124
Fig. 4.31 Variation of Normalized Active Length with $w_L/L$ – Effect of $\beta$	124
Fig. 4.32 Variation of Normalized Normal Displacement with Normalized Distance - Effect of $\beta$	125
Fig. 4.33 Variation of Normalized Tension with Normalized Distance – Effect of $\beta$	125
Fig. 4.34 Variation of Maximum Normalized Tension with $w_L/L$ - Effect of $\beta$	126
Fig. 4.35 Variation of Inclination at $x=L$ with $w_L/L$ – Effect of $\beta$	126
Fig. 4.36 Variation of Maximum Normalized Normal Component of Tension with $w_L/L$ -Effect of $\beta$	127
Fig. 4.37 Variation of Maximum Normalized Horizontal Component of Tension with $w_L/L$ -Effect of $\beta$	127
Fig. 4.38 Variation of Normalized Transverse Force with $w_L/L$ – Effect of $\beta$	128

# Chapter 1

## Introduction

### 1.1 General

Reinforcement of soils and ground has become one of the most preferred alternatives for the modern design of earth structures which are relatively more strong, economic and earthquake resistant than conventionally designed ones. New developments in many innovative uses of geosynthetics have offered engineering solutions for reinforcement, drainage, separation, and stabilization. Unlike the conventional soil retaining structures, reinforced soil structures are relatively flexible and can withstand larger displacements and tensions without catastrophic failures. In many cases effective use of reinforcements necessitates the recognition of its mechanical behavior in combination with the properties of the soil to be reinforced. Response of the reinforced soil structures in particular, depends on the soil-reinforcement interface characteristics.

Typical reinforced earth or soil structures are retaining walls, embankments, nailed slopes, subgrades beneath pavements, etc. (Fig. 1.1). These structures are designed to resist disturbing forces by transferring them back to the soil through interface shear stresses between the soil – reinforcement and tensile forces within the reinforcement elements. The soil-reinforcement interaction mechanism can be simplified into two types: soil sliding over the reinforcement or *direct shear mechanism* and pullout of the reinforcement from the soil or *pullout mechanism*. The two interaction mechanisms are depicted in Fig. 1.2. The interface shear strength and stress – displacement response are evaluated by the modified direct shear test in which one half of the box contains the soil while the reinforcing material is bonded such that it interacts with the soil. The pull-out test is used to determine directly the resistance offered by the reinforcing element. In the latter test, it is presumed that the reinforcement is acted upon by an axial force while in practically all cases the kinematics of deformation (Fig. 1.3) dictates both the force and the displacement to be oblique to the reinforcing element.

Almost all the available design methods incorporate only the axial pull-out mechanism and do not consider oblique pull or displacement of the reinforcement (Fig.

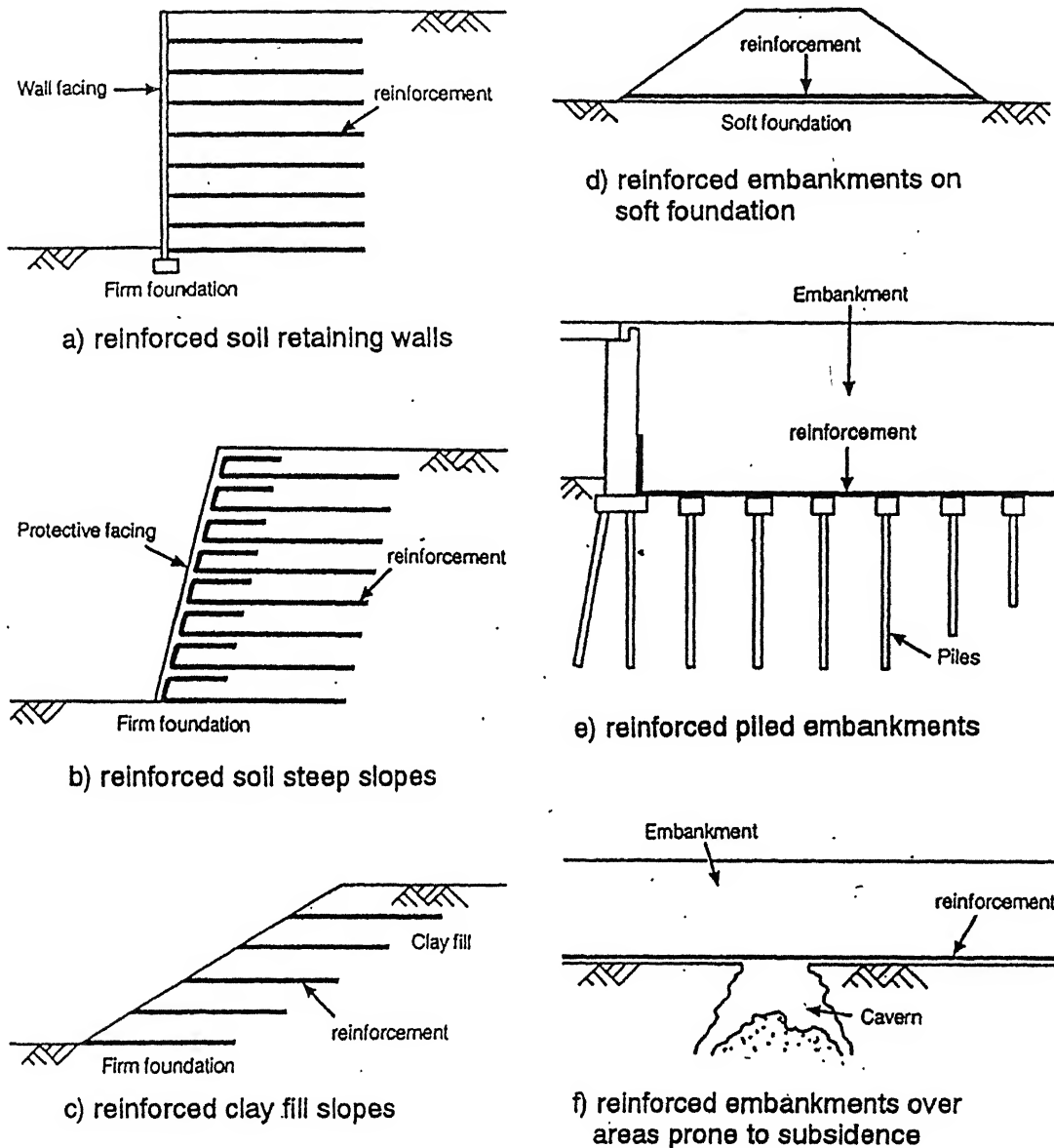


Fig. 1.1 Common Applications of Reinforced Soil

1.4). Under the action of axial pull, the normal stresses on the reinforcement – soil the same as the gravity stresses. Consequently, the shear resistance mobilized at the interface is proportional to these normal stresses. However, under the action of oblique force or displacement, the soil beneath the reinforcement mobilizes additional normal stresses as the reinforcement deforms transversely. As a result, the shear resistance

mobilized could be considerably different in case of reinforcement subjected to oblique force. The response of sheet reinforcement to an oblique force is a combination of

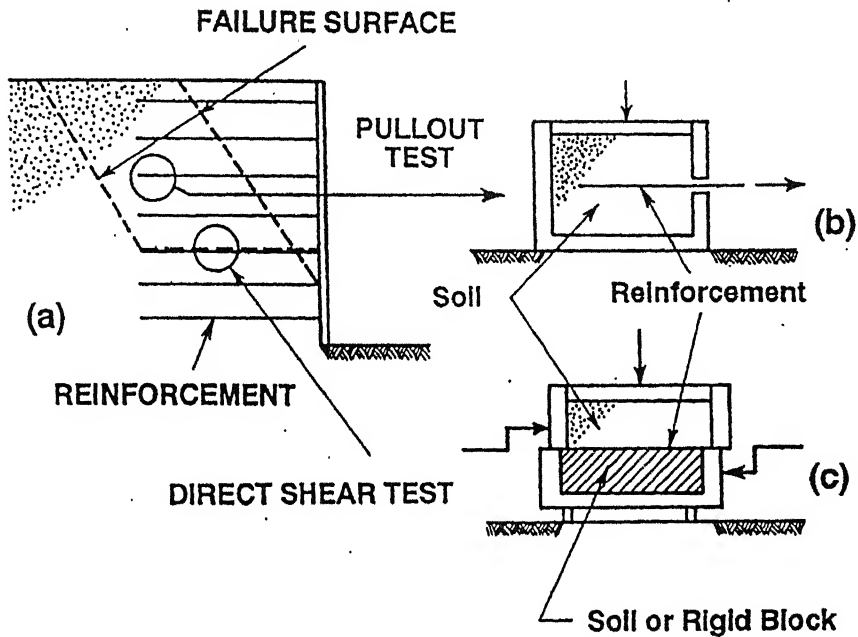


Fig. 1.2 Typical Reinforced soil mechanism showing two Possible Interaction Mechanisms

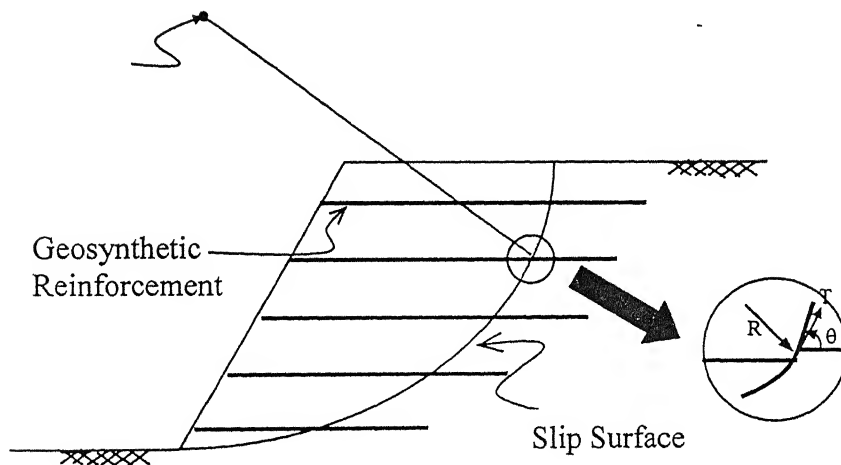


Fig. 1.3 Kinematics of Reinforcement – Soil Interaction

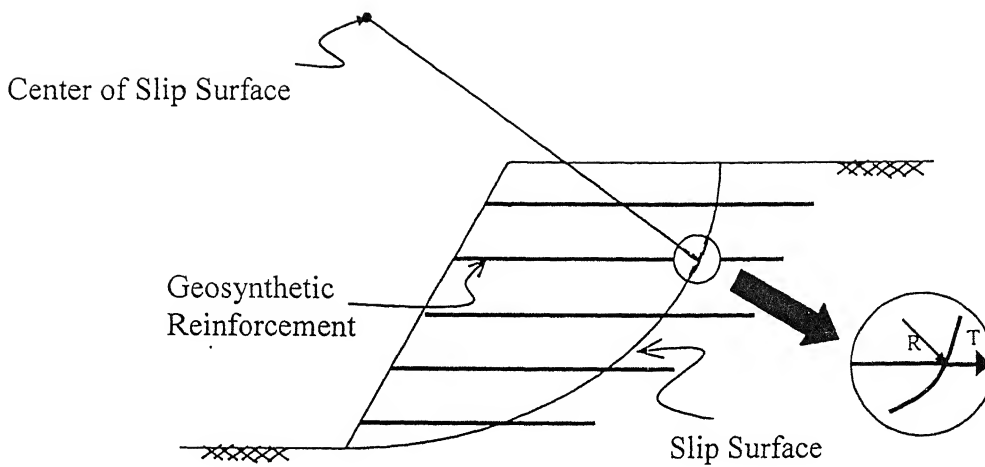


Fig. 1.4 A Typical Pullout Mechanism

responses due to transverse and axial forces. In this work, a method is proposed for the analyses of reinforcement subjected to transverse force or displacement.

## 1.2 Objective

An attempt has been made to formulate and analyze the sheet reinforcement subjected to a transverse downward displacement/force. Literatures explaining the soil-reinforcement interaction due to application of transverse displacement/force are scarce. This thesis work is a small contribution to the current state of science and art of theoretical formulation and numerical analysis for the interface earth reinforcement interactions.

## 1.3 Scope and organization

A simple mathematical model is developed to study the response of inextensible as well as extensible sheet reinforcement subjected to transverse downward displacement/force. The analyses is carried out assuming (i) full resistance is mobilized along sheet-soil interface and (ii) the shear stresses along soil-reinforcement interface is mobilized as a function of the horizontal displacement of the interface between the sheet and the soil subjected to a maximum value (i.e, full shear resistance). To begin with, the stress-displacement response of the subgrade is assumed to be linear (linear subgrade). Latter, a realistic case of hyperbolic stress-displacement response of the soil is considered (non-linear subgrade). The outline of the analyses carried out is presented in the form of a flow chart in Fig. 1.5.

A review of the existing literature (chapter 2) indicates that the analyses of sheet reinforcement subjected to oblique force are scarce.

Chapter 3 deals with the analyses of inextensible reinforcement subjected to a downward transverse force. A simple model is developed and the analyses are carried out for a wide range of soil and soil-interface characteristics.

Chapter 4 focuses on the analyses of extensible sheet reinforcement due to application of transverse displacement/force.

Summary and conclusions based on the present study are given in chapter 5.

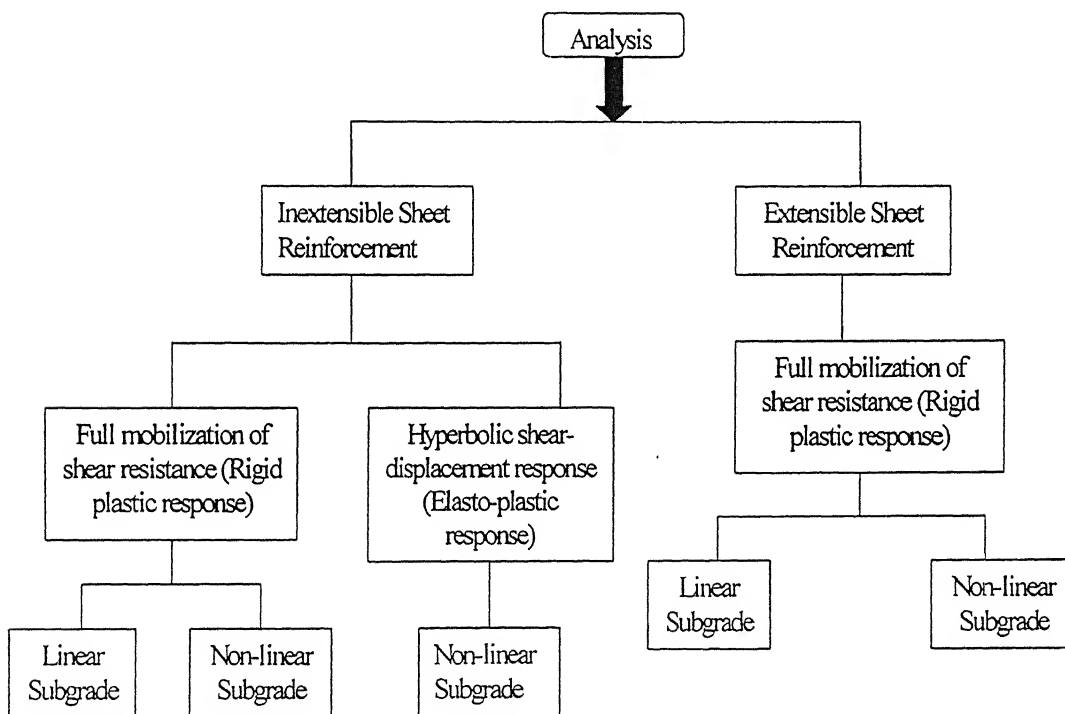


**Fig. 1.5 Outline of the Analyses**

# Chapter 2

## Literature Review

### 2.1 General

In the last three decades, there has been a significant growth in the engineering application of geosynthetics for stabilizing earth structures. All efforts are being made to understand the soil-inclusion/reinforcement characteristics with respect to the overall mechanism of the composite medium. Till date, there is no significant study with regard to the behavior of sheet reinforcement subjected to an oblique downward force. The response of soil due to an oblique force is a combination of responses due to axial and transverse forces. This chapter mainly deals with the review of a) Soil-reinforcement mechanisms, b) the theoretical and experimental studies on the reinforced earth due to pullout force c) studies related to present work and d) the studies on the bearing capacity of reinforced ground.

### 2.2 Soil-Reinforcement Mechanism

Jewell (1992) proposed two limiting modes of soil-reinforcement interaction mechanism: soil sliding over the reinforcement (direct shear mechanism) and the pullout of the reinforcement from the soil (pullout mechanism). Fig. 2.1 shows the conceptual sketches for these cases.

The direct shear resistance between the reinforcement and the soil has two components, namely: the shear resistance between the soil and the reinforcement plane surface and the soil to soil shear resistance (Fig. 2.2). Jewell et al. (1984) proposed the general expression for direct sliding resistance as

$$F_s = \sigma_n A [\alpha_{ds} \tan \delta + (1 - \alpha_{ds}) \tan \phi_{ds}] \quad (2.1)$$

where  $\sigma_n$  is normal stress at shear plane,  $A$  is total area,  $\phi_{ds}$  is friction angle of soil in direct shear,  $\delta$  is skin friction angle between soil and reinforcement shear surface, and  $\alpha_{ds}$  is ratio between the reinforcement shear area and total shear area.

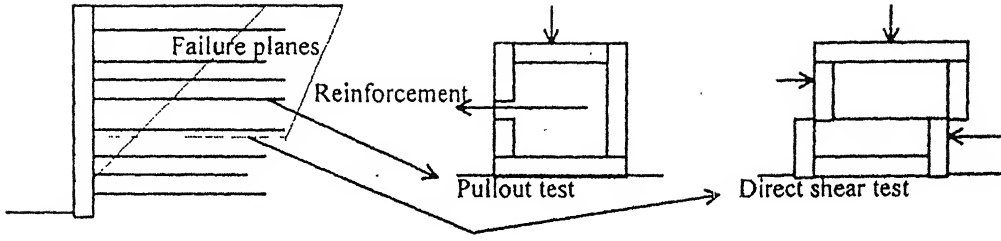


Fig. 2.1 Two possible interaction Mechanism in Reinforced Soils (Jewell, 1992)

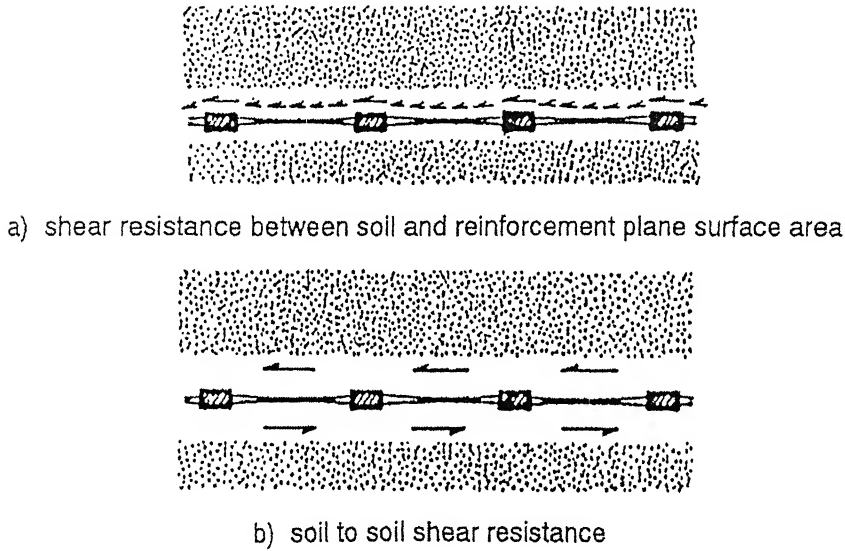


Fig. 2.2 Components of direct Shear Resistance for Geogrid reinforcement

The pullout resistance consists also of two components, namely: friction resistance and bearing resistance (Fig. 2.3). The frictional resistance can be calculated as

$$F_s = 2(A_l + A_t)\sigma_n \tan \delta \quad (2.2)$$

where  $A_l$  is frictional area of longitudinal members at the reinforcement plane surface and  $A_t$  is frictional area of transverse members at the reinforcement plane surface. The bearing resistance is evaluated by bearing capacity theory as follows:

$$F_b = (cN_c + \sigma_n N_q)A_b \quad (2.3)$$

Where  $c$  is cohesion of backfill soil,  $\sigma_n$  is applied normal pressure at the soil/reinforcement interface,  $N_c, N_q$  are bearing capacity factors and  $A_b$  is the bearing area of transverse members.

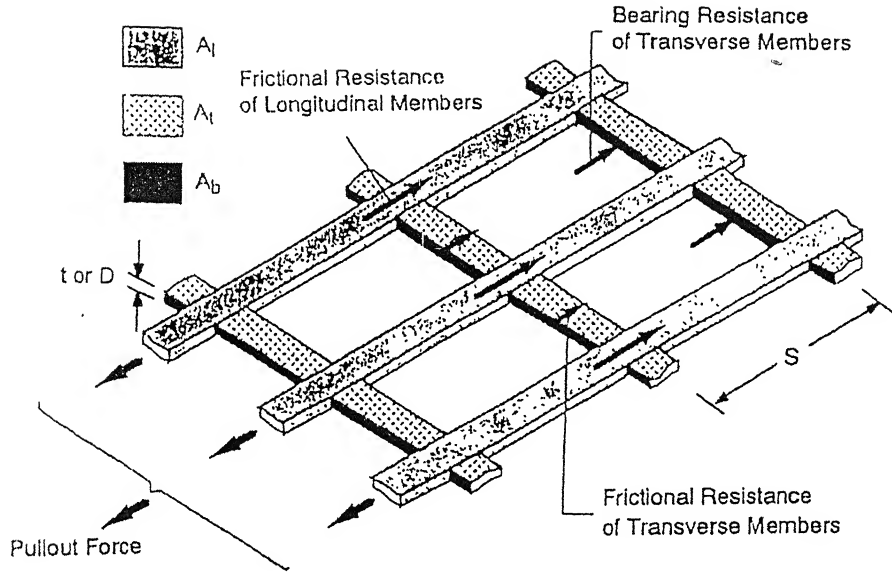


Fig. 2.3 Components of Pullout Resistance for Grid Reinforcement

Different assumptions have been used for determining the bearing capacity factors. Peterson and Anderson (1980) proposed a general bearing failure mechanism (Fig. 2.4a) and proposed the following bearing capacity factors

$$N_q = \exp(\pi \cdot \tan \phi) \tan^2 \left( \frac{\pi}{4} + \frac{\phi}{2} \right) \quad (2.4)$$

$$N_c = \cot \phi (N_q - 1) \quad (2.5)$$

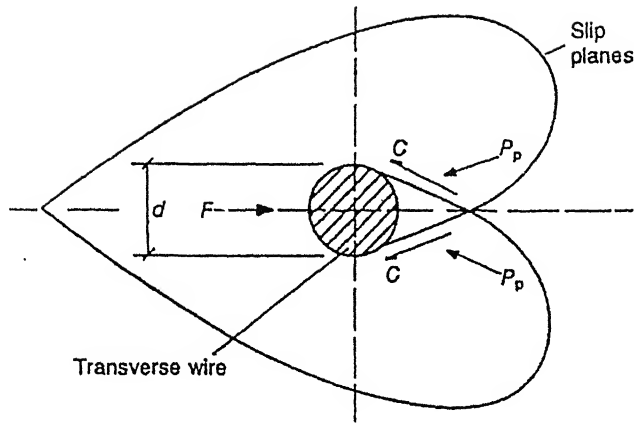
Jewell et al. (1984) assumed a punching shear failure mechanism (Fig. 2.4b) and thus

$$N_q = \exp \left[ \left( \frac{\pi}{2} + \phi \right) \tan \phi \right] \tan \left( \frac{\pi}{4} + \frac{\phi}{2} \right) \quad (2.6)$$

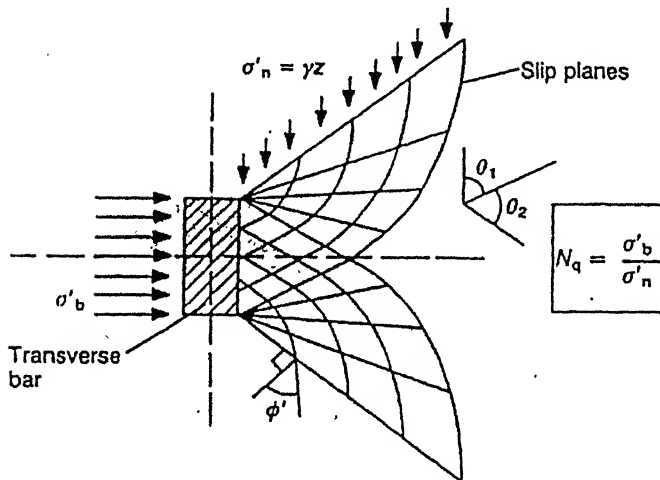
$$N_c = \cot \phi (N_q - 1) \quad (2.7)$$

The general bearing failure and punching shear failure mechanisms form the upper and lower bounds (Palmiera and Miligan, 1989; Jewell, 1990) of the pullout bearing resistance.

Palmiera and Miligan (1989) observed loss in pullout load with decreased spacing of transverse members due to increased interference.



(a) General Bearing Failure Mechanism  
(After Peterson and Anderson, 1980)



(b) Punching Shear Failure Mechanism  
(After Jewell, Milligan, Sarsby and Dubois, 1984)

Fig. 2.4 Pullout Bearing Resistance Mechanism

## 2.3 Analytical and Experimental Studies on Pullout Response

Farrag et al. (1993) presented the testing equipment, specimen preparation and testing procedures for load controlled and displacement rate controlled pullout tests for geosynthetic reinforced granular soils. The influence of test type, confining pressure, soil density, boundary conditions, and geotextile characteristics on pullout load-displacement response of selected geogrids embedded in sand were evaluated.

Bergado and Chai (1994) proposed expressed a new bearing capacity equation to calculate the maximum pullout force of extensible grid reinforcement by incorporating the influence of rigidity and spacing ratio ( $s/D$ , where  $s$  is the bearing member spacing and  $D$  is the bearing member thickness).

Alfaro et al. (1995) proposed the combined two-dimensional (caused due to soil-reinforcement interface friction) and three-dimensional mechanism (caused due to the confinement of the dilating zone of soil around the reinforcement) to evaluate the pullout resistance of geogrid strip reinforcement embedded in dense granular soil.

Lopes and Ladeira (1996) studied the interactive behavior of high density polyethylene uniaxial geogrid specimens in a well graded, gravelly sand, and the effects of specimen geometry, soil height and sleeve length using a large pullout box.

Sobhi and Wu (1996) presented an interface pullout formula for predicting and interpreting pullout test results for extensible sheet reinforcement. The model was based on three postulates. They are: a) *The postulate of stationary confining soil* states that the confining soil remains stationary at all times during the a pull out test, b) *the postulate of interface shear stress mobilization* assumes that the shear stress induced at the soil-reinforcement interface along the active length (the distance along the reinforcement at which the tension in the reinforcement equals zero) is uniform and is equal to the limiting interface shear stress and c) *the postulate of cumulative deformation frictional resistance* developed within the elongated length of the reinforcement is significant and must be accounted for in the analytical model. The analytical solution was used to predict the active length of the reinforcement, pullout force to induce pullout failure, coefficient of interface friction for the soil and the reinforcement and reinforcement displacement along the length.

Wilson-Fahmy et al. (1996) considered the long-term pullout behavior of polymeric geogrids. The experimental results indicate that the pullout strength after 1,000 hr sustained loading could be assumed to be equal to the short-term pullout strength.

Gurung (1999) proposed a new model for the pullout test on highly extensible reinforcement. A bilinear shear stress-displacement relationship was assumed. A relative stiffness parameter,  $\alpha = \frac{2k_s L^2}{E_r t_r}$ , a relative displacement parameter,  $\beta = \frac{w_m}{L}$ ,

the stiffness ratio and  $R_k = \frac{k_{s2}}{k_{s1}}$  were introduced in the governing non-linear equation for a pullout phenomenon. The variation of normalized displacements, strains and normalized pullout forces along the reinforcement length for wide range of parameters,  $\alpha$ ,  $\beta$  and  $R_k$  were presented. The proposed model predicted reasonably with the response from field pullout tests. Later, a model was proposed for a non-linear (hyperbolic) response of the soil and variations were given similar to that for a bilinear model.

Gurung (2000) proposed an analytical model for strip anchor reinforcement and incorporated a hyperbolic shear stress-displacement relation for the soil-reinforcement interface shear stress during pull out tests. A new concept of an anchorage factor (anchor to strip reinforcement capacities), the relative stiffness and the displacement parameters were defined to explain the pullout behavior. The normalized load-displacement relationship and the variations of pullout force and displacement with distance along the reinforcement, at different anchorage factors, are presented. The degree of reduction in the pullout displacements for the increased capacity of the anchor reinforcement was illustrated.

## 2.4 Studies relating to Oblique Force along Reinforcement

Leschinsky and Reinschmidt (1985) in the stability analysis of membrane-reinforced slopes based on limit equilibrium and variational extremization considered that a membrane at the failure surface would bend at an unknown angle,  $\theta$ , as the collapse begins. The tension developed in the membrane was assumed along this angle,  $\theta$  (Fig.2.5).

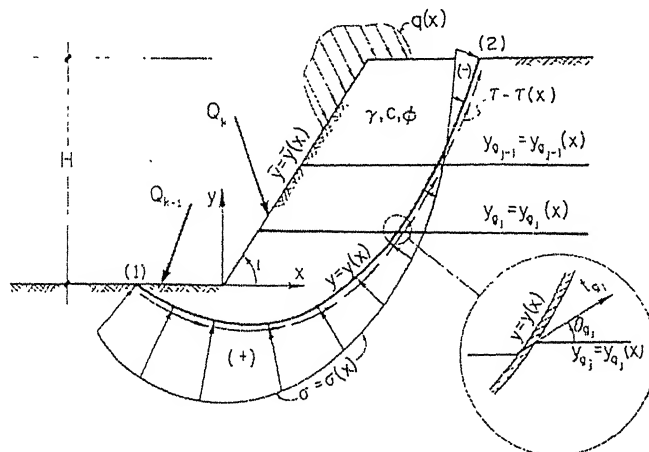


Fig 2.5 Forces considered in the stability Analysis

Degenkamp and Dutta (1988) presented the chain tension at the anchor point and the chain configuration inside the soil for an anchoring system consisting of a pile with an embedded connection between the anchor pile and the mooring chain (Fig. 2.6). They proposed a two-dimensional static analysis to evaluate the variations of tension and chain configuration inside the soil. They also proposed the effective width of the chain to be used in the calculation of soil resistance in bearing (EWB) and friction (EWS).

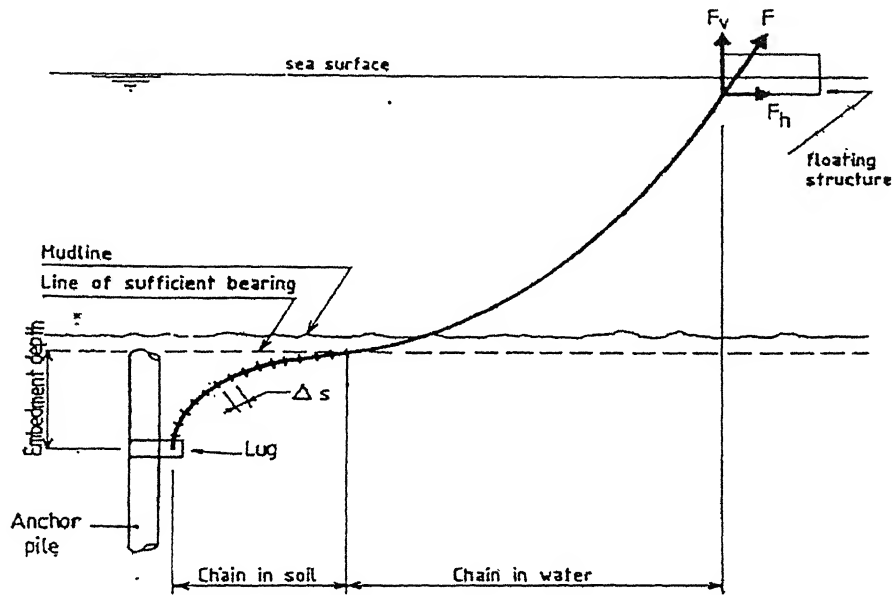


Fig. 2.6 Chain Configuration between Floating Structure and embedded Pile Lug

Leschinsky and Boedeker (1990) investigated the internal and external stability analyses of geosynthetic reinforced soil structures for two extreme inclinations of reinforcement tensile resistance, orthogonal to the radius vector defining the geosynthetic sheet, and horizontal, signifying the as installed position. The assumed horizontal tensile resistance produced values of required tensile resistance that are slightly larger than those for orthogonal geosynthetic force.

Athanasopoulos (1993) placed the geotextile reinforcement perpendicular to the plane of shear in a direct shear tests on unsaturated clay samples reinforced with woven and non-woven geotextiles. The pullout force is resisted by the horizontal component of tension developed along the reinforcement in the shear zone (Fig. 2.7). The value of tension,  $T$ , developed in the sheet of reinforcement is given by

$$T = A_v K_o \sigma_v \tan \delta \quad (2.8)$$

The shear strength increase,  $\Delta\tau$ , of reinforced soil with vertical orientation of reinforcement is given by

$$\Delta\tau = \frac{T}{A_f} (\sin \theta + \cos \theta \tan \phi) \quad (2.9)$$

where  $\Delta\tau$  is the difference of peak strength between reinforced and unreinforced sand,  $A_f$  is the sheared area of sand in the direct shear test,  $\theta$  is the angle defined in Fig. 2.7, and  $\phi$  is the angle of internal friction of sand.

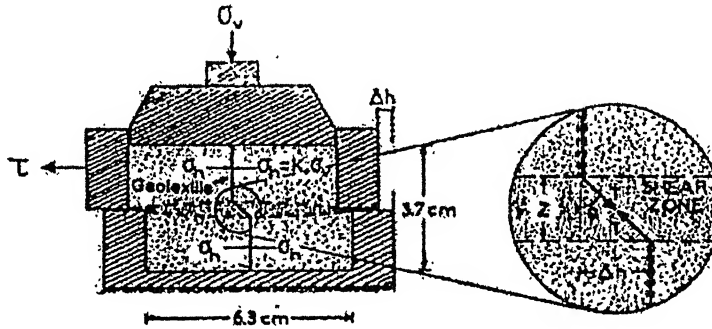


Fig. 2.7 Direct Shear testing of Soil Sample reinforced with a Sheet of Geotextile

Neubecker and Randolph (1994) presented analytical expressions that describe the anchor chain profile in uniform soil and soil with strength increasing linearly with depth. Analytical expressions have also been derived that relate the chain tension to the inclination angle for any general soil-strength profile.

Burd (1995) proposed an analytical model for a plane strain membrane mechanism of reinforcement under the application of a monotonic load. He postulated a method for the determination of the active length of the reinforcement.

## 2.5 Bearing Capacity of Reinforced soils

Binquet and Lee (1975) addressed the analytical problem of the bearing capacity of a strip footing on a granular soil containing horizontal layers of tensile reinforcing. Fig. 2.8a shows the assumed failure surface. Zone I-immediately below the foundation was assumed to settle along with the foundation under the application of load and on each side of zone I, the soil was pushed downward - this is zone II. Under the

application of bearing pressure by the foundation, the reinforcing ties at along  $a'$ ,  $c'$  and  $a$ ,  $c$  was assumed to take two right angle turns around two frictionless rollers (Fig. 2.8b).

Akinmusuru and Akinbolade (1981) reported some experimental works on square footings paced on a deep homogenous sand bed reinforced with flat strips of the rope fiber material. It was shown that depending on the strip arrangement, ultimate bearing capacity values can be increased by a factor up to three times that of unreinforced soil.

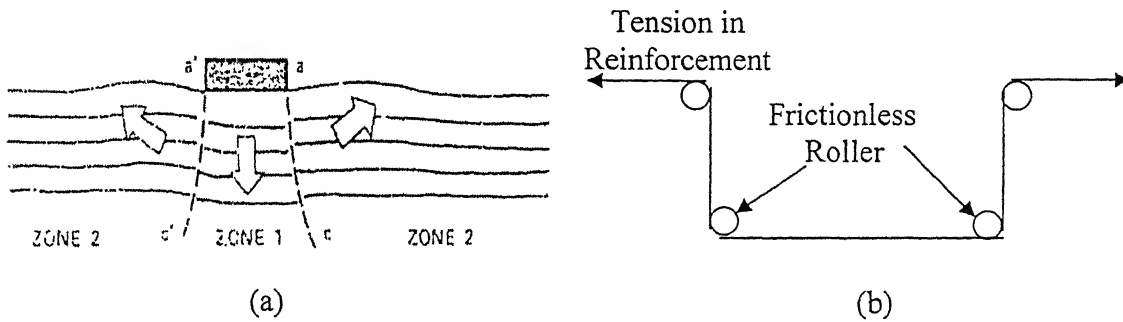


Fig. 2.8 Assumed Failure Mechanism under a foundation supported by reinforced earth

Brown and Poulos (1981) have applied the finite element method for the analysis of reinforced soil bed incorporating elasto-plastic soil model satisfying Mohr-Coulomb failure criterion, elastic reinforcement strip and a model for soil-reinforcement bonding which allows for slippage governed by a Mohr-coulomb failure criterion.

Giroud and Noiray (1981) have made a quasi-static analysis of the unpaved road mechanism with and without geotextile reinforcement. The analysis was based on the consideration of the “tension membrane” effect for the case of plane strain reinforced unpaved road deforming under the action of single application of dual wheel load. Assuming an allowable rut depth, load spread angle, suitable geometric configuration and firm anchorage of the reinforcement, the strain in the reinforcement can be calculated. Once the strain is known, the tension in the reinforcement can be estimated from the stiffness of the reinforcement. Design charts have been prepared for the reduction in road base thickness, due to reinforcing effect of geosynthetic for various traffic intensities.

Bourdeau et al. (1982) analysed the membrane action of the reinforcement on the load-settlement response of two-layered soil. The geotextile is introduced at the interface of the two layers. Probabilistic stress distribution was considered.

Haliburton and Barron's (1983) design method was based on small-scale model tests resting on dense sand. Results show that the bearing capacity of reinforced aggregate increases to more than twice and the load-deformation modulus three to five folds of the unreinforced system by optimum placement of the fabric.

Sawicki (1983) applied plasticity theory to estimate the ultimate bearing capacity of reinforced soil. Both rigid-plastic and elasto-plastic models have been applied for analyzing the microbehaviour of the reinforcement soil composite.

Fragaszy and Lawton (1984) conducted a series of laboratory model tests designed to determine the influence of soil density and reinforcing strip length on the load settlement behavior of reinforced sand. When bearing capacity ratio is calculated at a settlement equal to 10% of the footing width, the bearing capacity ratio is independent of soil density. When calculated at a settlement of 4% of the footing width, the percentage increase in the bearing capacity appears to be less for loose sands than for dense sands.

Guido et al. (1986) conducted laboratory model tests on bearing capacity of geogrid and geotextile reinforced earth slabs. The parameters like coefficient of friction between the geotextile and soil, pullout resistance between geogrid and soil, depth below the footing of the first layer of the reinforcement and tensile strength of the reinforcement were studied.

Watari et al. (1986) carried out field tests to study the effect of polymer net in compensating the shortages of bearing capacity of soft soil when construction fill is placed over the soft soil. Measurements were made of the settlement of the fill, heave and lateral movement in the soft clay stratum, the strain and hence tensile stresses in the polymer-nets during and after the spreading of earthfill. Bearing capacity of the reinforced soil has been estimated with the help of modified Terzaghi bearing capacity equation (Yamanouchi and Gotoh, 1979) as follows,

$$q_u = \alpha_s c N_c + T \left( \frac{2 \sin \theta}{B} + \frac{N_q}{R} \right) + \gamma D_f N_q \quad (2.10)$$

where  $\alpha_s$  is the shape factor of the footing,  $N_c$  and  $N_q$  are Terzaghi's bearing capacity factors,  $T$  is the polymer net tensile force per unit length,  $B$  is the banking strip width,  $R$  is the radius of the wedge formed and  $\theta$  is the angle formed by the tangent of the above circle at the footing edge (Fig. 2.9 )

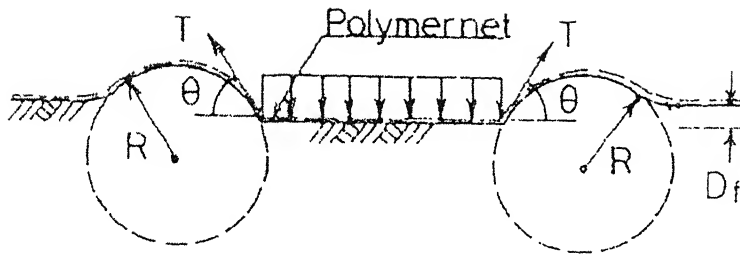


Fig. 2.9 Effect of Polymernet

Love et al. (1987) have developed a large strain finite element method to include the effect of thin reinforcement layer.

Nishigata and Yamaoka (1992) investigated the mechanism of geotextile reinforcement by conducting two-dimensional models. The contribution of vertical component of tensile force developed in the geotextile, restraint of soft subgrade soil and confinement of aggregate (sub-base) layer were considered. The equations for ultimate bearing capacity were given and a design chart is proposed for determination of aggregate thickness when the shear strength of the subgrade soil and required bearing capacity of the road system are known.

Mandal and Shah (1993) investigated the effect of bearing capacity by conducting model tests on footings on clay subgrades reinforced with geogrids placed horizontally. The improvement in bearing capacity was observed at nearly all levels of deformation in the geogrid reinforced clay subgrades.

Ghosh and Madhav (1994) developed a simple mathematical model to account for the membrane effect of a reinforcement layer on the load-settlement response of a reinforced granular fill-soft soil foundation system. The non-linear loading pressure-settlement response of the granular fill and soft soil, respectively, for plane strain loading condition are incorporated into the formulation.

Yetimoglu et al. (1994) investigated the bearing capacity of rectangular footings on geogrid-reinforced sands by performing laboratory model tests and FEM analyses. The bearing capacity of reinforced sand was found to increase with reinforcement layer number and reinforcement size when reinforcement was placed within a certain effective zone. In addition, the analysis indicated that increasing reinforcement stiffness beyond a certain value would not bring about further increase in the bearing capacity.

Shukla and Chandra (1995) developed a mechanical model for a geosynthetic-reinforced granular fill-soft system, which incorporates the effect of compaction of the granular fill on its load-settlement response. The model considers large deformations and both horizontal and vertical shear stress transfer at the fill-geosynthetic interface.

Das et al. (1996) conducted experiments on the laboratory model tests to determine the ultimate bearing capacity of a strip foundation on a saturated clay slope reinforced with a layer of geogrid. The maximum depth of the reinforcement that contributes to the improvement in bearing capacity was found to be about  $1.72 B$ , where  $B$  is the width of the footing.

Adams and Collin (1997) carried out 35 large-scale model tests to find out the effects of a single and multiple layers of geosynthetic reinforcement placed below the shallow footing. Two different types of geosynthetics, stiff biaxial geogrid and a geocell were used to carry out the tests. Results showed that the use of geosynthetics for foundation soil would increase the ultimate bearing capacity of shallow spread footings by a factor of 2.5.

## 2.6 Conclusions

A literature review shows that great deal of progress has been achieved with regard to pullout response of reinforced earth. But, the response of reinforcement subjected to an oblique/transverse force is not studied. The analysis of reinforcement due to a transverse force is covered in the subsequent chapters. Finally, based on the proposed model, a method for the estimation of the bearing capacity of a two-layered soil with a sheet reinforcement inclusion is presented.

## Chapter 3

# Analysis of Inextensible Sheet Reinforcement Subjected to a Transverse Force/Displacement

### 3.1 General

This chapter deals with the analysis of inextensible sheet reinforcement subjected to a transverse downward displacement applied at the free end. The analyses is carried out assuming (i) full shear resistance is mobilized along the sheet-soil interface and (ii) the shear stress is mobilized as a function of the horizontal displacement of the interface between the sheet and the soil subjected to a maximum value (i.e, full shear resistance). For the first case (full shear stress mobilization) the analyses are carried out assuming the response of the soil to transverse displacements to be linear (linear subgrade) as well as non-linear (non-linear subgrade). But for the case of shear stress mobilization as a function of horizontal displacement of the interface, only the non-linear subgrade response is considered in the analysis.

### 3.2 Problem Statement

An inextensible sheet reinforcement of length,  $L$ , is embedded at a depth,  $D_e$ , in a soil of unit weight,  $\gamma$  (Fig. 3.1). The interface shear resistance between the reinforcement and the soil is characterized by the angle,  $\phi_r$  ( $\leq \phi$ , the angle of shearing resistance of the soil). The problem is to determine the displacement profile of and the tension mobilized in the reinforcement due to transverse force,  $P$ , applied at point B. Alternatively, the displacement profile and the transverse force due to a given transverse displacement,  $w_L$ , of the point, B, are to be evaluated.

### 3.3 Analyses

#### 3.3.1 Linear Subgrade –Model I

##### 3.3.1.1 The Model

The inextensible reinforcement sheet acted upon by a transverse force,  $P$ , or a transverse displacement,  $w_L$ , is subjected to uniform normal stresses of intensity,  $q_t$  ( $=\gamma D_e$ )

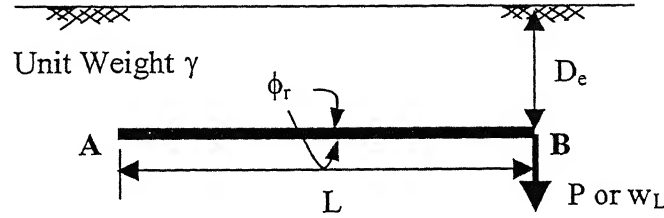


Fig. 3.1 Definition Sketch

on the top and stresses of intensity,  $q_b(x)$ , on the bottom surfaces of the reinforcement (Fig. 3.2a). The soil below the reinforcement generates additional stresses, i.e ( $q_b - q_t$ ) due to the downward displacement,  $w_L$ . The response is represented by a set of Winkler springs (Fig. 3.2 b). A typical linear stress-displacement response is considered for response of the soil and hence for the Winkler springs (Fig. 3.2 c).

Stress-displacement response of the subgrade or the Winkler springs is defined by the expression

$$(q_b - q_t) = k_s w \quad (3.1)$$

where  $w$  is the normal displacement and  $k_s$  is the modulus of subgrade reaction of the ground.

##### 3.3.1.2 Analysis

The equilibrium of forces on an element (Fig 3.3) of infinitesimal length,  $\Delta x$ , and unit width is considered. The tensile forces and the inclination of the left and right ends of the element are respectively,  $T$  and  $(T + \Delta T)$ , and  $\theta$  and  $(\theta + \Delta\theta)$  at distances  $x$  and  $(x + \Delta x)$  from the left end (Point A) of the sheet (Fig. 3.1).

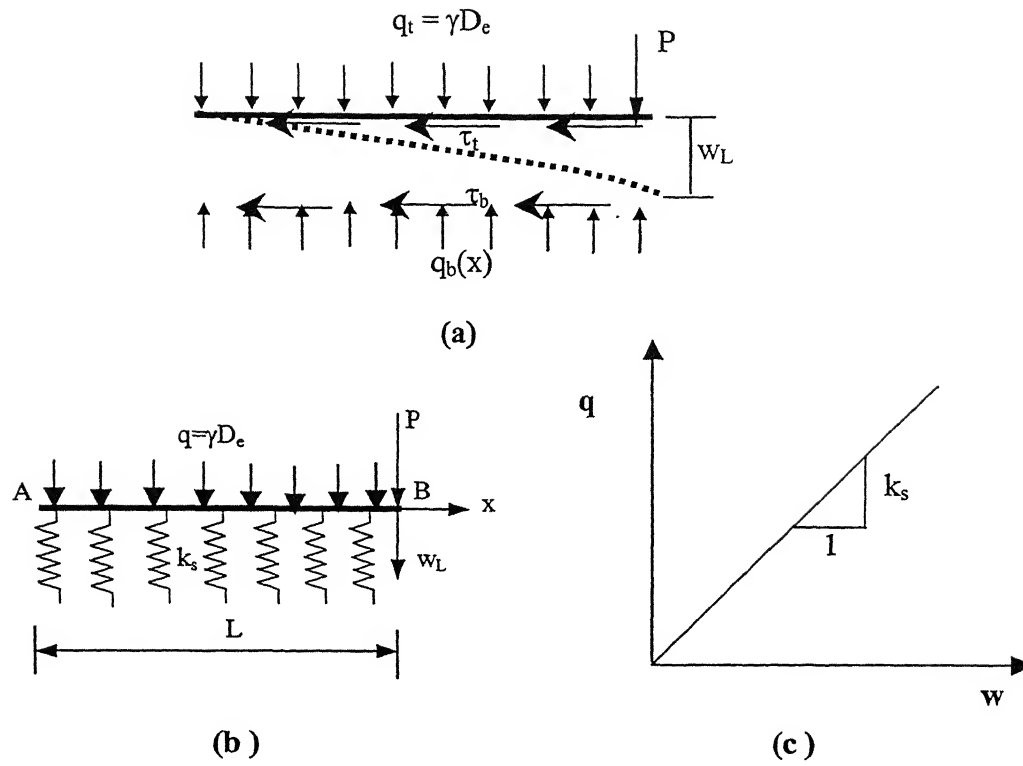


Fig 3.2(a) Forces acting on Sheet Reinforcement and (b) Idealization of Soil (c) Stress Displacement Response of Soil.

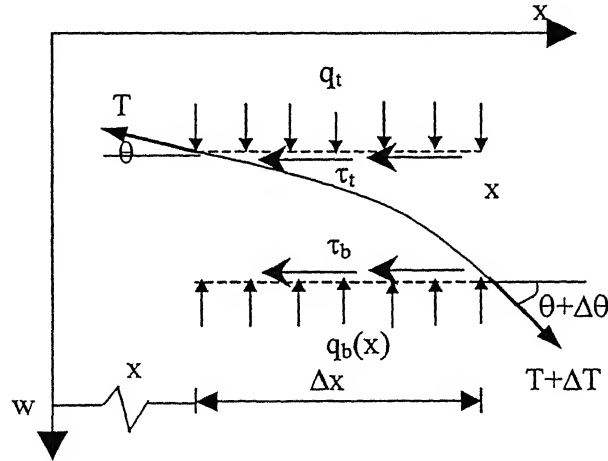


Fig. 3.3 Forces on Infinitesimal Element

Considering the equilibrium of forces in the horizontal and vertical directions, one gets

$$\sum F_x = (T + dT)\cos(\theta + d\theta) - T\cos\theta - (q_t + q_b)\tan\phi_r\Delta x = 0 \quad (3.2)$$

$$\sum F_y = (T + dT)\sin(\theta + d\theta) - T\sin\theta - (q_b - q_t)\Delta x = 0 \quad (3.3)$$

For small deformations, as  $\Delta\theta \rightarrow 0$ ,  $\cos \Delta\theta \rightarrow 1$  and  $\sin \Delta\theta \rightarrow 0$ . Neglecting second order terms, Eqs. 3.2 and 3.3 get simplified respectively to

$$\cos\theta\left(\frac{dT}{dx}\right) - T\sin\theta\left(\frac{d\theta}{dx}\right) - (q_t + q_b)\tan\phi_r = 0 \quad (3.4)$$

$$\sin\theta\left(\frac{dT}{dx}\right) + T\cos\theta\left(\frac{d\theta}{dx}\right) - (q_b - q_t) = 0 \quad (3.5)$$

Multiplying Eq. 3.4 by  $\cos\theta$  and Eq. 3.5 by  $\sin\theta$  and adding the two, one gets

$$\frac{dT}{dx} = (q_t + q_b)\cos\theta\tan\phi_r + (q_b - q_t)\sin\theta \quad (3.6)$$

Similarly, multiplying Eq. 3.4 by  $\sin\theta$  and Eq. 3.5 by  $\cos\theta$  and subtracting the latter from the former, one gets

$$-T\frac{d\theta}{dx} - (q_t + q_b)\tan\phi_r\sin\theta + (q_b - q_t)\cos\theta = 0 \quad (3.7)$$

But  $\tan\theta = dw/dx$ , where  $w$  is the normal displacement at a distance,  $x$ , from point A. Differentiating with respect to  $x$ , one gets

$$\frac{d\theta}{dx} = \cos^2\theta \frac{d^2w}{dx^2} \quad (3.8)$$

Combining Eqs. 3.1, 3.6, 3.7 and 3.8, the following equations are obtained

$$\frac{dT}{dx} = (q_t + q_b)\cos\theta\tan\phi_r + k_s w \sin\theta \quad (3.9)$$

$$-T\cos^2\theta \frac{d^2w}{dx^2} + K_s w \cos\theta = (q_t + q_b)\sin\theta\tan\phi_r \quad (3.10)$$

For small  $\theta$ , Eqs. 3.9 and 3.10 reduce to

$$\frac{dT}{dx} = (q_t + q_b)\tan\phi_r$$

$$=(q_b - q_i + 2q_i)\tan\phi_r$$

$$=(k_s w + 2\gamma D_e)\tan\phi_r \quad (3.11)$$

$$-T \frac{d^2 w}{dx^2} + k_s w = 0 \quad (3.12)$$

Eqs. 3.11 and 3.12 are the governing equations for the problem under consideration. Eqs. 3.11 and 3.12 are non-dimensionalised with  $X=x/L$ ,  $W=w/w_L$  and  $T^*=T/T_{\max p}$  where  $w_L$  is the normal displacement at the right end, i.e,  $x=L$  or  $X=1.0$  and  $T_{\max p}=2\gamma D_e L \tan\phi_r$ , the maximum axial pullout force. Eqs. 3.11 and 3.12 become

$$\frac{dT^*}{dX} = \frac{1}{2} \left( \mu \frac{w_L}{L} W + 2 \right) \quad (3.13)$$

$$-T^* \frac{d^2 W}{dX^2} + \frac{\mu W}{2 \tan\phi_r} = 0 \quad (3.14)$$

where  $\mu = \frac{k_s L}{\gamma D_e}$  is relative stiffness factor .

Eqs. (3.13) and (3.14) are the governing differential equations in normalized for the present model. The boundary conditions are: slope of and tension in the reinforcement are zero at the left end, i.e. at  $x$  (or  $X$ ) = 0, i.e.,  $dw/dx$  (or  $dW/dX$ ) = 0 and  $T$  (or  $T^*$ ) = 0, while at the right end, i.e. at  $x=L$ ,  $X = 1.0$ , the displacement  $w = w_L$  (or  $W = 1.0$ ). The problem has been posed with free end displacement,  $w_L$ , specified rather than specifying the force at  $x=L$  as it was found to be simpler. The transverse force,  $P$ , required to cause the displacement,  $w_L$ , is obtained as part of the response by integrating the soil reaction mobilized as

$$P = \int_0^L k_s w dx \quad (3.15)$$

### 3.3.1.3 Numerical Solution

The two force equilibrium equations, Eqs. 3.13 and 3.14, are to be solved together to obtain the results. As an analytical solution is not possible, a numerical finite

difference procedure is proposed. The reinforcement length,  $L$ , is divided into 'n' sub-elements each of length,  $\Delta L=L/n$  or  $\Delta X=1/n$  as shown in Fig. 3.4. Eqs. 3.13 and 3.14 in finite difference form become

$$\frac{T_{i+1}^* - T_i^*}{\Delta X} = \frac{1}{2} \left( \mu W_i \frac{w_L}{L} + 2 \right) \quad (3.16)$$

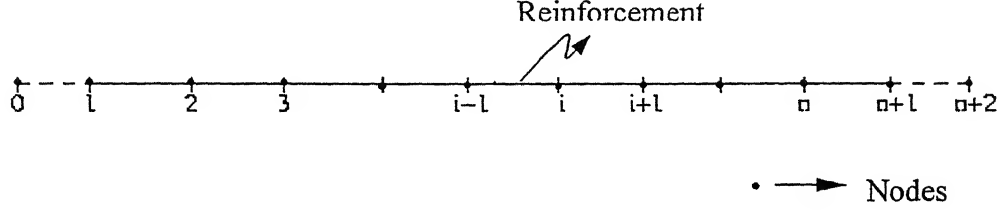


Fig 3.4 Discretisation of Reinforcement Length into Elements

$$-T_i^* \left( \frac{W_{i-1} - 2W_i + W_{i+1}}{\Delta X^2} \right) + \frac{\mu W_i}{2 \tan \phi_r} = 0 \quad (3.17)$$

Solving for normalized displacement and normalized tension, one gets

$$W_i = \frac{T_i^* n^2 (W_{i-1} + W_{i+1})}{\left( 2n^2 T_i^* + \frac{\mu}{2 \tan \phi_r} \right)} \quad (3.18)$$

$$T_{i+1}^* = \frac{1}{2} \left( \mu W_i \frac{w_L}{L} + 2 \right) + T_i^* \quad (3.19)$$

To obtain the displacement at node 1, the boundary condition  $dW/dX=0$  at  $X=0$  leads to the condition,  $W_0=W_2$  and Eq. 3.18 for node 1 becomes

$$W_1 = \frac{2n^2 T_1^* W_2}{\left( 2n^2 T_1^* + \frac{\mu}{2 \tan \phi_r} \right)} \quad (3.20)$$

At  $x=L$  or  $X=1.0$ ,  $i=n+1$  and  $W_{n+1}=1.0$ .

The transverse force,  $P$  is obtained from by numerical integration of Eq. (3.15) as

$$P = k_s \Delta x \left[ \frac{w_1 + w_{n+1}}{2} + \sum_{i=2}^n w_i \right] \quad (3.21)$$

The above equation in normalized form becomes

$$P^* = \mu \frac{w_o}{L} \frac{1}{n} \left[ \frac{W_1 + 1}{2} + \sum_{i=2}^n W_i \right] \quad (3.22)$$

A given free end displacement at the right end of the reinforcement, the response of the soil reinforcement is obtained by solving Eqs. (3.18) and (3.19) for the given boundary conditions. The corresponding normalized transverse force to enforce a given free end displacement is obtained by Eq. (3.22).

#### 3.3.1.4 Characteristics of the Model

A simple mathematical model has been developed to study the response of inextensible sheet reinforcement subjected to transverse displacement/force. With the application of an applied transverse load or displacement, reinforcement interacts with the soil and as a consequence shear stresses at the interface of and tensile forces in the reinforcement are generated. The reinforcement-soil interface is characterized by the interface friction angle ( $\phi_r$ ). The normal stresses generated due to transverse load application are assumed to increase linearly with normal displacement. But in reality, soil exhibits a non-linear relationship between stresses and the displacement. This drawback is overcome by assuming a hyperbolic relation between stress and displacement and the solution given in the subsequent section.

#### 3.3.1.5 Results and Discussions

Eqs. (3.18) and (3.19) are solved for reinforcement length (1 to 10 m), unit weight of soil,  $\gamma$  (15 to 20 kN/m<sup>3</sup>), depth of embedment,  $D_e$  (1 to 10 m), interface friction angle,  $\phi_r$ , (20° to 40°) and free end displacement,  $w_L$  (0.001L to 0.1L). The values of the coefficient of subgrade reaction,  $k_s$  obtained from Scott (1981) are shown in Table 3.1.

Table 3.1. Modulus of Subgrade Reaction in MN/m<sup>3</sup>

Soil Characteristics	Loose	Medium Dense	Dense
Dry or Moist Sand	6-18	18-90	90-300
Submerged Sand	7.5	24	90

The range of relative ground stiffness factor,  $\mu(=k_s L/\gamma D_e)$ , becomes 50-100,000.

Firstly, the convergence of the results has been checked by varying 'n', the number of elements into which the reinforcement discretised. It has been found that for 'n' values beyond 1000 the accuracy in the values of normalized tension,  $T^*$  or the normalized transverse force,  $P^*$ , were not affected at the right end. Hence  $n=1000$  has been chosen for further analyses.

The normalized displacement profiles,  $w/L$ , versus distance along the reinforcement,  $X$ , for a relatively small value of free end displacement of  $w_L/L$  of 0.01, and for relative stiffness factor,  $\mu$  values of 50, 200, 500, 1000 and 10000, and  $\phi_r$  values of  $25^\circ$  to  $35^\circ$  are presented in Fig. 3.5. For relatively compressible subgrades, i.e.  $\mu$  equal to 50, the displacements increase gradually from a short distance of about  $0.3L$  from the left end. The points of mobilization of transverse displacements move to the right with increasing values of  $\mu$ . The displacements get restricted to a smaller zone close to the right end for very stiff subgrade ( $\mu=10,000$ ). The effect of the reinforcement – subgrade interface shear angle on the displacement profiles is relatively small. Larger the value of  $\phi_r$ , more gradual are the increases in the transverse deformations, though this increase is not very significant. The effect of  $\phi_r$  decreases with increasing values of  $\mu$ . Thus the normal displacement profiles are almost independent of  $\phi_r$  for  $\mu=10,000$ . Similar set of results (Fig. 3.6) are obtained for relatively large free end displacement of  $w_L/L=0.1$ .

The variation of normalized displacement,  $w/L$ , with normalized distance,  $X$ , for different free end displacements of 0.025, 0.05 and 0.1 are shown in Fig. 3.7. For a given length of reinforcement, as free end displacement,  $w_L$ , increases the points of mobilization of transverse displacements move towards the left end indicating that large tracts of the soil offer resistance.

The variation in normalized tension,  $T^*$ , with distance,  $X$ , for different values of  $w_L/L$  and for  $\mu=500$  and  $\phi_r=30^\circ$ , is presented in Fig. 3.8. For very small values of  $w_L/L$ ,

e.g. 0.001, the tension increases linearly with distance,  $X$ . The tension increases sharply from a distance,  $x$ , of about  $0.75L$  and the rate of increase is non-linear for large free end displacements.

The effect of soil stiffness,  $\mu$ , on the variation of normalized tension along the length of the reinforcement is presented in Fig. 3.9. For relatively compressible soils ( $\mu \leq 50$ ), the tension varies almost linearly with distance along the length of reinforcement. But for large soil stiffness (e.g.  $\mu = 10,000$ ), the normal displacements become highly localized near the right end and hence tension increases sharply in that portion of the reinforcement length and the rate of increase of tension with  $x$  is highly non-linear.

The variation of maximum tension developed with free end displacement is shown in Fig. 3.10. The maximum tension is nearly independent of with free end displacement for relatively compressible soils ( $\mu = 50$ ). As  $\mu$  increases, the rate of increase of maximum tension with  $w_L/L$  also increases.

The variation of inclination,  $\theta_L$ , of the reinforcement at the right end, i.e at  $x=L$ , with  $w_L/L$  for relative stiffness factors of  $\mu = 50, 500, 2000, 5000$  and  $10000$  is portrayed in Fig. 3.11. As the normal displacements are highly localized for stiff soils (Fig. 3.5), the inclination of reinforcement with the horizontal at  $x=L$  is higher for such soils.  $(\theta)_L = 4^\circ$  for  $\mu = 50^\circ$  and  $39^\circ$  for  $\mu = 10,000$  at  $w_L/L = 0.01$  and for  $\phi_r = 30^\circ$ . The variation of  $\theta_L$  with  $w_L/L$  is linear for relatively compressible soils ( $\mu = 50$ ) and non-linear for relatively stiff soils ( $\mu = 10,000$ ).

The maximum tension developed as well as the inclination of reinforcement with the horizontal at  $x=L$  increase with the enforced free end transverse displacement. Thus, the normal component of maximum tension developed with free end displacement increases (Fig. 3.12) with  $w_L/L$ . The rate of increase of normal component of maximum tension developed increases with the relative stiffness of the soil. The normal component of maximum tension developed is negligible to very small for relatively compressible soils.

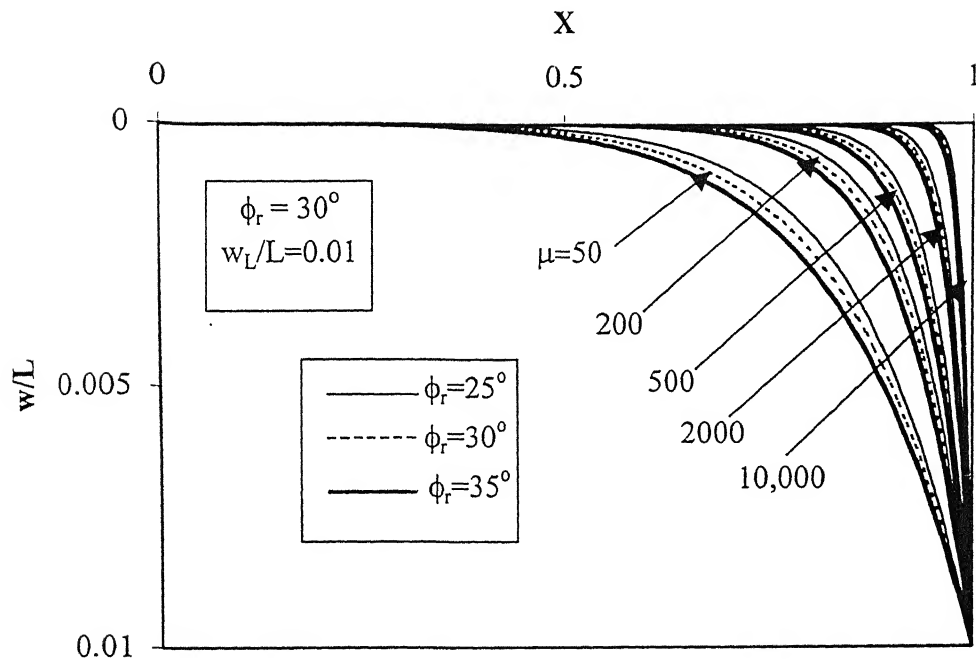


Fig. 3.5 Variation of Normalized Normal Displacement with Normalized Distance for  $w_L/L=0.01$  – Effect of  $\mu$ .

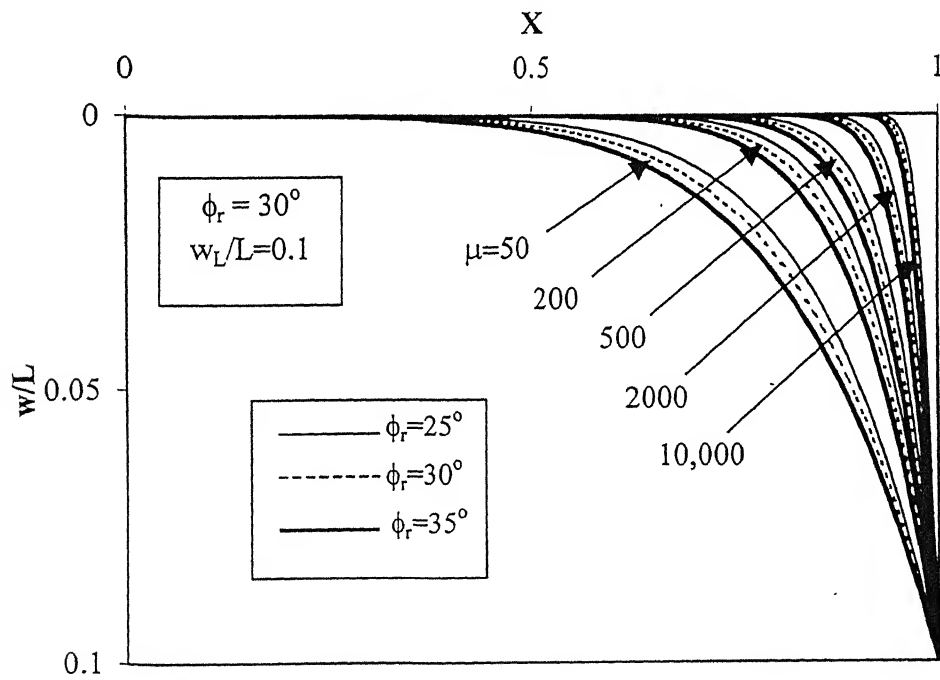


Fig. 3.6 Variation of Normalized Normal Displacement with Normalized Distance for  $w_L/L=0.1$  – Effect of  $\mu$ .

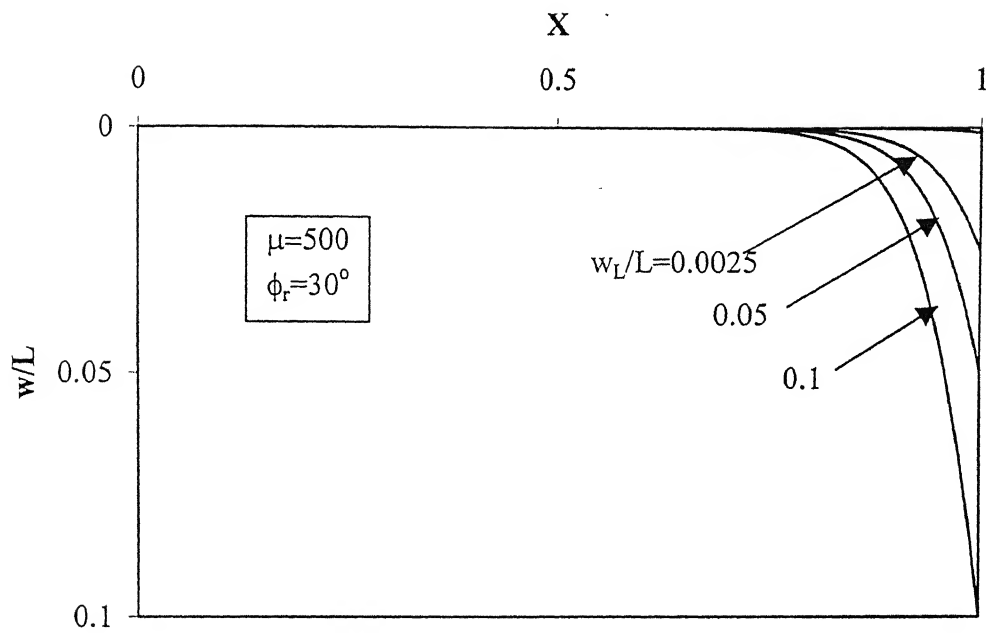


Fig. 3.7 Variation of Normalized Normal Displacement with Normalized Distance - Effect of  $w_L/L$

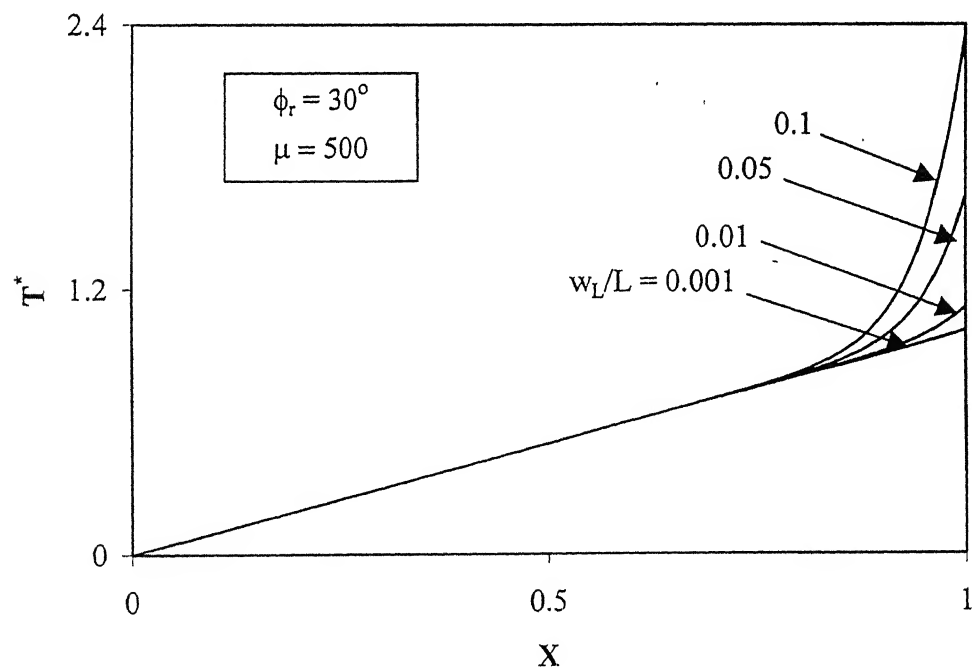


Fig. 3.8 Variation of Normalized Tension with Normalized Distance – Effect of  $w_L/L$

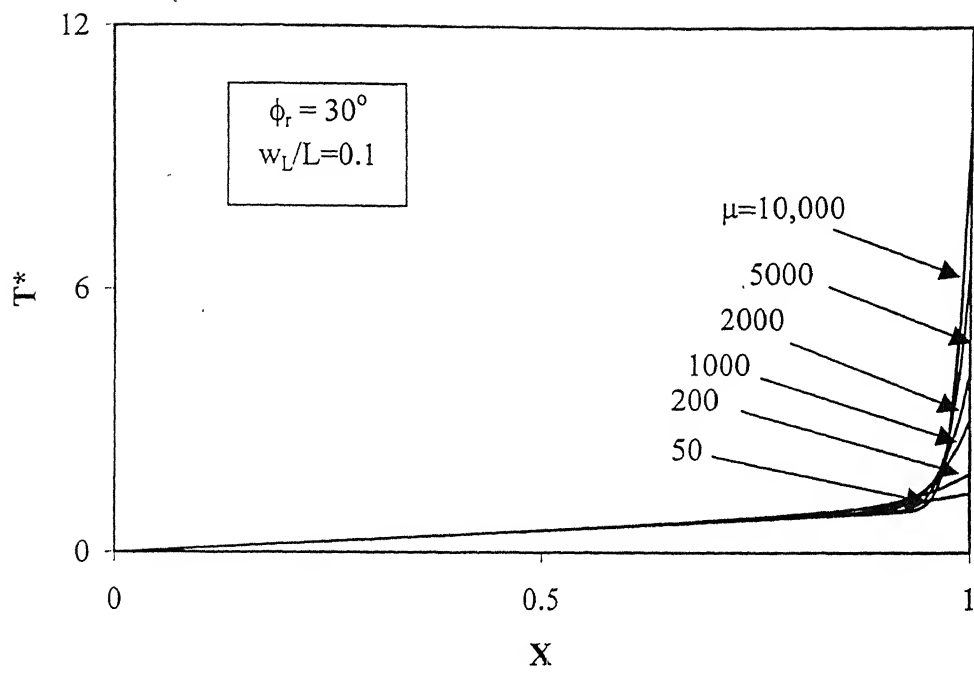


Fig. 3.9 Variation of Normalized Tension with Normalized Distance – Effect of  $\mu$

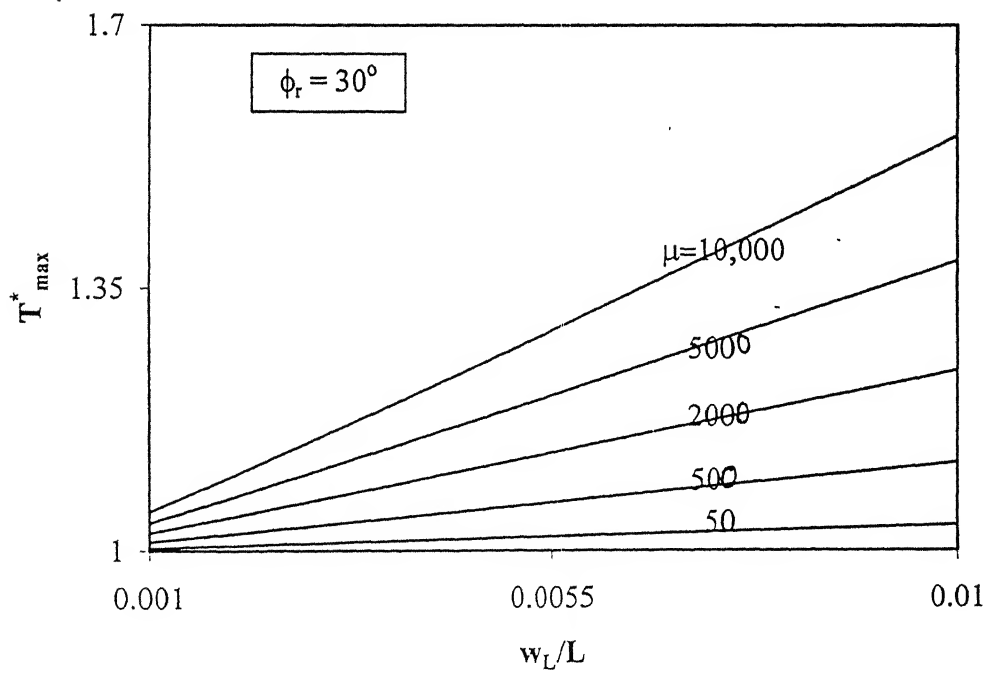


Fig. 3.10 Variation of Normalized Maximum Tension with  $w_L/L$  – Effect of  $\mu$

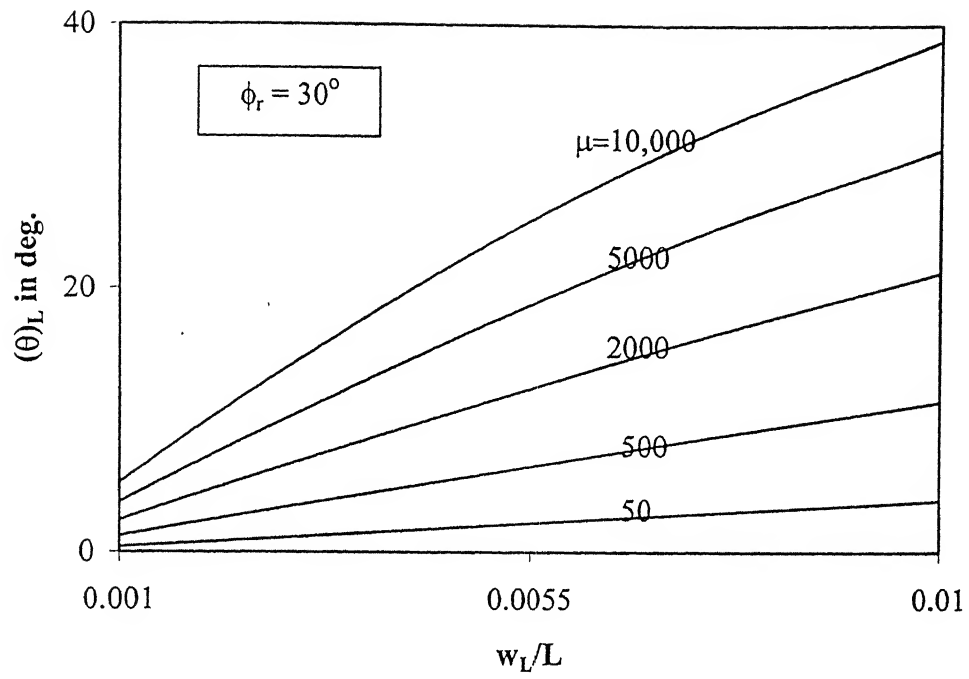


Fig 3.11 Variation of Maximum Inclination with  $w_L/L$  – Effect of  $\mu$

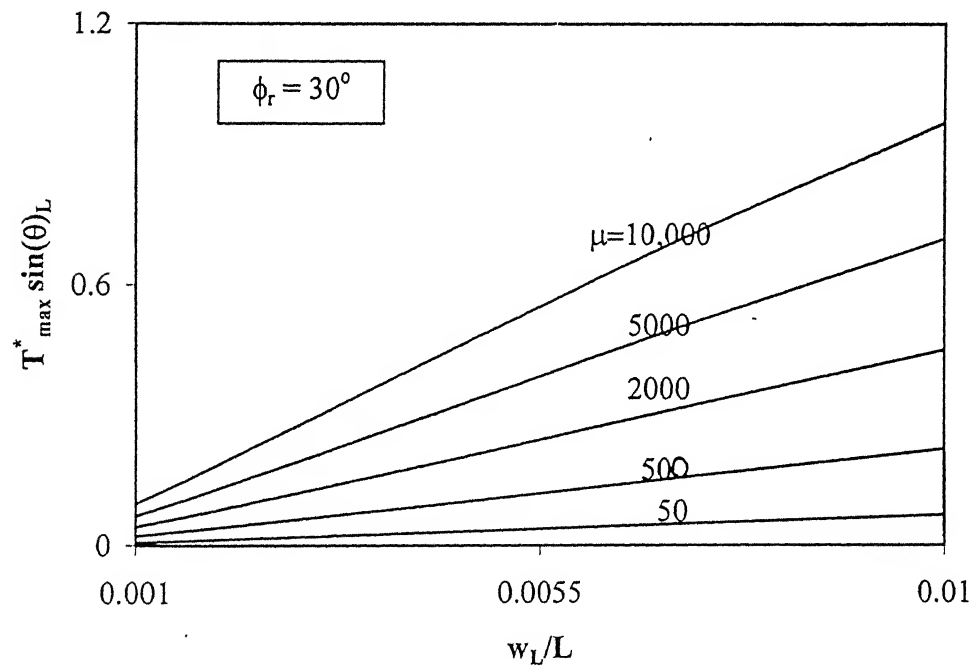


Fig. 3.12 Variation of Normalized Maximum Normal Component of Tension with  $w_L/L$  – Effect of  $\mu$

The variation of normalized horizontal component of tension with free end displacement,  $w_L/L$  for relative stiffness of soil,  $\mu=50, 500, 2000, 5000$  and  $10,000$  is depicted in Fig. 3.13. The horizontal component of tension developed can be interpreted as the axial pullout force the reinforcement can resist. For relatively compressible soils ( $\mu=50$ ), the pullout force equals the maximum axial pullout capacity. The normal stresses developed in the soil for relatively stiff soils at a given free end displacement are high. Thus the shear stresses developed are also high and hence the pullout force that the reinforcement can resist is greater than the axial pullout capacity ( $T_{\max}^* \cos \theta_L > 1.0$ ) for relatively stiff soils ( $\mu \geq 500$ ). The rate of increase of this pullout force increases with free end displacement with increasing stiffness of the soil.

The transverse force,  $P_L^*$ , mobilized for any free end displacement,  $w_L/L$ , at the free end is estimated from Eq. 3.22.  $P_L^*$  increases almost linearly (Fig. 3.14) for  $w_L/L$  in the range 0 to 0.01. Thus,  $P_L^*$  ranges from 0.034 to 0.068 for  $w_L/L$  equal to 0.005 while the values vary from 0.555 to 1.154 at  $w_L/L$  equal to 0.01 for  $\mu$  increasing from 50 to 10,000.

The transverse force,  $P_L^*$ , varies almost linearly with interface friction angle,  $\phi_r$  for different values of  $w_L/L$  and for  $\mu=500$  (Fig. 3.15). The rate of increase of  $P^*$  with  $\phi_r$  increases with free end displacement,  $w_L/L$ . A simple linear relation of the form  $P_L^* = a + b(\phi_r - 20)$  is proposed where  $a$  and  $b$  are constants. The variations of these constants,  $a$  and  $b$  with  $w_L/L$  are presented in Figs. 3.16a and 3.16b. The variation is linear with  $w_L/L$ .

The variation of maximum normalized tension,  $T_{\max}^*$ , developed in the reinforcement (at the end where transverse downward displacement is induced) with the relative stiffness of the soil,  $\mu$ , is presented in Fig. 3.17. For small free end displacements ( $w_L/L=0.001$ ), the reinforcement undergoes is very less. Hence there is no increments in the shear stresses along the reinforcement due to transverse downward displacement are very small. Thus,  $T_{\max}^*$  is independent of  $\mu$  for small  $w_L/L$ . But, for large free end displacements,  $\mu$  has a bearing on the development of  $T_{\max}^*$ . At relatively large free end displacements ( $w_L/L \geq 0.005$ ), the maximum tension developed increases with increase in the relative stiffness of the soil as the normal stresses cause a corresponding increase in the shear stresses.

For a given free end displacement, the transverse displacements become highly localized at the right end (Fig. 3.5) for relatively stiff soils. Hence, the inclination of

reinforcement,  $\theta_L$ , with the horizontal at  $x=L$ , increases with increase in relative stiffness,  $\mu$ . The rate of increase of  $\theta_L$  with  $\mu$  increases with increase in the free end displacement  $w_L/L$ .  $\theta_L$  ranges from  $0.3^\circ$  to  $5^\circ$  for  $w_L/L=0.001$  while the values vary from  $4^\circ$  to  $39^\circ$  for  $w_L/L=0.01$  for  $\mu$  values increasing from 50 to 10,000 (Fig. 3.18).

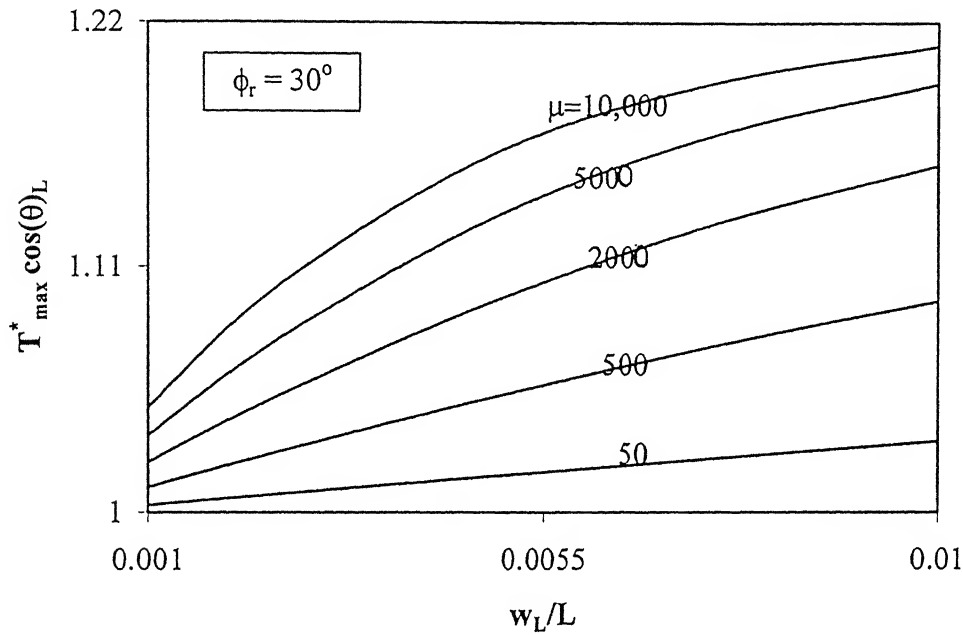


Fig. 3.13 Variation of Normalized Maximum Horizontal Component of Tension with  $w_L/L$  – Effect of  $\mu$

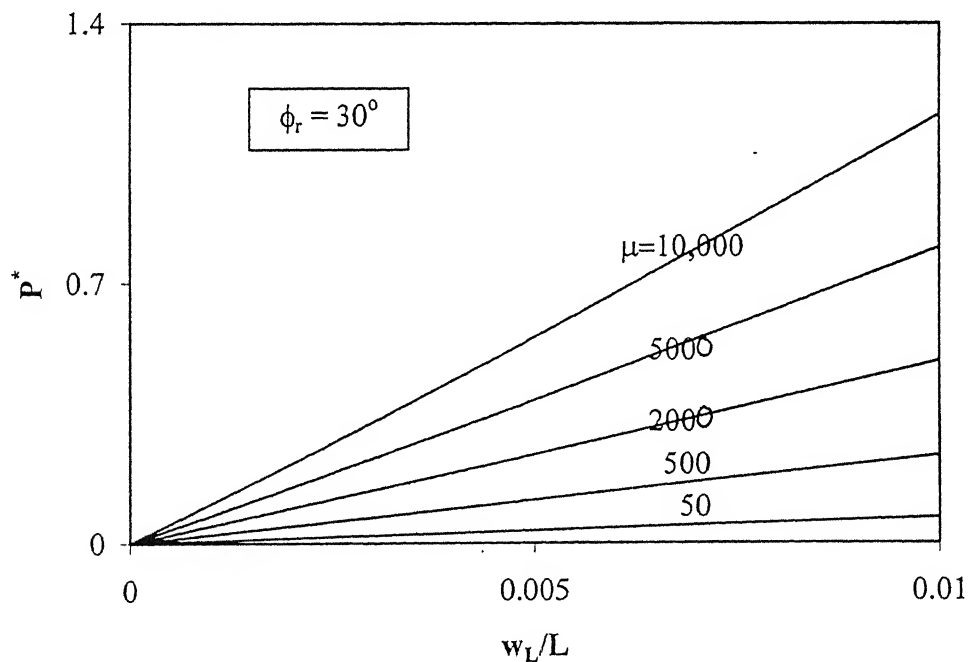


Fig. 3.14 Variation of Normalized transverse Force with  $w_L/L$  - Effect of  $\mu$

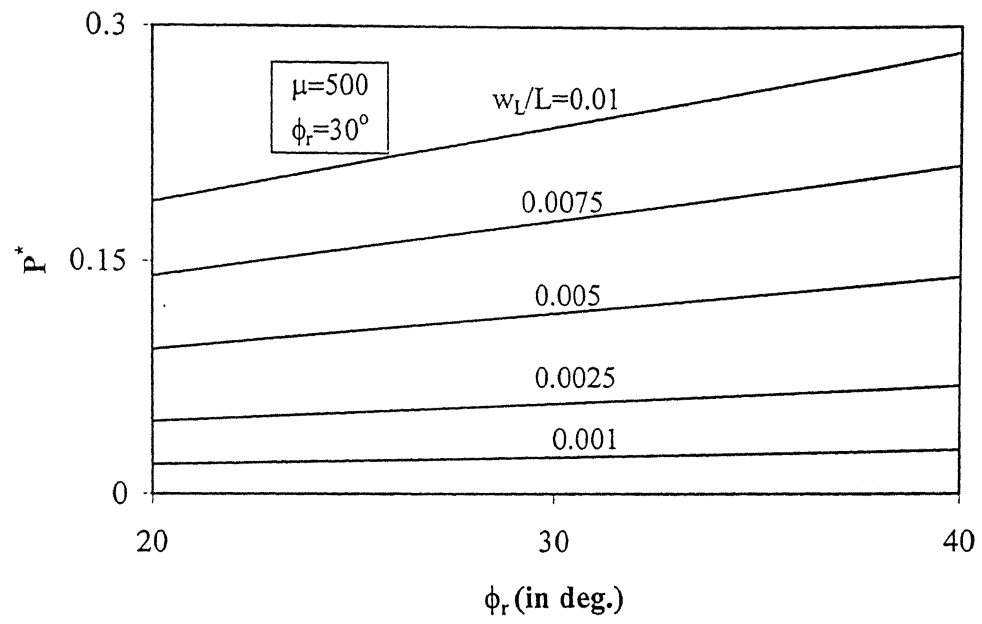


Fig. 3.15. Variation of Normalized transverse Force with Interface Friction angle

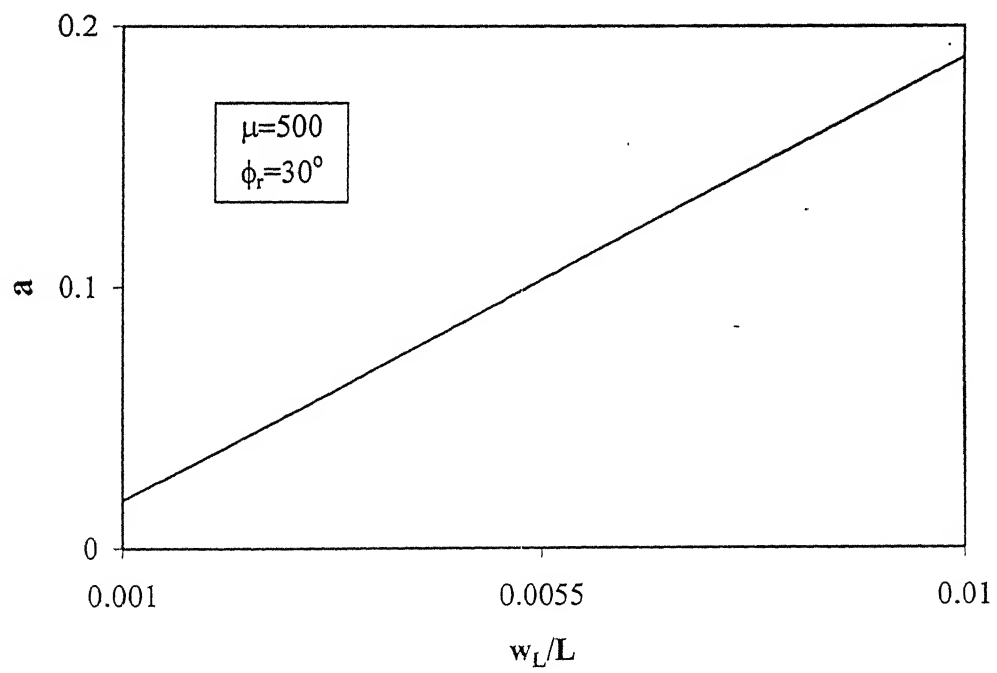


Fig. 3.16a Variation of 'a' with  $w_L/L$

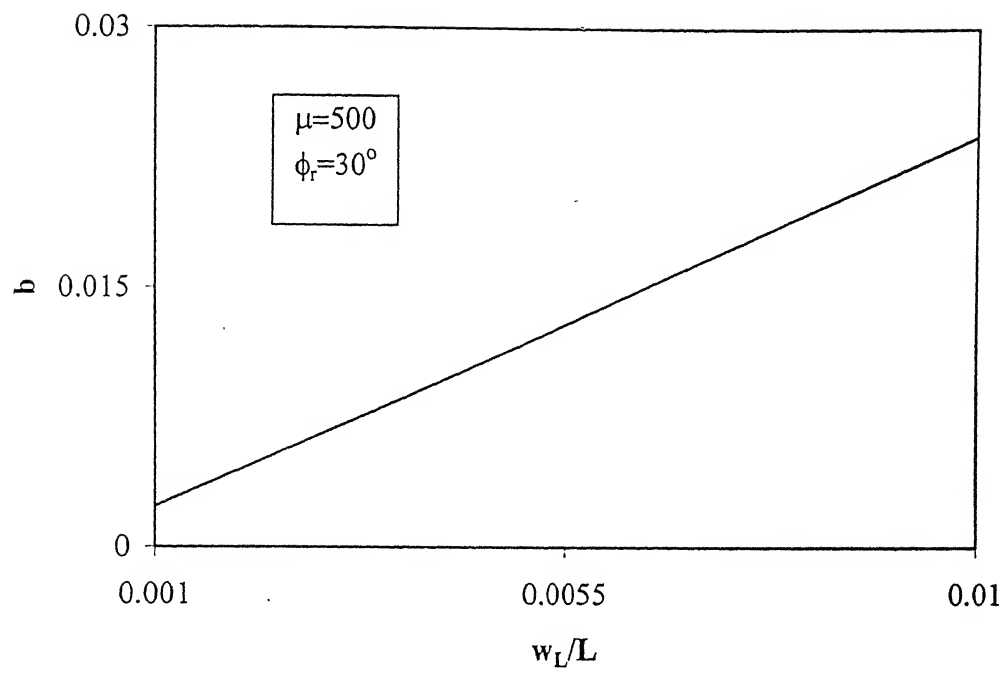


Fig. 3.16b Variation of 'b' with  $w_L/L$

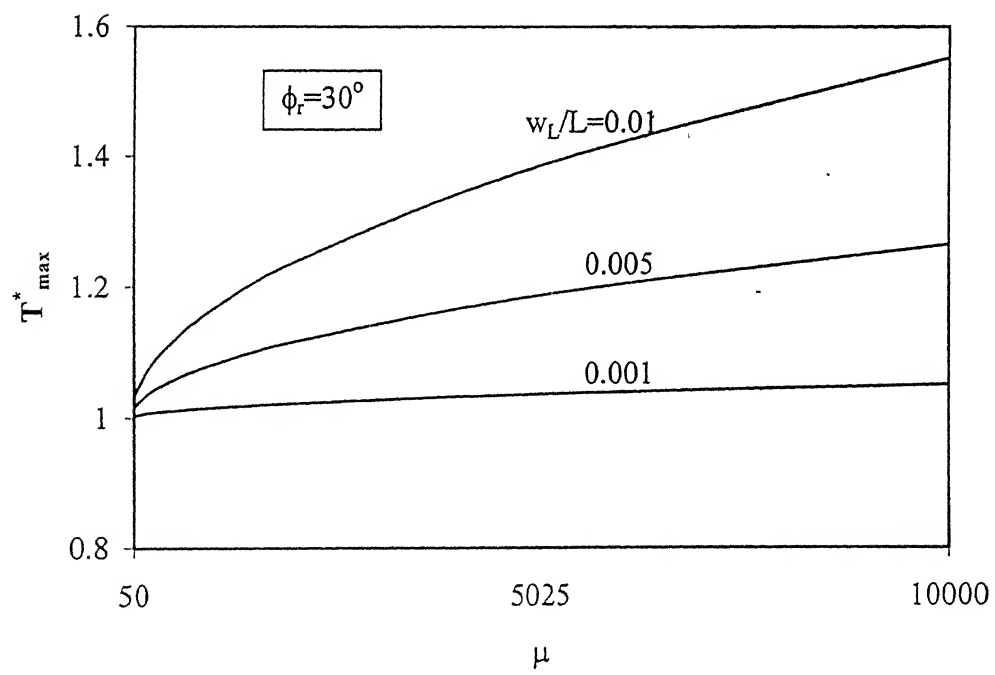


Fig. 3.17 Variation of Normalized Maximum Tension with  $\mu$

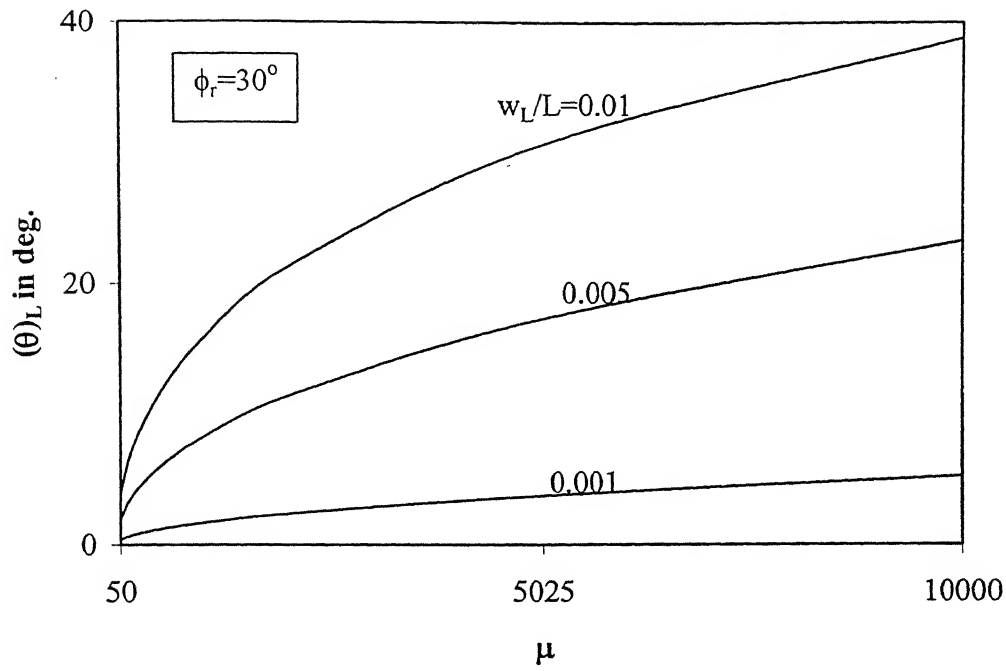


Fig. 3.18 Variation of Maximum Horizontal Inclination with  $\mu$

The variation of maximum normalized normal component of tension,  $T_{\max}^* \sin \theta_L$ , with relative stiffness of soil,  $\mu$ , is presented in Fig. 3.19. As the sheet is almost horizontal for  $w_L/L = 0.001$ ,  $T_{\max}^* \sin \theta_L$  ranges from mostly 0 to 0.1 for  $\mu = 50$  and 10,000 respectively. The rate of increase of  $T_{\max}^* \sin \theta_L$  increases with  $\mu$  and with increase in  $w_L/L$ , as both the inclination of reinforcement with horizontal  $\theta_L$ , and the maximum tension,  $T_{\max}^*$  developed increase.

The maximum normalized horizontal component of tension,  $T_{\max}^* \cos \theta_L$ , is almost independent of  $\mu$  and varies from 1.0 to 1.2 for  $w_L/L$  in the range 0.001 to 0.01 (Fig. 3.20).

The rate of increase of normalized transverse force,  $P^*$ , increases with relative stiffness,  $\mu$ , with increase in normalized free end displacement,  $w_L/L$  (Fig. 3.21).

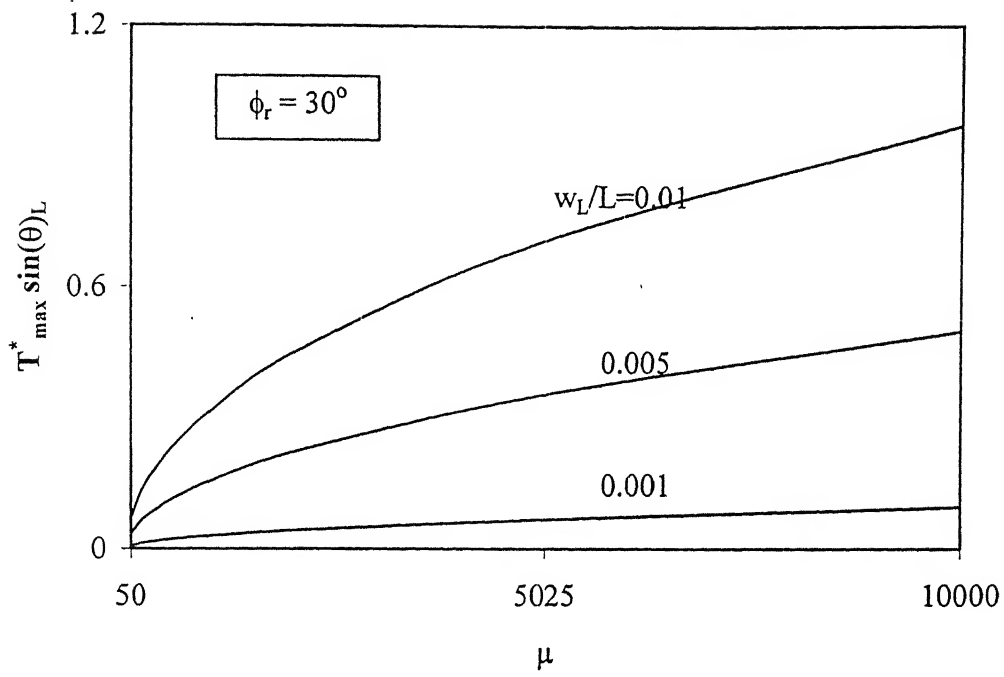


Fig. 3.19 Variation of Normalized Maximum Normal Component of Tension with  $w_L/L$  – Effect of  $\mu$

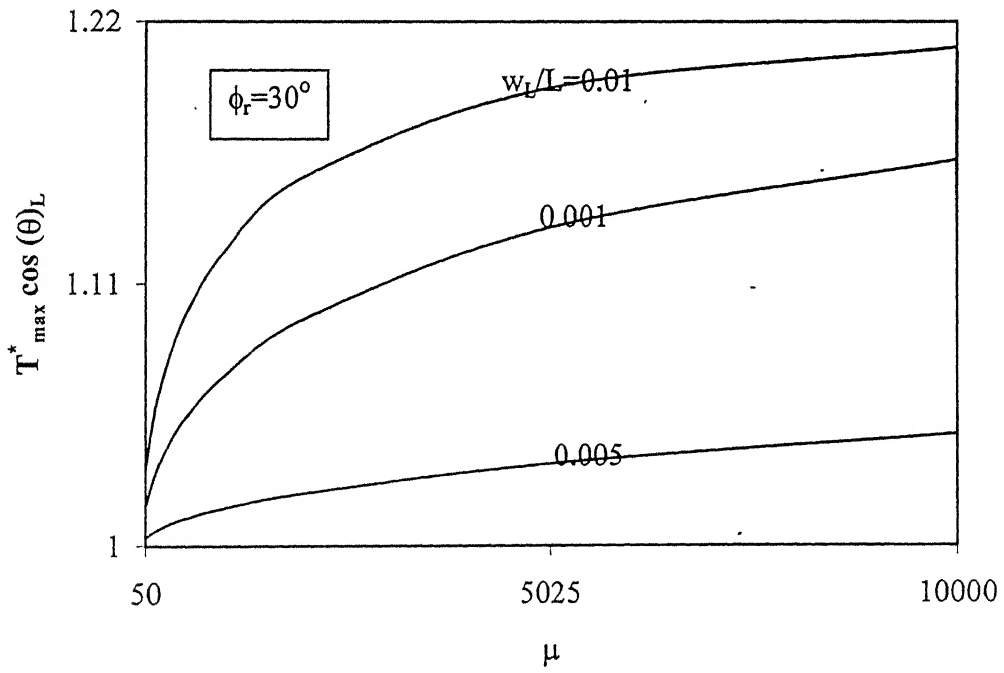


Fig. 3.20 Variation of Normalized Maximum Horizontal Component of Tension with  $w_L/L$  – Effect of  $\mu$

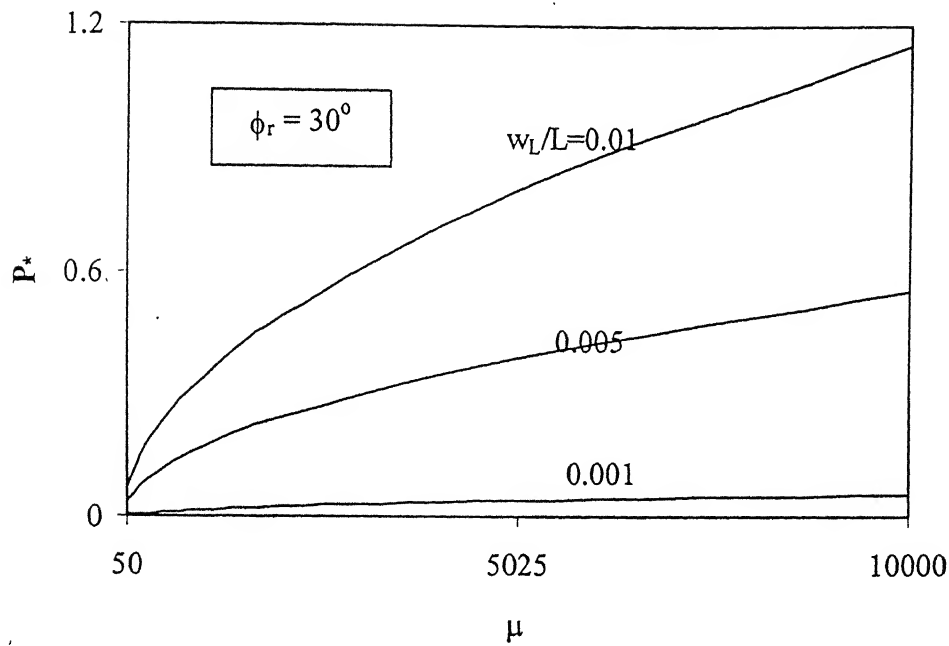


Fig. 3.21 Variation of Normalized Maximum Transverse Force with  $\mu$  – Effect of  $w_L/L$

### 3.3.2 Non-Linear Subgrade –Model II

In section 3.3.1, the stress-displacement response of the soil is beneath the reinforcement assumed to be linear. It is commonly found that the soil behavior over a wide range of stresses is non-linear and inelastic. The deformation of soil mass is controlled by interaction between the individual particles, especially by sliding, rolling and crushing. Since all of these cause non-linear and irreversible deformations, it is expected that the stress-strain relationship for soil will be strongly non-linear. Thus, the stress developed in the soil cannot increase neither linearly nor indefinitely with displacement. It is limited to the ultimate bearing resistance,  $q_{ult}$ , of the soil. Hence to simulate this condition, a hyperbolic stress-displacement response of the soil is assumed.

#### 3.3.2.1 The Model

The model is identical to the one explained in section 3.3.1.1. In this case, the response of the soil from below the reinforcement due to additional stresses, i.e.,  $(q_b - q_t)$  generated due to the application of the transverse force,  $P$ , is given by

$$(q_b - q_t) = \frac{k_s w}{1 + \frac{k_s w}{q_{ult}}} \quad (3.23)$$

where  $k_s$ ,  $q_{ult}$  and  $w$  are the initial modulus of subgrade reaction, the ultimate resistance and normal displacement of the soil respectively (Fig. 3.22).

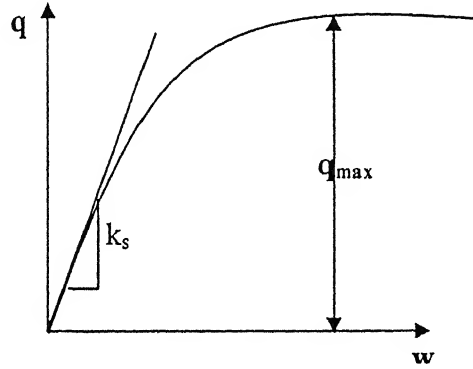


Fig. 3.22 Hyperbolic Response between stress,  $q$  and settlement,  $w$

### 3.3.2.2 Analysis

Considering the equilibrium of forces on an element of infinitesimal length,  $\Delta x$ , and unit width as described in section 3.3.1.2, one can derive

$$\frac{dT}{dx} = (q_t + q_b) \cos \theta \tan \phi_r + (q_b - q_t) \sin \theta \quad (3.24)$$

$$-T \frac{d\theta}{dx} - (q_t + q_b) \tan \phi_r \sin \theta + (q_b - q_t) \cos \theta = 0 \quad (3.25)$$

From Eq. 3.8,

$$\frac{d\theta}{dx} = \cos^2 \theta \frac{d^2 w}{dx^2} \quad (3.26)$$

Combining Eqs. (3.24), (3.25) and (3.26), the following equations are obtained

$$\frac{dT}{dx} = (q_t + q_b) \cos \theta \tan \phi_r + \left( \frac{k_s w}{1 + \frac{k_s w}{q_{ult}}} \right) \sin \theta \quad (3.27)$$

$$-T \cos^2 \theta \frac{d^2 w}{dx^2} + \left( \frac{K_s w}{1 + \frac{k_s w}{q_{ult}}} \right) = (q_z + q_b) \sin \theta \tan \phi_r \quad (3.28)$$

For small  $\theta$ , Eqs. (3.27) and (3.28) reduce to

$$\begin{aligned} \frac{dT}{dx} &= (q_t + q_b) \tan \phi_r \\ &= (q_b - q_t + 2q_t) \tan \phi_r \\ &= \left( \frac{k_s w}{1 + \frac{k_s w}{q_{ult}}} + 2\gamma D_e \right) \tan \phi_r \end{aligned} \quad (3.29)$$

$$-T \frac{d^2 w}{dx^2} + \frac{k_s w}{1 + \frac{k_s w}{q_{ult}}} = 0 \quad (3.30)$$

Eqs. (3.29) and (3.30) are the governing equations for the model that incorporates the non-linear response of the soil. Eqs. (3.29) and (3.30) are non-dimensionalised with  $X=x/L$ ,  $W=w/w_L$  and  $T^*=T/T_{\max p}$  where  $T_{\max p} = 2 \gamma D_e L \tan \phi_r$ , the maximum axial pullout force. Eqs. (3.29) and (3.30) in normalized form are

$$\frac{dT^*}{dX} = \frac{1}{2} \left( \frac{\mu \frac{w_L}{L} W}{1 + \beta W \frac{w_L}{L}} + 2 \right) \quad (3.31)$$

$$-T^* \frac{d^2 W}{dX^2} + \frac{\mu W}{2 \tan \phi_r \left( 1 + \beta W \frac{w_L}{L} \right)} = 0 \quad (3.32)$$

where  $\beta = \frac{k_s L}{q_{ult}}$  --- a parameter that quantifies the relative initial subgrade modulus with the ultimate resistance of the ground.

The boundary conditions for the present case are the same as explained in section 3.2.1.3 for the present case. The transverse force required to cause the displacement,  $w_L$ , is obtained by integrating the soil reaction mobilized as

$$P = \int_0^L \frac{k_s w}{1 + \frac{k_s w}{q_{ult}}} dx \quad (3.33)$$

### 3.3.2.3 Numerical Solution

The discretisation of reinforcement length into elements is as explained in section 3.2.1.4. Eqs. (3.31) and (3.32) in finite difference form become

$$\frac{T_{i+1}^* - T_i^*}{\Delta X} = \frac{1}{2} \left( \frac{\mu W_i \frac{w_L}{L}}{1 + \beta W_i \frac{w_L}{L}} + 2 \right) \quad (3.34)$$

$$-T_i^* \left( \frac{W_{i-1} - 2W_i + W_{i+1}}{\Delta X^2} \right) + \frac{\mu W_i}{2 \tan \phi_r \left( 1 + \beta W_i \frac{w_L}{L} \right)} = 0 \quad (3.35)$$

Solving for normalized displacement and normalized tension, one gets

$$W_i = \frac{T_i^* n^2 (W_{i-1} + W_{i+1})}{\left( 2n^2 T_i^* + \frac{\mu}{2 \tan \phi_r \left( 1 + \beta W_i \frac{w_L}{L} \right)} \right)} \quad (3.36)$$

$$T_{i+1}^* = \frac{1}{2n} \left( \frac{\mu W_i \frac{w_o}{L}}{1 + \beta W_i \frac{w_L}{L}} + 2 \right) + T_i^* \quad (3.37)$$

To obtain the displacement at node 1, the boundary condition  $dW/dx=0$  at  $X=0$  leads to the condition,  $W_o=W_2$  and Eq. (3.36) for node 1 becomes

$$W_1 = \frac{2n^2 T_1^* W_2}{\left( 2n^2 T_1^* + \frac{\mu}{2 \tan \phi_r \left( 1 + \beta W_i \frac{w_L}{L} \right)} \right)} \quad (3.38)$$

At  $x=L$  or  $X=1.0$ ,  $i = n+1$  and  $W_{n+1}=1.0$  and at  $X=0$  or  $i=1$ ,  $T = T^* = 0.0$  (no tension).

As the reinforcement sheet is discretized into 'n' elements and the transverse force,  $P$ , is obtained by numerical integration as

$$P = \sum_{i=1}^n \left( \frac{k_s w}{1 + \frac{k_s w}{q_{ult}}} \right) dx \quad (3.39)$$

The transverse force in normalized form is

$$P^* = \frac{P}{\gamma D_e L} = \frac{1}{n} \frac{w_L}{L} \sum_{i=1}^n \frac{\mu W_i}{1 + \beta W_i \frac{w_L}{L}} \quad (3.40)$$

A given free end displacement at the right end of the reinforcement, the response of the soil reinforcement is obtained by solving Eqs. (3.37) and (3.38) for the given boundary conditions. The corresponding normalized transverse force to enforce a given free end displacement is obtained by Eq. (3.40). The displacement, tension profiles and other variations along the length of reinforcement are presented in the following section.

#### 3.3.2.4 Characteristics of the Model

A simple mathematical model has been developed to study the behavior of reinforcement sheet subjected to transverse force for a non-linear subgrade and full shear resistance mobilized along the reinforcement-soil interface. The reinforcement is characterized by the interface friction angle ( $\phi_r$ ) only. Unlike the previous model, the stresses generated due to the application of a transverse force are limited to the ultimate resistance of the soil. A limitation of the model is that under large displacement or applied transverse load, the assumption of small angles is not appropriate.

### 3.3.2.5 Results and Discussions

Based on the formulation presented in the preceding sections, the analysis of reinforcement subjected to transverse force is carried out for a wide range of parameters,  $\mu$ ,  $\beta$ ,  $w_L/L$  and  $\phi_r$ . Considering the ultimate resistance,  $q_{ult}$ , to lie in the range, 300 to 1000 kN/m<sup>2</sup>, the value of  $\beta(=k_s L/q_{ult})$  works out to be in the range 50 and 3000.

Fig. 3.23 shows the normalized displacement profile,  $w/L$ , with normalized distance along the reinforcement,  $X$ , for a free end displacement of  $w_L/L=0.1$ , [ $\beta(=k_s L/q_{ult})$ ]=1000 and  $\phi_r=30^\circ$  for relative stiffness,  $\mu$ , of 50, 250, 500, 1000, 2000, 5000 and 100,000. For relatively compressible subgrades ( $\mu=50$ ), the transverse displacements are mobilized over the entire length of reinforcement. The points of mobilization of transverse displacement move to the right with increasing relative stiffness of the soil. The displacements become highly localized near the right end for very stiff subgrades ( $\mu=100,000$ ).

The normalized displacement profiles,  $w/L$  vs  $X$  for  $\beta=100, 500, 1000, 2000$  and 3000 for typical values of  $\mu=1000$ ,  $\phi_r=30^\circ$  and  $w_L/L=0.1$  are presented in Fig 3.24. With decreasing  $\beta(=k_s L/q_{ult})$ , the points of mobilization of transverse displacements move to the right end. Thus as the ultimate resistance of the soil increases, the displacements become localized at the right end. For  $\beta=3000$  and 500, the displacements are mobilized from about 0.35L and 0.78L respectively from the left end.

Fig. 3.25 presents the variation of normalized tension,  $T^*$ , with normalized distance,  $X$ . For very soft to very stiff soils,  $T^*$  increases linearly with  $X$  for nearly 0.4L from left end. The distance from the left end where the non-linearity between  $T^*$  vs  $X$  starts increases with increasing  $\mu$  values. The rate of increase of  $T^*$  with  $X$  also increases with  $\mu$ . The maximum tension values increase from about 1.0 for  $\mu=50$  to about 1.8 for  $\mu=10,000$ . The highly localized displacement behavior for very stiff soils is the reason for sharp increase in  $T^*$  values.

The mobilized friction at the interface between the reinforcement and the soil and hence the tension developed in the reinforcement increase with the ultimate resistance of the soil and hence larger  $T^*$  values for smaller  $\beta(=k_s L/q_{ult})$  values (Fig. 3.25). The pattern of curves shown in Fig. 3.27 is similar to those in Fig. 3.24. Since for  $\beta=100$ , the normalized displacement,  $W$ , increases from a point about 0.25L from the

(free) end, the normal stresses, the shear stresses and the tension mobilized increase rapidly from that point onwards.

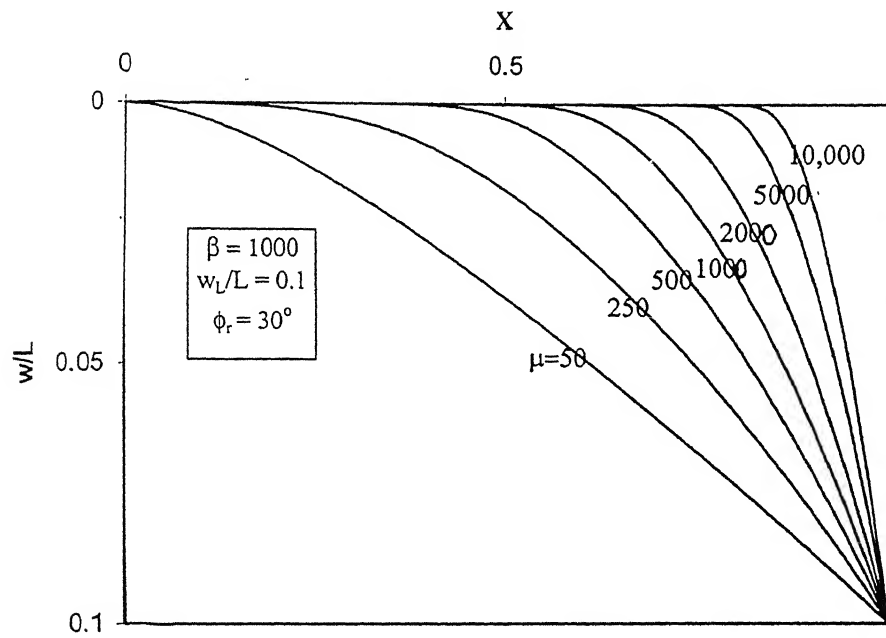


Fig. 3.23 Variation of Normalised Displacement with Normalized Distance –Effect of  $\mu$

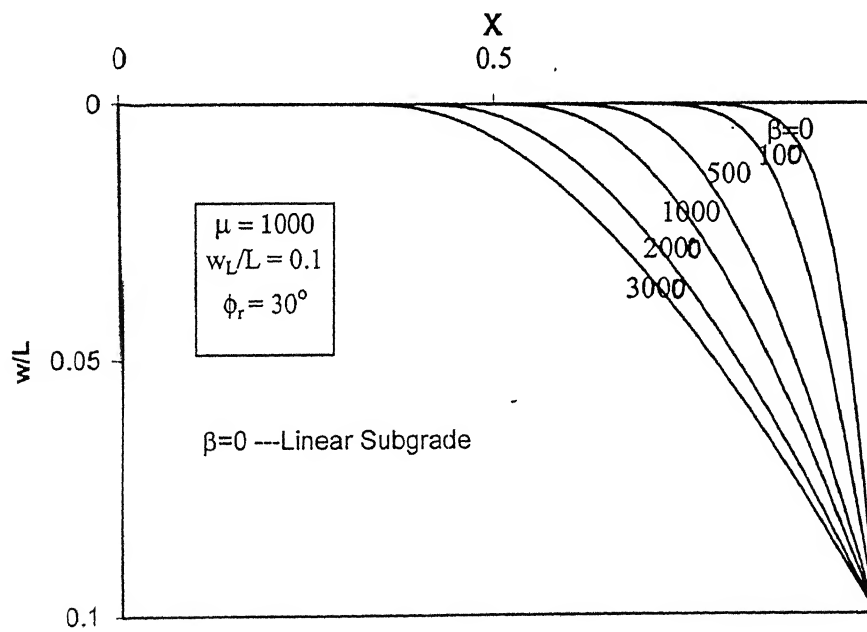


Fig. 3.24 Variation of Normalised Displacement with Normalised Distance- Effect of  $\beta$

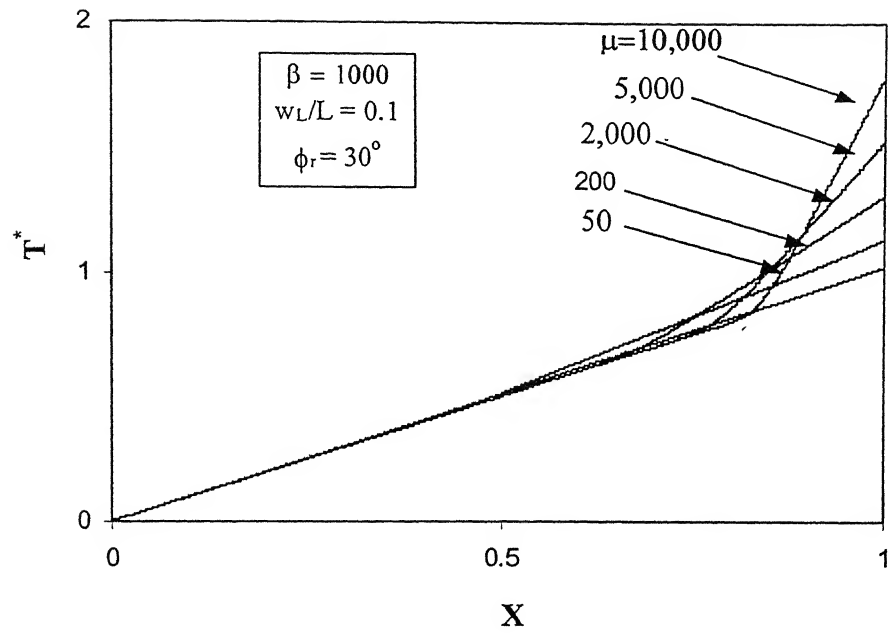


Fig. 3.25 Variation of Normalized Tension with Normalized Distance – Effect of  $\mu$

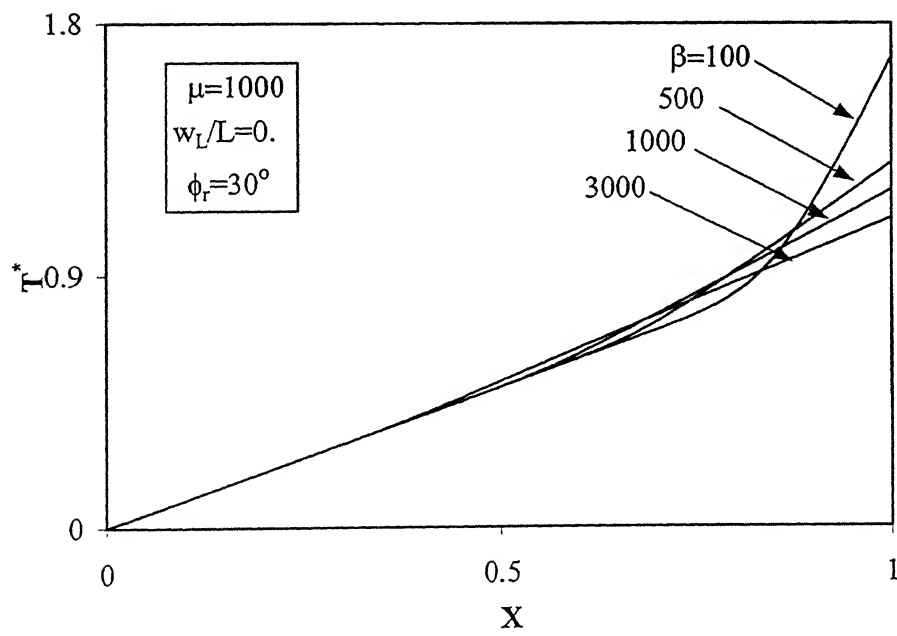


Fig. 3.26 Variation of Normalized Tension with Normalized Distance – Effect of  $\beta$

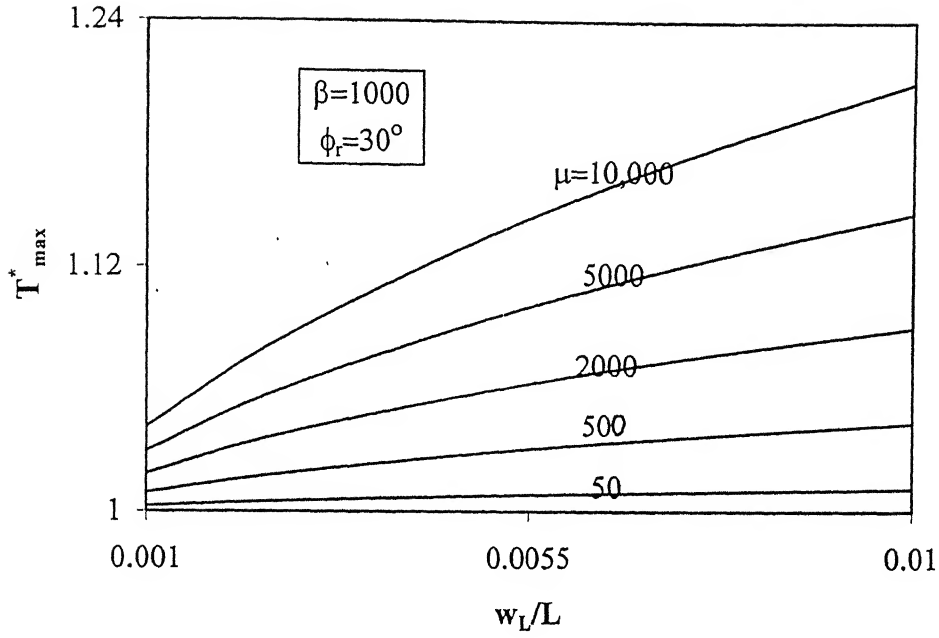


Fig. 3.27 Variation of Maximum Normalized Tension with Normalized Free End Displacement – Effect of  $\mu$

Fig. 3.28 depicts the variation of maximum normalized tension,  $T_{max}^*$  developed at the right end with  $w_L/L$  for  $\mu=50, 500, 1000, 5000$  and  $10000$ . For very soft soils ( $\mu=50$ ), the increase in normal stresses generated due to the application of transverse displacement/ force/ is negligible and hence the maximum tension developed is equal to the axial pullout capacity of reinforcement ( $T_{max}^* = 1.0$ ). As the stiffness of the soil increases ( $\mu \geq 500$ ), normal stresses on the reinforcement due to transverse displacement/force increase. As a result, larger shear stresses are mobilized and the maximum tension mobilized become greater than the axial pullout capacity,  $T_{max}^* \geq 1.0$ . The initial rate of increase of maximum tension with  $w_L/L$  increases with  $\mu$ . At larger enforced displacements, the rate of increase of  $T_{max}^*$  with  $w_L/L$  decreases.

The variation of inclination of reinforcement,  $\theta_L$ , at right end ( $x=L$ ) with normalized free end displacement,  $w_L/L$ , is presented in Fig. 3.29. The rate of increase of inclination,  $\theta_L$ , with  $w_L/L$  increases with increase in the relative stiffness,  $\mu$ . For relatively compressible soils ( $\mu=50$ ),  $\theta_L$  is equal to  $2^\circ$  whereas the inclination is as high as  $19^\circ$  for relatively stiff soils ( $\mu=10,000$ ) for  $w_L/L=0.01$ ,  $\beta=1000$  and  $\phi_r=30^\circ$ .

The same trend as observed for the variation of normalized maximum tension,  $T_{max}^*$ , with free end displacement,  $w_L/L$ , is followed for the variation of normal

component of the maximum tension,  $T^*_{\max} \sin \theta_L$ , developed at the right end (Figs. 3.29 and 3.27).

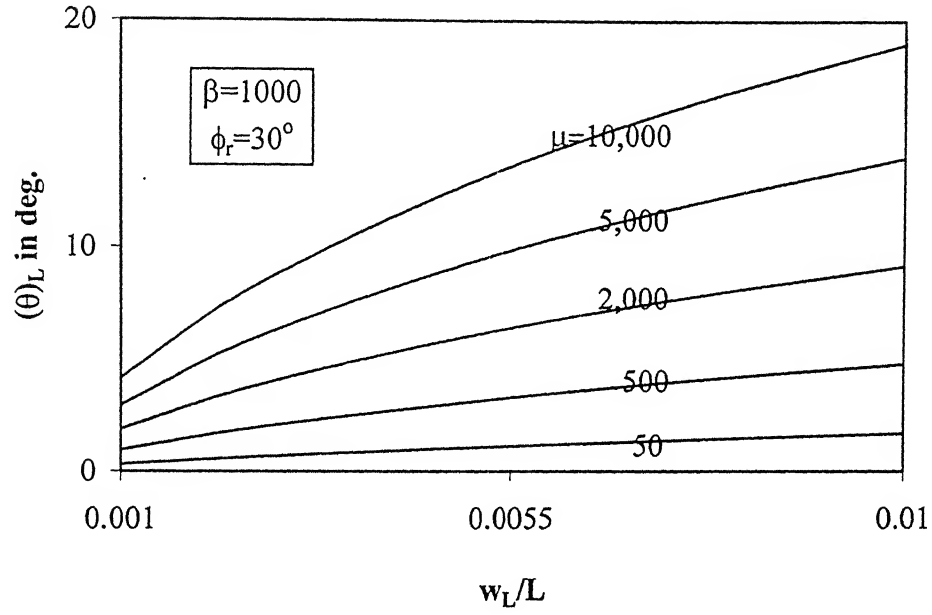


Fig. 3.28 Variation of Maximum Inclination of Reinforcement with Horizontal with  $w_L/L$  -Effect of  $\mu$

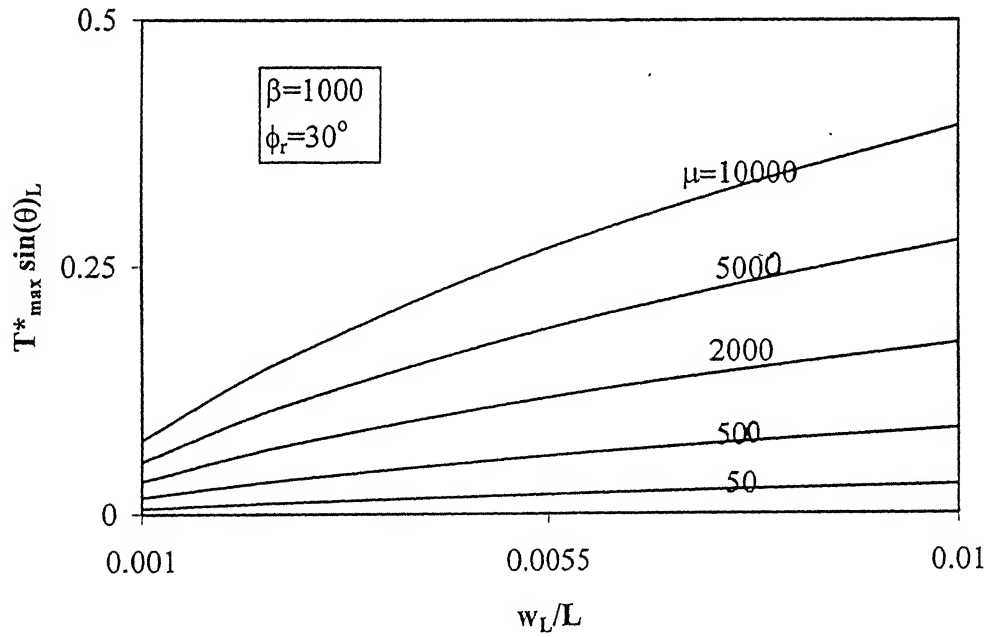


Fig. 3.29 Variation of Maximum Normalized Normal Tension with Normalized Free End Displacement for Different  $\mu$

The variation of horizontal component of maximum tension,  $T_{\max}^* \cos \theta_L$ , with normalized free end displacement,  $w_L/L$ , is shown in Fig.3.30. The trend is similar to that of the variation of normalized maximum tension with  $w_L/L$ . The normal stresses developed in relatively compressible soils ( $\mu=50$ ) are less and hence the shear resistance developed along the reinforcement-soil interface is also less. Thus, for relatively compressible soils ( $\mu=50$ ), the pullout capacity due to transverse displacement/force almost equals the axial pullout capacity. For  $\mu=50$ , the pullout force due to transverse force is just 1% more than the axial pullout for a free end displacement,  $w_L$ , equal to  $0.01L$  and for  $\beta=1000$  and  $\phi_r=30^\circ$  whereas the pullout force is 14% more than the axial pullout capacity for the same free end displacement and parameters but for  $\mu=10,000$ .

The variation of normalized transverse force,  $P^*$ , calculated from Eq. (3.40) with  $w_L/L$  for different  $\mu$  values of 50, 250, 1000, 2000, 5000 and 10000 is shown in Fig. 3.31. For very soft soils ( $\mu = 50$ ), very small magnitude of normalized transverse force of 0.02 is sufficient to lead to a free end displacement of  $w_L/L=0.01$ , with  $\beta=1000$  and  $\phi_r=30^\circ$ , whereas, normalized transverse force of 0.42 is required to cause the same free end displacement for  $\mu=10,000$  and with same set of parameters. The rate of increase of  $P^*$  with  $w_L/L$  increases with increase in relative stiffness of soil,  $\mu$ . For a given soil, the rate of increase of  $P^*$  with  $w_L/L$  is more at small free end displacements,  $w_L$ .

The variation of maximum tension,  $T_{\max}^*$ , with normalized free end displacement,  $w_L/L$ , is presented in Fig. 3.32. The rate of increase of  $T_{\max}^*$  with  $w_L/L$  increases with decrease in  $\beta$  ( $=k_s L/q_{ult}$ ).

The transverse displacements are highly localized for soils that have high ultimate resistance (i.e. low  $\beta$  magnitude) whereas the transverse displacements are mobilized over larger lengths of reinforcement for soils with low ultimate resistance (i.e. large  $\beta$  value). Hence, the inclination of reinforcement,  $\theta_L$ , at the right end (i.e at  $x=L$ ) for soils with  $\beta=3000$  is as low as  $4^\circ$  compared to soils with  $\beta=100$  for  $w_L/L$  equal to 0.01,  $\mu=1000$  and  $\phi_r=30^\circ$ . The rate of increase of inclination with  $w_L/L$  increases with decrease in  $\beta$  (Fig. 3.33).

The trend of variation of normal component of maximum tension,  $T_{\max}^* \sin \theta_L$ , is similar to that of maximum normalized tension,  $T_{\max}^*$ , with normalized free end displacement,  $w_L/L$  (Fig. 3.34).  $T_{\max}^* \sin \theta_L$  increases linearly with  $w_L/L$  and the rate of increase increases with decrease in  $\beta$ .

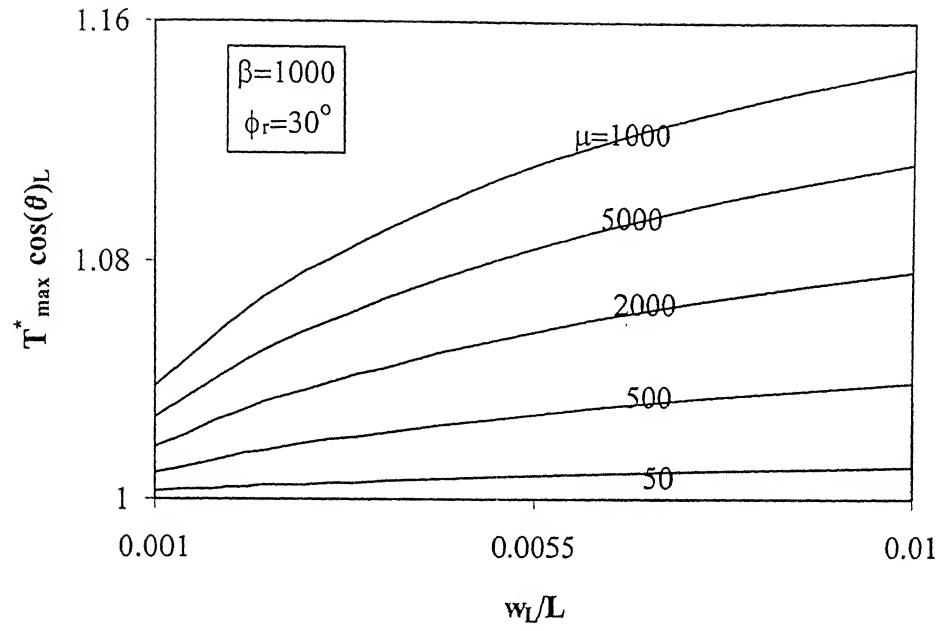


Fig. 3.30 Variation of Maximum Normalized Horizontal Component of Tension with Normalized Free End Displacement - Effect of  $\mu$

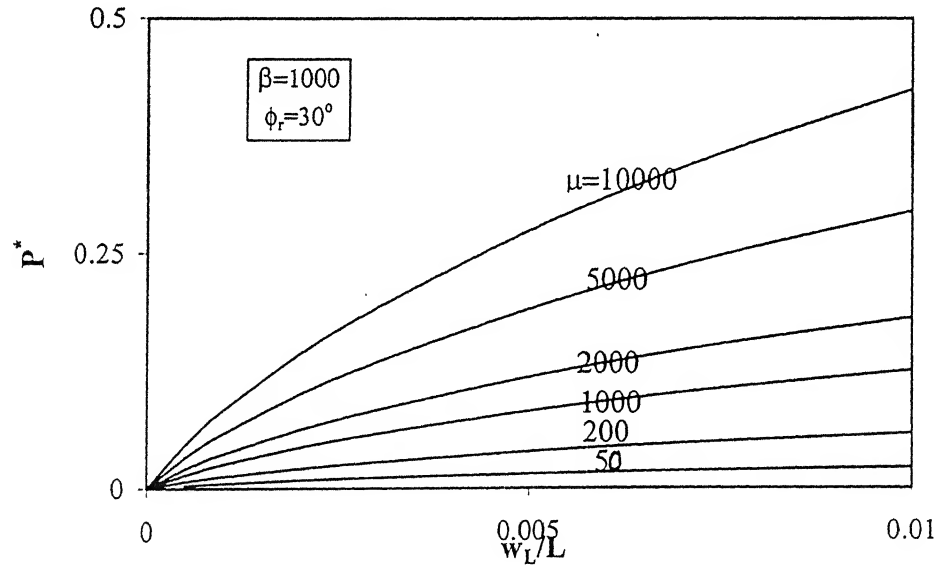


Fig. 3.31 Variation of Normalized Transverse Force with Normalized Free End Displacement - Effect of  $\mu$

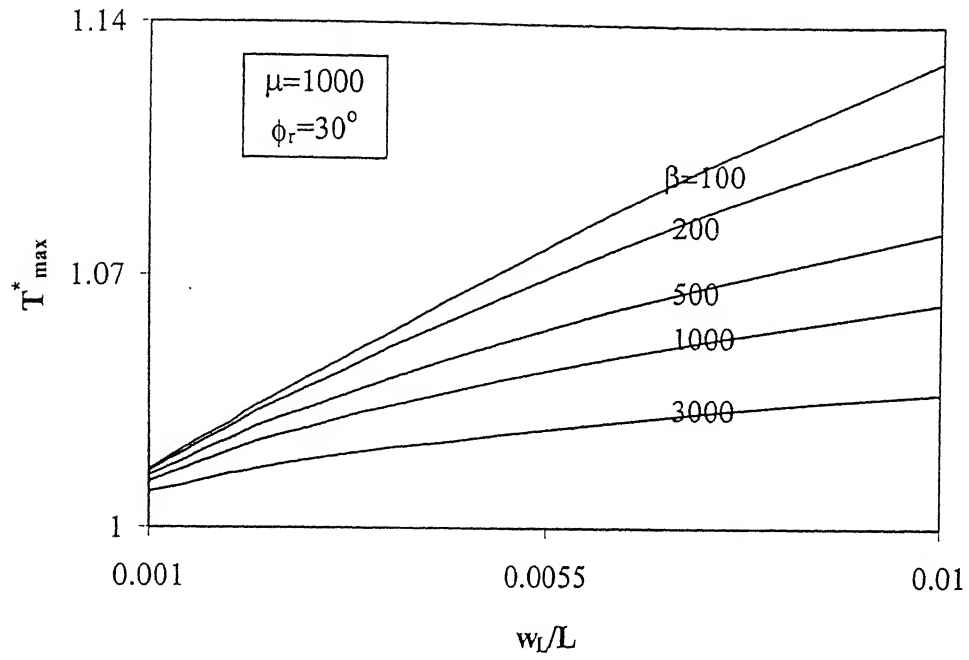


Fig. 3.32 Variation of Maximum Normalized Tension with Normalized Free End Displacement – Effect of  $\beta$

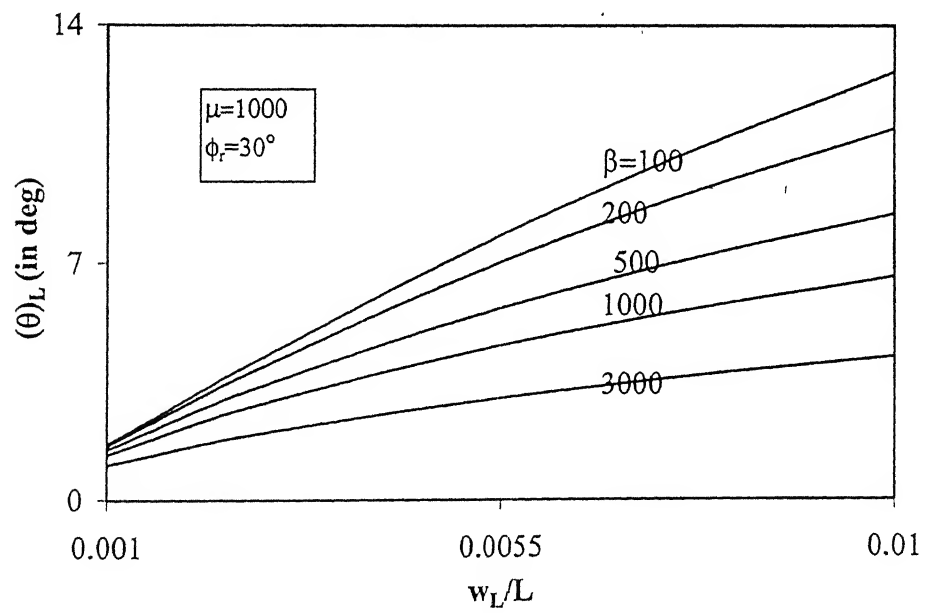


Fig. 3.33 Variation of Maximum Inclination of Reinforcement with Horizontal with  $w_L/L$  – Effect of  $\beta$

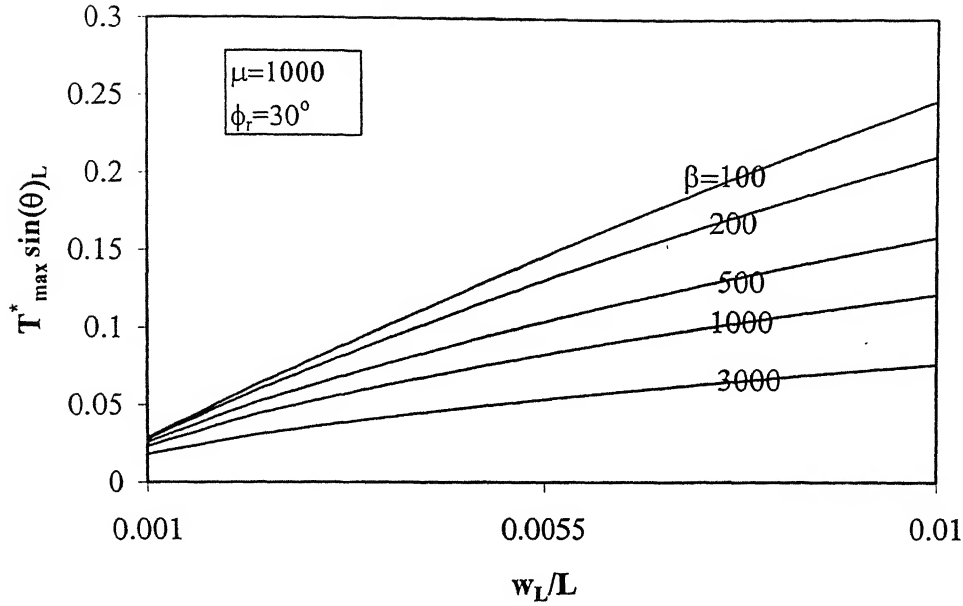


Fig. 3.34 Variation of Maximum Normalized Normal Tension with Normalized Free End Displacement for Different  $\beta$

The normal stresses developed in relatively weak soils (i.e large  $\beta$ ) are less and so is the shear resistance developed along the reinforcement-soil interface due to which the pullout force for soils with  $\beta=3000$  is just 3% more than the axial pullout capacity when compared to an increase of 10% for  $\beta=100$  for  $w_L/L=0.01$ ,  $\mu=1000$  and  $\phi_r=30^\circ$  (Fig. 3.35).

The variation of normalized transverse force,  $P^*$ , with normalized free end displacement,  $w_L/L$ , for  $\beta(=k_s L/\gamma D_e)$  values of 100, 200, 500, 1000, 2000 and 3000 is presented in Fig. 3.36 for relative stiffness,  $\mu=100$  and  $\phi_r=30^\circ$ . The rate of increase of  $P^*$  with  $w_L/L$  increases with increase in  $\beta$  value. Larger normal stresses are mobilized over greater lengths (Fig.3.24) for increasing  $\beta$  values and hence  $P^*$  increases with increase in  $w_L/L$ .

The variation of normalized maximum tension,  $T_{max}^*$ , developed at the right end (at  $x=L$ ), with relative stiffness of the soil,  $\mu$ , is presented in Fig. 3.37 for normalized free end displacements,  $w_L/L$ , equal to 0.001, 0.005 and 0.01 for  $\beta=1000$  and  $\phi_r=30^\circ$ . The rate of increase of  $T_{max}^*$  with  $\mu$  increases with increase in free end displacement,  $w_L/L$ . The normal stresses developed in the relatively compressible soils are less compared to those for stiff soils. Hence, the maximum tension developed is lower for

relatively compressible soils and higher for relatively stiff soils at a given free end displacement.  $T_{\max}^*$  for stiff soils ( $\mu=10,000$ ) is 20% more than that for relatively compressible soils ( $\mu=50$ ).

The variation of inclination,  $\theta_L$ , of reinforcement at  $x=L$  with relative stiffness,  $\mu$ , is presented in Fig. 3.38. The phenomena of localization of transverse displacement increases with increase in stiffness of soil and hence an increase in inclination with increase in stiffness is observed. The effect of this localization is higher at higher free end displacements and leads to an increase in the rate of increase of  $\theta_L$  with  $\mu$  with increase in  $w_L/L$ .

The trend of variation of normalized normal component of maximum tension,  $T_{\max}^* \sin \theta_L$ , with relative stiffness,  $\mu$ , (Fig. 3.39) is similar to that of the variation of  $T_{\max}^*$  with  $w_L/L$  (Fig. 3.37).

The rate of increase of normalized horizontal component of tension,  $T_{\max}^* \cos \theta_L$ , with relative stiffness,  $\mu$ , increases with increase in normalized free end displacement,  $w_L/L$ .  $T_{\max}^* \cos \theta_L$  increases from 1.00 to 1.03 for  $w_L/L=0.001$  for  $\mu$  increasing from  $\mu=50$  to 10,000 for  $\beta=1000$  and  $\phi_r=30^\circ$  compared to an increase from 1.01 to 1.14 for the same increase in  $\mu$  values and same set of parameters (Fig. 3.40). Thus the effect of  $\mu$  in increasing the resistance to pullout force is negligible.

The rate of increase of normalized transverse force,  $P^*$ , with relative stiffness of the soil,  $\mu$ , increases with increase in normalized free end displacement,  $w_L/L$  (Fig. 3.41).

The normal stresses developed in the soil decrease with decrease in ultimate resistance of the soil [i.e, with increasing  $\beta(=k_s L/q_{ult})$ ] and hence the maximum tension,  $T_{\max}^*$ , mobilized in the reinforcement decreases with increasing  $\beta$  values. The rate of decrease in  $T_{\max}^*$  with  $\beta$  is high for  $\beta$  in the range 0 to 1500 (Fig. 3.42). The effect of  $\beta$  on the mobilization of maximum tension is insignificant for small free end displacements ( $w_L/L=0.001$ ).

The phenomenon of localization of transverse displacements becomes predominant with increase in ultimate resistance of the soil (i.e with decrease in  $\beta$  values). Hence, the inclination of reinforcement at  $x=L$  is larger at low values of  $\beta$  and the inclination decreases with increase in  $\beta$  value (Fig. 3.43). The effect of  $\beta$  on

inclination of reinforcement at  $x=L$  is negligible at small free end displacements ( $w_L/L=0.001$ ).

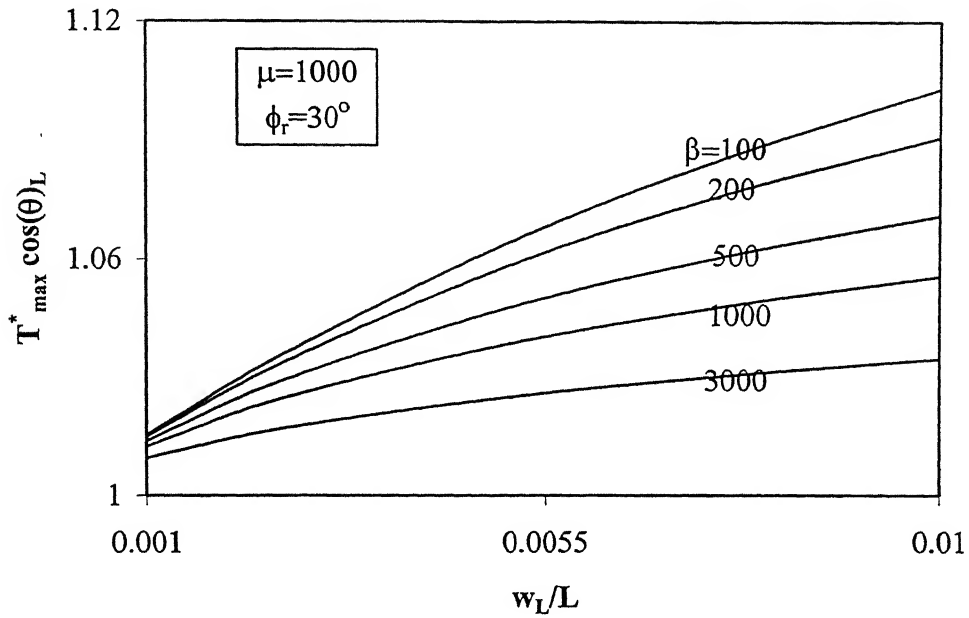


Fig. 3.35 Variation of Maximum Normalized Normal Tension with Normalized Free End Displacement for Different  $\beta$

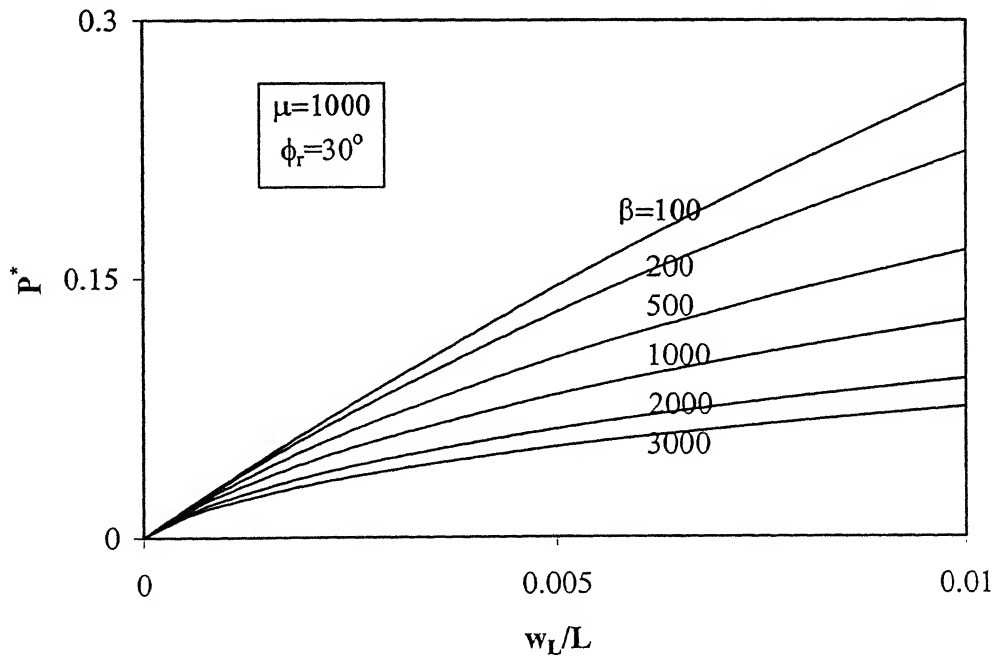


Fig. 3.36 Variation of Normalized Transverse Force with Normalized Free End Displacement - Effect of  $\beta$

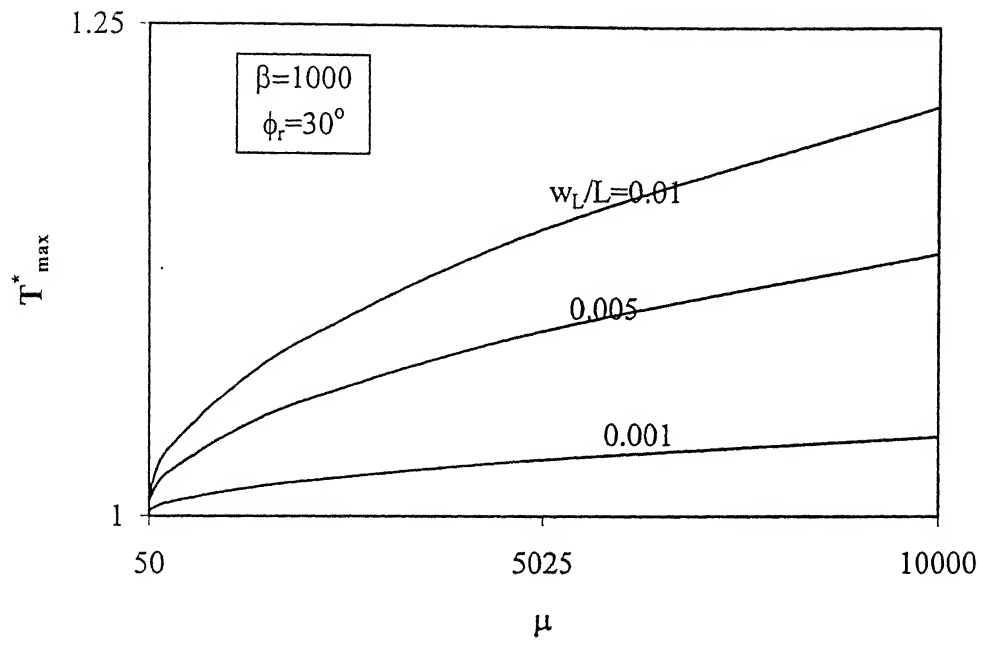


Fig. 3.37 Variation of Normalized Tension with  $\mu$ .

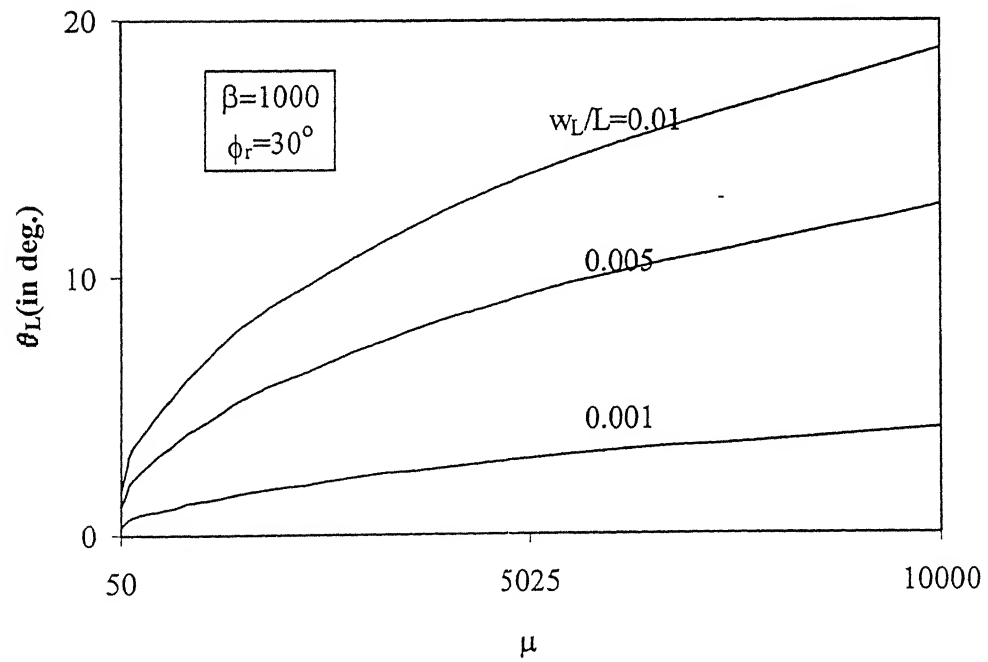


Fig. 3.38 Variation of Inclination of Reinforcement with  $\mu$ .

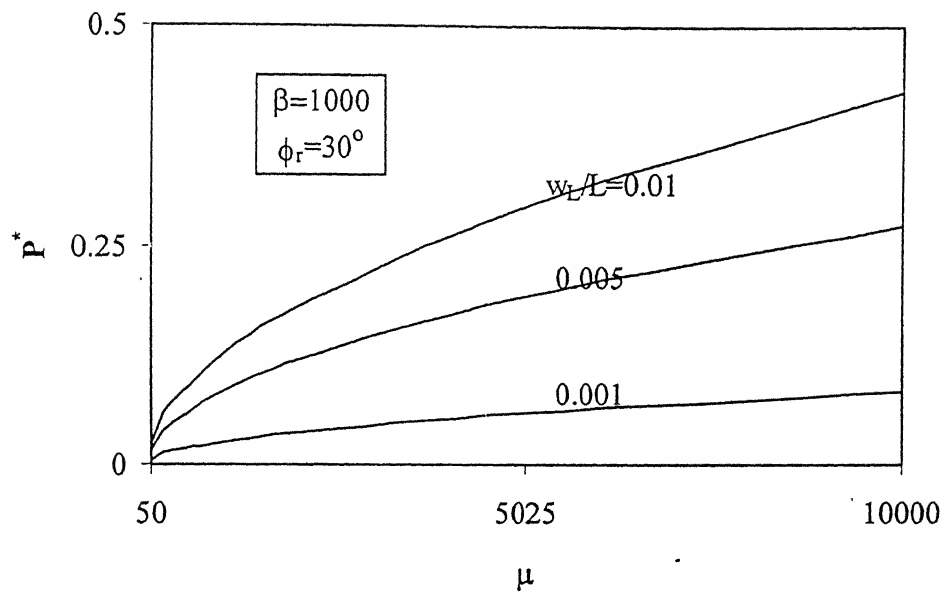


Fig. 3.41 Variation of Normalized Transverse Force with  $\mu$

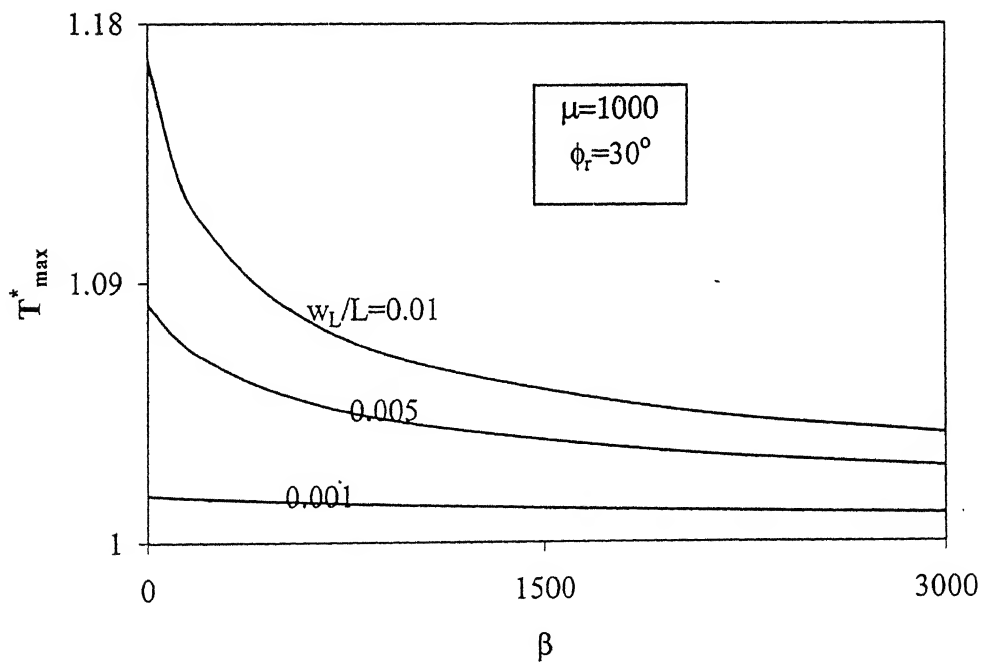


Fig. 3.42 Variation of Normalized Maximum Tension with  $\beta$

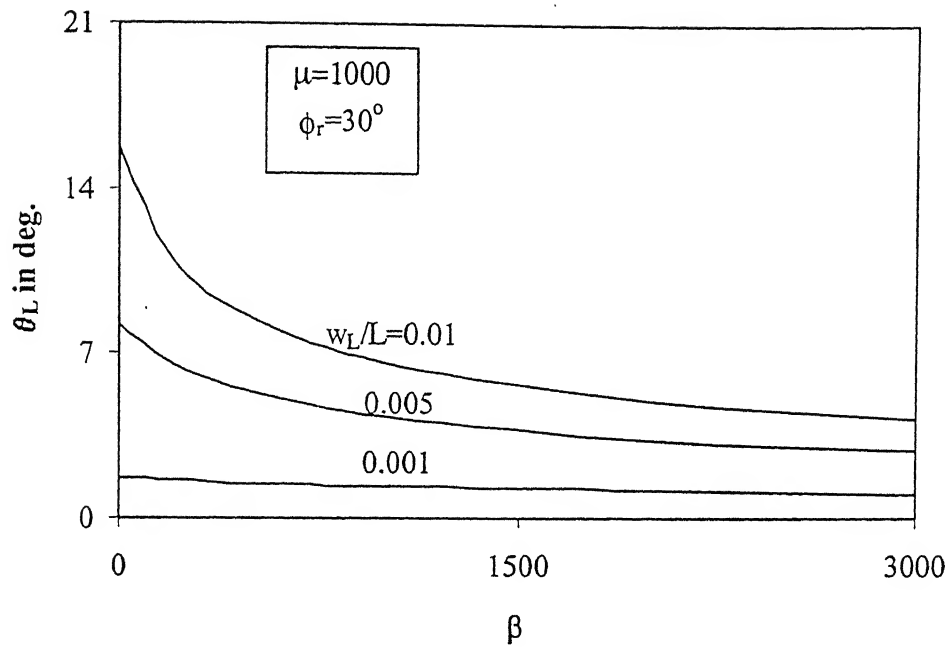


Fig. 3.43 Variation of Inclination of Reinforcement with  $\beta$

The inclination decreases from  $1.5^\circ$  to  $1^\circ$  with increase in  $\beta$  from 0 (i.e. for the case of linear subgrade) to 3000 for  $w_L/L = 0.001$  whereas it decreases from  $16^\circ$  to  $4^\circ$  for  $w_L/L = 0.01$  for  $\mu=1000$  and  $\phi_r=30^\circ$ .

The trend of variation of normalized normal component of maximum tension,  $T_{\max}^* \sin \theta_L$ , and normalized horizontal component of maximum tension,  $T_{\max}^* \cos \theta_L$ , with  $\beta$  is similar to the variation of normalized maximum tension,  $T_{\max}^*$ , with  $w_L/L$  (Figs. 3.44 and 3.45).

Large shear resistance is developed at reinforcement –soil interface at low  $\beta$  values due to large normal stresses developed. Hence  $P^*$  decreases with increase in  $\beta$  values. The rate of decrease of  $P^*$  with  $w_L/L$  is high for  $\beta$  in the range 0-1500 and the rate decreases thereafter. The transverse force required to cause small free end displacements ( $w_L/L=0.001$ ) is almost independent of  $\beta$  values (Fig. 3.46).

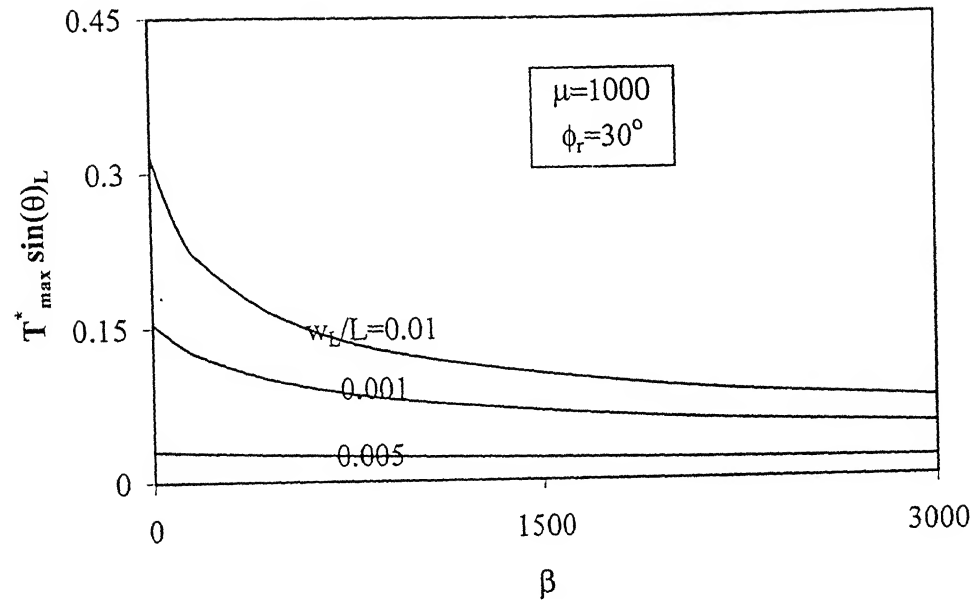


Fig. 3.44 Variation of Normalized Normal Component of Maximum Tension with  $\beta$

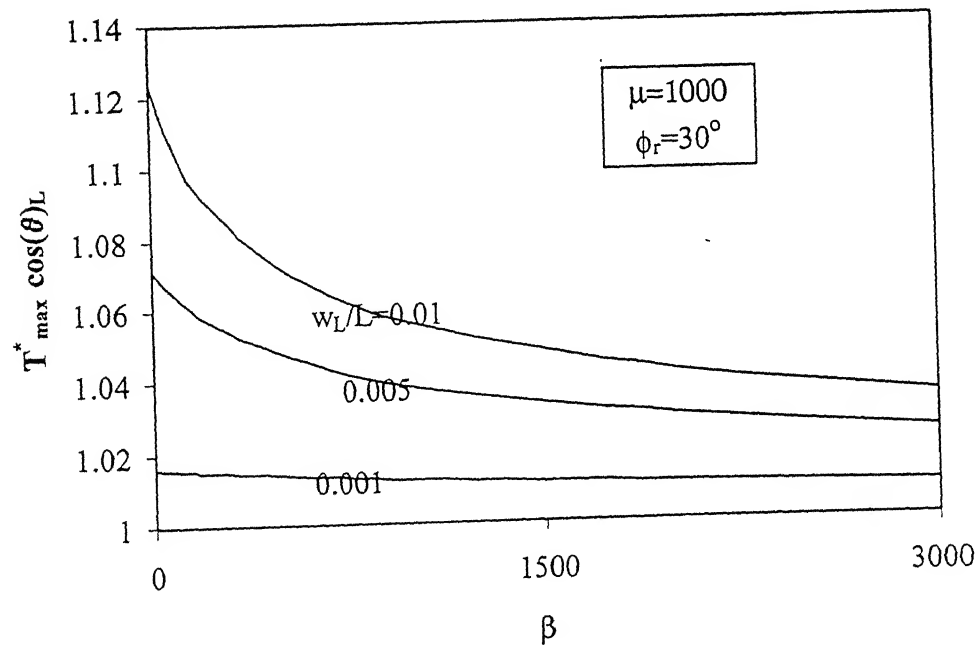


Fig. 3.45 Variation of Normalized Horizontal Component of Maximum Tension with  $\beta$

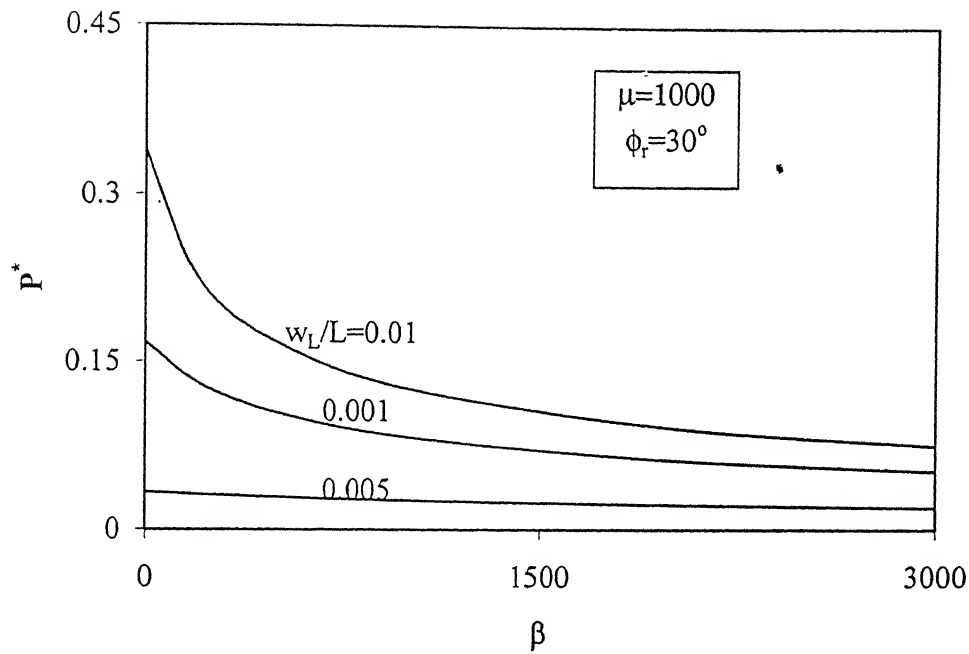


Fig. 3.46 Variation of Normalized Transverse Force with  $\beta$

### 3.3.3 Non-Linear Subgrade and Non-Linear Shear Mobilization

In section 3.3.2, full mobilization of shear resistance is assumed between the sheet and the soil irrespective of the magnitude of horizontal displacement of the interface (i.e. ideal rigid plastic type behavior of shear-displacement as shown in Fig. 3.47a is assumed).

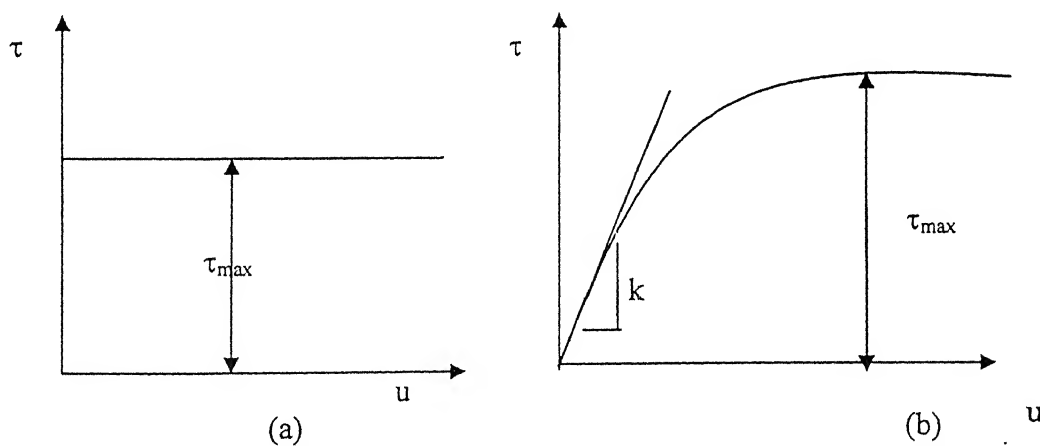


Fig. 3.47 Shear Stress-Displacement Response of Soil (a) Ideal Rigid Plastic and (b) Elasto-Plastic Responses.

Eqs. (3.41) and (3.42) are the governing equations for full mobilization of interface shear resistance.

$$\tau_b = q_b \tan \phi_r \quad (3.41)$$

$$\tau_t = q_t \tan \phi_r \quad (3.42)$$

But in actuality, the shear stress mobilized depends on the horizontal displacement at the interface between the reinforcement sheet and the soil with the maximum value limited to the stresses given by Eqs. (3.41) and (3.42). Hence to simulate this condition, a hyperbolic relation between the mobilized shear and the horizontal displacement of the interface between the sheet and the soil is considered (Elasto plastic behavior of shear-displacement as shown in Fig. 3.47b).

### 3.3.3.1 The Model

The model is identical to the one explained in section 3.2.2.1 except for the relation between the shear stress mobilized and the horizontal displacement of reinforcement sheet and soil given by

$$\tau = \frac{k_\tau u}{1 + \frac{k_\tau u}{\tau_{\max}}} \quad (3.43)$$

where  $k_\tau$ ,  $\tau_{\max}$  and  $u$  are the initial slope of shear-horizontal displacement curve, the ultimate shear stress and the relative horizontal displacement between the sheet and the soil respectively.

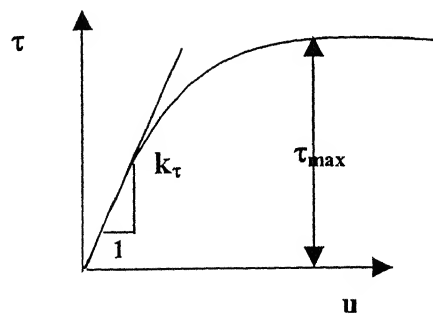


Fig. 3.48 Hyperbolic Response between Shear Resistance,  $\tau$  and Horizontal Displacement,

### 3.3.3.2 Analysis

Considering the equilibrium of forces of an element of infinitesimal length,  $\Delta x$ , and unit width as described in section 3.2.1.3, one can derive

$$\sum F_x = (T + dT)\cos(\theta + d\theta) - T\cos\theta - (\tau_t + \tau_b)\Delta x = 0 \quad (3.44)$$

$$\sum F_y = (T + dT)\sin(\theta + d\theta) - T\sin\theta - (q_b - q_t)\Delta x = 0 \quad (3.45)$$

For small deformations, as  $\Delta\theta \rightarrow 0$ ,  $\cos \Delta\theta \rightarrow 1$  and  $\sin \Delta\theta \rightarrow 0$ . Neglecting second order terms, Eqs. 3.44 and 3.45 get simplified respectively to

$$\cos\theta\left(\frac{dT}{dx}\right) - T\sin\theta\left(\frac{d\theta}{dx}\right) - (\tau_t + \tau_b) = 0 \quad (3.46)$$

$$\sin\theta\left(\frac{dT}{dx}\right) + T\cos\theta\left(\frac{d\theta}{dx}\right) - (q_b - q_t) = 0 \quad (3.47)$$

Multiplying Eq. 3.46 by  $\cos\theta$  and Eq. 3.47 by  $\sin\theta$  and adding the two, one gets

$$\frac{dT}{dx} = (\tau_t + \tau_b)\cos\theta + (q_b - q_t)\sin\theta \quad (3.48)$$

Similarly, multiplying Eq. 3.46 by  $\sin\theta$  and Eq. 3.47 by  $\cos\theta$  and subtracting the latter from the former, one gets

$$-T\frac{d\theta}{dx} - (\tau_t + \tau_b)\sin\theta + (q_b - q_t)\cos\theta = 0 \quad (3.49)$$

Using the relation given by Eq. (3.43),

$$\tau_t = \frac{k_t u}{1 + \frac{k_t u}{(\tau_{\max})_t}} \quad (3.50)$$

where  $(\tau_{\max})_t$  is the maximum shear that can be mobilized at the top of reinforcement sheet.

$$(\tau_{\max})_t = q_t \tan\phi_r = \gamma D_e \tan\phi_r \quad (3.51)$$

Substituting Eq. 3.51 in Eq. 3.50, one gets

$$\tau_t = \frac{k_t u}{1 + \frac{k_t u}{\gamma D_e \tan \phi}} \quad (3.52)$$

$$\text{Similarly, } \tau_b = \frac{k_t u}{1 + \frac{k_t u}{(\tau_{\max})_b}} \quad (3.53)$$

Where  $(\tau_{\max})_b$  is the maximum shear that can be mobilized at the bottom of the reinforcement sheet.

$$\begin{aligned} (\tau_{\max})_b &= q_b \tan \phi_r \\ &= \left( \gamma D_e + \frac{k_s w}{1 + \frac{k_s w}{q_{ult}}} \right) \tan \phi_r \end{aligned} \quad (3.54)$$

Substituting Eq. 3.54 in Eq. 3.53, one gets

$$\tau_b = \frac{k_t u}{1 + \frac{k_t u}{\left( \gamma D_e + \frac{k_s w}{1 + \frac{k_s w}{q_{ult}}} \right) \tan \phi_r}} \quad (3.55)$$

But  $\tan \theta = dw/dx$ , where  $w$  is the normal displacement at a distance,  $x$ , from point A.

Differentiating with respect to  $x$ , one gets

$$\frac{d\theta}{dx} = \cos^2 \theta \frac{d^2 w}{dx^2} \quad (3.56)$$

For a subgrade with non-linear (hyperbolic) response, (Fig. 3.22)

The increment in normal stress due to the normal displacement of the reinforcement sheet is

$$q_b - q_t = \frac{k_s w}{1 + \frac{k_s w}{q_{ult}}} \quad (3.57)$$

Substituting Eqs.(3.52),(3.55), (3.56) and (3.57) in Eqs.(3.48) and (3.49), one gets

$$\frac{dT}{dx} = \left[ \frac{k_\tau u}{1 + \frac{k_\tau u}{\gamma D_e \tan \phi}} + \frac{k_\tau u}{1 + \frac{k_\tau u}{\left( \gamma D_e + \frac{k_s w}{1 + \frac{k_s w}{q_{ult}}} \right) \tan \phi_r}} \right] \cos \theta + \frac{k_s w}{1 + \frac{k_s w}{q_{ult}}} \sin \theta \quad (3.58)$$

$$-T \cos^2 \theta \frac{d^2 w}{dx^2} + \left( \frac{K_s w}{1 + \frac{k_s w}{q_{ult}}} \right) \cos \theta = \left[ \frac{k_\tau u}{1 + \frac{k_\tau u}{\gamma D_e \tan \phi}} + \frac{k_\tau u}{1 + \frac{k_\tau u}{\left( \gamma D_e + \frac{k_s w}{1 + \frac{k_s w}{q_{ult}}} \right) \tan \phi_r}} \right] \sin \theta \quad (3.59)$$

For small  $\theta$ , Eqs. 3.58 and 3.59 reduce to

$$\frac{dT}{dx} = \left( \frac{\frac{k_r u}{1 + \frac{k_r u}{\gamma D_e \tan \phi}} + \frac{k_r u}{1 + \frac{k_r u}{\left( \gamma D_e + \frac{k_s w}{1 + \frac{k_s w}{q_{ult}}} \right) \tan \phi_r}} \right) \quad (3.60)$$

$$-T \frac{d^2 w}{dx^2} + \left( \frac{K_s w}{1 + \frac{k_s w}{q_{ult}}} \right) = 0 \quad (3.61)$$

Eqs. 3.60 and 3.61 are the governing equations for the model that incorporates non-linear subgrade and non-linear shear-horizontal displacement responses of the soil and the interface. Eqs. 3.60 and 3.61 are non-dimensionalised with  $X=x/L$ ,  $W=w/w_L$ ,  $U=u/L$ ,  $T^*=T/T_{\max}$  where  $T_{\max}=2 \gamma D_e L \tan \phi_r$ , the maximum axial pullout force. Eqs. (3.60) and (3.61) in normalized form are

$$\frac{dT^*}{dX} = \frac{1}{2 \tan \phi_r} \left( \frac{\frac{\eta U}{1 + \frac{\eta U}{\tan \phi_r}} + \frac{\eta U}{1 + \frac{\eta U}{\left( \frac{\mu \frac{w_L}{L} W}{1 + \beta W \frac{w_L}{L}} + 1 \right) \tan \phi_r}} \right) \quad (3.62)$$

$$-T^* \frac{d^2 W}{dX^2} + \frac{\mu W}{2 \tan \phi_r \left( 1 + \beta W \frac{w_L}{L} \right)} = 0 \quad (3.63)$$

where  $\mu = \frac{k_s L}{\gamma D_e}$  and  $\beta = \frac{k_s L}{q_{ult}}$  are defined in section 3.2.1.3 and 3.2.2.2 respectively.

$\eta = \frac{k_r L}{\gamma D_e}$  -Relative initial shear stiffness factor for the soil.

The boundary conditions for the present case are the same as detailed in section 3.2.1.3. Eqs. (3.33), (3.34) and (3.35) derived for the determination of transverse force for a given transverse/ vertical displacement,  $w_L$ , hold good for this case also.

### 3.3.3.3 Numerical Solution

The discretisation of inextensible reinforcement length into elements is as explained in section 3.2.1.4. Eqs. 3.62 and 3.63 in finite difference form become

$$\frac{T_{i+1}^* - T^*}{\Delta X} = \frac{1}{2 \tan \phi_r} \left( \frac{\eta U}{1 + \frac{\eta U}{\tan \phi_r}} + \frac{\eta U}{1 + \left( \frac{\mu \frac{w_L}{L} W}{1 + \beta W \frac{w_L}{L}} + 1 \right) \tan \phi_r} \right) \quad (3.64)$$

$$-T_i^* \left( \frac{W_{i-1} - 2W_i + W_{i+1}}{\Delta X^2} \right) + \frac{\mu W_i}{2 \tan \phi_r \left( 1 + \beta W_i \frac{w_L}{L} \right)} = 0 \quad (3.65)$$

Solving for normalized displacement and normalized tension, one gets

$$T_{i+1}^* = T_i^* + \frac{1}{2(n-1)\tan\phi_r} \left( \frac{\eta U}{1 + \frac{\eta U}{\tan\phi_r}} + \frac{\eta U}{1 + \frac{\eta U}{\left( \frac{\mu \frac{w_L}{L} W}{1 + \beta W \frac{w_L}{L}} + 1 \right) \tan\phi_r}} \right) \quad (3.66)$$

$$W_i = \frac{T_i^* n^2 (W_{i-1} + W_{i+1})}{\left( 2n^2 T_i^* + \frac{\mu}{2 \tan\phi_r \left( 1 + \beta W_i \frac{w_L}{L} \right)} \right)} \quad (3.67)$$

### 3.3.3.4 Calculation of Horizontal Displacement along the Length of Reinforcement

The inextensible sheet reinforcement is divided into 'n<sub>e</sub>' elements (Fig. 3.49) each of length Δx. 1, 2, 3... n, (n+1) are the nodes in the original undeformed position of the sheet. w<sub>1</sub>, w<sub>2</sub>, w<sub>3</sub>, ..., w<sub>n</sub>, w<sub>n+1</sub> indicate the vertical displacement profile of the sheet due to an application of transverse force. It is assumed that the (n+1)<sup>th</sup> node deforms vertically downwards [indicated by (n+1)<sup>↓</sup>] which is true for small transverse forces applied. Thus the horizontal displacement of (n+1)<sup>th</sup> node is zero. From (n+1)<sup>th</sup> node, a distance equal to elemental length Δx is marked along the vertical displacement profile (indicated by n<sup>↓</sup>) to locate the position of n<sup>th</sup> node in the deformed position. The horizontal displacement of n<sup>th</sup> is determined by the horizontal distance between n<sup>th</sup> and n<sup>↓</sup> assuming in-extensible reinforcement. The same procedure is adopted to locate (n-1)<sup>th</sup> node starting from n<sup>↓</sup> node and so on. Thus the horizontal displacements of all the nodal points along the reinforcement sheet are evaluated.

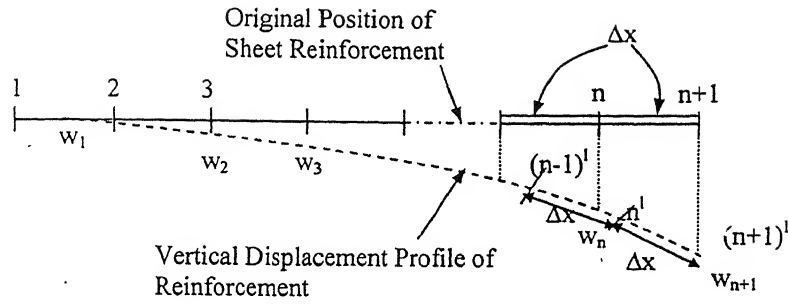


Fig. 3.49 Procedure for Calculation of Horizontal Displacements along the Reinforcement

### 3.3.3.5 Characteristics of the Model

Unlike the previous model, the shear stress mobilized along the length of the sheet is taken as a function of the horizontal displacement of the reinforcement sheet, limited by the ultimate shear resistance that can be developed between the sheet and the soil. A limitation of this model is that under large displacement or applied transverse load, the assumption of small angles is not appropriate.

### 3.3.3.6 Results and Discussions

Based on the above formulation, the analysis of reinforcement subjected to transverse displacement/force is carried out for a ranges of parameters  $\mu$ ,  $\beta$ ,  $w_L/L$ ,  $\phi_r$  and  $\eta$ . The value of initial shear stiffness,  $k_r$ , is taken as (1-10) times the initial subgrade modulus,  $k_s$ . Hence, the effect of  $\eta(=k_r L/\gamma D_e)$  on the response of the reinforcement is studied in the range 10 to 1,000,000.

Fig. 3.50 shows the normalized displacement profiles with normalized distance for  $w_L/L=0.1$ ,  $\beta=1000$ ,  $\eta=500$  and  $\phi_r=30^\circ$ , for relative stiffness factor of soil,  $\mu$ , equal to 200, 500, 1000, 2000, 3000 and 10000. For relatively compressible subgrades ( $\mu \leq 200$ ), the transverse displacements are mobilized over the entire length of the reinforcement whereas the transverse displacements get highly localized towards the right end for stiffer subgrades ( $\mu=10,000$ ). A comparison of response of Model II (non-linear subgrade with full shear mobilized along sheet-soil interface) with the present model reveals that for a non-linear shear stress-displacement model (Figs. 3.23 and 3.50), the transverse displacements get mobilized over larger lengths of reinforcement. For

$w_L/L=0.1$ ,  $\mu=500$ ,  $\beta=1000$  and  $\phi_r=30^\circ$ , the length over which transverse displacements are mobilized is  $0.6L$  measured from the point of application of displacement/transverse force for full shear mobilization case while it is  $0.75L$  for the above same parameters but with non-linear shear mobilization-horizontal displacement parameter,  $\eta=500$ .

Fig.3.51 shows the variation of transverse displacement profiles with normalized distance for different values of  $\beta(=k_sL/q_{ult})$  values for  $\mu=500$ ,  $\eta=500$ ,  $w_L/L=0.1$  and  $\phi_r=30^\circ$ . The points of mobilization of transverse displacements move towards the left end with decrease in ultimate resistance of the soil (i.e with increase in  $\beta$  value).

The effect of relative initial shear mobilization factor,  $\eta$ , on the variation of transverse displacement profiles,  $W$ , with normalized distance,  $X$ , is presented in Fig. 3.52. As the non-linearity of the relationship between the shear stress mobilization and horizontal displacement of interface between reinforcement and sheet increases (i.e as  $\eta$  increases), the length of mobilization of transverse displacements increases. Very large  $\eta$  values ( $\eta=10,000$ ) indicate that the shear stress mobilized approaches the full or maximum shear mobilization between the reinforcement and the soil. Hence for  $\eta$  values beyond 2000, no change in the transverse displacement profile is evident.

The variation of normalized horizontal displacement,  $U$ , of reinforcement with normalized distance,  $X$ , for different relative stiffnesses of soil,  $\mu$ , is presented in Fig. 3.53 at  $\beta=1000$ ,  $\eta=500$ ,  $w_L/L=0.1$  and  $\phi_r=30^\circ$ . The straight horizontal portion response indicates the rigid body movement for that portion of the reinforcement. The points marked on the curve indicate the extent up to which the rigid body movement takes place from the left end. The length over which rigid body movement of reinforcement occurs from left end, increases with increasing stiffness of the soil. The length over which rigid body movement of reinforcement occurs is  $0.35L$  from the left end for  $\mu=50$  whereas it is  $0.8L$  for  $\mu=10,000$ . The horizontal displacement at the right end ( $x=L$ ) is zero as the sheet is assumed to undergo a purely vertical translation at that end. The rate of decrease of horizontal displacements of reinforcement from the point of rigid body translation to zero is high in case of relatively stiff soils ( $\mu=10,000$ ).

The variation of normalized horizontal displacement of reinforcement,  $U$ , with normalized distance,  $X$ , for  $\beta(=k_sL/q_{ult})$  equal to 100, 500, 1000, 2000 and 3000 is presented in Fig. 3.54 for  $\mu=500$ ,  $\eta=500$ ,  $w_L/L=0.1$  and  $\phi_r=30^\circ$ . As the ultimate resistance of the soil increases (i.e, for decreasing  $\beta$  values), the length over which the

rigid translatory movement of reinforcement takes place also increases. It is about  $0.75L$  for  $\beta=100$  whereas it is about  $0.35L$  for  $\beta=3000$  at  $\mu=500$ ,  $\eta=500$ ,  $w_L/L=0.1$  and  $\phi_r=30^\circ$ . The rate of decrease of horizontal displacements of reinforcement from rigid body translation to zero is high in case of soils with high ultimate resistance (low  $\beta$  value).

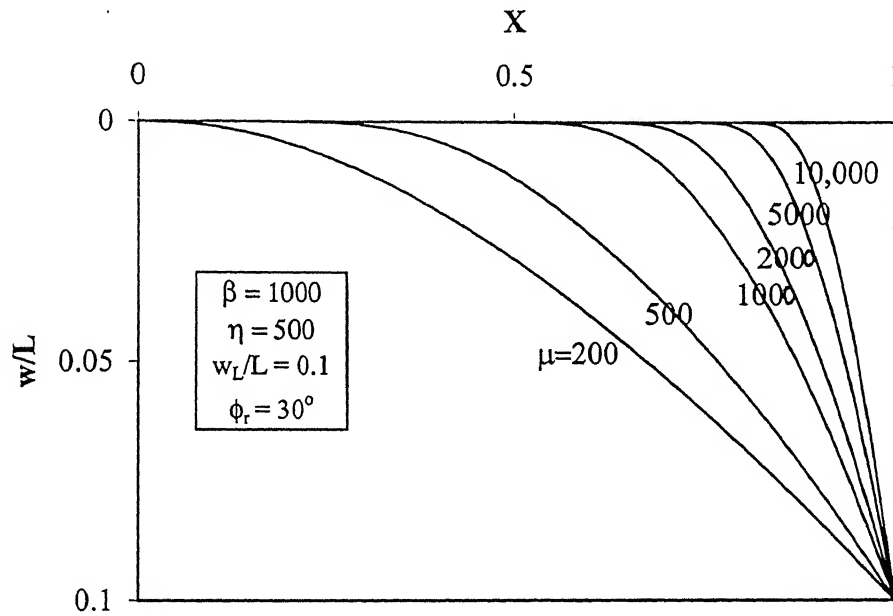


Fig. 3.50 Variation of Normalized Displacement with Normalized Distance –Effect of  $\mu$

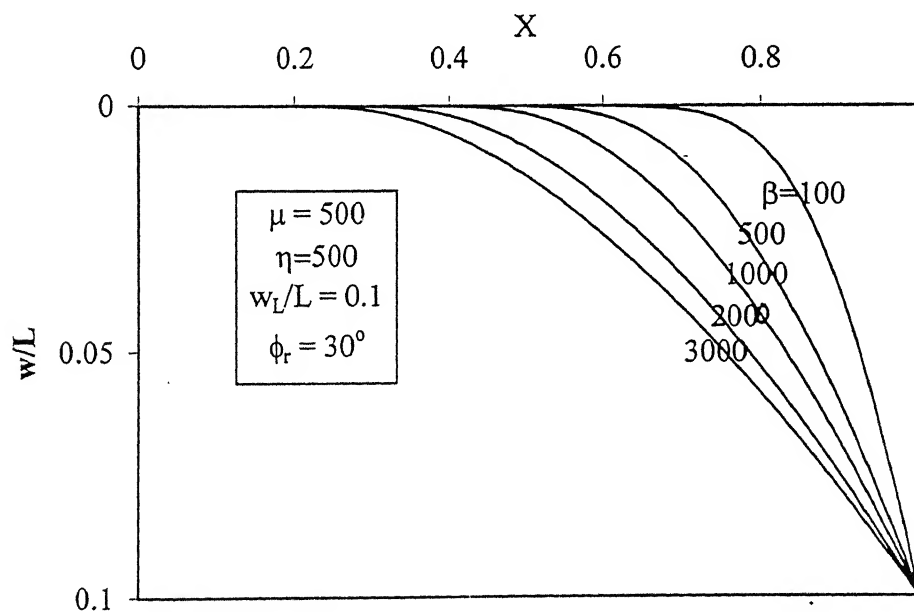


Fig. 3.51 Variation of Normalized Displacement with Normalized Distance –Effect of  $\beta$

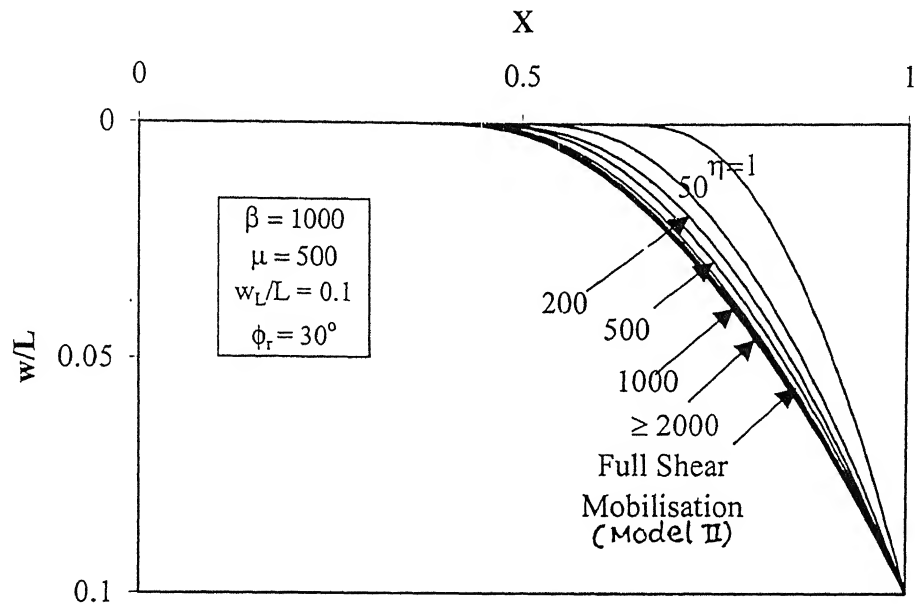


Fig. 3.52 Variation of Normalised Displacement with Normalised Distance – Effect of  $\eta$

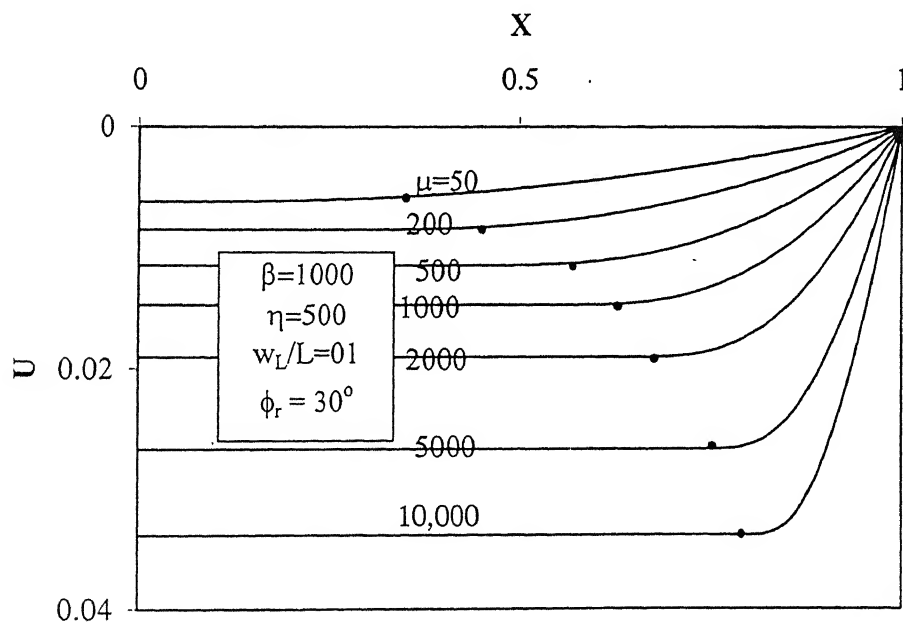


Fig. 3.53 Variation of Horizontal Displacement with Normalised Distance – Effect of  $\mu$

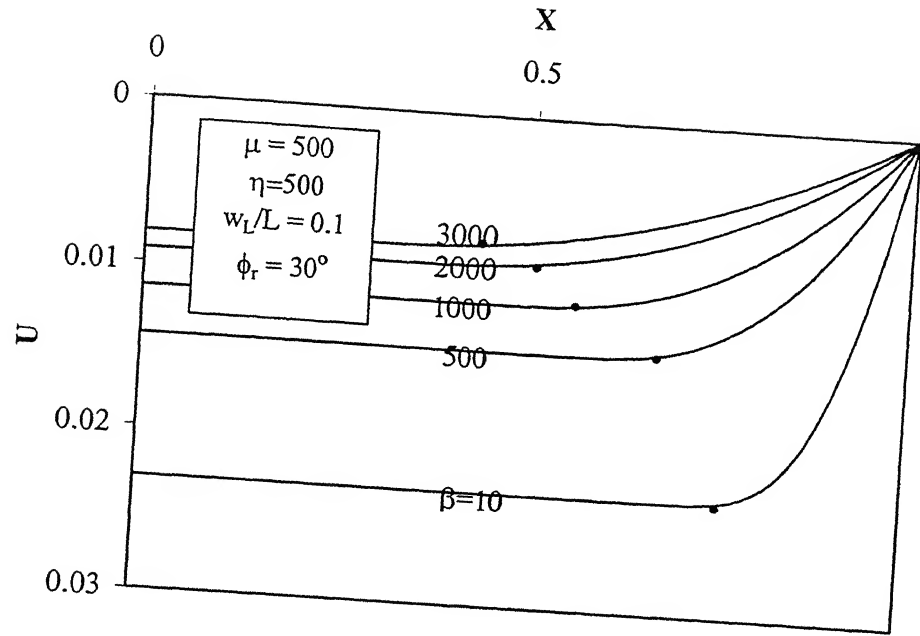


Fig. 3.54 Variation of Horizontal Displacement with Normalised Distance – Effect of  $\beta$

The effect of relative initial shear stiffness,  $\eta$ , on the variation of normalized horizontal displacement of reinforcement with the normalized distance is presented in Fig. 3.55. There is no significant difference in the horizontal displacements for  $\eta \geq 2000$  as the shear mobilized between the sheet and the reinforcement reaches the maximum shear that can be mobilized. The length over which the rigid body type of movement of reinforcement takes place decreases with increase in the relative initial shear stiffness of the soil. The length of reinforcement undergoing rigid body translation is about  $0.7L$  for  $\eta=10$  compared to  $0.5L$  for  $\eta \geq 2000$ .

The variation of normalized tension with normalized distance for relative stiffness of soil, for  $\mu$  equal to 50, 200, 500, 1000, 2000, 5000 and 10000 is presented in Fig. 3.56 for  $\beta=1000$ ,  $\eta=500$ ,  $w_L/L=0.1$  and  $\phi_r=30^\circ$ . For a given soil, tension increases linearly with distance along the reinforcement for a length of about  $0.6L$  measured from the left end. But near the end where transverse displacement/force is applied, the reinforcement undergoes notable transverse displacements in addition to the horizontal displacements of the interface. The increase in shear resistance along the interface is due to increase in normal stresses because of mobilization of transverse displacements. Hence, tension increases non-linearly as one move towards the end where transverse

displacement/load is applied. As the displacement of interface is zero at the right end, the rate of increase of tension decreases as one approaches the right end ( $x=L$ ).

Similar variation can be observed with the parameter  $\beta (=k_s L/q_{ult})$  (Fig. 3.57).

The effect of relative initial shear stiffness,  $\eta$ , on the variation of normalized tension,  $T^*$ , with normalized distance,  $X$ , is shown in Fig 3.58. For a given horizontal displacement of the interface, the shear mobilized will be larger for large  $\eta$  (as non-linearity increases with increasing  $\eta$ ). Hence the shear mobilized along the reinforcement increases with increasing  $\eta$  values. For  $\eta \geq 2000$ , the tension developed along the length remains the same as the shear mobilized approaches the maximum value. Hence the curves showing the variation of tension with distance for  $\eta \geq 2000$  and full shear mobilization case overlap each other.

The rate of increase of maximum normalized tension,  $T^*_{max}$ , developed at the right end with normalized free end displacement,  $w_L/L$ , increases with increase in relative stiffness of the soil (Fig 3.59). Large normal stresses are induced in the soil over larger lengths for large free end displacements. Hence, the shear resistance along the interface increases and so does the maximum tension developed at  $x=L$ . The tension is found to increase linearly with  $w_L/L$  for relatively compressible soils ( $\mu=50$ ) but becomes non-linear for stiff soils ( $\mu=10,000$ ).

The transverse displacement profile becomes highly localized with increase in the enforced free end displacement,  $w_L$ . Hence, large inclinations of reinforcement are observed for large  $w_L/L$  (Fig 3.60). The variation of horizontal inclination,  $\theta_L$ , with normalized free end displacement,  $w_L/L$ , is linear for relatively compressible soils but becomes non-linear with increase in the relative stiffness of the soil. The rate of increase of  $\theta_L$  with  $w_L/L$  increases with increase in the stiffness of soil.

The variation of normalized normal component of maximum tension,  $T^*_{max} \sin \theta_L$ , is linear with normalized free end displacement,  $w_L/L$ , for  $w_L$  in the range of  $0.001L$  to  $0.01L$  and for  $\mu$  in the range  $50$  to  $10,000$  for  $\beta=1000$ ,  $\eta=500$  and  $\phi_r=30^\circ$  (Fig. 3.61). The rate of increase of  $T^*_{max} \sin \theta_L$  with  $w_L/L$  increases with increase in the relative stiffness of the soil,  $\mu$ . The normal component of maximum tension developed is insignificant for relatively compressible soils ( $\mu=50$ ).  $T^*_{max} \sin \theta_L$  being equal to  $0.02$  for  $w_L/L=0.01$  for  $\beta=1000$ ,  $\eta=500$  and  $\phi_r=30^\circ$ .

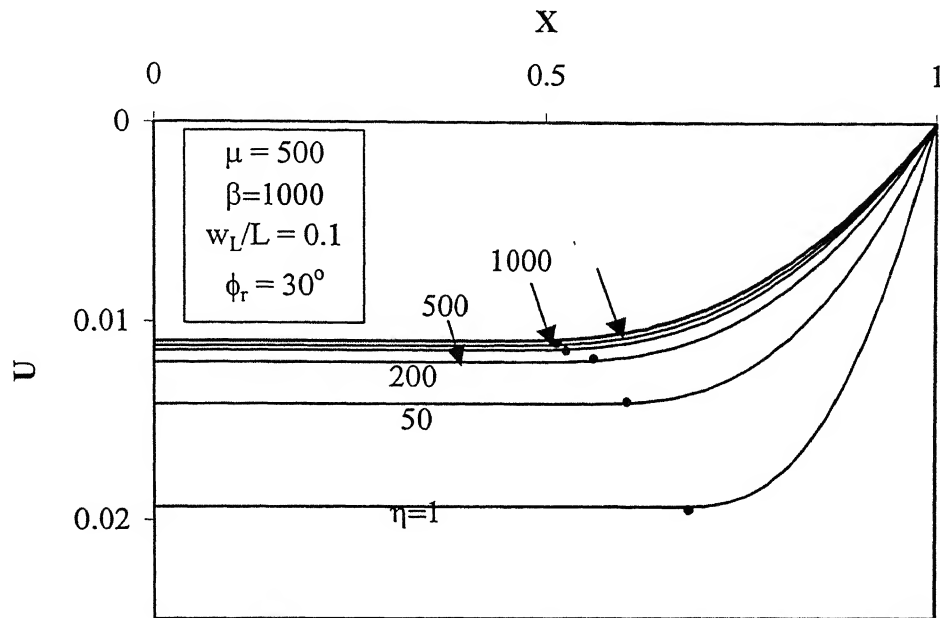


Fig. 3.55 Variation of Horizontal Displacement with Normalised Distance – Effect of  $\eta$

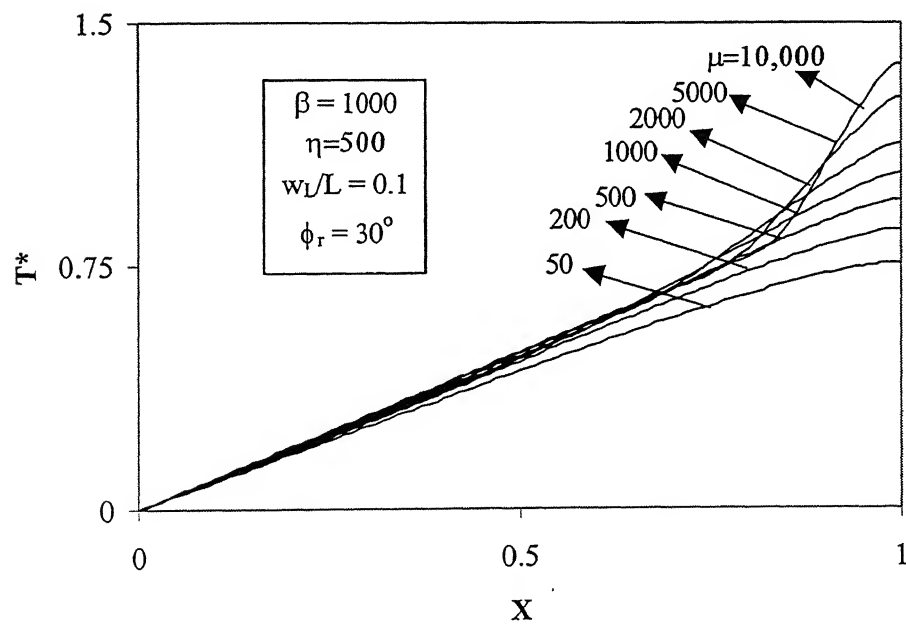


Fig. 3.56 Variation of Normalised Tension with Normalised Distance- Effect of  $\mu$

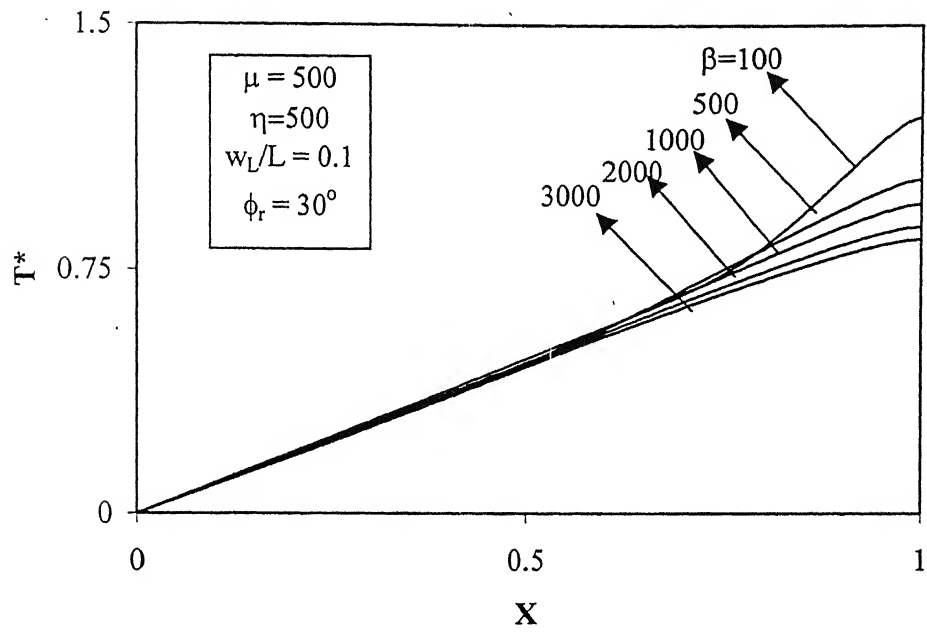


Fig. 3.57 Variation of Normalized Tension with Normalized Distance- Effect of  $\beta$

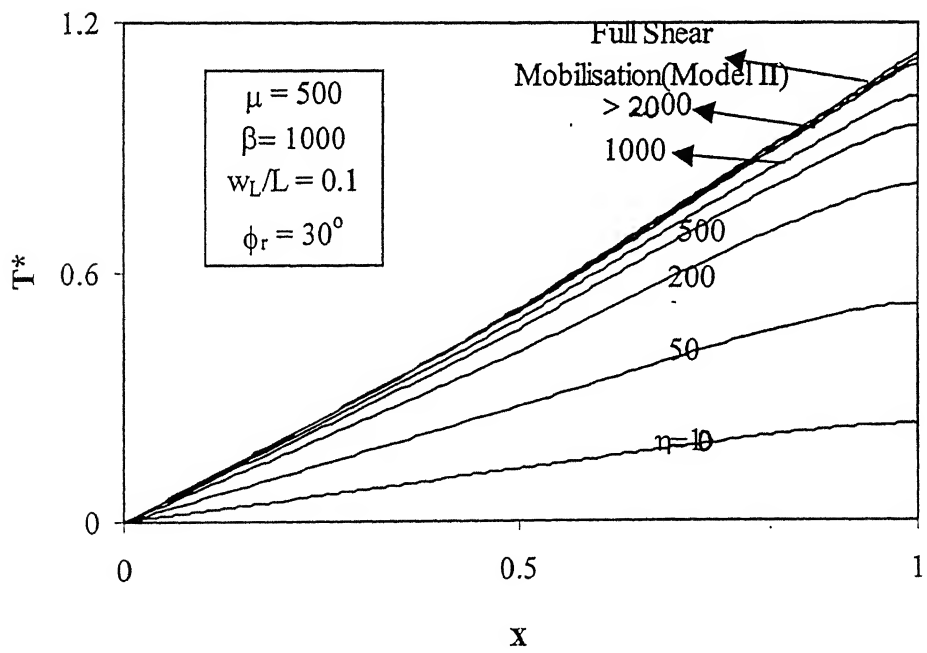


Fig. 3.58 Variation of Normalized Tension with Normalized Distance- Effect of  $\eta$

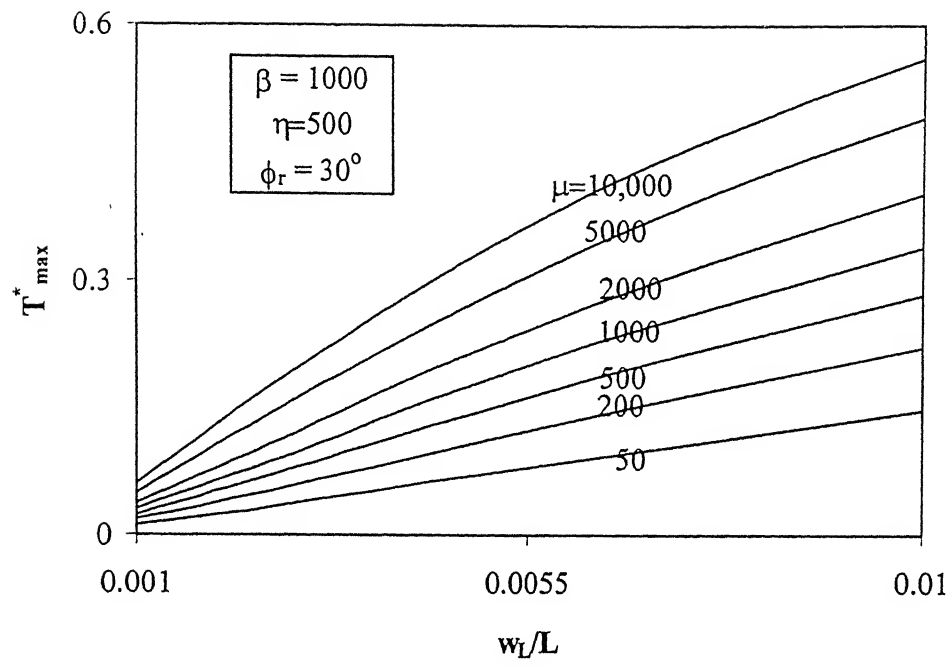


Fig.3.59 Variation of Normalized Maximum Tension with Normalized Distance- Effect of  $\mu$

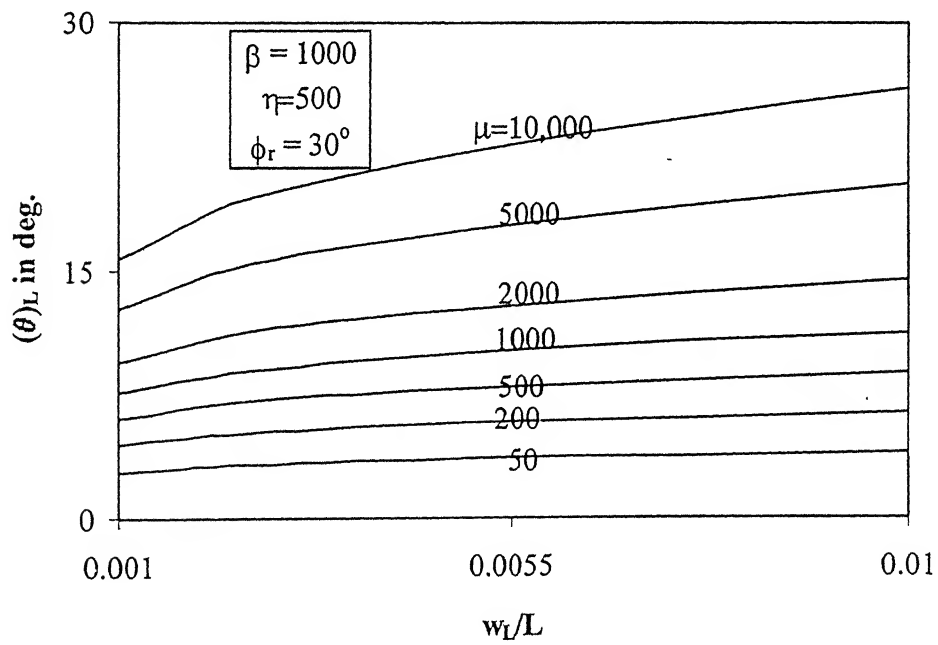


Fig. 3.60 Variation of Inclination of Reinforcement at  $x=L$  with  $w_L/L$ - Effect of  $\mu$

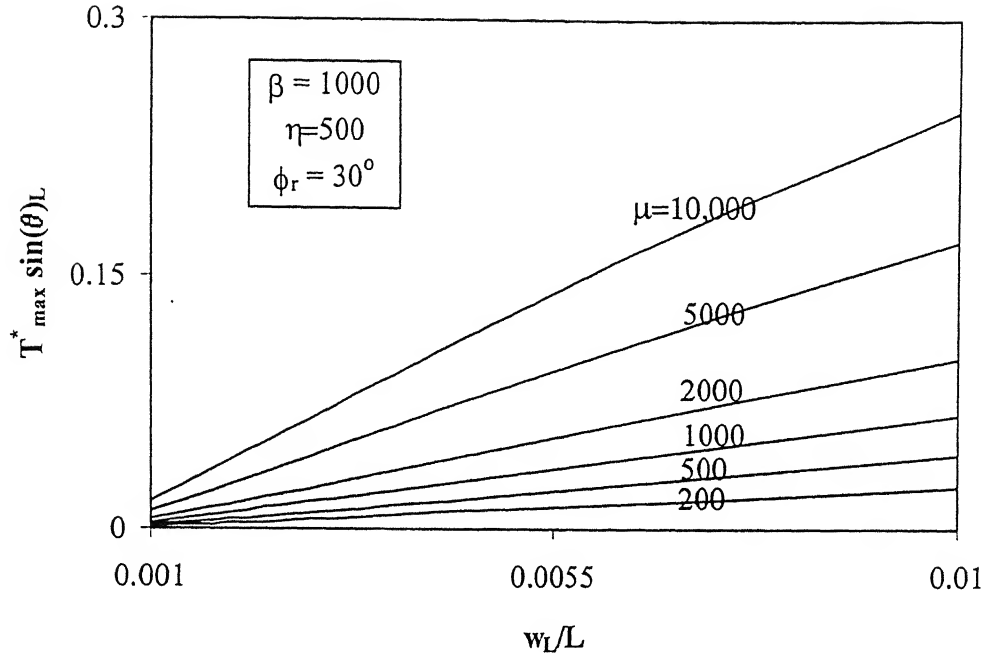


Fig. 3.61 Variation of Maximum Normalized Normal Component of Tension with  $w_L/L$  – Effect of  $\mu$

The variation of normalized horizontal component of tension, normal range  $0.001L$  to  $0.01L$  and  $\mu$  in the range  $50$  to  $10,000$ . The rate of increase of  $T^*_{\max} \cos \theta_L$  with  $w_L/L$  increases with increase in  $\mu$  (Fig 3.62)

The variation of normalized transverse force,  $P^*$ , with  $w_L/L$  for relative stiffness of the soil,  $\mu$ , equal to  $200, 500, 1000, 2000, 5000$  and  $10,000$  is presented in Fig.3.63. The rate of increase of transverse force with  $w_L/L$  increases with increase in relative stiffness of soil,  $\mu$ . The variation of  $P^*$  with  $w_L/L$  is almost linear in the range  $\mu=200$  to  $10,000$  for  $\beta=1000, \eta=500$  and  $\phi_r=30^\circ$  (Fig 3.63)

Large normal stresses are induced in the soil over larger lengths of reinforcement for greater free end displacements,  $w_L$ . Hence the large shear resistance mobilized along the sheet-soil interface cause an increase in the maximum tension,  $T^*_{\max}$ , developed at  $x=L$  with  $w_L/L$ . The variation of  $T^*_{\max}$ , with  $w_L/L$  is linear for  $\beta$  in the range  $100-3000$  for  $\mu=500, \eta=500$  and  $\phi_r=30^\circ$  (Fig. 3.64).

Due to localization of transverse displacements at large free end displacements,  $w_L$ , the inclination of reinforcement, at  $x=L$  increases with  $w_L/L$ . The effect of localization increases with increase in the ultimate resistance of the soil,  $q_{ult}$  (i.e for low  $\beta$  values). Hence, the rate of increase of  $\theta_L$ , with  $w_L/L$  increases with increase in  $\beta$

values (Fig 3.65). The variation of normalized normal component of tension,  $T_{\max}^* \sin \theta_L$ , with normalized free end displacement,  $w_L/L$ , is presented in Fig. 3.66. The variation is almost linear for  $w_L$  in the normal range of  $0.001L$  to  $0.01L$  but becomes non-linear for smaller  $\beta$  values ( $\beta \leq 500$ ).

The trend of variation of normalized horizontal component of tension,  $T_{\max}^* \cos \theta_L$ , with normalized free end displacement,  $w_L/L$ , (Fig. 3.67) is similar to that of the variation of  $T_{\max}^*$  with  $w_L/L$  (Figs. 3.64)

The variation of normalized transverse force,  $P^*$ , with normalized end displacement,  $w_L/L$ , is shown in Fig. 3.68. The trend of variation is similar to that of the variation of  $T_{\max}^* \sin \theta_L$  with  $w_L/L$ . The rate of increase of  $P^*$  with  $w_L/L$  increases with decreasing  $\beta$ .

The normalized maximum tension varies linearly with normalized free end displacement,  $w_L/L$ , for smaller initial shear stiffness of the soil ( $\eta \leq 1000$ ) but the variation becomes non-linear as the shear stiffness increases (i.e at higher  $\eta$  value). The rate of increase of  $T_{\max}^*$  with  $w_L/L$  decreases for large free end displacement,  $w_L$ , for higher  $\eta$  values (Fig. 3.69).

The effect of localization of transverse displacements near the right end for increasing free end displacements causes an increase in inclination of reinforcement,  $\theta_L$ , at  $x=L$ . The rate of increase of  $\theta_L$  increases with decreasing  $\eta$  values (Fig. 3.70).

The variation of normalized normal component of maximum tension,  $T_{\max}^* \sin \theta_L$ , is linear with normalized free end displacement,  $w_L/L$ , for  $w_L$  in the range of  $0.001$  to  $0.01L$  and  $\eta$  in the range  $10$ - $10,000$  for  $\mu=500$ ,  $\beta=1000$  and  $\phi_r=30^\circ$  (Fig. 3.71).

The variation of normalized horizontal component of tension,  $T_{\max}^* \cos \theta_L$ , with  $w_L/L$  (Fig. 3.72) is similar to that of the variation of  $T_{\max}^* \sin \theta_L$  with  $w_L/L$  (Fig. 3.71). The variation of normalized transverse force,  $P^*$ , with  $w_L/L$  is linear for smaller relative initial shear stiffness,  $\eta$ , but becomes non-linear at high  $\eta$  ( $\eta$  of the order of  $10,000$ ) as the relationship between shear stress –displacement becomes highly non-linear (Fig. 3.73).

The rate of increase of normalized tension,  $T^*$ , with normalized free end displacement is high for relatively compressible soils ( $\mu < 2000$ ) but the rate decreases at higher stiffnesses of the soil (Fig. 3.74).

The effect of localization of transverse displacements near the right end increases with increase in the relative stiffness of the soil,  $\mu$ . Hence the inclination of reinforcement with horizontal,  $\theta_L$ , at  $x=L$  increases with  $\mu$ . The rate of increase of  $\theta_L$  is high for relatively compressible soils ( $\mu \leq 5000$ ) (Fig. 3.75).

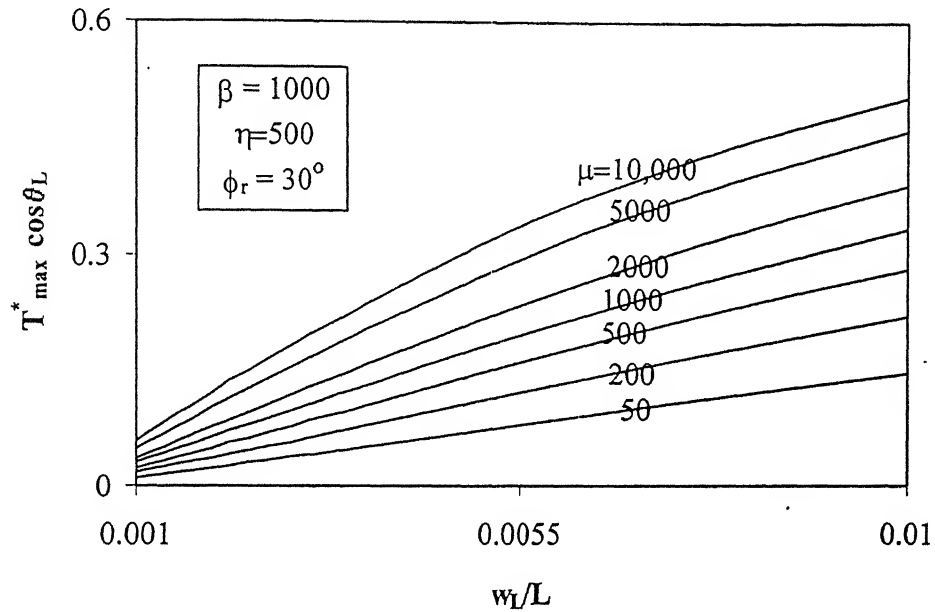


Fig. 3.62 Variation of Normalized Maximum Horizontal Component of Tension with  $w_L/L$  – Effect of  $\mu$

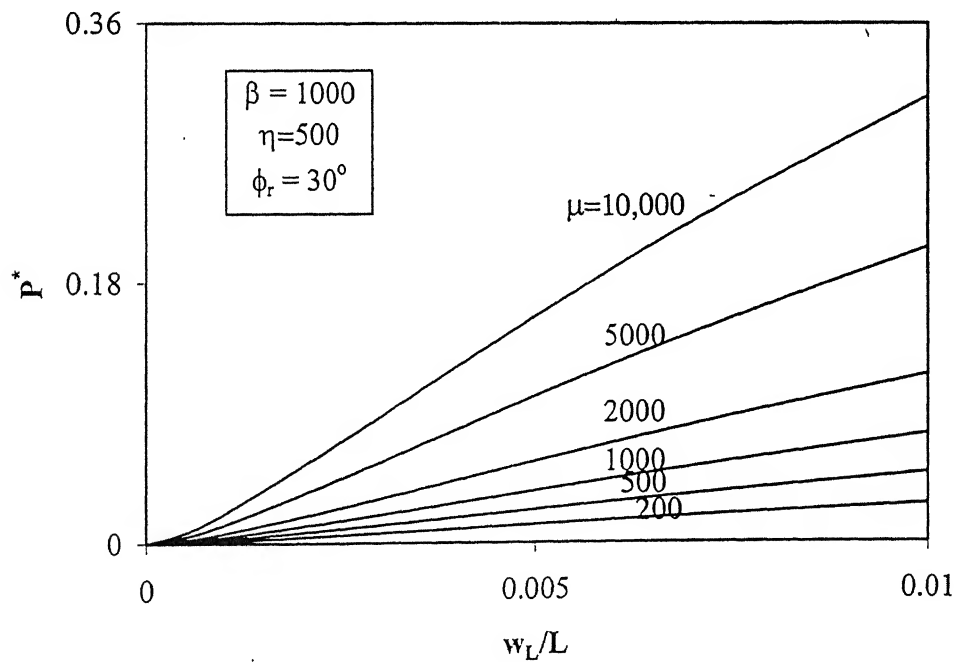


Fig. 3.63 Variation of Normalized Transverse Force with  $w_L/L$  - Effect of  $\mu$

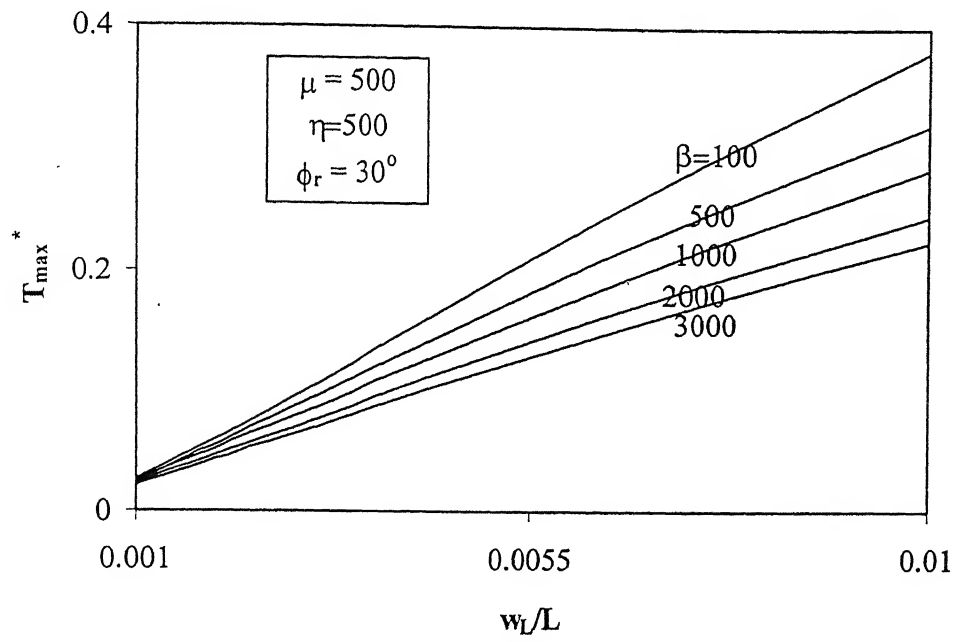


Fig. 3.64 Variation of Normalized Maximum Tension with  $w_L/L$  - Effect of  $\beta$

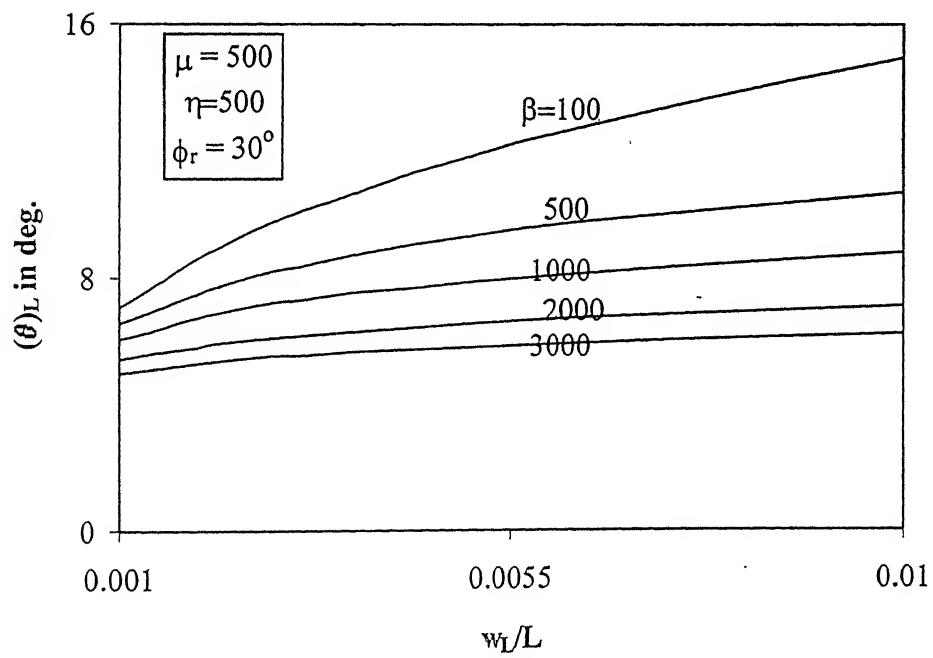


Fig. 3.65 Variation of Inclination of Reinforcement at  $x=L$  - Effect of  $\beta$

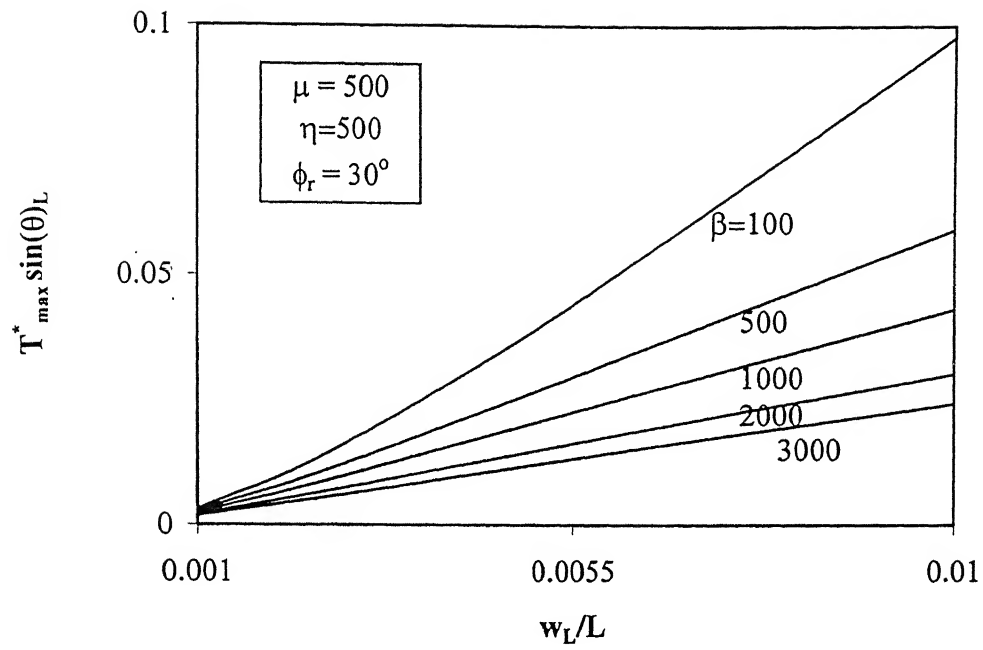


Fig. 3.66 Variation of maximum Normalized Normal Component of Tension with  $w_L/L$  – Effect of  $\beta$

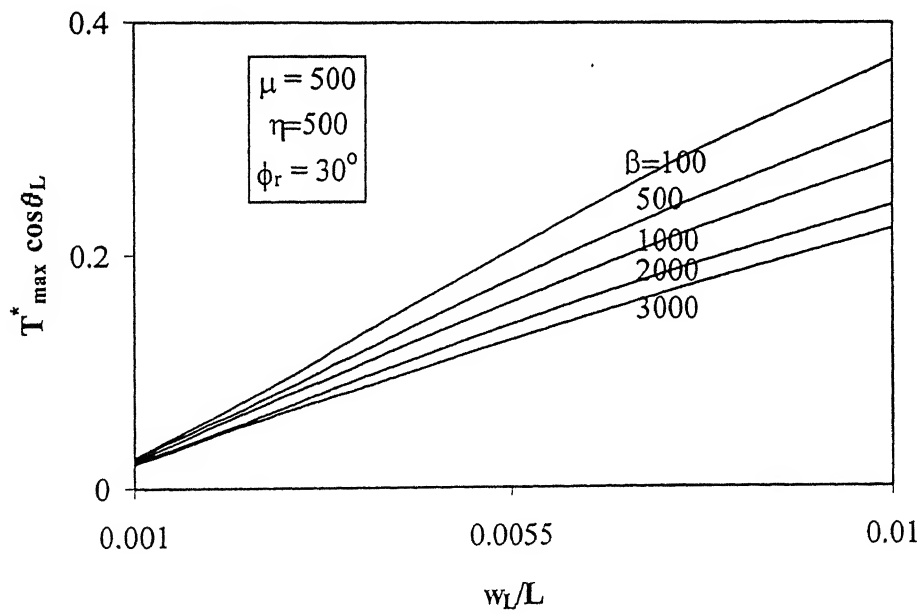


Fig. 3.67 Variation of Maximum Normalized Horizontal Component of Tension with  $w_L/L$  – Effect of  $\beta$

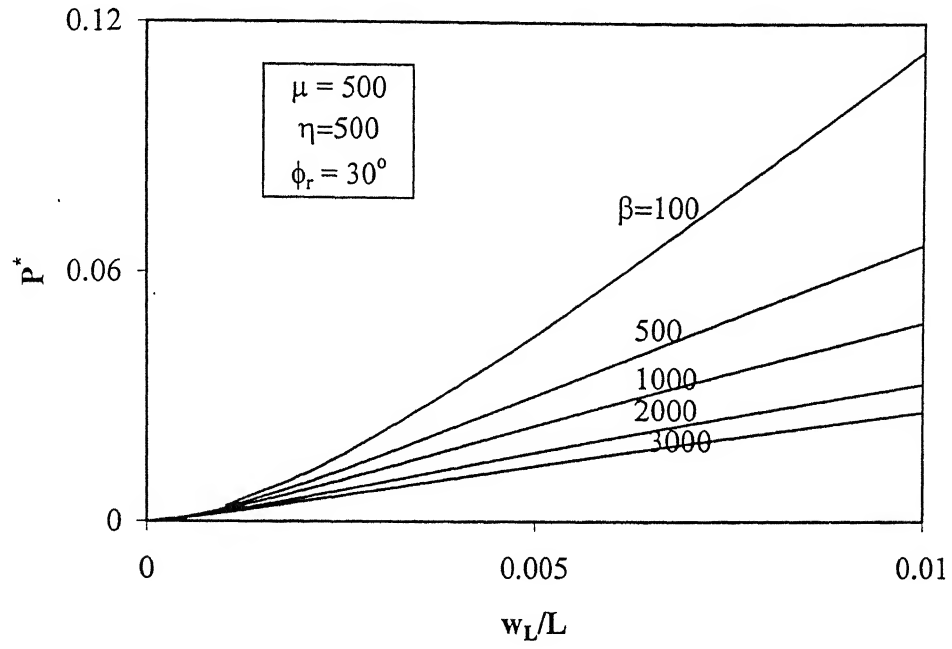


Fig. 3.68 Variation of Normalized Transverse Force with  $w_L/L$  - Effect of  $\beta$

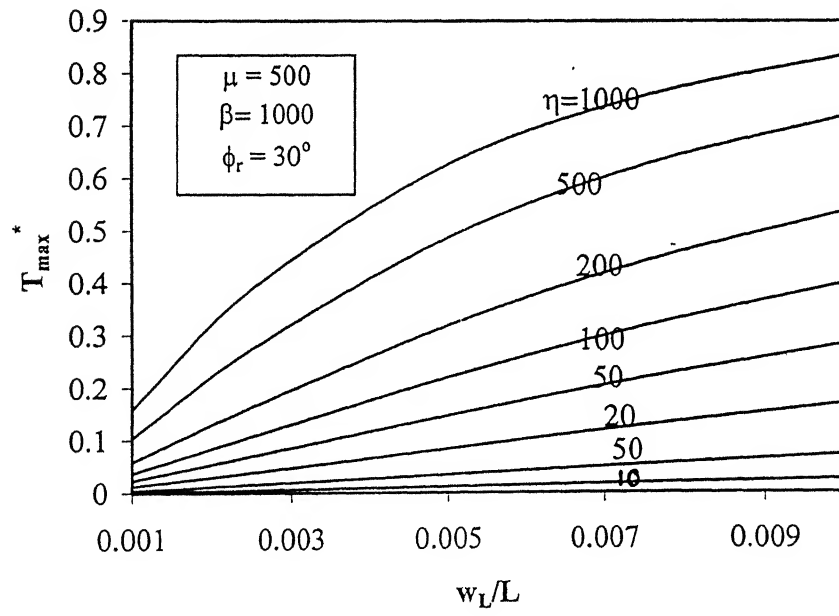


Fig. 3.69 Variation of Normalized maximum Tension with  $w_L/L$  - Effect of  $\eta$

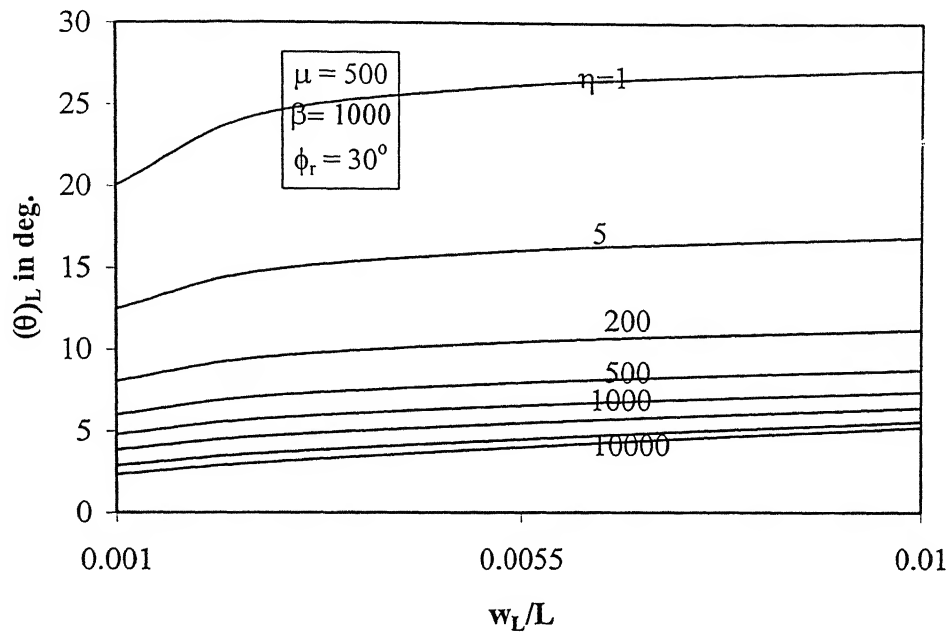


Fig. 3.70 Variation of Inclination of Reinforcement at  $x=L$  – Effect of  $\eta$

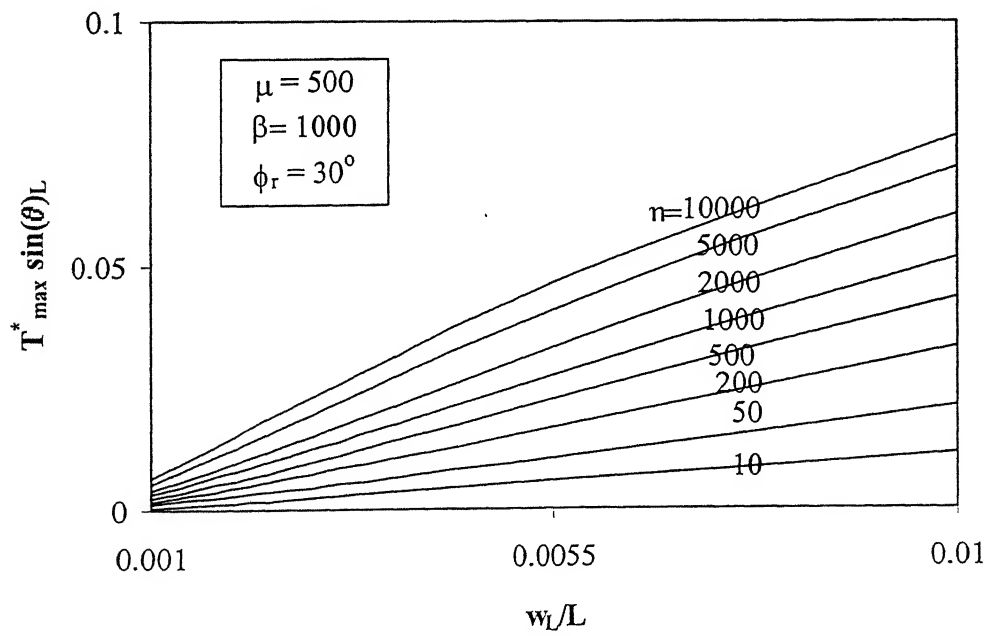


Fig. 3.71 Variation of maximum Normalized Normal Component of Tension with  $w_L/L$  – Effect of  $\eta$

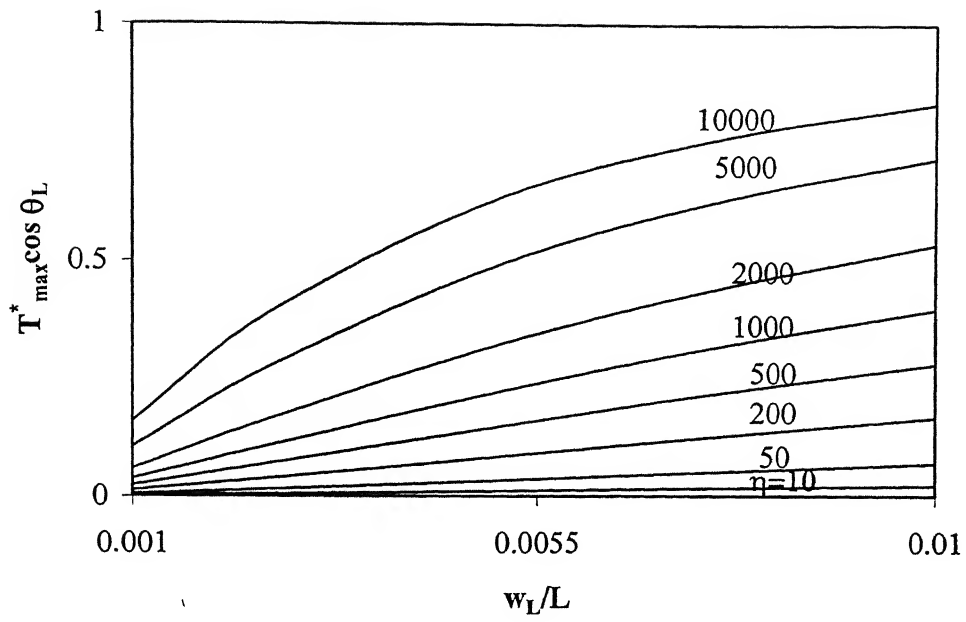


Fig. 3.72 Variation of Maximum Normalized Horizontal Component of Tension with  $w_L/L$  – Effect of  $\eta$

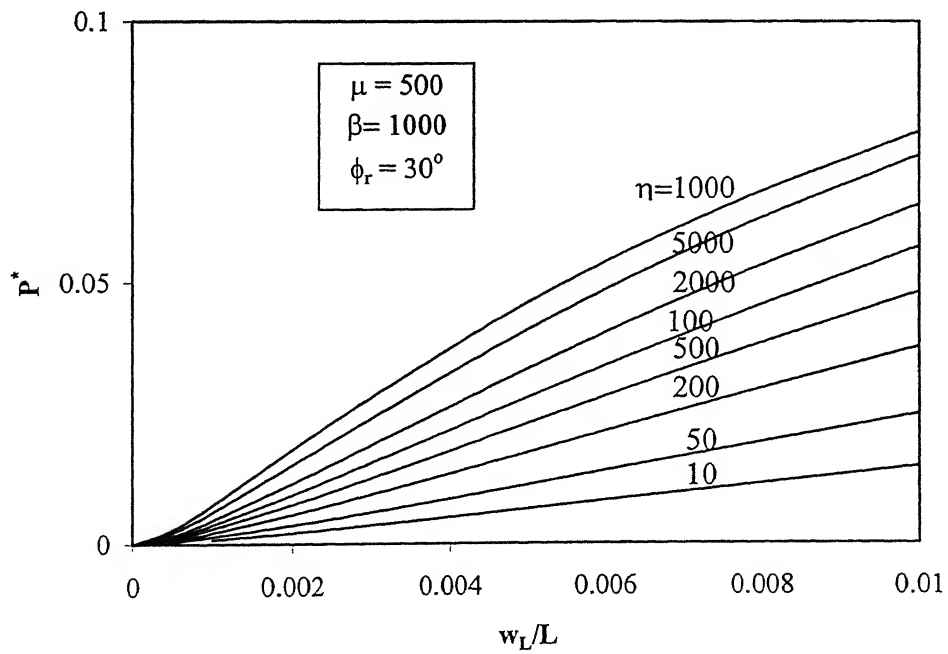


Fig. 3.73 Variation of Normalised Transverse Force with  $w_L/L$  - Effect of  $\eta$

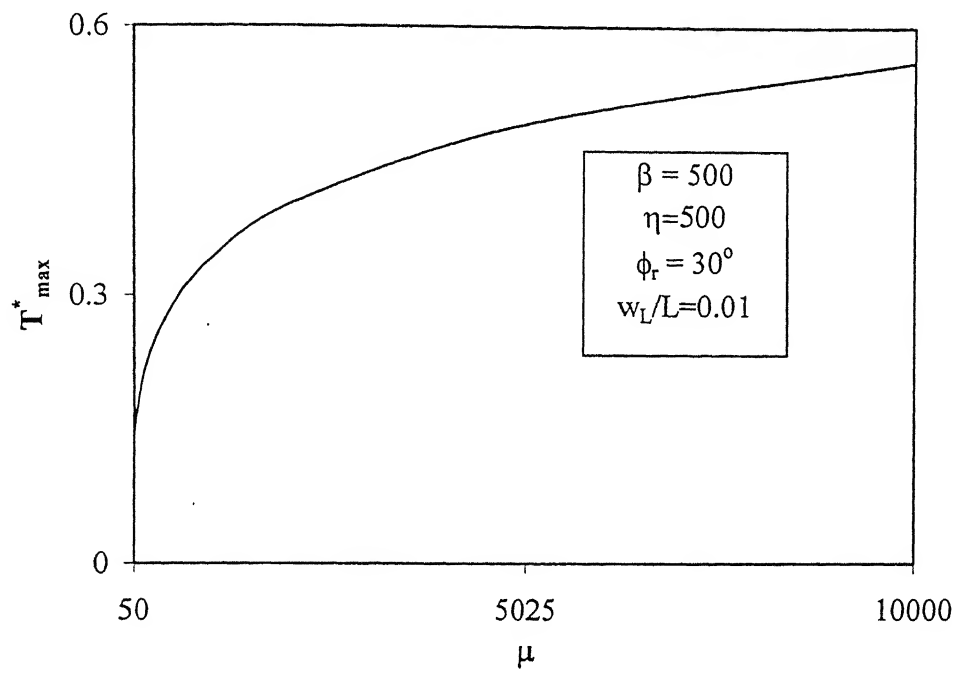


Fig. 3.74 Variation of Normalized Maximum Tension with  $\mu$

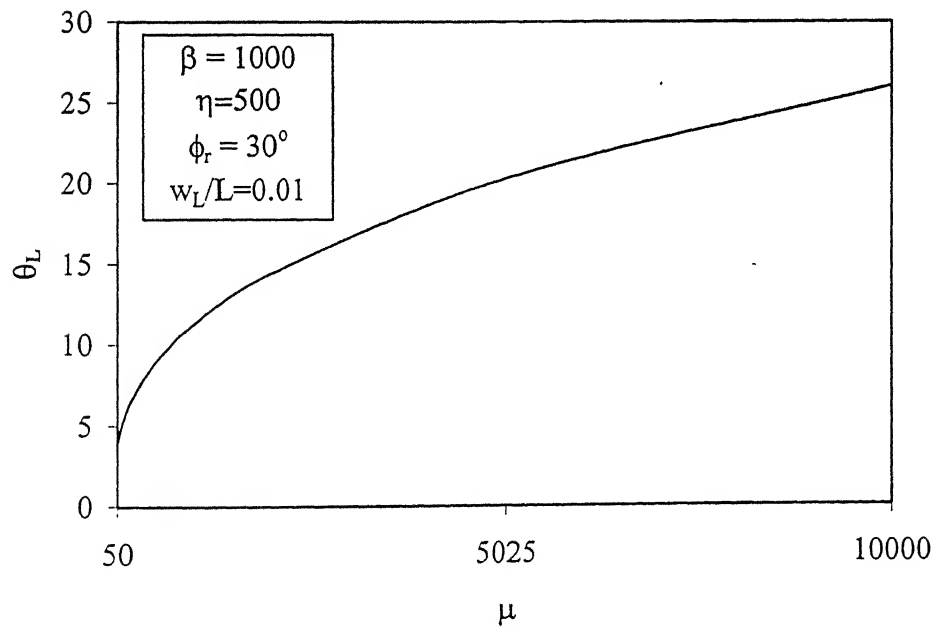


Fig. 3.75 Variation of Inclination of Reinforcement at  $x=L$  with  $\mu$

The trends of variations of normalized normal component of tension,  $T_{\max}^* \sin \theta_L$  (Fig. 3.76) and normalized horizontal component of tension,  $T_{\max}^* \cos \theta_L$ , (Fig. 3.77) with relative stiffness of soil,  $\mu$  are similar to that of the variation of  $T_{\max}^*$  with  $\mu$  (Fig. 3.74). The pullout force is less than the axial capacity for the entire range of  $\mu$  from 50-10,000 for a free end displacement,  $w_L$  equal to  $0.01L$ , and for  $\beta=1000$ ,  $\eta=500$  and  $\phi_r=30^\circ$ .

The variation of normalized transverse force,  $P^*$ , with relative stiffness of soil,  $\mu$ , is presented in Fig. 3.78. The transverse force required to enforce a given free end displacement,  $w_L$ , increases with  $\mu$  because of increase in the shear resistance along the reinforcement-soil interface due to mobilization of higher normal stresses.

The normal stresses developed in the soil decrease with increase in ultimate resistance of the soil (i.e with decreasing  $\beta(=k_s L/q_{ult})$  value) and hence the variation of normalized maximum tension,  $T_{\max}^*$ , with  $\beta$  as shown in Fig. 3.79 is observed.

The inclination of reinforcement,  $\theta_L$ , decreases asymptotically with increasing  $\beta$  (Fig. 3.80) because of the phenomena of localization of transverse displacements near the right end for large  $\beta$  values.

The trends of variations of  $T_{\max}^* \sin \theta_L$  (Fig. 3.81) and  $T_{\max}^* \cos \theta_L$  (Fig. 3.82) with  $\beta$  are similar to that of  $T_{\max}^*$  with  $\beta$  (Fig. 3.80). The pullout force is just 22% of the axial pullout capacity for  $\beta=1000$ ,  $\mu=500$ ,  $\eta=500$ ,  $w_L/L=0.01$  and  $\phi_r=30^\circ$ .

The normalized transverse force,  $P^*$ , decreases with increase in  $\beta$  but becomes constant at large  $\beta$  (Fig. 3.83) when the shear resistance mobilized at the interface reaches the maximum shear resistance.

The shear resistance mobilized along the reinforcement is higher for relatively higher shear stiffness of the interface (i.e for large  $\eta$  value). At some stage, the shear stress reaches the maximum value equal to the full mobilization case. Hence, the rate of increase of tension decreases with increase in  $\eta$  value and for large  $\eta$  ( $\eta=10,000$ ), it becomes nearly constant indicating the full shear mobilization condition (Fig. 3.84)

The maximum inclination of the reinforcement,  $\theta_L$ , decreases rapidly for small initial shear stiffness of soil but becomes nearly constant at large  $\eta$  values ( $\eta \geq 5,000$ ) (Fig. 3.85).

The trends of variations of normalized normal component of tension,  $T_{\max}^* \sin \theta_L$  (Fig. 3.86) and normalized horizontal component of tension,  $T_{\max}^* \cos \theta_L$  (Fig. 3.87), with  $\eta$  are similar to the variation of maximum tension developed at  $x=L$  with  $\eta$  (Fig. 3.84).

The normalized transverse force,  $P^*$ , increases with  $\eta$  due to increase in the shear resistance mobilized along the interface. At large  $\eta$ , the shear resistance reaches the full (maximum) shear resistance along the interface and hence becomes almost constant. The  $\eta \geq 5000$ ,  $P^*$  becomes almost constant for  $\mu=500$ ,  $\beta=1000$ ,  $\phi_r=30^\circ$  and  $w_L/L=0.01$  (Fig. 3.88).

The variation of normalized shear mobilized ( $\tau^* = \tau/\gamma D_e$ ) along the reinforcement for varying  $\eta$  is shown in Fig. 3.89. The shear mobilized remains constant for some portion of the length measured from the left end because of the rigid body movement over this portion of reinforcement. As the mobilization of transverse displacement and displacement of interface takes place, the shear mobilized increases from the constant value but reaches a value of zero at the right end where transverse force is applied (since the displacement of interface is assumed zero at this point). For  $\eta \geq 2000$ , there is no further increment in shear mobilization as the shear mobilization reaches its ultimate value.

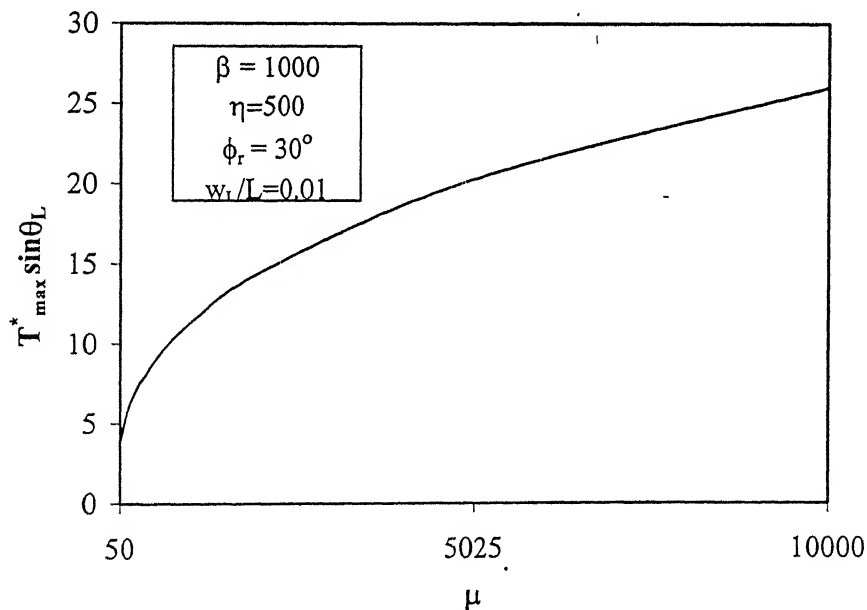


Fig. 3.76 Variation of Normalized Maximum Normal Component of Tension with  $\mu$

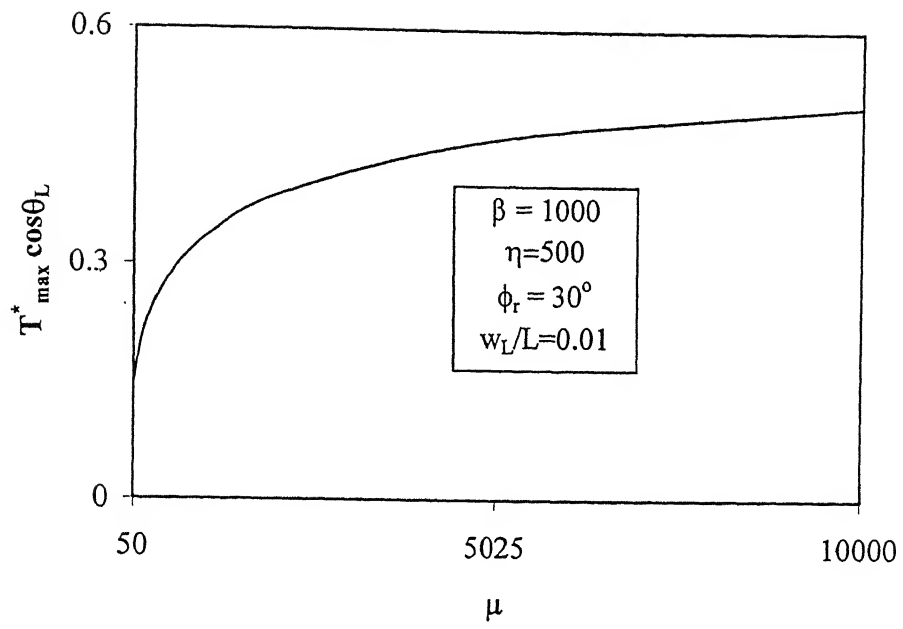


Fig. 3.77 Variation of Normalized Maximum Horizontal Component of Tension with  $\mu$

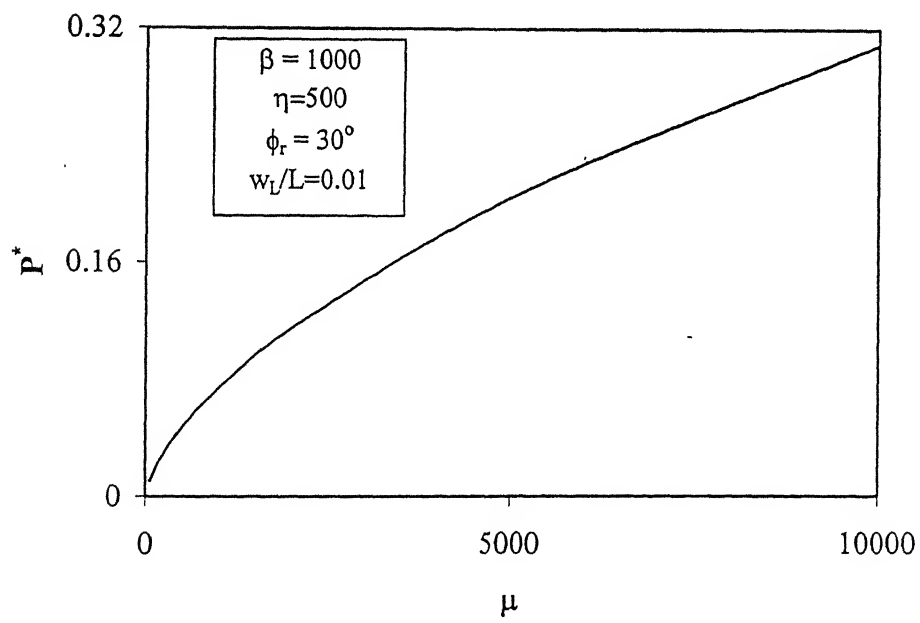


Fig. 3.78 Variation of Normalized Transverse Force with  $\mu$

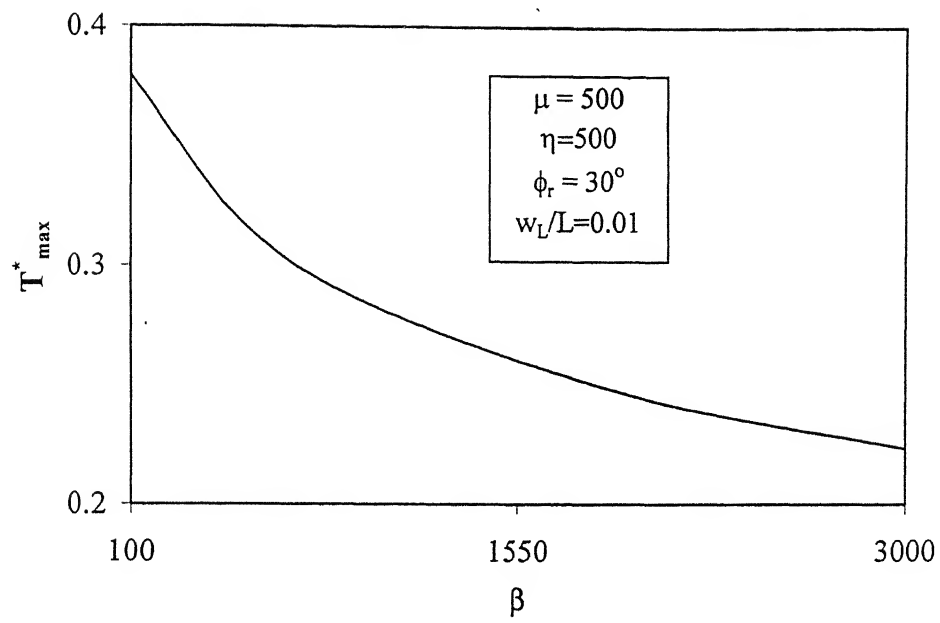


Fig. 3.79 Variation of Normalized Maximum Tension with  $\beta$

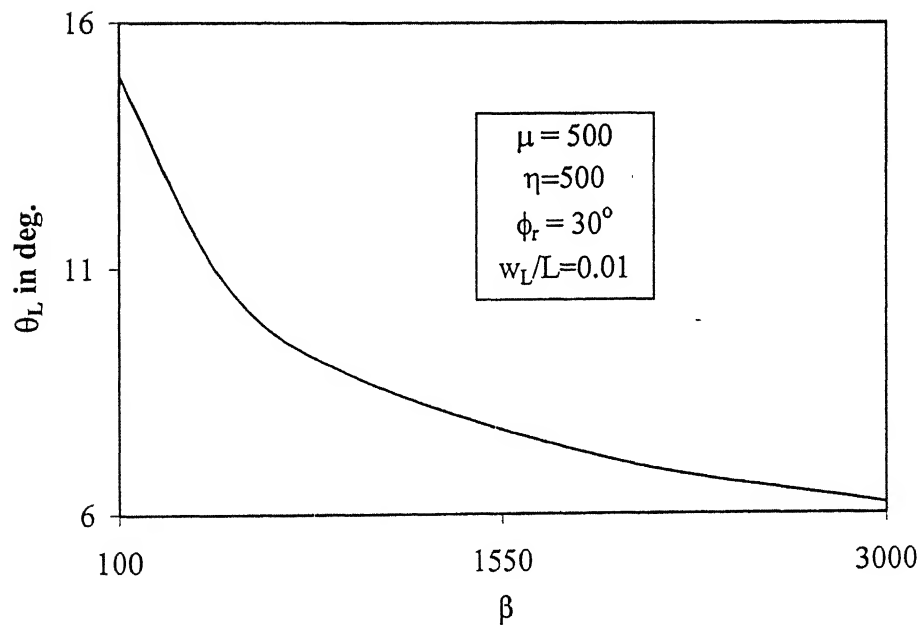


Fig. 3.80 Variation of Inclination of Reinforcement at  $x=L$  with  $\beta$

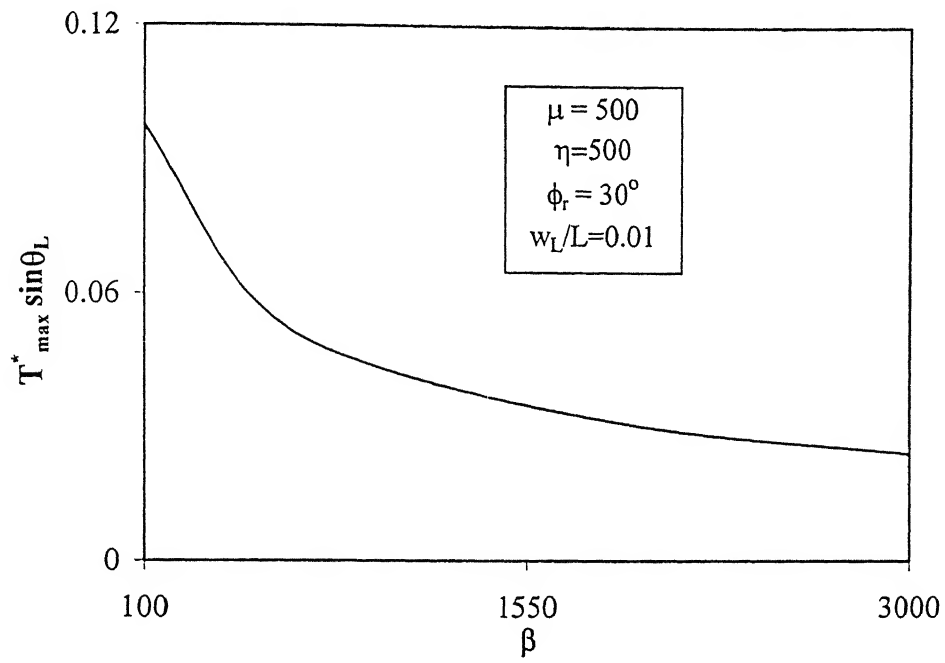


Fig. 3.81 Variation of Normalized Maximum Normal Component of Tension with  $\beta$

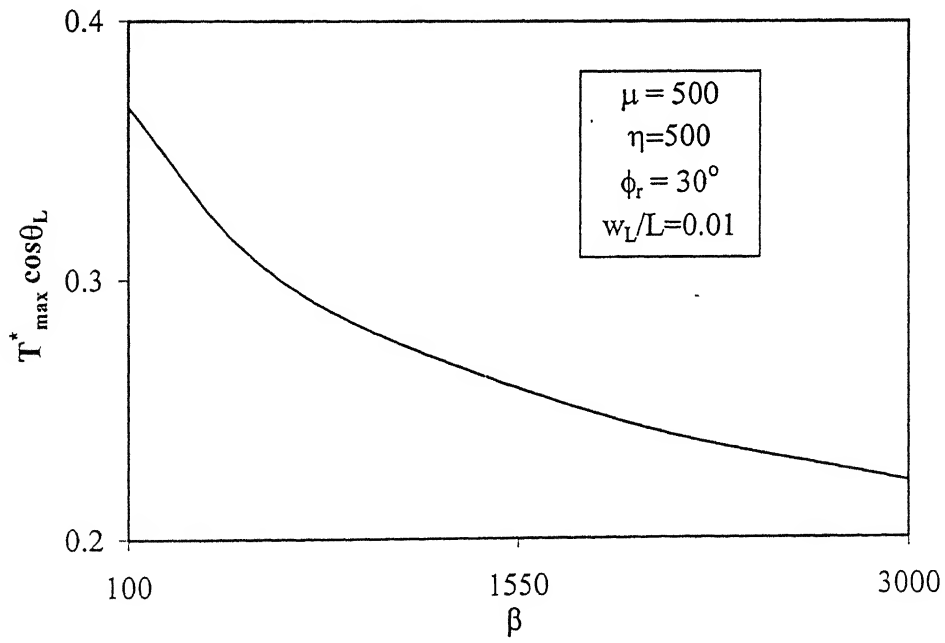


Fig. 3.82 Variation of Normalized Maximum Horizontal Component of Tension with  $\beta$

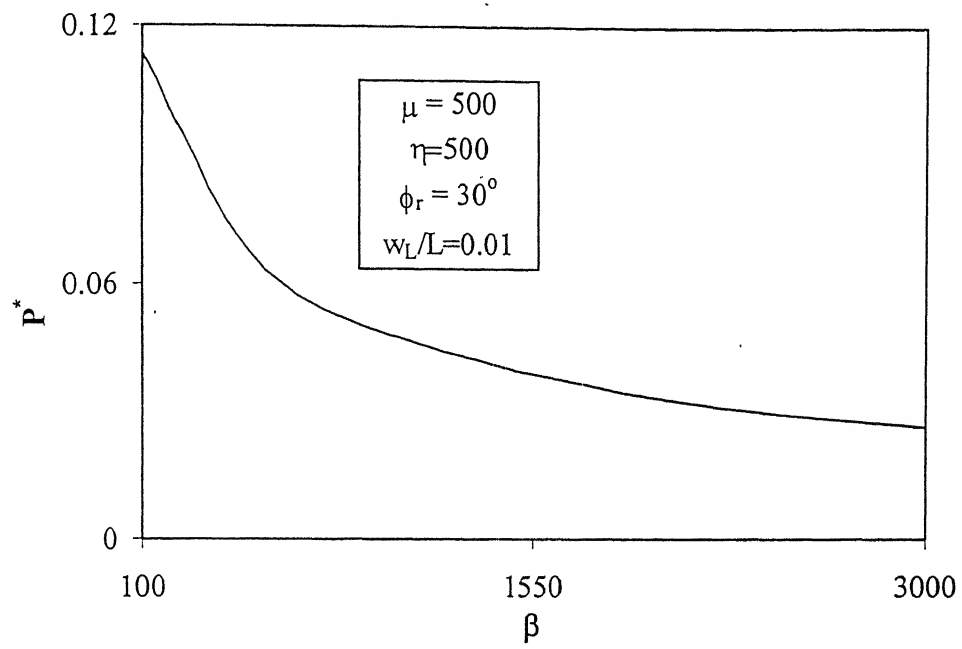


Fig. 3.83 Variation of Normalized Transverse Force with  $\beta$

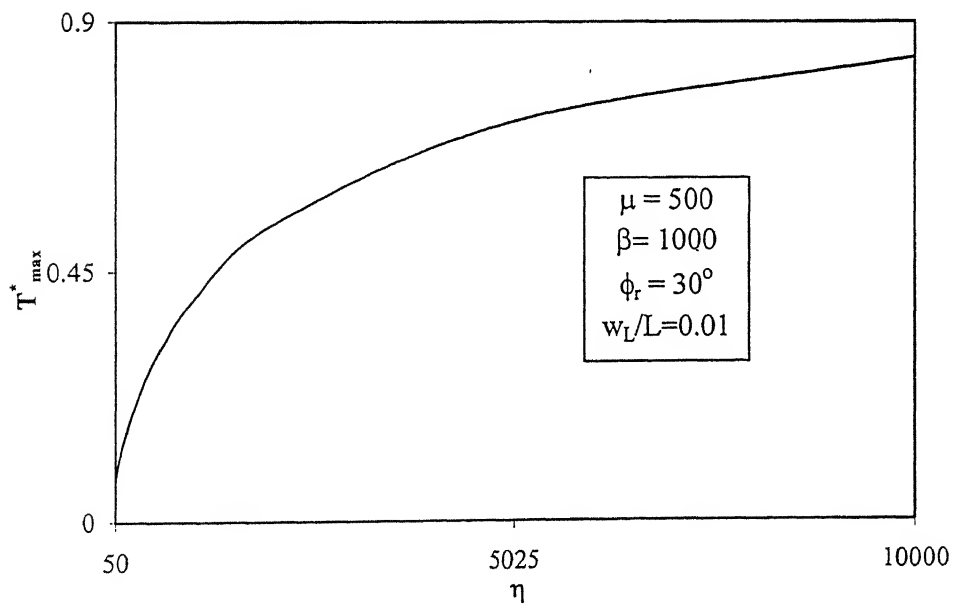


Fig. 3.84 Variation of Normalized Maximum Tension with  $\eta$

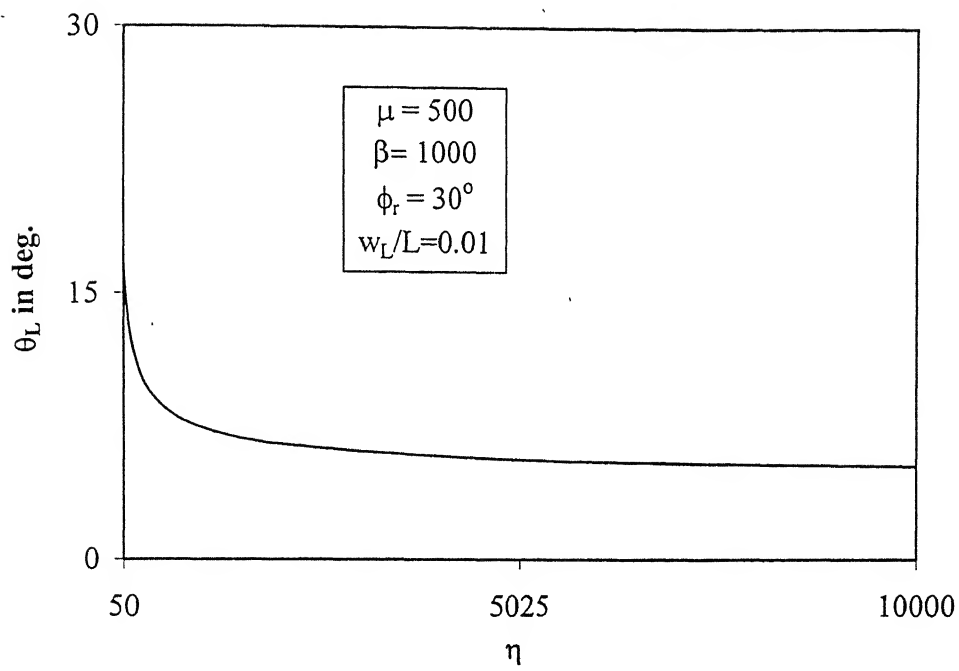


Fig. 3.85 Variation of Inclination of Reinforcement at  $x=L$  with  $\eta$

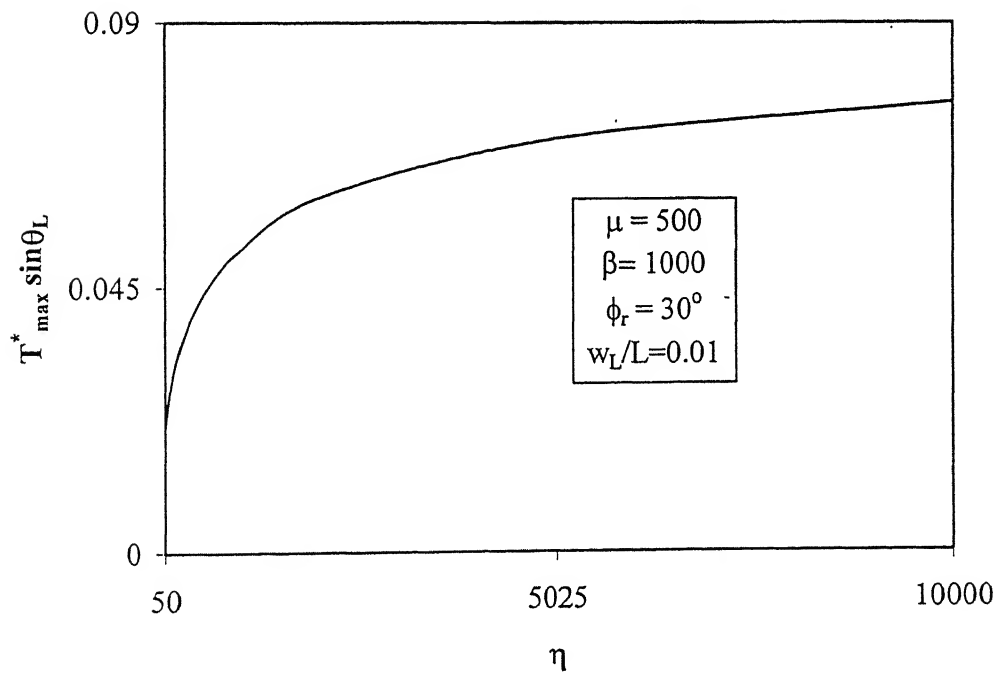


Fig. 3.86 Variation of Normalized Maximum Normal Component of Tension with  $\eta$

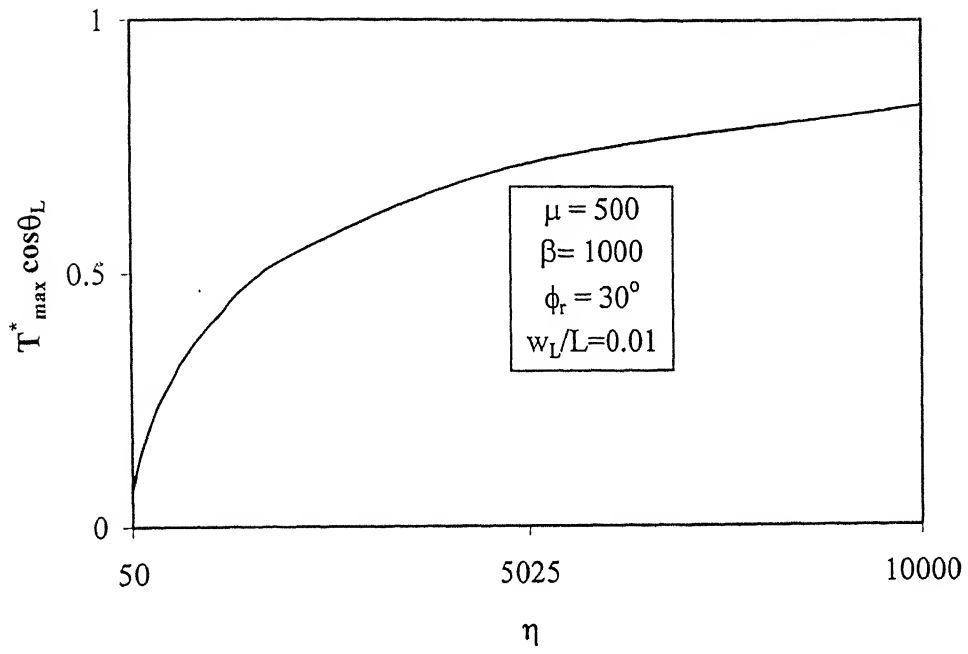


Fig. 3.87 Variation of Normalized Maximum Horizontal Component of Tension with  $\eta$

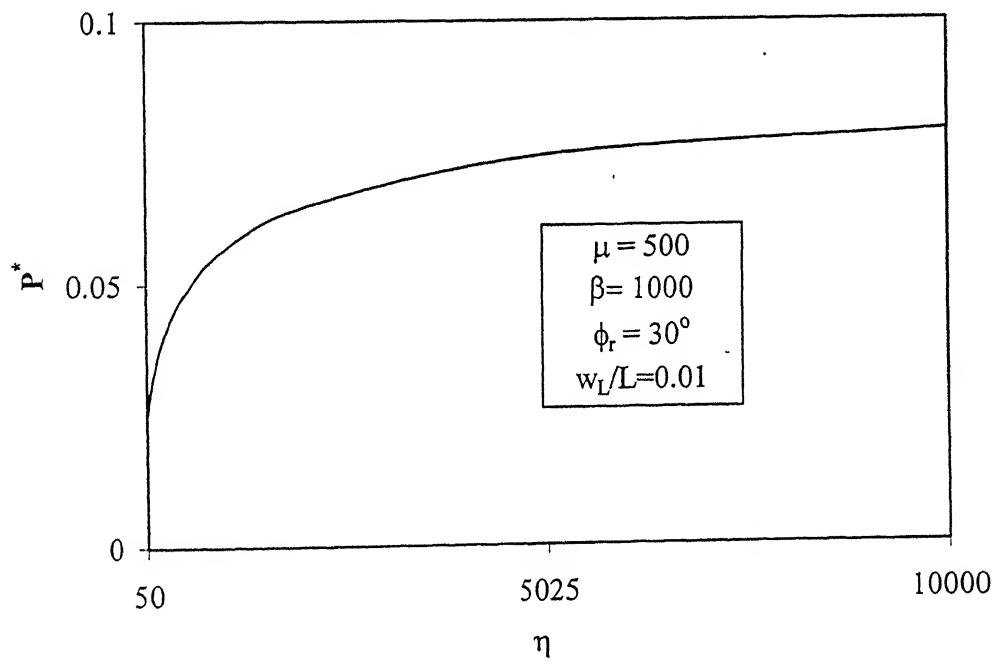


Fig. 3.88 Variation of Normalized Transverse Force with  $\eta$

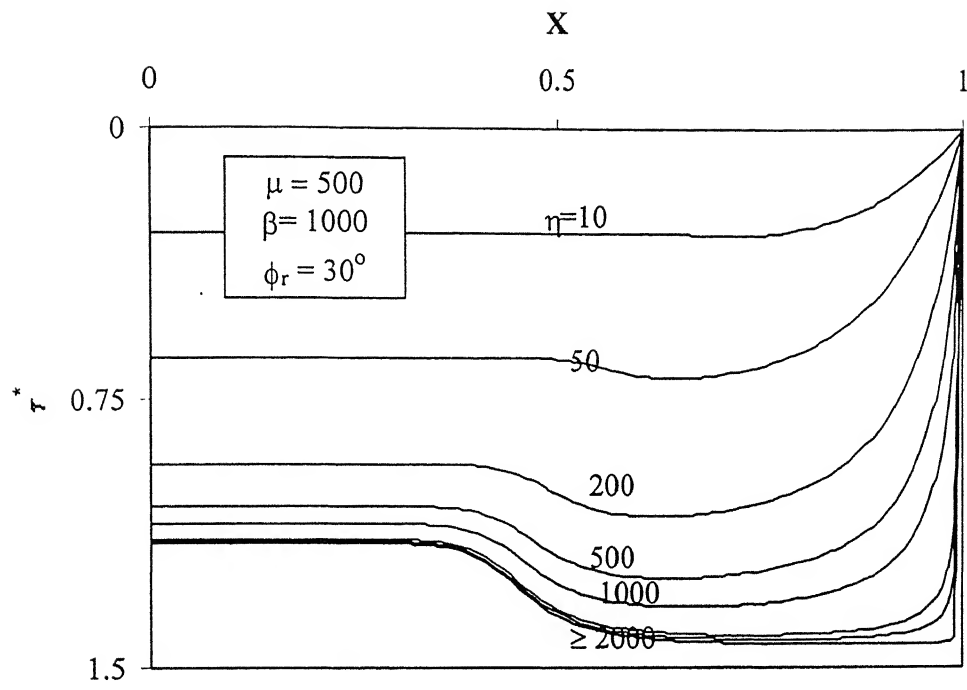


Fig 3.89 Variation of Normalized shear Resistance with Normalized distance

## Chapter 4

# Analyses for Extensible Reinforcement subjected to Transverse Downward Force/Displacement

### 4.1 General

The previous models dealt with the analyses of an inextensible reinforcement subjected to a transverse downward displacement at the right end. This chapter focuses on the analyses of an extensible reinforcement subjected to free end transverse downward displacement. Burd (1995) in the analysis of membrane action in reinforced unpaved roads, proposed a method for the determination of length of extensible reinforcement over which shear stress is mobilized. Burd's theory is applied to the present problem to locate the position on the reinforcement where tension becomes zero. The length over which the shear stress is mobilized is defined as the "active length of reinforcement". The main difference in the analyses of inextensible and extensible reinforcements lies in the fact that the shear stresses are mobilized over the entire length of an inextensible reinforcement whereas they are mobilized only over the active length for an extensible reinforcement. The analyses are carried out assuming full mobilization of shear resistance along the sheet-soil interface. The analysis is carried out for two cases: (i) assuming the response of the soil to transverse displacements to be linear (linear subgrade) and (ii) assuming the response of the soil to transverse displacements to be non-linear (non-linear subgrade).

### 4.2 Problem Statement

An extensible sheet reinforcement of stiffness,  $J$ , and length,  $L$ , is embedded at a depth,  $D_e$ , in a soil of unit weight,  $\gamma$  (Fig. 4.1). The interface shear resistance between the reinforcement and the soil is characterized by the angle,  $\phi_r$  ( $\leq \phi$ , the angle of shearing resistance of the soil). The problem is to analyze the displacement profile of and the tension mobilized in the reinforcement due to transverse force,  $P$ , applied at point B. Alternatively, the displacement profile and the transverse force due to a given transverse displacement,  $w_L$ , of the point, B, are to be evaluated.

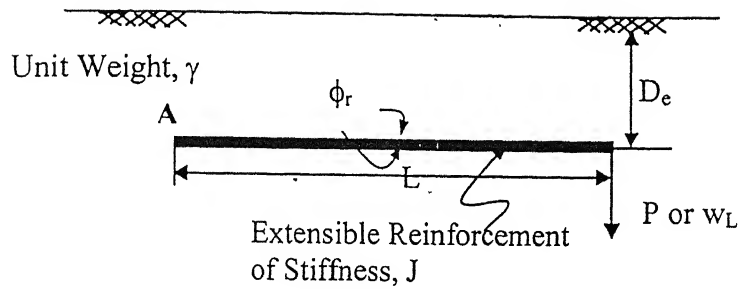


Fig. 4.1 Definition Sketch

### 4.3 Procedure for Locating Active Length of Reinforcement

AB is the undeformed shape of the extensible reinforcement (Fig. 4.2). As the reinforcement is extensible, some portion  $A-A^1$  of the reinforcement remains intact whereas the portion of the reinforcement between  $A^1$  and B undergoes transverse as well as horizontal displacements under the application of transverse displacement/force at point B. Thus the shear stresses are mobilized only in the stretch  $A^1-B$  of the reinforcement as shown in Fig. 4.2. No tension is mobilized at and to the left of point  $A^1$ . This length ' $A^1B$ ' over which the shear stresses are mobilized is defined as the "active length of reinforcement",  $x_o$ . The active length of reinforcement,  $x_o$ , is obtained by equating the change of reinforcement length associated with change in geometry to the length increase compatible with the strains associated with the developed tensile

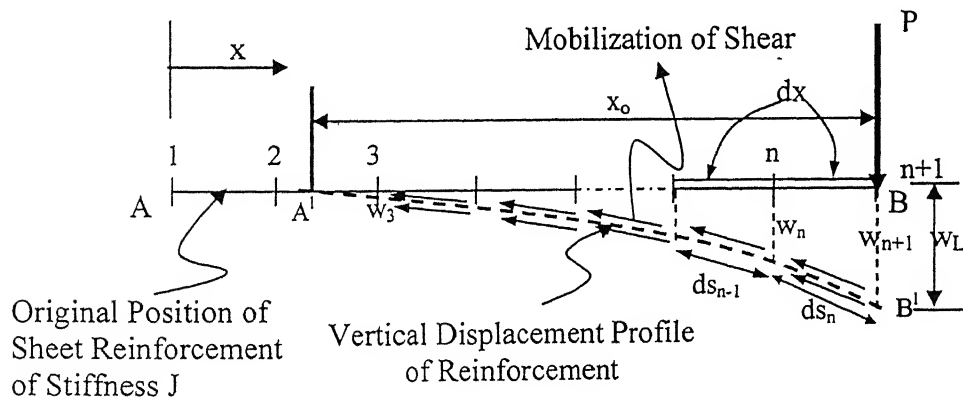


Fig. 4.2. Deformed Shape and Shear Stress Mobilization of Extensible Reinforcement

stresses along the reinforcement. Thus the increased length of the portion of reinforcement,  $A^1B$ , due to tensile stresses along the reinforcement should equal the

length between  $A^1-B^1$  obtained from the change in geometry of the portion,  $A^1B$  due to the application of downward displacement/force. To locate the position of  $A^1$ , the reinforcement length is discretized into ' $n_e$ ' elements [1,2,3....(n+1) nodes]. The position of  $A^1$  is located by traversing from  $(n+1)^{th}$  node towards node 1. As there is no shear stress mobilized to the left of  $A^1$ , the tension developed at all nodes to the left of and at  $A^1$  is zero. Supposing that  $A^1$  corresponds to some node  $j$  ( $1 \leq j < n+1$ ), the extended length of reinforcement between  $A^1-B$ , calculated from the reinforcement strains is

$$L_\epsilon^1 = x_o + \int_{L-x_o}^L \frac{T(x)}{J} dx \quad (4.1)$$

where  $T(x)$  is the tension developed in the reinforcement at distance  $x$ .

In finite difference form, the above equation becomes

$$L_\epsilon^1 = x_o + \sum_{i=j}^n \frac{T_i(x)}{J} dx_i \quad (4.2)$$

where  $T_i(x)$  is the average tension developed in the  $i^{th}$  element.

The length of reinforcement between  $A^1-B$ , calculated from the change in geometry due to enforced transverse displacement/force at point B, is given by

$$L_g^1 = \int_{L-x_o}^L \sqrt{1 + \left( \frac{dw}{dx} \right)^2} dx \quad (4.3)$$

In finite difference form, Eq. (4.3) becomes

$$L_g^1 = \sum_{i=j}^n \sqrt{1 + \left( \frac{dw_i}{dx_i} \right)^2} dx_i \quad (4.4)$$

Eqs. (4.2) and (4.4) after normalizing reduce to

$$L_\epsilon^1 = X_o + \sum_{i=j}^n \frac{T_i^*(x)}{J^*} \sqrt{\left( \frac{w_L}{L} \right)^2 (w_{i+1} - w_i)^2 + \left( \frac{1}{n-1} \right)^2} \quad (4.5)$$

$$L_g^1 = \sum_{i=n}^j \sqrt{\left( \frac{w_L}{L} \right)^2 (w_{i+1} - w_i)^2 + \left( \frac{1}{n-1} \right)^2} \quad (4.6)$$

where  $L_e^{\star} = L_e^{\star} / L$ ,  $L_g^{\star} = L_g^{\star} / L$ ,  $X_o = x_o / L$ ,  $T^{\star} = T / T_{\max}$ ,  $T_{\max} = 2\gamma D_e L \tan \phi_r$  – the maximum pullout force and  $J^{\star} = J / 2\gamma D_e L \tan \phi_r$ , the relative stiffness of the reinforcement.

$X_o$  is to be located iteratively. Suppose in the process of node traversing to locate  $X_o$ , one is at node 'k', the boundary conditions to solve the governing equations for a given model (linear subgrade/non-linear subgrade) are: the tension developed in the reinforcement at and all nodes to the left of 'k' are zero, i.e.  $T_i = 0.0$ , for  $1 \leq i \leq k$  and the slope at node 'k' is zero, i.e.,  $(dw/dx)_i$  [or  $(dW/dX)_i$ ] = 0 at  $i=k$ . while at the right end, i.e. at  $x=L$  or  $X = 1.0$ , the displacement  $w = w_L$  (or  $W = 1.0$ ).

Using the above boundary conditions, the governing equations for assumed model (Linear subgrade model/Non-linear subgrade model) and the stiffness of the reinforcement for a given free end displacement at the right end are solved to obtain the displacement profile and the tensions developed along the reinforcement.  $L_e^{\star}$  and  $L_g^{\star}$  are evaluated from Eqs. (4.5) and (4.6) and equated. In case they are unequal, another immediate node to the left of node k, i.e. (k-1) is selected and the above procedure repeated. This process of node traversing is continued until the lengths,  $L_e^{\star}$  and  $L_g^{\star}$  computed from Eqs. (4.5) and (4.6) equal. To start with, k is taken to be at node (n+1) and 'k' is traversed from node (n+1) towards 1. The maximum value of  $X_o$  can be 1.0 i.e,  $x_o=L$ , the full length of reinforcement (the case in which the shear stresses are mobilized for the entire length of the reinforcement).

## 4.4 Analyses

### 4.4.1 Linear Subgrade – Model I

#### 4.4.1.1 The Model

The extensible reinforcement sheet acted upon by a transverse force, P, or a transverse displacement,  $w_L$ , is subjected to uniform normal stresses of intensity,  $q_t$  ( $=\gamma D_e$ ) on the top and stresses of intensity,  $q_b(x)$ , on the bottom surfaces of the reinforcement (Fig. 4.3a). The soil below the reinforcement generates additional

stresses, i.e.  $(q_b - q_t)$  due to the downward displacement,  $w_L$ . The response is represented by a set of Winkler springs (Fig. 4.3b). A typical linear stress-displacement response is considered for response of the soil and hence for the Winkler springs (Fig. 4.3c).

Stress-displacement response of the subgrade or the Winkler springs is defined by the expression

$$(q_b - q_t) = k_s w \quad (4.7)$$

where  $w$  is the normal displacement and  $k_s$  is the modulus of subgrade reaction of the ground.

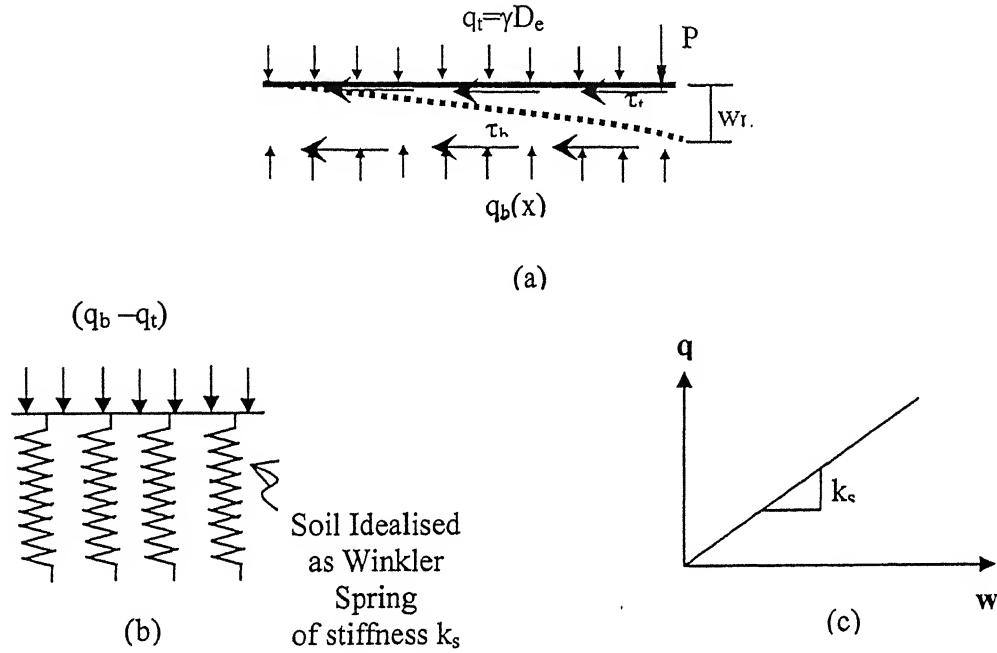


Fig. 4.3 (a) Forces acting on Sheet Reinforcement and (b) Idealization of Soil (c) Stress Displacement Response of Soil.

#### 4.4.1.2 Analysis

The equilibrium of forces on an element (Fig 4.4) of infinitesimal length,  $\Delta x$ , and unit width is considered. The tensile forces and the inclination of the left and right ends of the element are respectively,  $T$  and  $(T + \Delta T)$ , and  $\theta$  and  $(\theta + d\theta)$  at distances  $x$  and  $(x + \Delta x)$  from the left end (Point A) of the sheet (Fig. 4.4).

Considering the equilibrium of forces in the horizontal and vertical directions, one gets

$$\sum F_x = (T + dT) \cos(\theta + d\theta) - T \cos \theta - (q_t + q_b) \tan \phi_r \Delta x = 0 \quad (4.8)$$

$$\sum F_y = (T + dT) \sin(\theta + d\theta) - T \sin \theta - (q_b - q_t) \Delta x = 0 \quad (4.9)$$

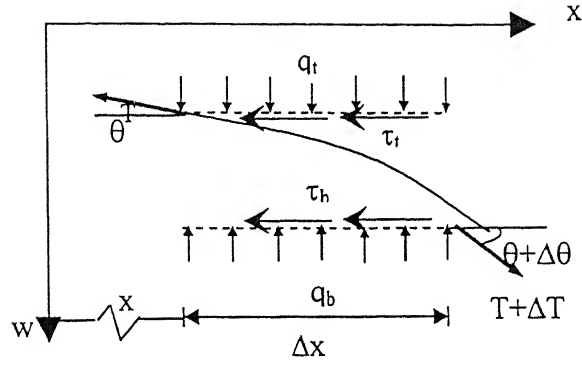


Fig. 4.4 Forces on Infinitesimal Element

For small deformations, as  $\Delta\theta \rightarrow 0$ ,  $\cos \Delta\theta \rightarrow 1$  and  $\sin \Delta\theta \rightarrow 0$ . Neglecting second order terms, Eqs. 4.8 and 4.9 get simplified respectively to

$$\cos \theta \left( \frac{dT}{dx} \right) - T \sin \theta \left( \frac{d\theta}{dx} \right) - (q_t + q_b) \tan \phi_r = 0 \quad (4.10)$$

$$\sin \theta \left( \frac{dT}{dx} \right) + T \cos \theta \left( \frac{d\theta}{dx} \right) - (q_b - q_t) = 0 \quad (4.11)$$

Multiplying Eq. 4.9 by  $\cos \theta$  and Eq. 4.10 by  $\sin \theta$  and adding the two, one gets

$$\frac{dT}{dx} = (q_t + q_b) \cos \theta \tan \phi_r + (q_b - q_t) \sin \theta \quad (4.12)$$

Similarly, multiplying Eq. 4.10 by  $\sin \theta$  and Eq. 4.11 by  $\cos \theta$  and subtracting the latter from the former, one gets

$$-T \frac{d\theta}{dx} - (q_t + q_b) \tan \phi_r \sin \theta + (q_b - q_t) \cos \theta = 0 \quad (4.13)$$

But  $\tan \theta = dw/dx$ , where  $w$  is the normal displacement at a distance,  $x$ , from point A. Differentiating with respect to  $x$ , one gets

$$\frac{d\theta}{dx} = \cos^2 \theta \frac{d^2 w}{dx^2} \quad (4.14)$$

Combining Eqs. 4.7, 4.12, 4.13 and 4.14, the following equations are obtained

$$\frac{dT}{dx} = (q_i + q_b) \cos \theta \tan \phi_r + k_s w \sin \theta \quad (4.15)$$

$$-T \cos^2 \theta \frac{d^2 w}{dx^2} + K_s w \cos \theta = (q_i + q_b) \sin \theta \tan \phi_r \quad (4.16)$$

For small  $\theta$ , Eqs. 4.15 and 4.16 reduce to

$$\begin{aligned} \frac{dT}{dx} &= (q_i + q_b) \tan \phi_r \\ &= (q_b - q_i + 2q_i) \tan \phi_r \\ &= (k_s w + 2\gamma D_e) \tan \phi_r \end{aligned} \quad (4.17)$$

$$-T \frac{d^2 w}{dx^2} + k_s w = 0 \quad (4.18)$$

Eqs. 4.17 and 4.18 are the governing equations for the problem under consideration. Eqs. 4.17 and 4.18 are non-dimensionalised with  $X=x/L$ ,  $W=w/w_L$  and  $T^*=T/T_{\max}$  where  $w_L$  is the normal displacement at the right end, i.e,  $x=L$  or  $X=1.0$  and  $T_{\max}=2\gamma D_e L \tan \phi_r$ , the maximum axial pullout force. Eqs. 4.17 and 4.18 become

$$\frac{dT^*}{dX} = \frac{1}{2} \left( \mu \frac{w_e}{L} W + 2 \right) \quad (4.19)$$

$$-T^* \frac{d^2 W}{dX^2} + \frac{\mu W}{2 \tan \phi_r} = 0 \quad (4.20)$$

where  $\mu = \frac{k_s L}{\gamma D_e}$  is relative stiffness factor.

#### 4.4.1.3 Numerical Solution

As an analytical solution is not possible, a numerical finite difference procedure is proposed. The reinforcement length,  $L$ , is divided into 'n' sub-elements each of length,  $\Delta L=L/n$  or  $\Delta X=1/n$  as shown in Fig. 4.5. Eqs. 4.19 and 4.20 in finite difference form become

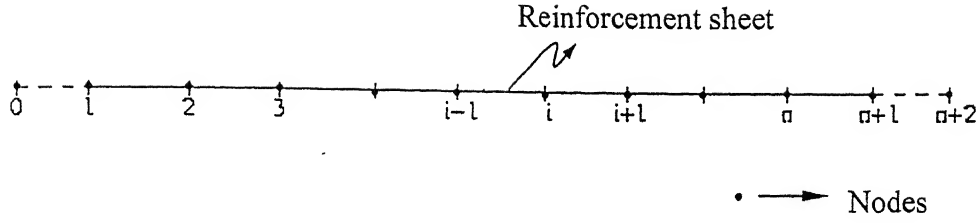


Fig. 4.5 Discretisation of Reinforcement Length into Elements

$$\frac{T_{i+1}^* - T_i^*}{\Delta X} = \frac{1}{2} \left( \mu W_i \frac{w_o}{L} + 2 \right) \quad (4.21)$$

$$-T_i^* \left( \frac{W_{i-1} - 2W_i + W_{i+1}}{\Delta X^2} \right) + \frac{\mu W_i}{2 \tan \phi_r} = 0 \quad (4.22)$$

Solving for normalized displacement and normalized tension, one gets

$$W_i = \frac{T_i^* n^2 (W_{i-1} + W_{i+1})}{\left( 2n^2 T_i^* + \frac{\mu}{2 \tan \phi_r} \right)} \quad (4.23)$$

$$T_{i+1}^* = \frac{1}{2} \left( \mu W_i \frac{w_o}{L} + 2 \right) + T_i^* \quad (4.24)$$

The procedure as described in section 4.3 is used to locate  $x_o$  using the above governing Eqs. (4.23) and (4.24) for the model. The displacement and the tensions corresponding to the node at which  $X_o$  is attained are the actual displacement profile and the tensions along the reinforcement for the extensible reinforcement.

The transverse force,  $P$ , required to cause the displacement,  $w_L$ , is obtained as part of the response by integrating the soil reaction mobilized as

$$P = \int_0^L k_s w dx \quad (4.25)$$

As the reinforcement length is discretised into 'n' elements and transverse force,  $P$ , is obtained as

$$P = k_s \Delta x \left[ \frac{w_1 + w_{n+1}}{2} + \sum_{i=2}^n w_i \right] \quad (4.26)$$

The transverse force in normalized form is

$$P^* = \frac{P}{\gamma D_e L} = \mu \frac{w_o}{L} \frac{1}{n} \left[ \frac{W_1 + 1}{2} + \sum_{i=2}^n W_i \right] \quad (4.27)$$

For a given free end displacement,  $w_L/L$ , applied at the free end, the variations of various quantities are presented and discussed in the section 4.4.2.4. The procedure as detailed in section 4.3 is adopted to arrive at the active length of reinforcement, normal displacement profiles and the tension profiles along the reinforcement. The normalized transverse force required to enforce the free end displacement,  $w_L/L$ , is then obtained by Eq. (4.27).

#### 4.4.1.4 Characteristics of the Model

A simple mathematical model has been developed to study the response of extensible sheet reinforcement subjected to transverse displacement/force. With the application of an applied transverse load or displacement, reinforcement interacts with the soil and as a consequence shear stresses at the interface of and tensile forces in the reinforcement are generated. The reinforcement-soil interface is characterized by the interface friction angle ( $\phi_r$ ). The normal stresses generated due to transverse load application are assumed to increase linearly with normal displacement. But in reality, soil exhibits a non-linear relationship between stress and displacement. This drawback is overcome by assuming a hyperbolic relation between stress and displacement and the solution obtained is given in the subsequent section. The model proposed herein takes into account the stiffness of reinforcement in the analysis. A limitation of this model is that under large displacements or applied transverse load, the assumption of small angles is not appropriate. Consideration of active length,  $x_o$ , appears to be appropriate in the context of extensible reinforcements.

#### 4.4.1.5 Results and Discussions

The stiffness of the geosynthetic reinforcement,  $J$ , range from 0-10,000 kN/m. Hence, the relative stiffness of reinforcement,  $J^* (= J/2\gamma D_e L \tan\phi_r)$ , is found to vary from 1 to 1,000.

For a given stiffness of reinforcement, the normalized active length of reinforcement,  $X_o$ , increases with increase in free end displacement (Fig.4.6). The rate

of increase of  $X_0$  increases with the reinforcement stiffness. For  $J^*=1.0$ , a length of only  $0.06L$  mobilizes shear resistance whereas shear resistance is mobilized over the entire length for  $J^*=5000$  for  $\mu=500$ ,  $w_L/L \geq 0.005$  and  $\phi_r=30^\circ$ . The full shear resistance is mobilized over the entire length even at small free end displacements for very stiff reinforcements ( $X_0=L$  at  $w_L/L=0.0075$  for  $J^*=2000$ ,  $\mu=500$  and  $\phi_r=30^\circ$ ).

The effect of relative stiffness of reinforcement,  $J^*$ , on the variation of normalized normal displacement with normalized distance is presented in Fig. 4.7. The point of mobilization of transverse displacements moves towards the left end with increasing relative stiffness of the reinforcement. The length over which the transverse displacements are mobilized for extensible reinforcement with relative stiffness,  $J^*$ , equal to 1, is just  $0.05L$  whereas it is about  $0.15L$  for reinforcement with  $J^*=50$  for  $w_L/L=0.01$ ,  $\mu=500$  and  $\phi_r=30^\circ$ . For very stiff (inextensible reinforcement), the normal displacement profile is identical to the one obtained by considering the shear mobilization for the entire length (Model 1a). The normal displacement profile obtained for  $J^* \geq 1000.0$  and from Model 1a are identical for  $w_L/L=0.01$ ,  $\mu=500$  and  $\phi_r=30^\circ$ .

The variations of normalized tension with normalized distance for relative stiffness of the reinforcement,  $J^*=1, 10, 50, 100, 250, 500$  and  $\geq 1000$  for  $w_L/L=0.01$ ,  $\mu=500$  and  $\phi_r=30^\circ$ , are depicted in Fig. 4.8. As the stiffness increases, large tracts of reinforcement-soil interfaces mobilize shear resistance. For  $J^*=1$ , shear resistance is mobilized only over a length of  $0.01L$  from the right end whereas for  $J^* \geq 1000$ , shear resistance is mobilized over the entire length of reinforcement. For a given relative stiffness of the reinforcement, the tension increases linearly over the initial portion of the reinforcement, the variation becoming non-linear near the right end of the reinforcement where large mobilization of transverse displacements takes place. Due to mobilization of transverse displacements, the normal stresses developed in the soil are high. This results in large increase of the shear resistance mobilized that gets translated into larger increase of tension. Hence, non-linearity in the variation of normalized tension with normalized distance is observed near the right end.

The variation of maximum tension, i.e.  $T^*$  at  $X=1$ , developed with  $w_L/L$  is presented in Fig. 4.9 for  $J^*=1, 10, 50, 100, 250, 500, 1,000, 2,000$  and  $5,000$ . The maximum tension developed for highly extensible reinforcement ( $J^*=1$ ) is negligible because shear stresses are mobilized over small tracts of reinforcement. The variation of maximum tension developed is linear with  $w_L/L$  in the range  $0.001$  and  $0.01$  for  $J^*$

varying from 1 to 1000 for  $\mu = 500$  and  $\phi_r = 30^\circ$ . The rate of increase of maximum tension increases with increasing relative stiffness of the reinforcement. The maximum normalized tension is just 0.08 for relative stiffness of reinforcement,  $J^* = 1$ , whereas it is

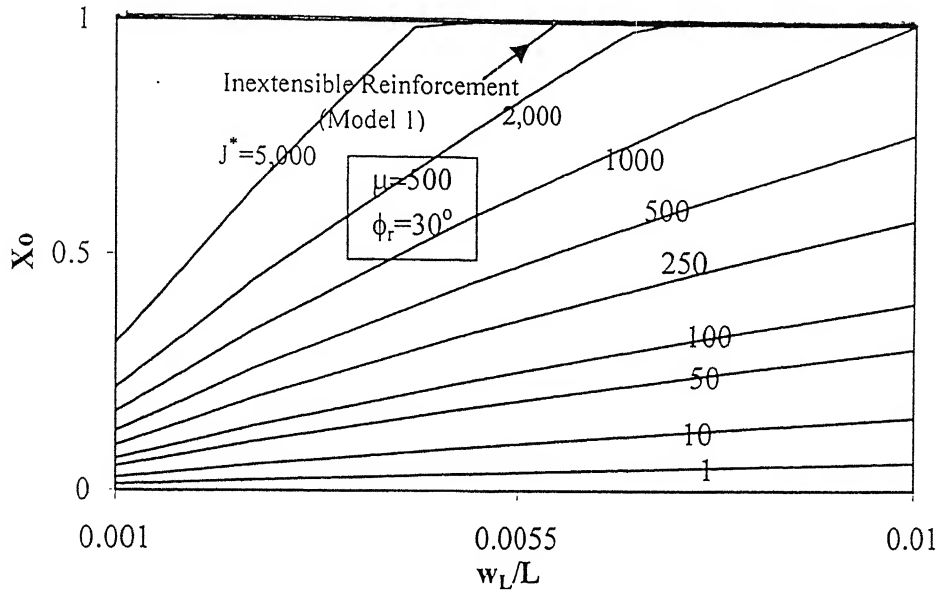


Fig 4.6 Variation of Normalized Active Length with  $w_L/L$  – Effect of  $J^*$

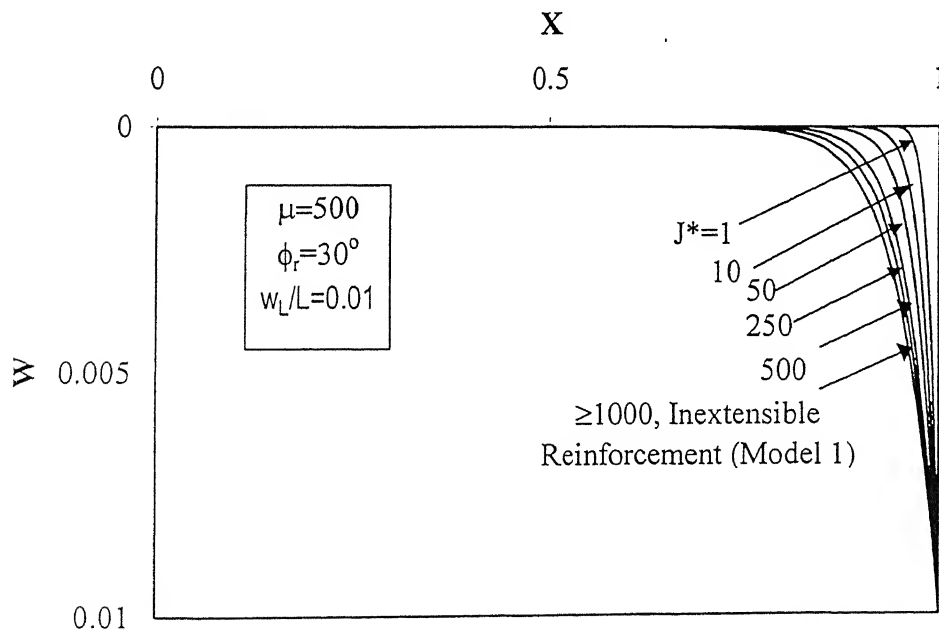


Fig. 4.7 Variation of Normalized Normal Displacement with Normalized Distance – Effect of  $J^*$ .

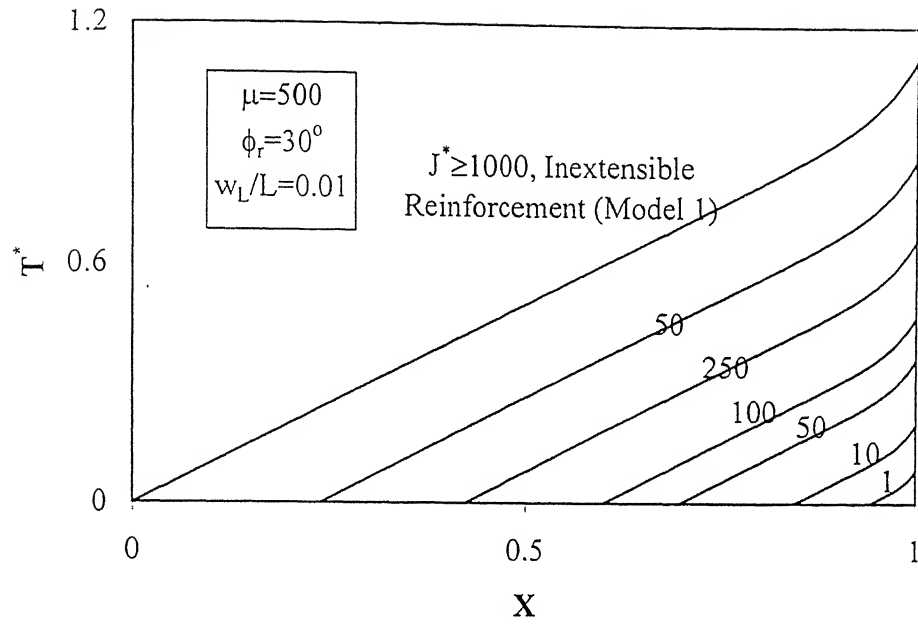


Fig. 4.8 Variation of Normalised Tension with Normalised Distance – Effect of  $J^*$ .

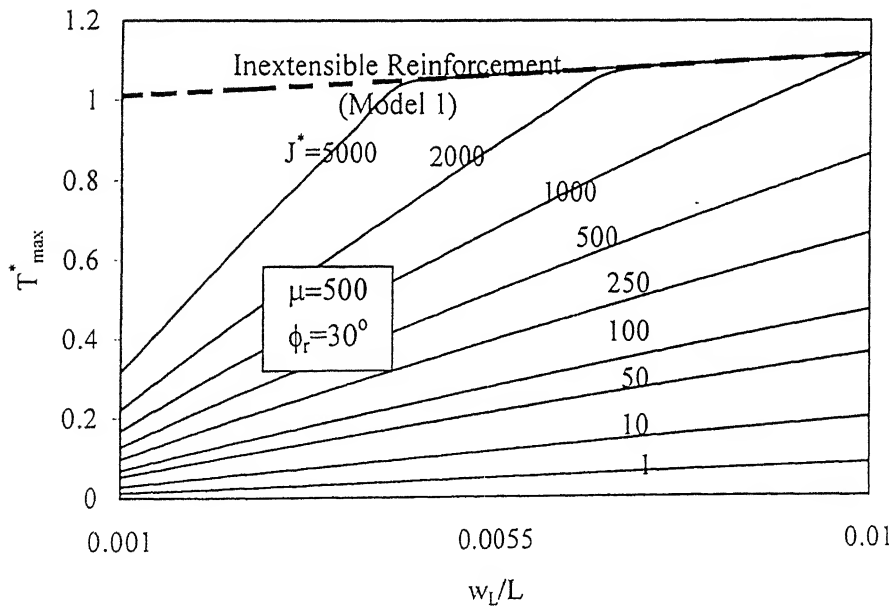


Fig. 4.9 Variation of Normalized Maximum Tension with  $w_L/L$  – Effect of  $J^*$ .

as high as 1.12 for inextensible reinforcement (Model 1) at  $w_L/L=0.01$  and for  $\mu=500$  and  $\phi_r=30^\circ$ . The maximum tension developed for  $J^*=1000$  and in an inextensible reinforcement are the same at  $w_L/L=0.01$  for  $\mu=500$  and  $\phi_r=30^\circ$ . The shear resistance get mobilized over the entire length of reinforcement for  $w_L/L \geq 0.075$  for  $J^*$  equal to 2000 and  $w_L/L \geq 0.005$  for  $J^*=5000$ . Thus, as the relative stiffness of reinforcement increases, the shear resistance gets mobilized over the entire length of reinforcement for small normalized free end displacements,  $w_L/L$ .

The normal displacements are confined to a small portion near the right end for highly extensible reinforcements for a given free end displacement at the right end (Fig. 4.8). Hence, the inclinations of highly extensible reinforcements with the horizontal at  $x=L$  is quite high. The inclination of reinforcement with relative stiffness,  $J^*=1$ , is as high as  $38^\circ$  at  $x=L$  whereas it is  $11.5^\circ$  at  $J^*=1000$  for  $\mu=500$  and  $\phi_r=30^\circ$  (Fig. 4.10). The rate of increase of inclination of reinforcement with the horizontal increases with the increase in the free end displacement. For  $J^*$  equal to 2000, the maximum inclination of the reinforcement for  $w_L/L \geq 0.005$  is the same as that of inextensible reinforcement.

The rate of increase of normalized normal component of tension,  $T_{\max}^* \sin \theta_L$ , increases with normalized free end displacement,  $w_L/L$  (Fig. 4.11). The normalized component of maximum tension varies linearly with free end displacement for highly extensible reinforcements ( $J^*=1$ ). But the non-linearity increases with increase in the stiffness of the reinforcement.

The variation of normalized horizontal component of maximum tension,  $T_{\max}^* \cos \theta_L$ , with the normalized free end displacement,  $w_L/L$ , is portrayed in Fig. 4.12. The trend of the variation of the normal horizontal component of maximum tension ( $T_{\max}^* \cos \theta_L$ ) is similar to that of the variation of normalized maximum tension,  $T_{\max}^*$ , with normalized free end displacement (Fig. 4.9). The pullout force is much less than the axial pullout capacity for highly extensible reinforcements in the normal displacement range considered. The pullout force is only 6% of the axial pullout capacity for reinforcement with relative stiffness,  $J^*=1.0$ , for a normalized free end displacement,  $w_L/L$  equal to 0.01 and for  $\mu=500$  and  $\phi_r=30^\circ$ . For highly stiff reinforcement ( $J^*=5000$ ), the pullout force is greater than the axial pullout capacity for  $w_L/L \geq 0.004$  for  $\mu=500$  and  $\phi_r=30^\circ$ .

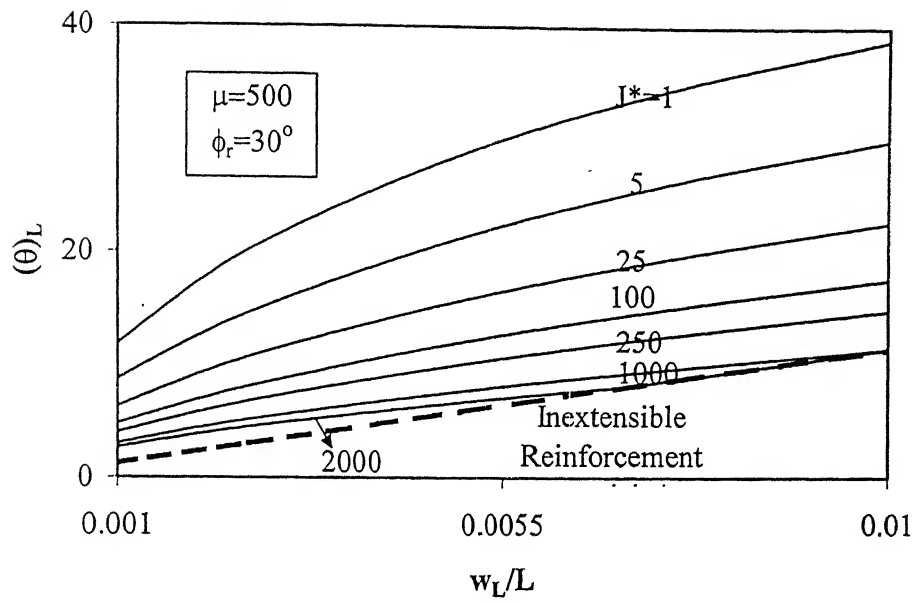


Fig. 4.10 Variation of Maximum Inclination with  $w_L/L$  – Effect of  $J^*$ .

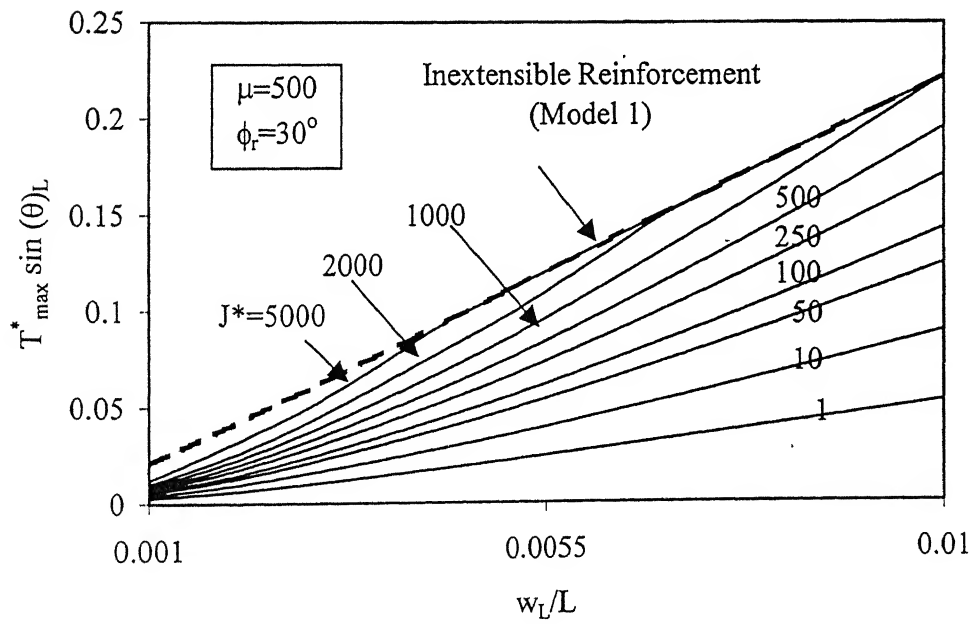


Fig. 4.11 Variation of Maximum Normalized Normal component of Tension with  $w_L/L$  – Effect of  $J^*$ .

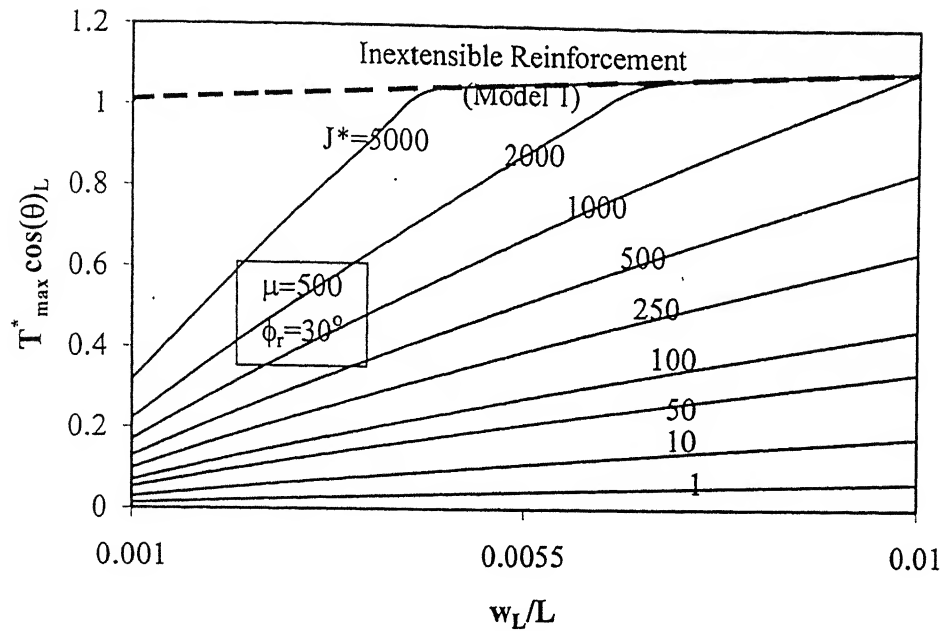


Fig. 4.12 Variation of Maximum Normalized Horizontal component of Tension with  $w_L/L$  – Effect of  $J^*$ .

The variation of normalized transverse force,  $P^*$ , with  $w_L/L$  for  $J^*=1, 10, 50, 100, 250, 500, 1000$  and  $2000$  and for  $\mu=500$  and  $\phi_r=30^\circ$  is presented in Fig. 4.13. For  $J^*=1.0$ , a normalized transverse force of  $0.05$  is sufficient to enforce a normalized free end displacement of  $w_L/L=0.01$  whereas it increases to  $0.24$  a very stiff or inextensible reinforcement for the same enforced  $w_L/L$ . This is due to the fact that active length of reinforcement,  $x_o$ , increases with increase in the stiffness of the reinforcement for any given free end displacement. The variation of normalized transverse force,  $P^*$ , is linear with normalized free end displacement,  $w_L/L$ , for relatively extensible reinforcements but becomes non-linear as the relative stiffness of the reinforcement increases. The rate of increase of normalized transverse force increases with free end displacement for increasing relative stiffness of reinforcement. For relative stiffness as high as  $5000$ , the normalized transverse force approaches that for an inextensible reinforcement at a free end displacement of  $w_L/L \geq 0.005$ .

The variation of normalized active length of reinforcement,  $X_o$ , with normalized free end displacements,  $w_L/L$ , for  $J^*=100$  and  $\phi_r=30^\circ$  is presented in Fig. 4.14 for relative soil stiffness,  $\mu$ , of  $50, 100, 2000, 5000, 10,000$  and  $100,000$ . The active length of reinforcement increases with the stiffness of the soil for a given free end

displacement,  $w_L$ . The active length of reinforcement,  $x_o$ , increases from  $0.27L$  for  $\mu=50$  to  $0.91L$  for  $\mu=100,000$  at  $w_L/L=0.01$  for  $J^*=100$  and  $\phi_r=30^\circ$ . The rate of increase of  $X_o$  with  $w_L/L$  increases with increase in relative stiffness,  $\mu$  of the soil.

The variation of normal displacement profiles,  $W$ , with normalized distance,  $X$ , for  $J^*=100$  and  $\phi_r=30^\circ$  for relative stiffness of soil,  $\mu$ , of 50, 200, 500, 2000 and 10,000 is presented in Fig. 4.15. The points of mobilization of transverse displacements move towards the left end with decreasing relative stiffness of the soil,  $\mu$ . The length over which mobilization of transverse displacements takes place for extensible reinforcement is less compared to that for inextensible reinforcement. For extensible reinforcements with  $J^*=100$ ,  $\phi_r=30^\circ$  and  $\mu=50$ , the transverse displacements are mobilized only over a length of  $0.25L$  from the right end but it is  $0.06L$  for  $\mu=10,000$  the same set of parameters (Fig. 4.15).

The variation of normalized tension,  $T^*$ , with normalized distance,  $X$ , for soils of relative stiffness,  $\mu$ , equal to 50, 200, 500, 2000 and 10,000 for  $w_L/L=0.01$ ,  $J^*=100$  and  $\phi_r=30^\circ$  is depicted in Fig. 4.16. As the stiffness of soil increases, large tracts of reinforcement mobilize shear resistance. For  $\mu=50$ , shear resistance is mobilized only over a length of  $0.18L$  whereas for  $\mu=10,000$ , shear resistance is mobilized for a length of  $0.66L$  from the right end for  $w_L/L=0.01$ ,  $J^*=100$  and  $\phi_r=30^\circ$ . The normalized tension,  $T^*$ , increases linearly along the reinforcement for relatively compressible soils ( $\mu=50$ ). The variation of  $T^*$  with  $X$  is linear away from the right end but becomes non-linear near the right end for relatively stiff soils ( $\mu=10,000$ ).

The maximum tension,  $T_{max}^*$ , developed in the reinforcement varies linearly with  $w_L/L$  for  $\mu$  in the range 50-10,000 for  $J^*=100$  and  $\phi_r=30^\circ$ . The rate of increase of maximum tension increases with increasing relative stiffness of the reinforcement (Fig. 4.17). Large tracts of reinforcement-soil interfaces mobilize shear resistance in addition to development of large normal stresses for relatively stiff soils. Hence,  $T_{max}^*$  as high as 1.12 is developed for  $\mu=10,000$  when compared to 0.29 developed for  $\mu=50$  for  $J^*=100$  and  $\phi_r=30^\circ$ .

The inclination of extensible reinforcement with horizontal for stiff soils is quite high as the transverse displacements are confined close to the right end (Fig. 4.18). The rate of increase of inclination with horizontal increases with  $w_L/L$ . The inclination of

reinforcement with horizontal with  $\mu=10,000$  is as high as  $44^\circ$  at  $x=L$  whereas it is  $8^\circ$  for  $\mu=50$  for  $J^*=100$  and  $\phi_r=30^\circ$

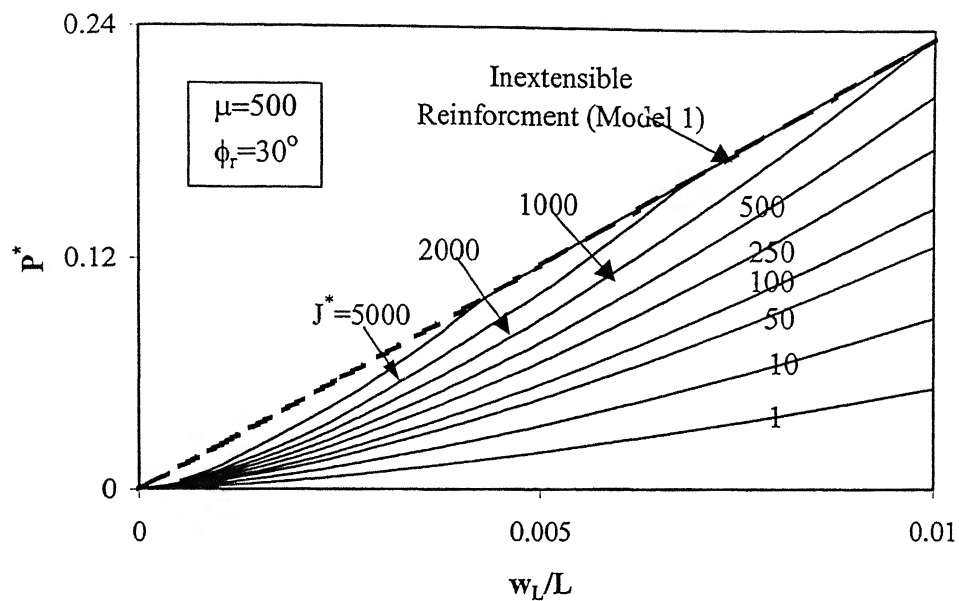


Fig. 4.13 Variation of Normalized Transverse Force with  $w_L/L$  – Effect of  $J$

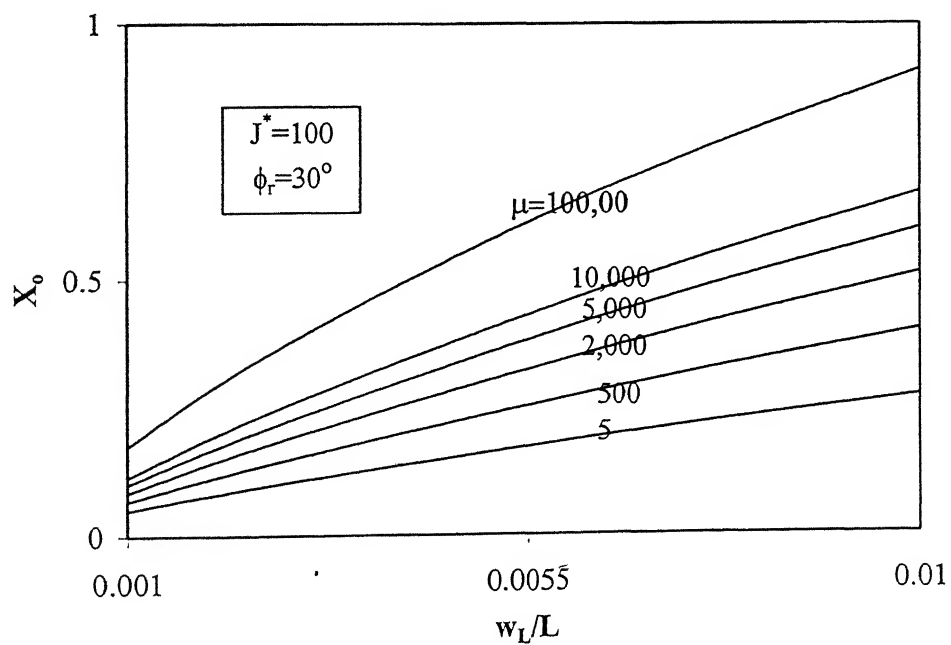


Fig. 4.14 Variation of Normalized Active Length with  $w_L/L$  – Effect of  $J^*$

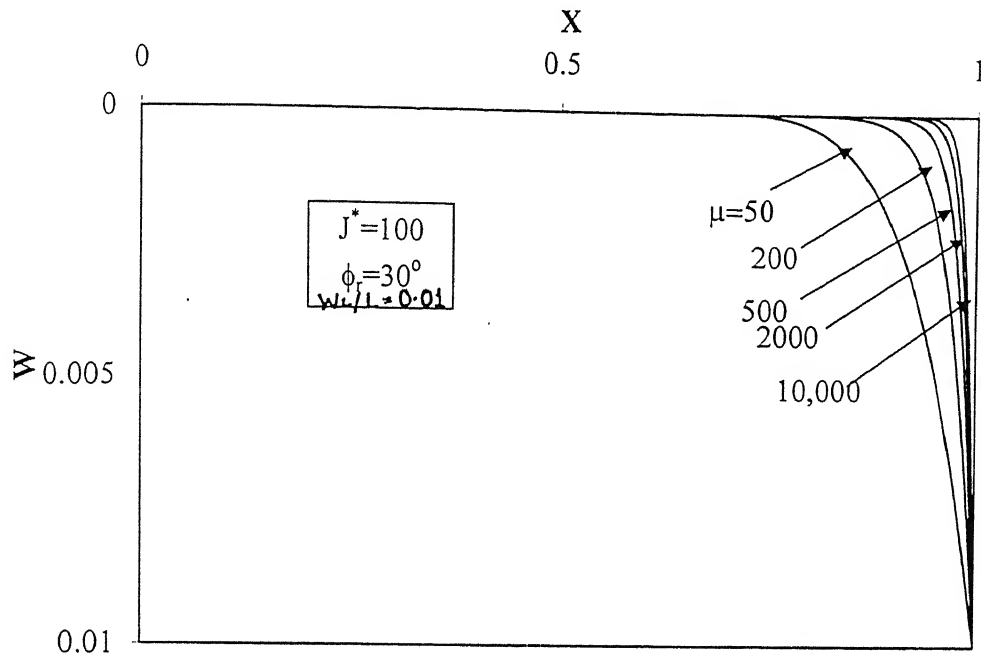


Fig. 4.15 Variation of Normalized Normal Displacement with Normalized Distance – Effect of  $J^*$ .

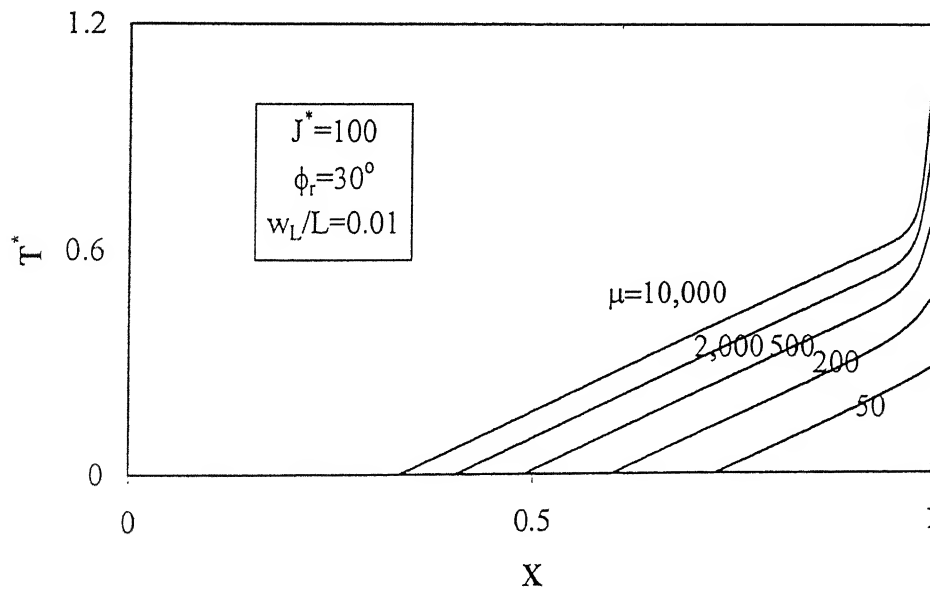


Fig. 4.16 Variation of Normalized Tension with Normalized Distance – Effect of  $J^*$ .

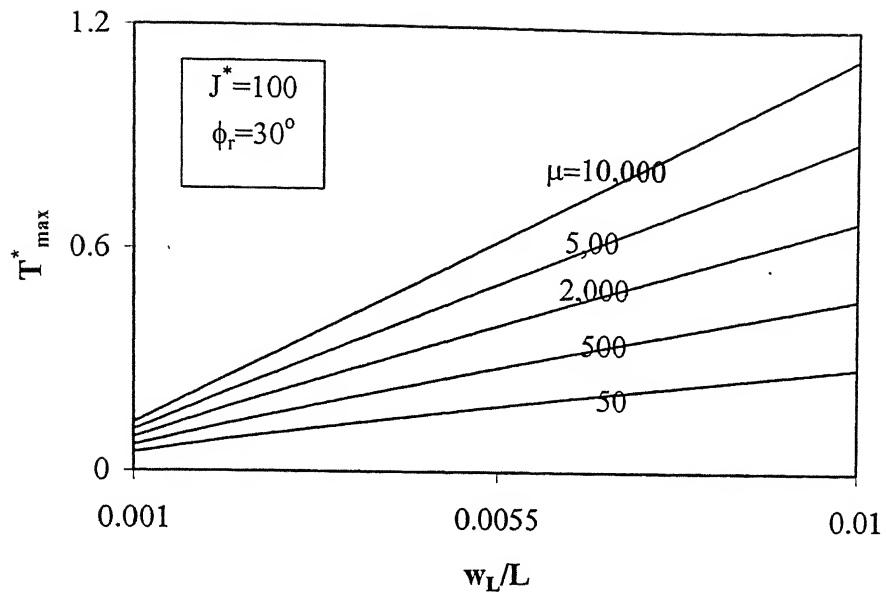


Fig. 4.17 Variation of Normalized Tension with  $w_L/L$ — Effect of  $\mu$

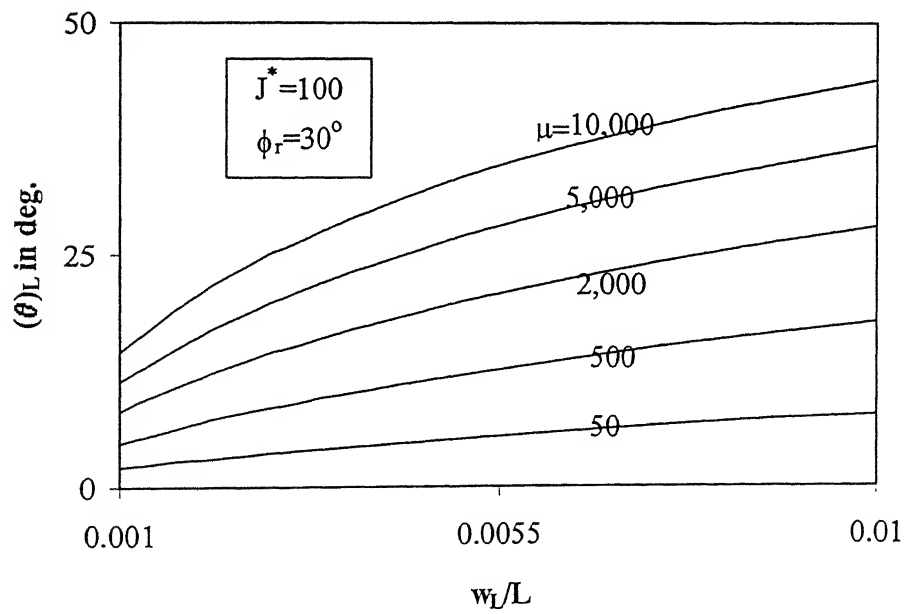


Fig. 4.18 Variation of Maximum Inclination with  $w_L/L$  – Effect of  $\mu$

The rate of increase of normalized normal component of tension,  $T_{\max}^* \sin \theta_L$ , increases with normalized free end displacement,  $w_L/L$  (Fig. 4.19). The variation of  $T_{\max}^* \sin \theta_L$  with  $w_L/L$  is almost linear for relatively compressible soils but becomes non-linear for stiff soils.

The variation of normalized horizontal component of tension,  $T_{\max}^* \cos \theta_L$ , with the normalized free end displacement,  $w_L/L$ , is portrayed in Fig. 4.20. The variation of  $T_{\max}^* \cos \theta_L$  with  $w_L/L$  is similar to that of the variation of normalized maximum tension,  $T_{\max}^*$ , with normalized free end displacement (Fig. 4.16). The pullout force is only 28% of the axial pullout capacity for relatively compressible soils ( $\mu=50$ ) whereas it increases to 81% of the axial pullout capacity for relatively stiff soils ( $\mu=10,000$ ) for  $J^*=100$ ,  $w_L/L=0.01$  and  $\phi_r=30^\circ$ .

The variation of normalized transverse force,  $P^*$ , with normalized free end displacement,  $w_L/L$  is linear for relatively compressible soils ( $\mu \leq 500$ ) but becomes non-linear with increase in relative stiffness of the soil (Fig. 4.21). A normalized transverse force of 0.03 is sufficient to enforce a normalized transverse displacement of 0.01 for  $\mu=50$  whereas it increases to 0.96 for  $\mu=10,000$  for the same enforced free end displacement. This is due to the fact that the active length of reinforcement,  $x_o$ , increases with increase in the relative stiffness of the soil for any given free end displacement. The rate of increase of normalized transverse force increases with free end displacement for increasing relative stiffness of the soil.

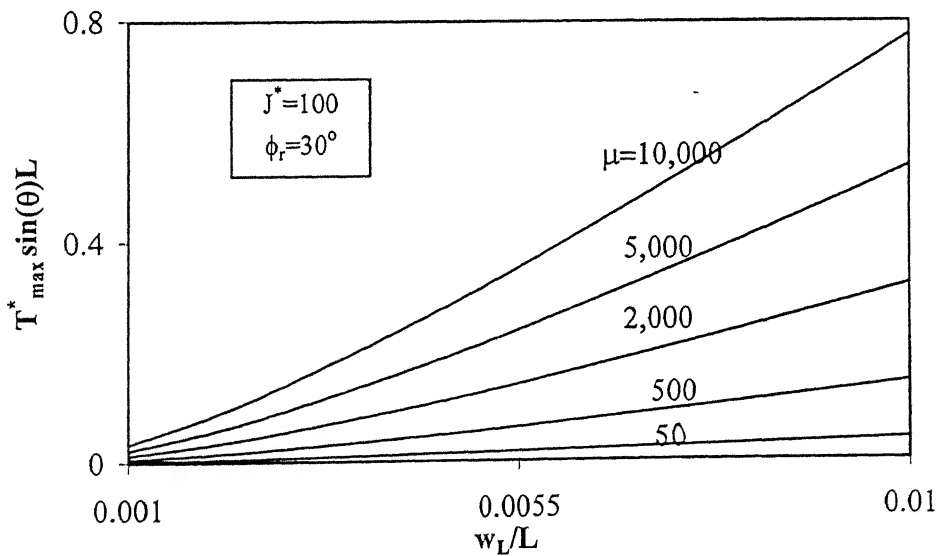


Fig. 4.19 Variation of Maximum Normalized Normal component of Tension with  $w_L/L$   
Effect of  $J^*$

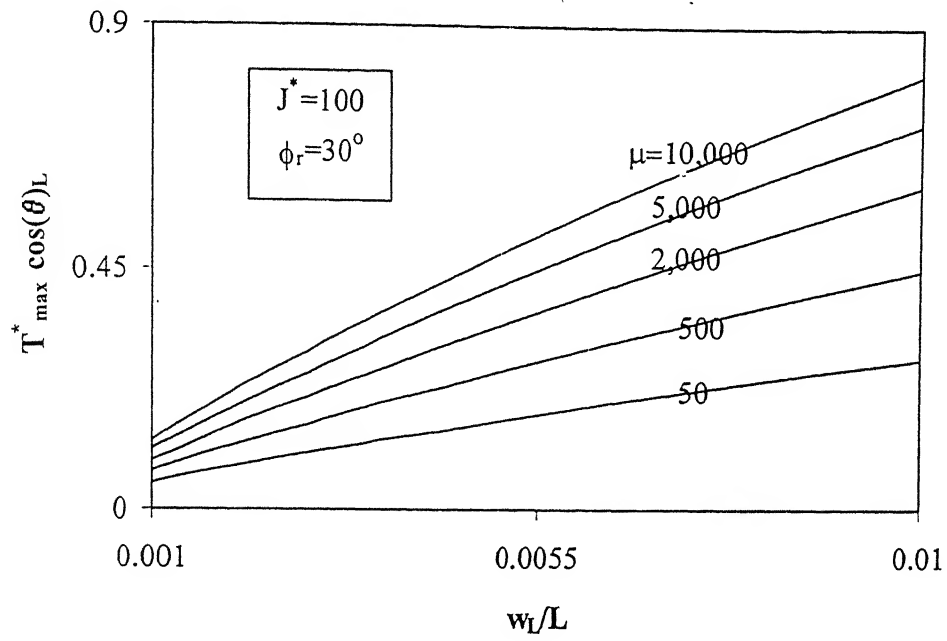


Fig. 4.20 Variation of Maximum Normalized Horizontal component of Tension with  $w_L/L$  – Effect of  $J^*$

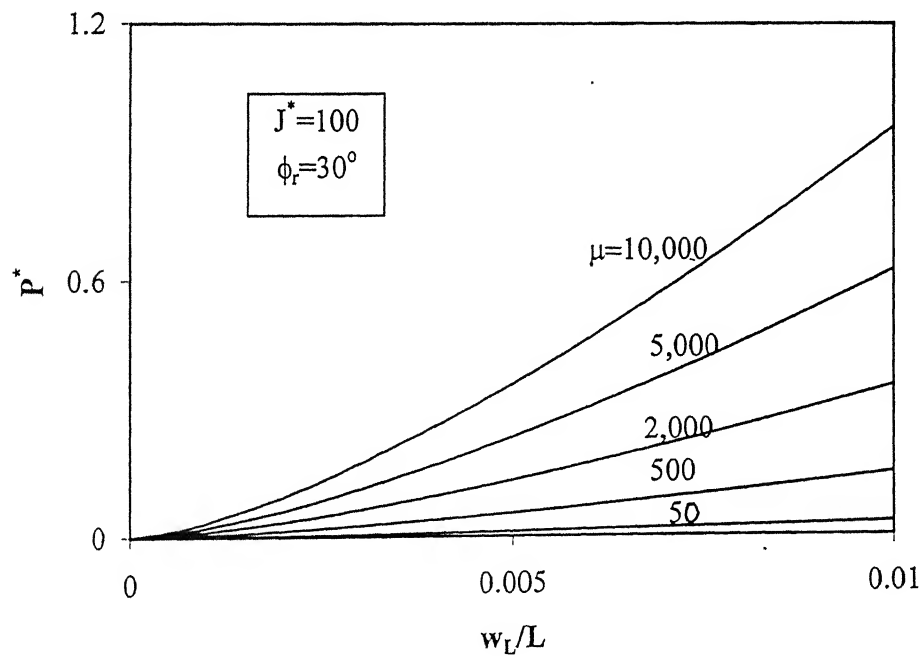


Fig. 4.21 Variation of Normalized Transverse Force with  $w_L/L$  – Effect of  $J^*$

#### 4.4.2 Non-Linear Subgrade - Model II

The stress developed in the soil cannot increase with displacement neither linearly nor indefinitely. Hence, to simulate such a condition, a hyperbolic stress-displacement response of the soil is assumed by restricting the maximum stress developed in the soil to that of its ultimate resistance.

##### 4.4.2.1 The Model

The model is identical to the one explained in section 4.4.1.1. In this case, the response of the soil due to additional stresses, i.e.,  $(q_b - q_t)$ , generated beneath the reinforcement due to the application of the transverse force,  $P$ , is given by

$$(q_b - q_t) = \frac{k_s w}{1 + \frac{k_s w}{q_{ult}}} \quad (4.28)$$

where  $k_s$ ,  $q_{ult}$  and  $w$  are the initial modulus of subgrade reaction, the ultimate resistance and normal displacement of the soil respectively (Fig. 4.22).

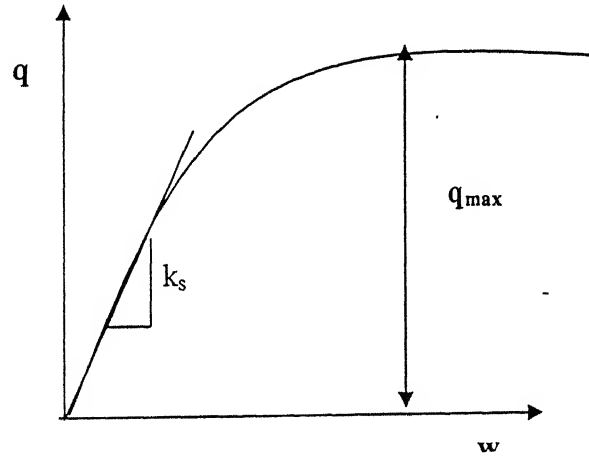


Fig. 4.22 Hyperbolic Response between stress,  $q$ , and settlement,  $w$

##### 4.4.2.2 Analysis

Considering the equilibrium of forces on an element (Fig. 4.4) of infinitesimal length,  $\Delta x$ , and unit width as described in section 4.4.1.2 one can derive

$$\frac{dT}{dx} = (q_t + q_b) \cos \theta \tan \phi_r + (q_b - q_t) \sin \theta \quad (4.29)$$

$$-T \frac{d\theta}{dx} - (q_t + q_b) \tan \phi_r \sin \theta + (q_b - q_t) \cos \theta = 0 \quad (4.30)$$

From Eq. 4.14,

$$\frac{d\theta}{dx} = \cos^2 \theta \frac{d^2 w}{dx^2} \quad (4.31)$$

Combining Eqs. (4.28), (4.29), (4.30) and (4.31), the following equations are obtained

$$\frac{dT}{dx} = (q_t + q_b) \cos \theta \tan \phi_r + \left( \frac{k_s w}{1 + \frac{k_s w}{q_{ult}}} \right) \sin \theta \quad (4.32)$$

$$-T \cos^2 \theta \frac{d^2 w}{dx^2} + \left( \frac{K_s w}{1 + \frac{k_s w}{q_{ult}}} \right) = (q_z + q_b) \sin \theta \tan \phi_r \quad (4.33)$$

For small  $\theta$ , Eqs. (4.32) and (4.33) reduce to

$$\begin{aligned} \frac{dT}{dx} &= (q_t + q_b) \tan \phi_r \\ &= (q_b - q_t + 2q_t) \tan \phi_r \\ &= \left( \frac{k_s w}{1 + \frac{k_s w}{q_{ult}}} + 2\gamma D_e \right) \tan \phi_r \end{aligned} \quad (4.34)$$

$$-T \frac{d^2 w}{dx^2} + \frac{k_s w}{1 + \frac{k_s w}{q_{ult}}} = 0 \quad (4.35)$$

Eqs. (4.34) and (4.35) are the governing equations for the model that incorporates the non-linear response of the soil. Eqs. (4.34) and (4.35) are non-dimensionalised with

$X=x/L$ ,  $W=w/w_L$  and  $T^*=T/T_{\max}$  where  $T_{\max}=2 \gamma D_e L \tan \phi_r$ , the maximum axial pullout force. Eqs. (4.34) and (4.35) in normalized form are

$$\frac{dT^*}{dX} = \frac{1}{2} \left( \frac{\mu \frac{w_L}{L} W}{1 + \beta W \frac{w_L}{L}} + 2 \right) \quad (4.36)$$

$$-T^* \frac{d^2 W}{dX^2} + \frac{\mu W}{2 \tan \phi_r \left( 1 + \beta W \frac{w_L}{L} \right)} = 0 \quad (4.37)$$

where  $\beta = \frac{k_s L}{q_{ult}}$  --- a parameter that quantifies the relative initial subgrade modulus with the ultimate resistance of the ground.

The boundary conditions for the present case are the same as explained in section 4.4.1.3 for the present case. The transverse force required to cause the displacement,  $w_L$ , is obtained by integrating the soil reaction mobilized as

$$P = \int_0^L \frac{k_s w}{1 + \frac{k_s w}{q_{ult}}} dx \quad (4.38)$$

#### 4.4.2.3 Numerical Solution

The discretisation of reinforcement length into elements is as explained in section 4.4.1.3. Eqs. (4.36) and (4.37) in finite difference form become

$$\frac{T^*_{i+1} - T^*_i}{\Delta X} = \frac{1}{2} \left( \frac{\mu W_i \frac{w_L}{L}}{1 + \beta W_i \frac{w_L}{L}} + 2 \right) \quad (4.39)$$

$$-T^*_i \left( \frac{W_{i-1} - 2W_i + W_{i+1}}{\Delta X^2} \right) + \frac{\mu W_i}{2 \tan \phi_r \left( 1 + \beta W_i \frac{w_L}{L} \right)} = 0 \quad (4.40)$$

Solving for normalized displacement and normalized tension, one gets

$$W_i = \frac{T_i^* n^2 (W_{i-1} + W_{i+1})}{\left( 2n^2 T_i^* + \frac{\mu}{2 \tan \phi_r \left( 1 + \beta W_i \frac{w_L}{L} \right)} \right)} \quad (4.41)$$

$$T_{i+1}^* = \frac{1}{2n} \left( \frac{\mu W_i \frac{w_o}{L}}{1 + \beta W_i \frac{w_L}{L}} + 2 \right) + T_i^* \quad (4.42)$$

To obtain the displacement at node 1, the boundary condition  $dW/dx=0$  at  $X=0$  leads to the condition,  $W_0=W_2$  and Eq. (4.42) for node 1 becomes

$$W_1 = \frac{2n^2 T_1^* W_2}{\left( 2n^2 T_1^* + \frac{\mu}{2 \tan \phi_r \left( 1 + \beta W_1 \frac{w_L}{L} \right)} \right)} \quad (4.43)$$

As the reinforcement sheet is discretized into 'n' elements and the transverse force, P, is obtained by numerical integration as

$$P = \sum_{i=1}^n \left( \frac{k_s w}{1 + \frac{k_s w}{q_{ult}}} \right) dx \quad (4.44)$$

The transverse force in normalized form is

$$P^* = \frac{P}{\gamma D_e L} = \frac{1}{n} \frac{w_L}{L} \sum_{i=1}^n \frac{\mu W_i}{1 + \beta W_i \frac{w_L}{L}} \quad (4.45)$$

For a given free end displacement,  $w_L/L$ , applied at the free end, the variations of various quantities are presented and discussed in the section 4.4.2.4. The procedure as detailed in section 4.3 is adopted to arrive at the active length of reinforcement, normal displacement profiles and the tension profiles along the reinforcement. The normalized

transverse force required to enforce the free end displacement,  $w_L/L$ , is then obtained by Eq. (4.45).

#### 4.4.2.4 Characteristics of the Model

A simple mathematical model has been developed to study the behavior of an extensible sheet reinforcement sheet subjected to transverse force. The reinforcement-soil interface is characterized by the interface friction angle ( $\phi_r$ ) only. Unlike the previous model, the normal stresses generated due to the application of a transverse displacement/force are limited to the ultimate resistance of the soil. Also, the normal stress-displacement response of the soil is assumed to be non-linear (hyperbolic). A limitation of the model is that under large displacement or applied transverse load, the assumption of small angles is not appropriate. Consideration of active length,  $x_o$  ( $X_o = x_o/L$ ) appears to be appropriate in the context of extensible reinforcements.

#### 4.4.2.5 Results and Discussions

The variation of normalized active length of reinforcement,  $X_o$ , with normalized free end displacement,  $w_L/L$ , is presented in Fig.4.23. The active length of reinforcement increases linearly with  $w_L/L$  for relatively extensible reinforcements but increases non-linear for stiffer reinforcements.  $X_o$  is less than 1 in the normal range of  $w_L/L$  (0.001-0.01) and for  $J^*$  in the range 1-1000 for soils with relative stiffness,  $\mu$ , equal to 500,  $\beta(=k_s L/q_{ult})=1000$  and  $\phi_r=30^\circ$ . Thus, the interface shear resistance is mobilized only over a partial length of the reinforcement-soil interface.

The transverse displacements of reinforcement with relative stiffness,  $J^*$ , in the normal range 1-1,000 are less than those of inextensible reinforcements (Fig. 4.24). The length over which normal displacements are mobilized increases with increase in stiffness of reinforcement. The normal displacements are mobilized only over a small length of  $0.06L$  for  $J^*=1$  and over a length of  $0.36L$  for  $J^*=1,000$  for  $\mu=500$ ,  $\beta=1,000$  and  $\phi_r=30^\circ$ .

The normalized tension,  $T^*$ , varies almost linearly along the active length of the reinforcement. As the active length of reinforcement increases with stiffness (Fig. 4.23), the tension developed in the reinforcement also increases with stiffness of reinforcement (Fig. 4.25). For relative stiffness of reinforcement of 1000, the shear resistance starts mobilizing from a point  $0.28L$  from the left end ( $x=0$ ).

The normalized maximum tension,  $T_{\max}^*$ , varies almost linearly with the normalized free end displacement,  $w_L/L$ , applied at the right end of the reinforcement. The rate of increase of  $T_{\max}^*$  with  $w_L/L$  increases with relative stiffness of reinforcement,  $J^*$  (Fig. 4.26).  $T_{\max}^*$  values for extensible reinforcements are significantly smaller than those for inextensible ones in the normal displacement range,  $w_L/L$ , of 0.001-0.01.

The transverse displacement profiles (Fig. 4.24) indicate that the displacements are highly localized near the right end for relatively extensible reinforcements. Hence, the inclination of reinforcement is large (Fig. 4.27) for relatively extensible reinforcement compared to that of stiffer reinforcements. The inclination is as low as  $6^\circ$  for reinforcements with relative stiffness,  $J^*$ , equal to 1000 whereas it is about  $23^\circ$  for reinforcements with  $J^*=1$ .

The trend of variation of the normalized component of tension,  $T_{\max}^* \sin \theta_L$ , with  $w_L/L$  (Fig. 4.28) is similar to that of the variation of  $T_{\max}^*$  with  $w_L/L$  (Fig. 4.26).

The axial pullout force is less than the axial pullout capacity ( $T_{\max}^* \cos \theta_L < T_{\text{axial}}^*$ ) for relative stiffness of reinforcement,  $J^*$ , in the normal range within 1,000. The pullout force is 75% of the axial pullout capacity for  $J^*$  as high as 1,000 for an induced normalized free end displacement,  $w_L/L$ , equal to 0.01 for  $\mu=500$ ,  $\beta=1000$  and  $\phi_r=30^\circ$  (Fig. 4.29).

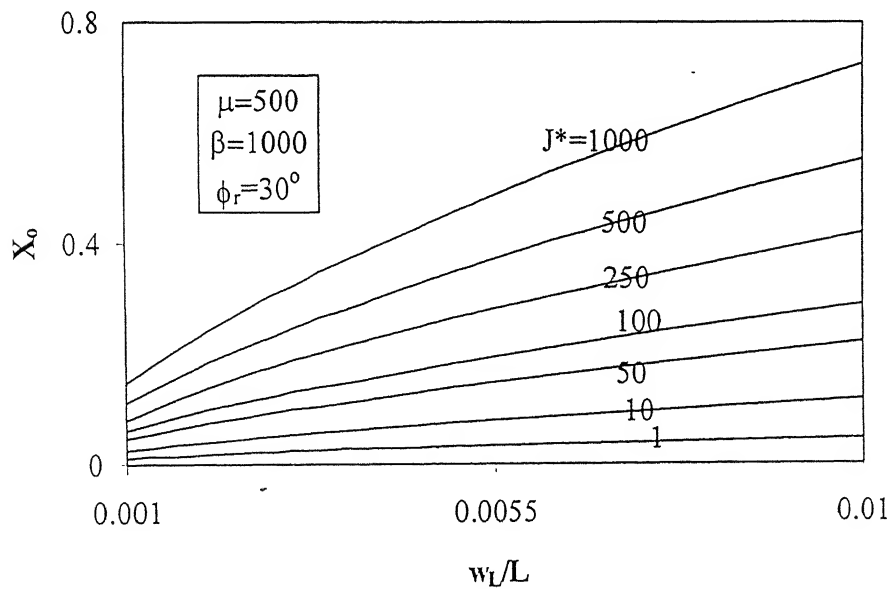


Fig. 4.23 Variation of Normalized Active Length with  $w_L/L$  – Effect of  $J^*$

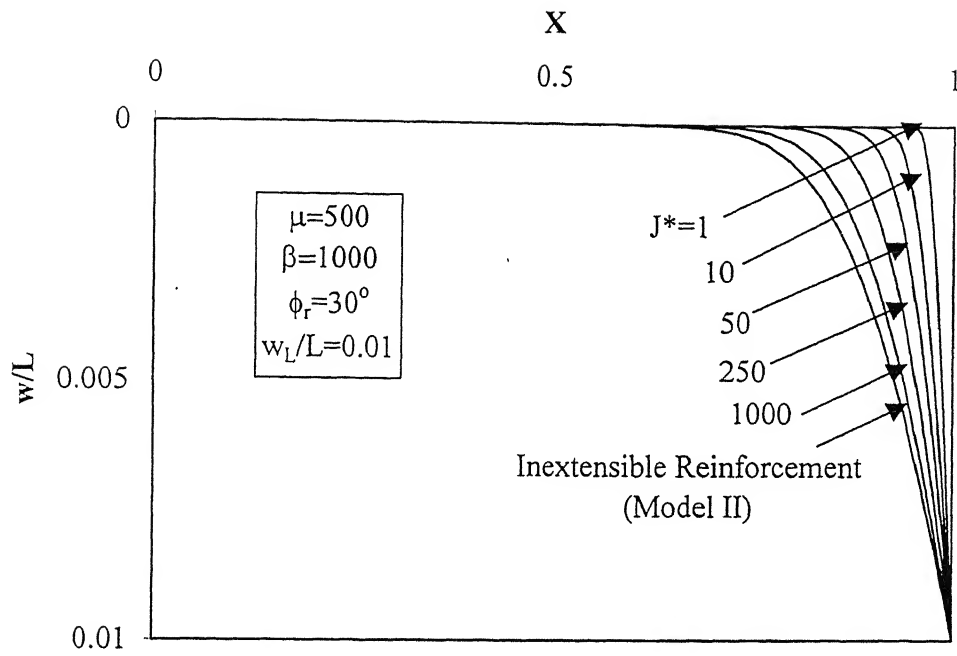


Fig. 4.24 Variation of Normalized Normal Displacement with Normalized Distance  
Effect of  $J^*$

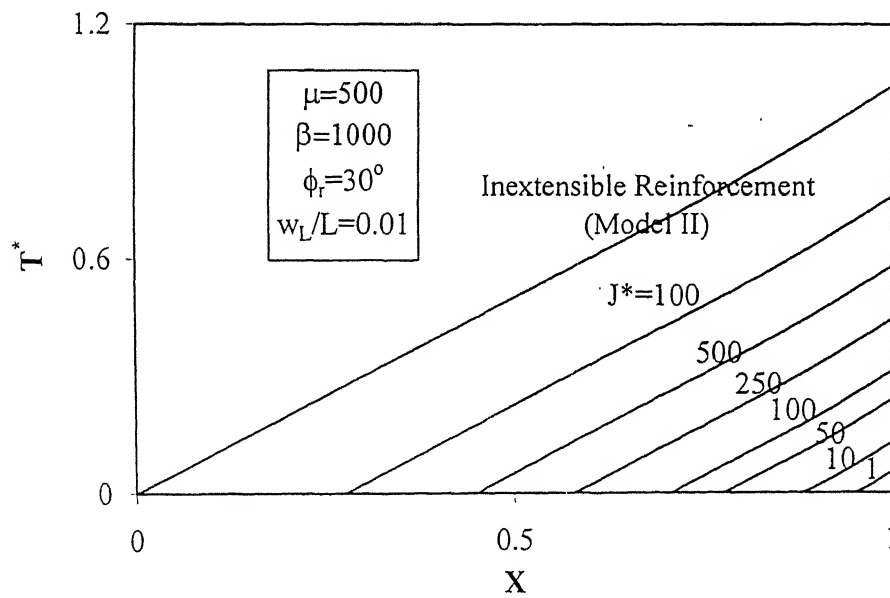


Fig. 4.25 Variation of Normalized Tension with Normalized Distance – Effect of  $J^*$

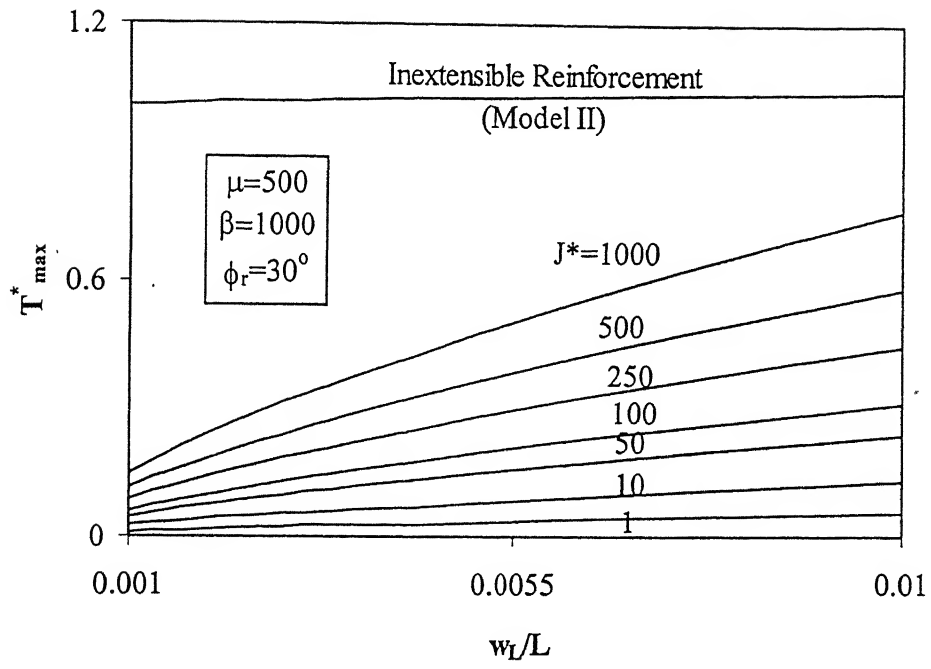


Fig. 4.26 Variation of Maximum Normalized Tension with  $w_L/L$  - Effect of  $J^*$

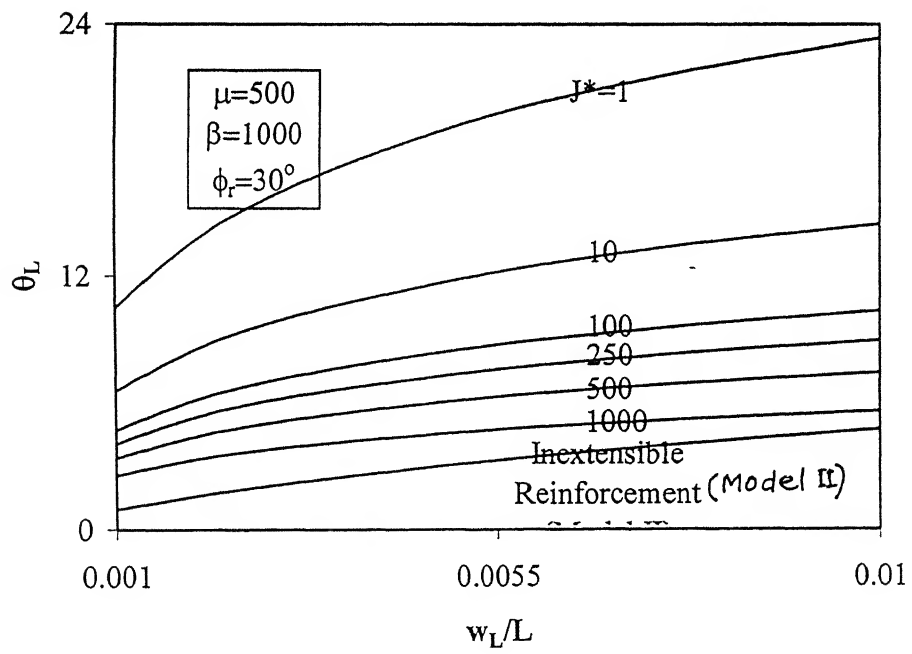


Fig. 4.27 Variation of Inclination at  $x=L$  with  $w_L/L$  - Effect of  $J^*$

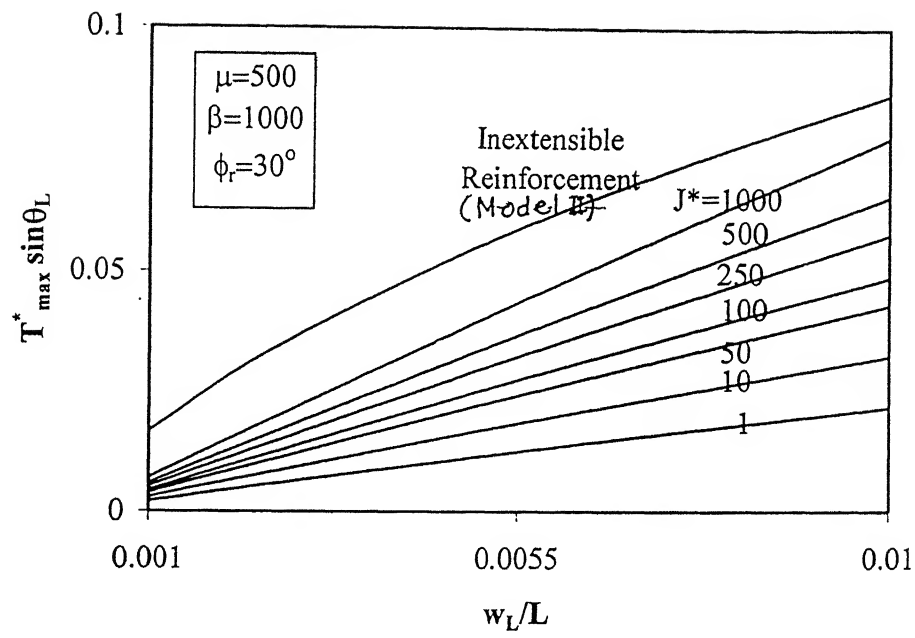


Fig. 4.28 Variation of Maximum Normalized Normal Component of Tension with  $w_L/L$  -Effect of  $J^*$

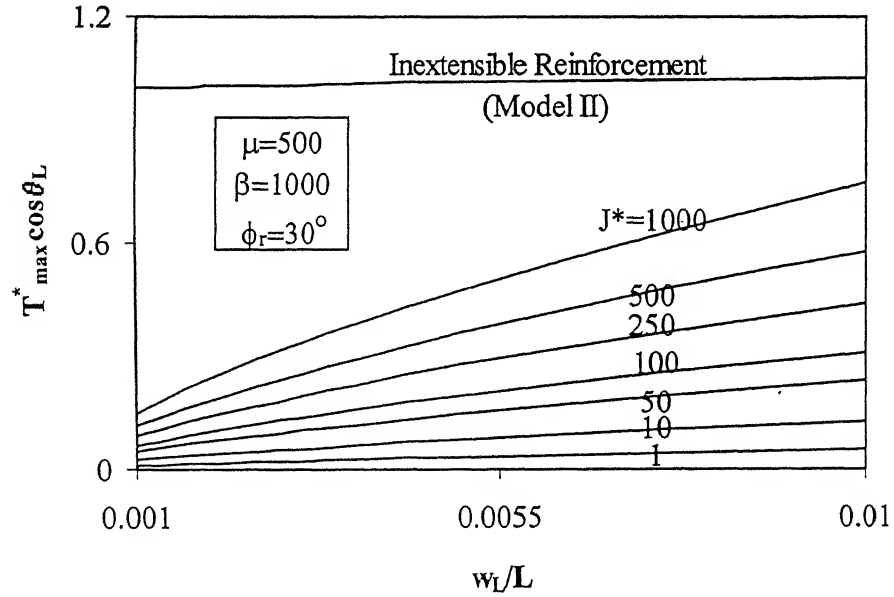


Fig. 4.29 Variation of Maximum Normalized Horizontal Component of Tension with  $w_L/L$  -Effect of  $J^*$

At large free end displacement, large normal stresses are induced in the soil over larger tracts of reinforcement and hence the normalized transverse force,  $P^*$ , increases with  $w_L/L$ . The variation is linear in the normal range of  $J^*$  (1-1,000). The rate of increase of  $P^*$  increases with  $J^*$  (Fig. 4.30).

The rate of increase of normalized active length of reinforcement,  $X_o$ , with  $w_L/L$  increases with decreasing  $\beta(=k_s L/q_{ult})$ .  $X_o$  is much less than 1.0 for  $\beta$  in the normal range of 100-3,000 indicating that only partial length of reinforcement is effective in offering shear resistance along the reinforcement-soil interface (Fig. 4.31)

The transverse displacements are highly localized near the right end for  $\beta(=k_s L/q_{ult})$  in the range 100-3000 for  $\mu=500$ ,  $J^*=250$  and  $\phi_r=30^\circ$  (Fig. 4.32).

The variation of normalized tension,  $T^*$ , along the reinforcement is linear for  $\beta$  in the normal range of 100-3000 for  $w_L/L$  equal to 0.01,  $\mu=500$ ,  $J^*=250$  and  $\phi_r=30^\circ$  (Fig. 4.33). The rate of increase of  $T^*$  with  $X$  increases with decrease in  $\beta$ . The tension in the reinforcement is mobilized only for a distance of  $0.5L$  from the right end for  $\beta=100$  whereas it is mobilized from a distance of  $0.36L$  for  $\beta=3000$  for  $w_L/L=0.01$ ,  $\mu=500$  and  $\phi_r=30^\circ$ .

Larger lengths of reinforcement mobilize shear resistance for soils with higher ultimate resistance (i.e. at low  $\beta$  values) (Fig. 4.31) and hence normalized maximum tension,  $T^*_{max}$ , increases with decreasing  $\beta$  at a given free end displacement.  $T^*_{max}=0.3$  for  $\beta=100$  whereas it is 0.20 for  $\beta=3,000$  for  $w_L/L=0.01$ ,  $\mu=500$  and  $\phi_r=30^\circ$  (Fig. 4.34).

The effect of localization of transverse displacements is higher (Fig. 4.35) near the right end for lower  $\beta$  values. Hence, higher inclinations are recorded for lower  $\beta$  values. The inclination of reinforcement is as high as  $17^\circ$  for  $\beta=100$  and it is  $7^\circ$  for  $\beta=3,000$  for  $w_L/L=0.01$ ,  $J^*=250$  and  $\mu=500$ .

The variation of normalized normal component of tension,  $T^*_{max} \sin \theta_L$ , is linear with  $w_L/L$  at lower  $\beta$  values but becomes non-linear at higher values of  $\beta$  (Fig. 4.36).

The trend of variation of normalized horizontal component of tension,  $T^*_{max} \cos \theta_L$ , with  $w_L/L$  (Fig. 4.37) is similar to that of the variation of  $T^*_{max}$  with  $w_L/L$  (Fig. 4.33). The pullout force is much less than the axial pullout capacity for  $\beta$  in the range of 100-3,000 and  $w_L/L$  in the range 0.0001-0.01. The pullout force is just 30% of the axial pullout capacity for  $\beta=100$  for  $w_L/L=0.01$ ,  $\mu=500$  and  $\phi_r=30^\circ$ .

The variation of normalized transverse force,  $P^*$ , with  $w_L/L$  (Fig. 4.38) is similar to that of the variation of  $T_{\max}^* \sin \theta_L$  with  $w_L/L$  (Fig. 4.36).

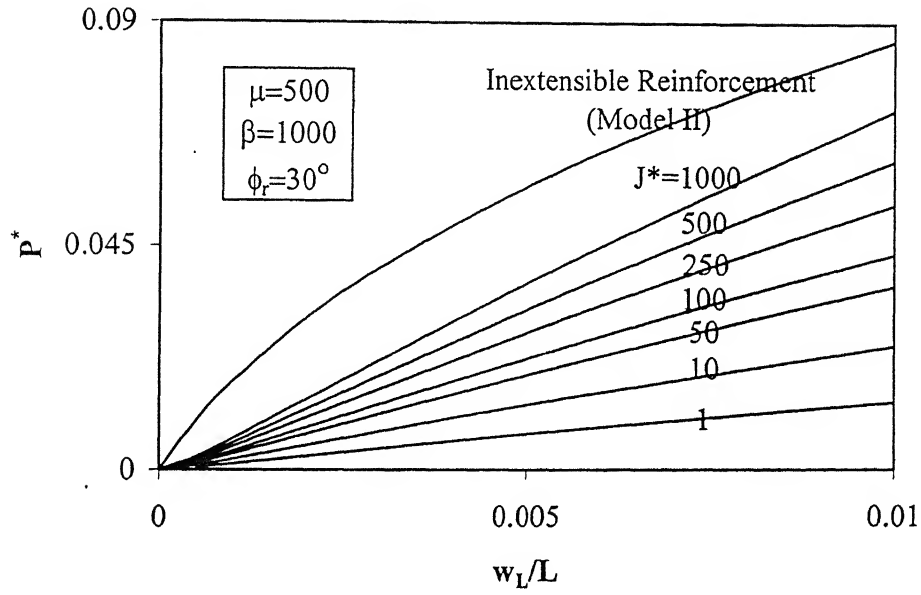


Fig. 4.30 Variation of Normalized Transverse Force with  $w_L/L$  – Effect of  $J^*$

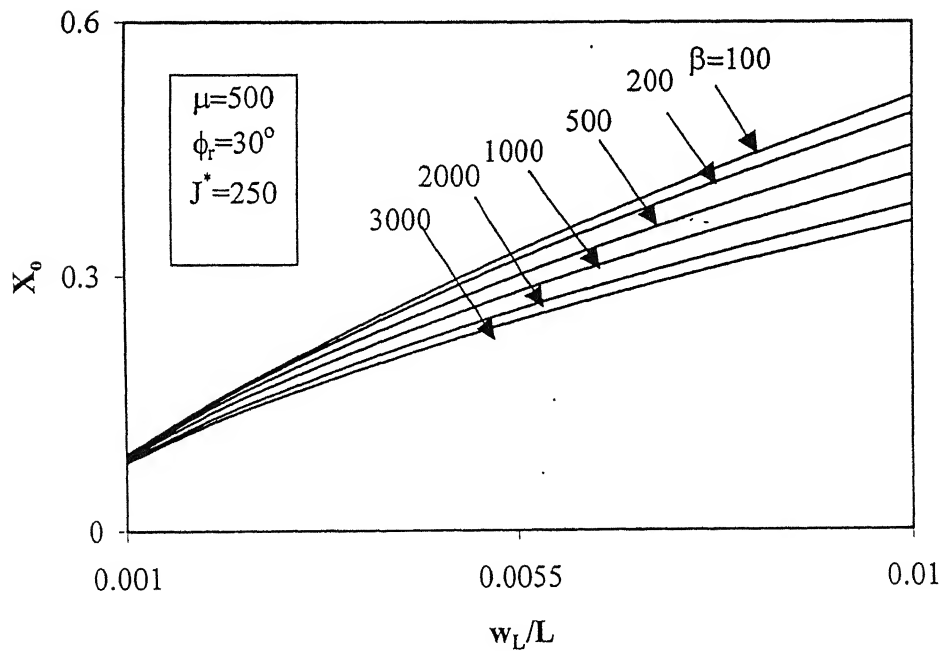


Fig. 4.31 Variation of Normalized Active Length with  $w_L/L$  – Effect of  $\beta$

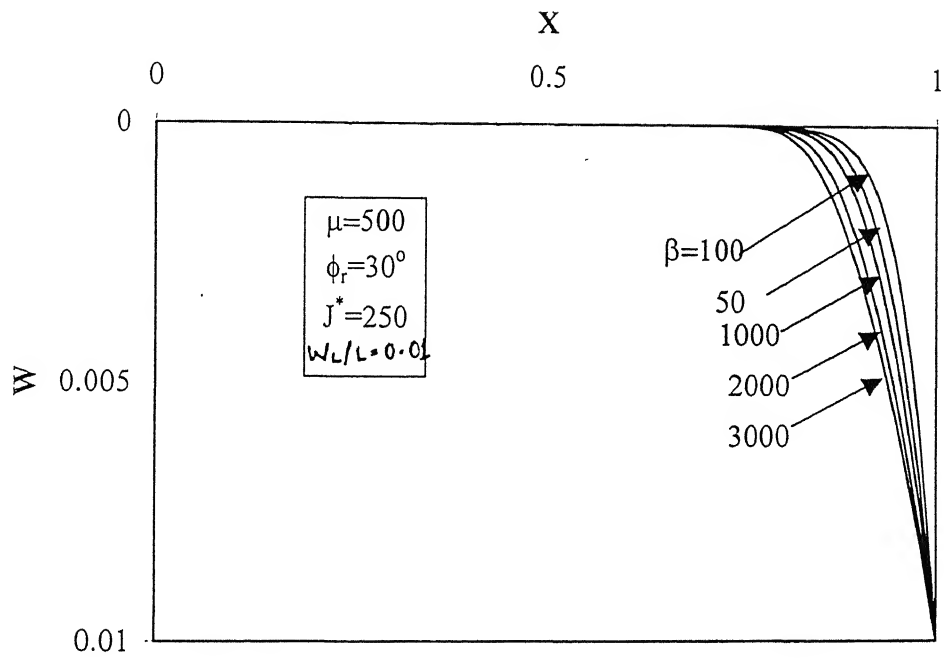


Fig. 4.32 Variation of Normalized Normal Displacement with Normalized Distance - Effect of  $\beta$

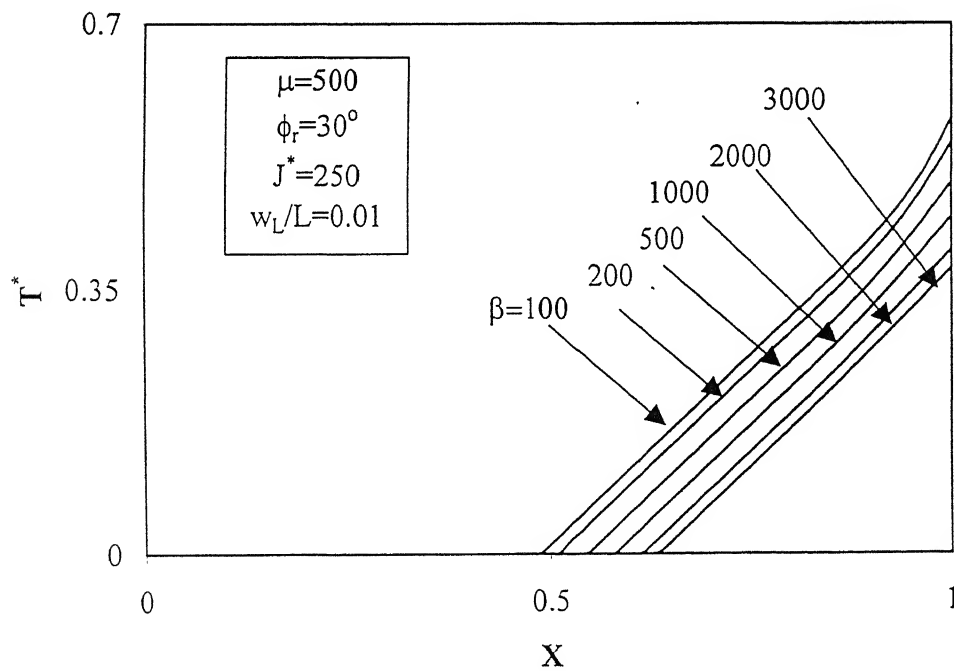


Fig. 4.33 Variation of Normalized Tension with Normalized Distance – Effect of  $\beta$

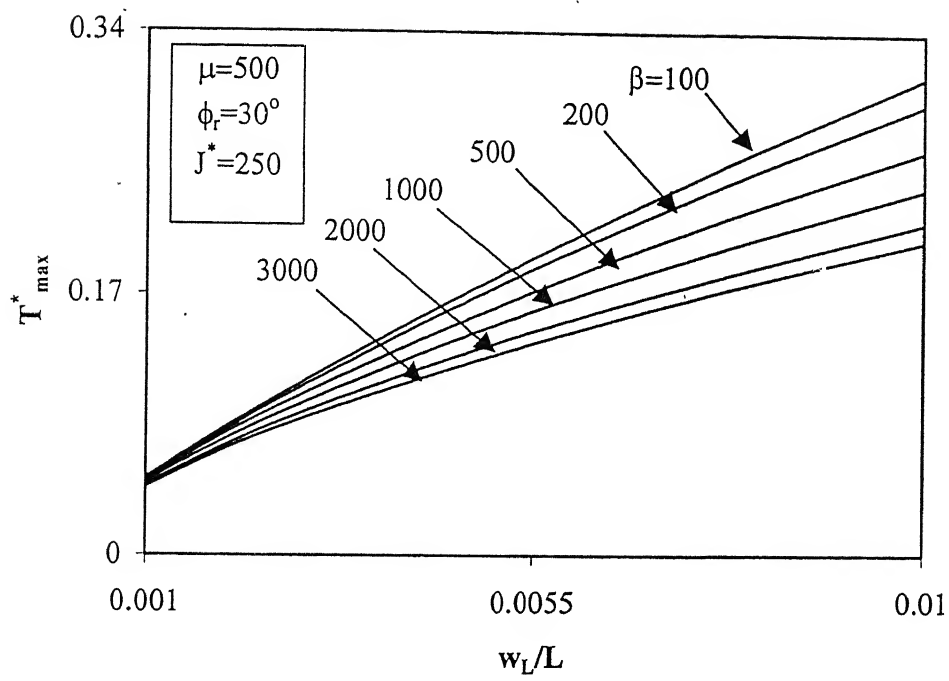


Fig. 4.34 Variation of Maximum Normalized Tension with  $w_L/L$  - Effect of  $\beta$

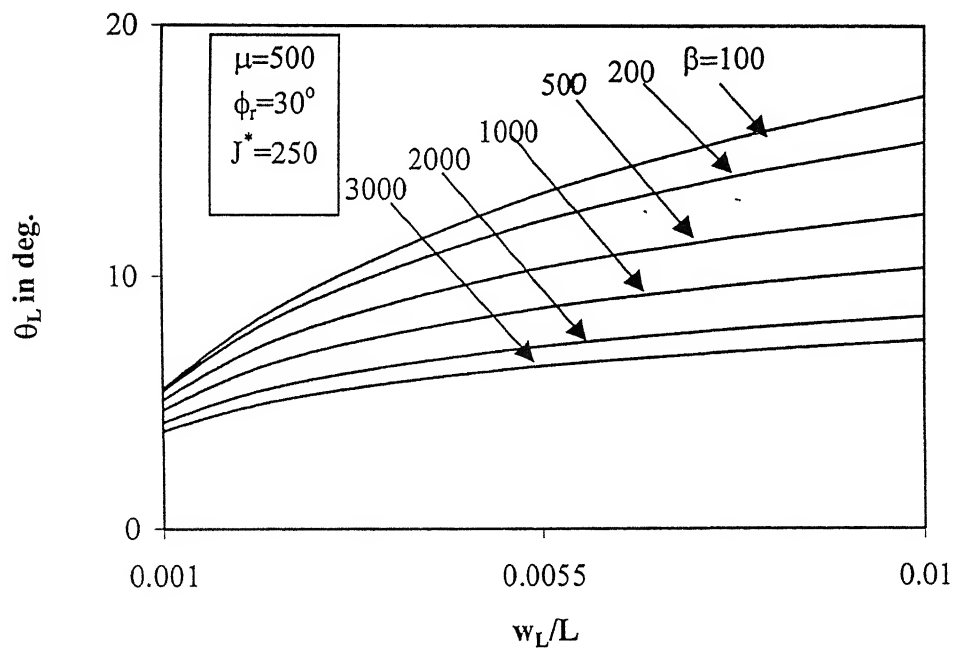


Fig. 4.35 Variation of Inclination at  $x=L$  with  $w_L/L$  - Effect of  $\beta$

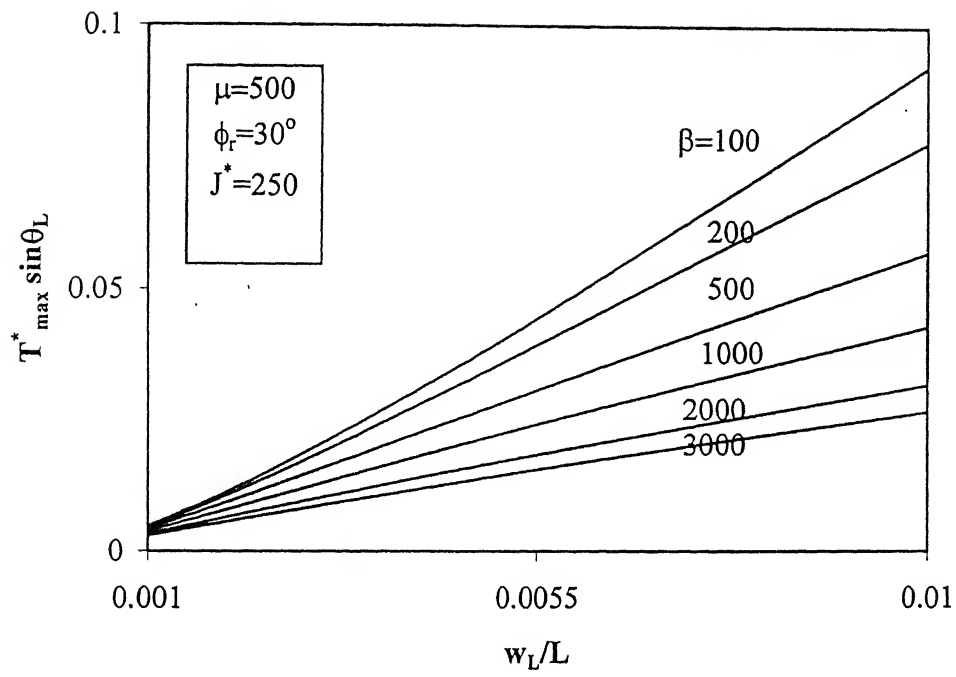


Fig. 4.36 Variation of Maximum Normalized Normal Component of Tension with  $w_L/L$  -Effect of  $\beta$

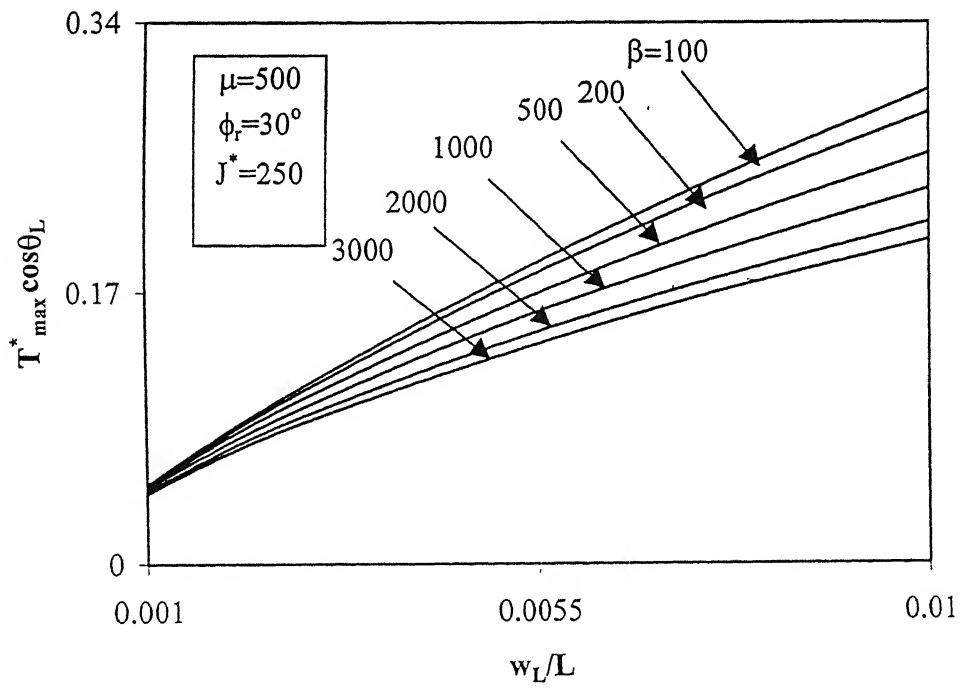


Fig. 4.37 Variation of Maximum Normalized Horizontal Component of Tension with  $w_L/L$  -Effect of  $\beta$

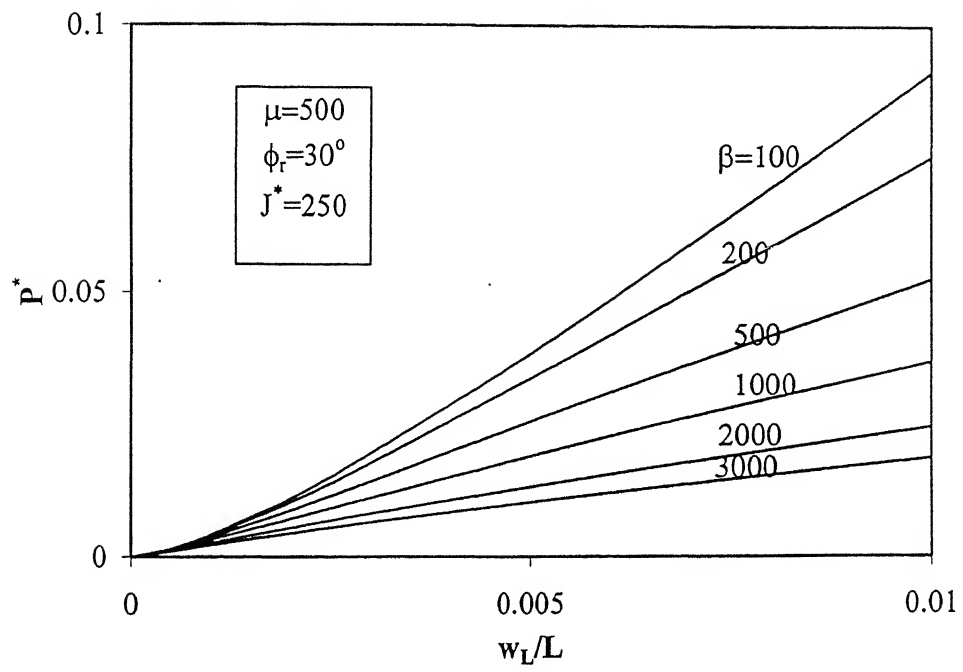


Fig. 4.38 Variation of Normalized Transverse Force with  $w_L/L$  – Effect of  $\beta$

- The pullout force due to transverse displacement is found to be greater than the axial pullout capacity for  $\mu$  in the range of 50-10,000 and  $w_L/L$  in the range 0.001-0.01 for  $\phi_r=30^\circ$ .

### **MODEL II: *Non- Linear Subgrade and Full Shear Mobilization***

- The points of mobilization of transverse displacement move to the right with decrease in the non-linearity parameter,  $\beta(=k_s L/q_{ult})$ . The transverse displacements are mobilized from a distance of  $0.75L$  from the left end for  $\beta=100$  and from a distance of  $0.35L$  for  $\beta=3000$  and for  $\mu=1000$ ,  $w_L/L=0.1$  and  $\phi_r=30^\circ$ .
- The maximum tension developed in the reinforcement, the inclination of the reinforcement at  $x=L$  and the transverse force required to cause the induced free end displacement predicted by this model for  $\beta=1000$ ,  $\mu=500$ ,  $w_L/L=0.01$  and  $\phi_r=30^\circ$  are less compared to those from Model 1 by 7%, 58 % and 63% respectively for the same set of parameters. This reduction in values is due to the assumption of non-linear normal stress-displacement response in which the maximum normal stress is limited by the ultimate bearing resistance of the soil,  $q_{ult}$ .
- The pullout force is 5% less for  $\beta=1000$ ,  $\mu=500$ ,  $w_L/L=0.01$  and  $\phi_r=30^\circ$  compared to the value based on model 1 for the same set of parameters. The pullout force due to transverse force/Displacement is not always greater than the axial pullout capacity.

### **MODEL 3: *Non-linear Subgrade and Non-Linear Shear Mobilization***

- The inextensible reinforcement undergoes rigid body translation over part of its length. The length over which this rigid body type translation takes place increases with increase in the stiffness of the soil. For a relatively stiff soils,  $\mu=10,000$ , a length of about  $0.8L$  from the left end undergoes rigid body translation whereas it is just  $0.35L$  for  $\mu=50$  for  $\beta=1000$ ,  $w_L/L=0.1$  and  $\phi_r=30^\circ$ . The rate of decrease of horizontal displacements of reinforcement from the point of rigid translation to zero at right end ( $x=L$ ) is high in case of relatively stiff soils ( $\mu=10,000$ ).

- The length of reinforcement over which rigid body translation occurs increases with decrease in  $\beta$  ( $=k_s L/q_{ult}$ ). For  $\beta=100$ , a length of  $0.75L$  from the left end exhibits rigid body translation compared to a length of  $0.35L$  for  $\beta=3000$  for  $\mu=1000$ ,  $w_L/L=0.1$  and  $\phi_r=30^\circ$ . The rate of decrease of horizontal displacements of reinforcement from the point of rigid translation to zero at right end ( $x=L$ ) is high in case of soils with high ultimate resistance (low  $\beta$  value).
- The length of rigid body translation increases with decrease in relative initial shear stiffness of soil,  $\eta(=k_r L/\gamma D_e)$ . A length of  $0.7L$  undergoes rigid body translation for  $\eta=10$  whereas a length of  $0.5L$  exhibits the same for  $\eta=1000$  for  $\beta=1000$ ,  $\mu=1000$ ,  $w_L/L=0.1$  and  $\phi_r=30^\circ$ .
- Beyond a certain initial shear stiffness of the soil (large  $\eta$ ), there are no variations in the transverse, axial, tension and shear resistance profiles along the length of the reinforcement. For  $\eta \geq 2000$ , the displacement, shear and tension profiles along the reinforcement do not show any variations along the reinforcement for  $\beta=1000$ ,  $\mu=1000$ ,  $w_L/L=0.01$  and  $\phi_r=30^\circ$ . For  $\eta \geq 2000$ , full shear resistance can be considered to have mobilized along the reinforcement-soil interface.
- The maximum tension developed and the transverse force to give a free end displacement of  $0.01$  are  $75\%$  and  $80\%$  less compared to the values model 1 whereas they are  $73\%$  and  $80\%$  less compared to the values based on model 2.
- The pullout force is  $74\%$  and  $23\%$  less compared to the values based on models 1 and 2. The pullout force is not always greater than the axial pullout capacity.

## ***EXTENSIBLE REINFORCEMENT***

The analyses of extensible reinforcement is carried out using two models: (i) Linear subgrade and full shear stress mobilized along the reinforcement and (ii) Non-linear subgrade and full shear mobilization.

### ***MODEL I: Linear Subgrade and Full Shear Mobilization***

- The active length of reinforcement increases with increase in the induced free end displacement and also increases with stiffness of the reinforcement for a given free end displacement.

- The entire length of reinforcement is active in offering shear resistance at a free end displacement,  $w_L$ , equal to  $0.007L$  for relative stiffness of reinforcement,  $J^*$ , equal to 2,000 whereas the entire length becomes active even at a free end displacement,  $w_L$ , equal to  $0.005L$  for  $J^*=5,000$  for  $\mu=500$  and  $\phi_r=30^\circ$ .
- For a given relative stiffness of the soil, the points of mobilization of transverse displacements move towards the right end for decreasing relative stiffness of the reinforcement,  $J^*$ . The transverse displacements get mobilized from a distance of  $0.95L$  for  $J^*=1$  and at a distance of  $0.8L$  for  $J^*=250$  for  $\mu=500$  and  $\phi_r=30^\circ$ .

## **MODEL II: *Non-Linear Subgrade and Full Shear Mobilization***

- The active length of reinforcement increases with decrease in the ultimate resistance of the soil (i.e for low  $\beta$ ). The active length of reinforcement is  $0.51L$  for  $\beta=100$  and  $0.364L$  for  $\beta=3000$  for  $\mu=500$ ,  $J^*=250$  and  $\phi_r=30^\circ$ .
- The pullout force is much less than the axial pullout capacity for relative stiffness of the reinforcement,  $J^*$  in the range of 1-1000 for  $\beta=3000$ ,  $\mu=500$  and  $\phi_r=30^\circ$ .

## APPENDIX I

### EVALUATION OF BEARING CAPACITY OF REINFORCED BED

**Problem Statement:** A strip footing of width,  $B$ , is placed in a sand layer with unit weight,  $\gamma$  and friction angle,  $\phi$ , at a depth,  $D_f$  below the ground level. A clay deposit with undrained cohesion,  $c_u$ , and subgrade modulus,  $k_s$ , underlies the sand layer. The base of the footing is at a depth  $H$  above the clay deposit. A reinforcement of length with interface friction angle,  $\phi_r$ , and stiffness,  $J$  is placed at the interface. The bearing capacity of such a system is presented in this section.

A model is presented to determine the bearing capacity of a footing resting on a sand layer underlain by a clay deposit with a sheet reinforcement placed at the interface of the two layers (Fig. I.1). A punching shear failure is assumed in the top layer followed by general shear failure in the bottom soil layer as shown in Fig. I.2 (Meyerhof, 1974). This type of failure occurs when the depth  $H$  is relatively small compared to the width of footing,  $B$ .

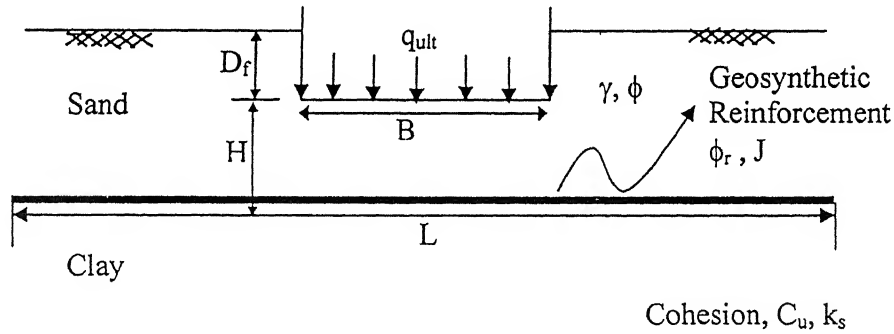


Fig. 1. Reinforced Foundation Bed

The ultimate bearing capacity,  $q_u$ , for the unreinforced case is

$$q_u = c_u N_c + \frac{\gamma H^2}{B} \left( 1 + \frac{2D}{H} \right) K_s \tan \phi + \gamma D \quad (\text{Meyerhof, 1974}) \quad (\text{I.1})$$

where  $N_c$  is the bearing capacity factor of clay layer and  $K_s$  is the punching shear coefficient obtained from Fig. 2 (Meyerhof, 1974) as a function of friction angle,  $\phi$ , of the sand.

Eq. (I.1) in normalized form becomes

$$q_u^* = 1 + \lambda (H^*)^2 \left( 1 + \frac{2D^*}{H^*} \right) K_s \tan \phi + \lambda D^* \quad (I.2)$$

where  $q_u^* = \frac{q_u}{c_u N_c}$ ,  $\lambda = \frac{\gamma B}{c_u N_c}$ ,  $H^* = \frac{H}{B}$  and  $D^* = \frac{D}{B}$

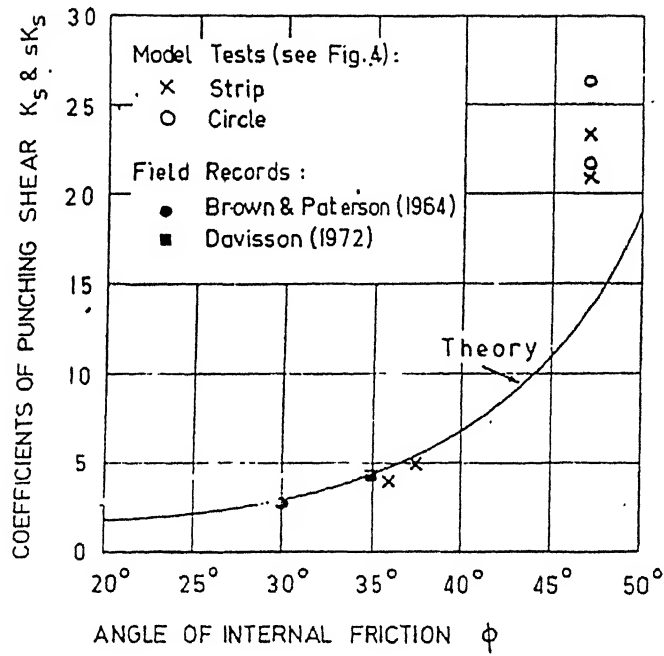


Fig. I.2. Coefficients of Punching Shearing Resistance.

The original shape 'ABCD' of sheet reinforcement is assumed to take the shape 'AEFD' due to punching mode of failure (Fig. I.3).



The improvement in bearing capacity is estimated for an inextensible reinforcement placed at the interface between the sand and clay deposit.

Model 3 (Chapter 3) based on non linear response of subgrade and non-linear shear-displacement response of the interface and inextensible reinforcement is considered to arrive at the tension developed in the reinforcement (Eqs. 3.66 and 3.67 and Fig. 3.47)

$$T_R^* = f\left(\mu, \eta, \beta, \frac{w_L}{L}\right)$$

$$\text{where } \mu = \frac{1}{2} \frac{k_s}{\gamma} \frac{\left(\frac{L}{B} - 1\right)}{\left(\frac{D}{B} + \frac{H}{B}\right)}$$

$$\eta = \frac{1}{2} \frac{k_r}{\gamma} \frac{\left(\frac{L}{B} - 1\right)}{\left(\frac{D}{B} + \frac{H}{B}\right)} \text{ and}$$

$$\beta = \frac{1}{2} \frac{k_s B}{c N_c} \left(\frac{L}{B} - 1\right)$$

The improvement in bearing capacity for this case is studied for typical values of  $\frac{\gamma B}{c N_c} = 0.35$ ,  $\frac{H}{B} = 0.5$ ,  $\frac{D}{B} = 0.5$ ,  $\frac{L}{B} = 4.0$ ,  $\phi = 35^\circ$  and  $30^\circ$ . The bearing capacity ratio of

unreinforced system,  $q_u^*$ , is found to be 2.0. for  $\frac{\gamma B}{c N_c} = 0.35$ ,  $\frac{H}{B} = 0.5$ ,  $\frac{D}{B} = 0.5$ ,  $\frac{L}{B} = 4.0$ ,  $\phi = 35^\circ$  and  $\phi_r = 30^\circ$ .

The variations of bearing capacity ratio of reinforced foundation bed,  $q_{uR}^*$ , with  $\mu$ ,  $\beta$ ,  $\eta$  for the above parameters for  $\frac{w}{B} = 0.015$  is depicted in Figs. I.4, I.5 and I.6.

## ***II Extensible Reinforcement***

The improvement in bearing capacity for an extensible reinforcement placed just above the clay layer is presented in this section.

Model II (chapter 4) based on non-linear subgrade and full shear mobilization is considered) to arrive at the tension developed in the reinforcement (section 4.4.2). The

improvement in bearing capacity for this case is studied for typical values of  $\frac{\gamma B}{c_u N_c} = 0.35$ ,

$\frac{H}{B} = 0.5$ ,  $\frac{D}{B} = 0.5$ ,  $\frac{L}{B} = 4.0$ ,  $\phi = 35^\circ$ , where  $J^* = \frac{J}{\gamma(D+H)(L/B-1)\tan\phi_r}$ ,  $J$  being the

stiffness of reinforcement.

The value of the bearing capacity ratio of unreinforced system,  $q_u^*$ , for the above parameters is found to be 2.0.

The variations of bearing capacity ratio of the reinforced system,  $q_{ur}^*$ , with  $\beta$  and  $J^*$  for  $\frac{w}{B} = 0.015$  considering the above parameters is depicted in Figs. I.7 and I.8.

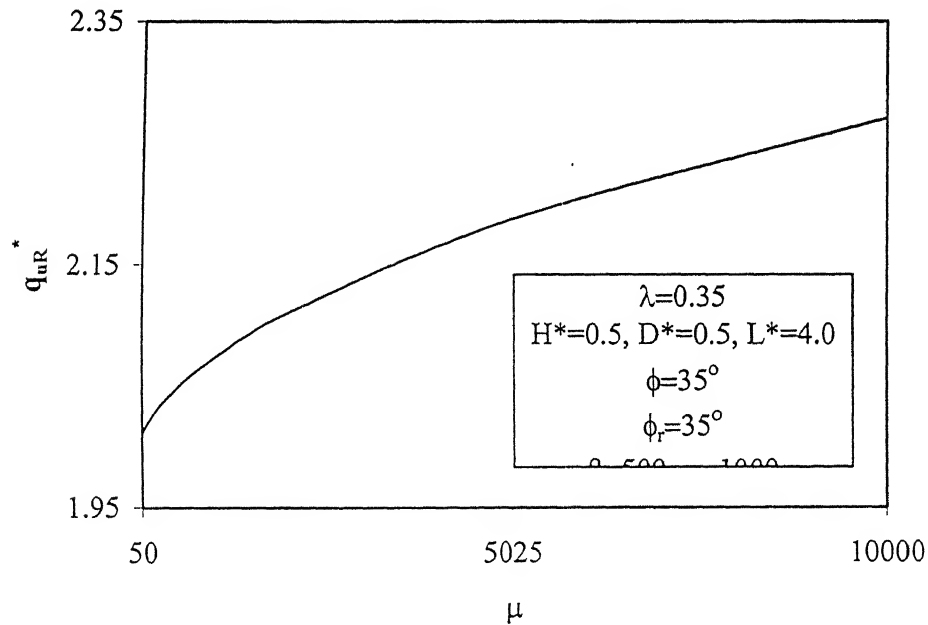


Fig. I.4. Variation of Normalized Bearing Capacity with  $\mu$  with Inextensible Reinforcement

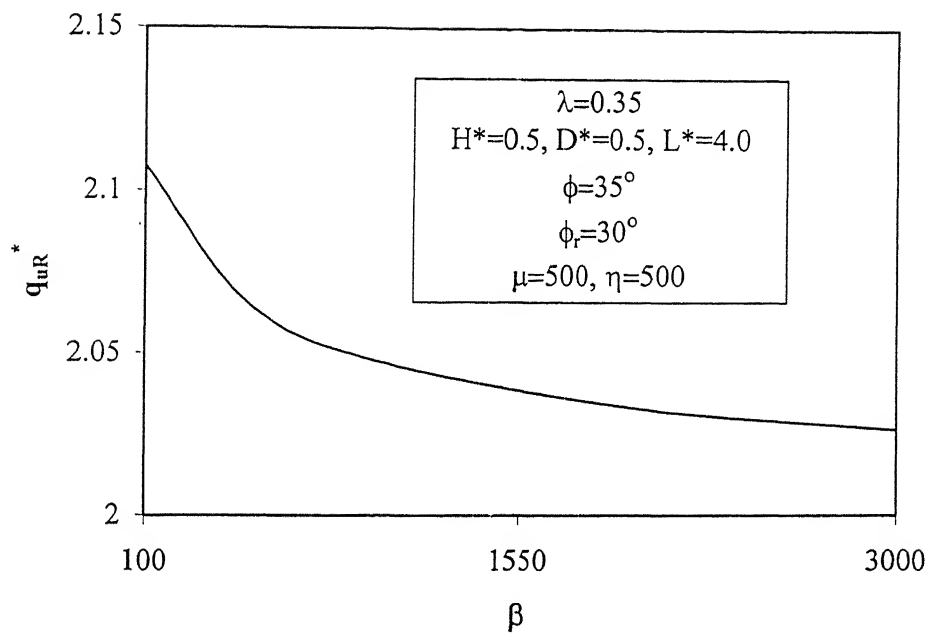


Fig. I.5. Variation of Normalized Bearing Capacity with  $\beta$  with Inextensible Reinforcement

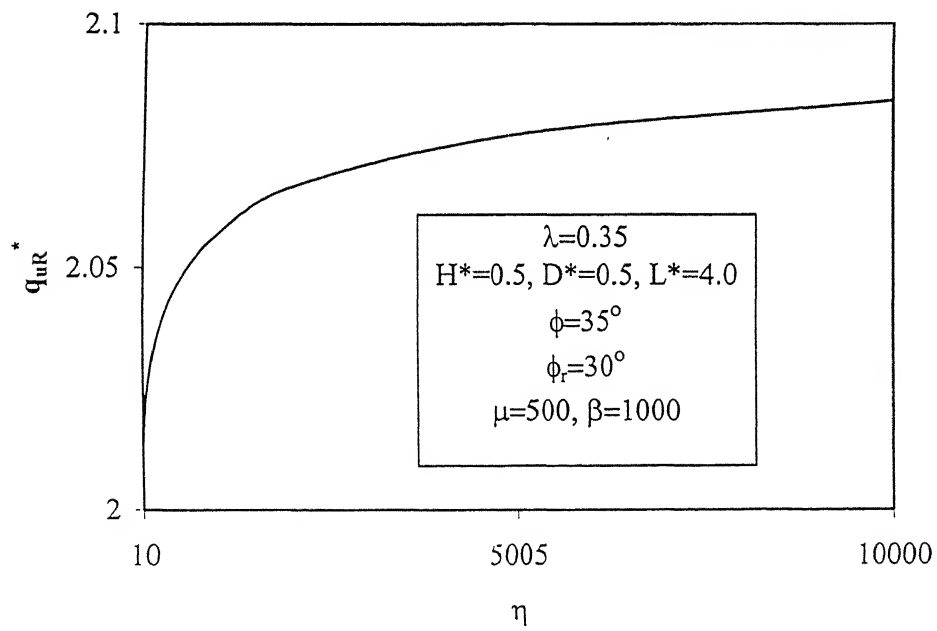


Fig. I.6. Variation of Normalized Bearing Capacity with  $\eta$  with Inextensible Reinforcement

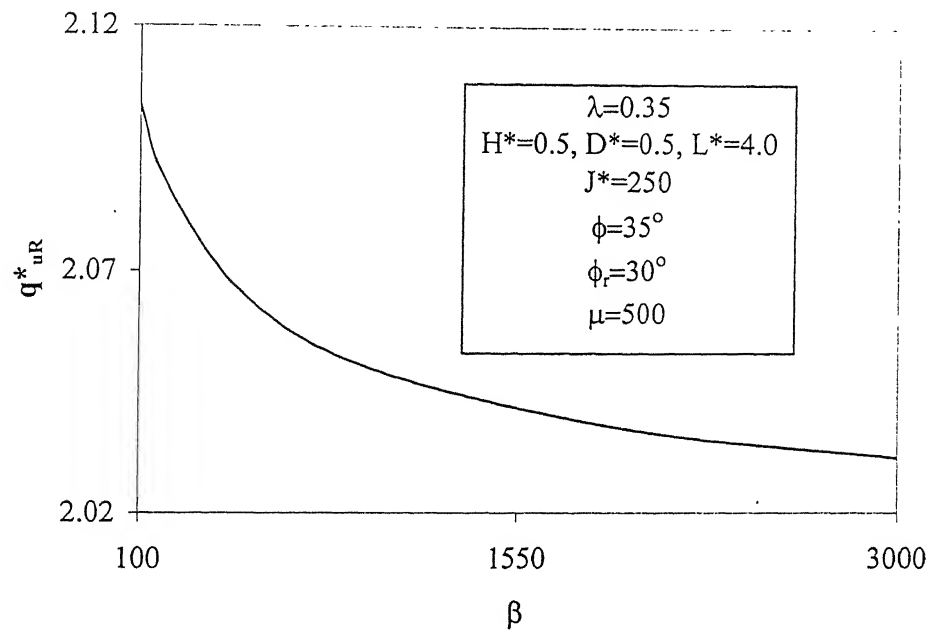


Fig I.7. Variation of Normalized Bearing Capacity with  $\beta$  with Extensible Reinforcement

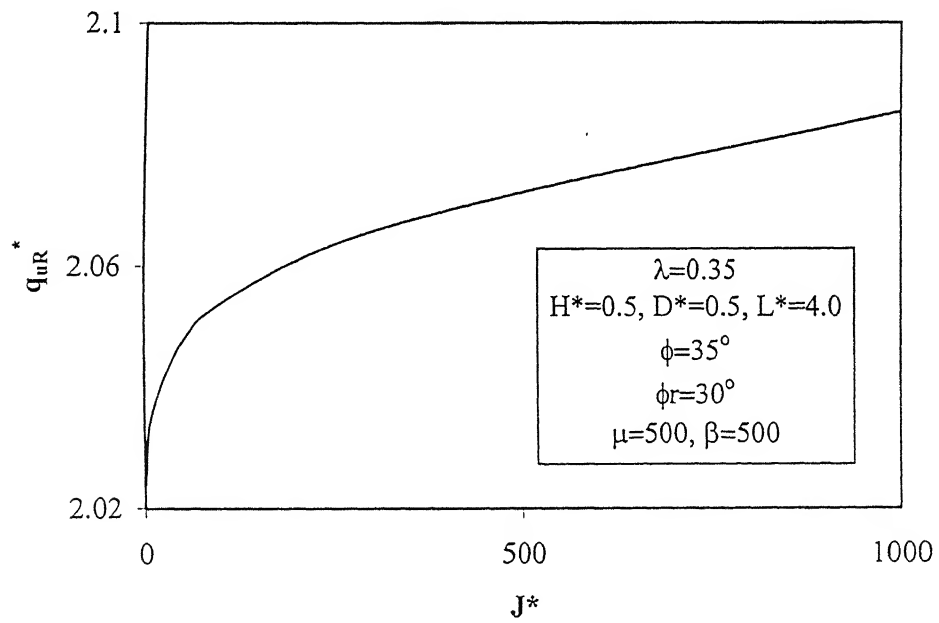


Fig. I.8. Variation of Normalized Bearing Capacity with  $J^*$  Extensible Reinforcement

## APPENDIX I

### EVALUATION OF BEARING CAPACITY OF REINFORCED BED

**Problem Statement:** A strip footing of width,  $B$ , is placed in a sand layer with unit weight,  $\gamma$  and friction angle,  $\phi$ , at a depth,  $D_f$ , below the ground level. A clay deposit with undrained cohesion,  $c_u$ , and subgrade modulus,  $k_s$ , underlies the sand layer. The base of the footing is at a depth  $H$  above the clay deposit. A reinforcement of length with interface friction angle,  $\phi_r$ , and stiffness,  $J$  is placed at the interface. The bearing capacity of such a system is presented in this section.

A model is presented to determine the bearing capacity of a footing resting on a sand layer underlain by a clay deposit with a sheet reinforcement placed at the interface of the two layers (Fig. I.1). A punching shear failure is assumed in the top layer followed by general shear failure in the bottom soil layer as shown in Fig. I.2 (Meyerhof, 1974). This type of failure occurs when the depth  $H$  is relatively small compared to the width of footing,  $B$ .

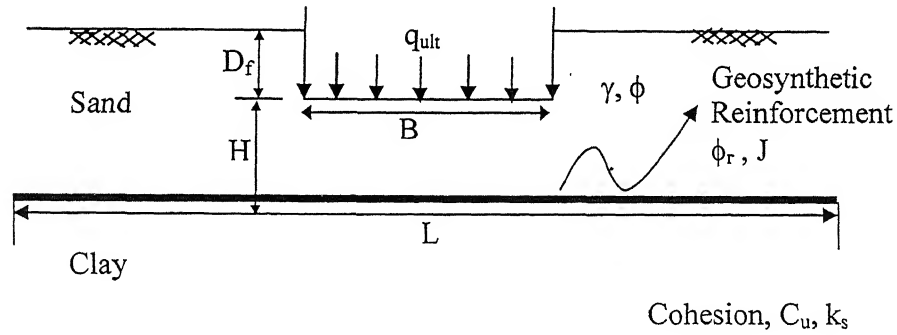


Fig. 1. Reinforced Foundation Bed

The ultimate bearing capacity,  $q_u$ , for the unreinforced case is

$$q_u = c_u N_c + \frac{\gamma H^2}{B} \left( 1 + \frac{2D}{H} \right) K_s \tan \phi + \gamma D \quad (\text{Meyerhof, 1974}) \quad (\text{I.1})$$

where  $N_c$  is the bearing capacity factor of clay layer and  $K_s$  is the punching shear coefficient obtained from Fig. 2 (Meyerhof, 1974) as a function of friction angle,  $\phi$ , of the sand.

Eq. (I.1) in normalized form becomes

$$q_u^* = 1 + \lambda (H^*)^2 \left( 1 + \frac{2D^*}{H^*} \right) K_s \tan \phi + \lambda D^* \quad (I.2)$$

where  $q_u^* = \frac{q_u}{c_u N_c}$ ,  $\lambda = \frac{\gamma B}{c_u N_c}$ ,  $H^* = \frac{H}{B}$  and  $D^* = \frac{D}{B}$

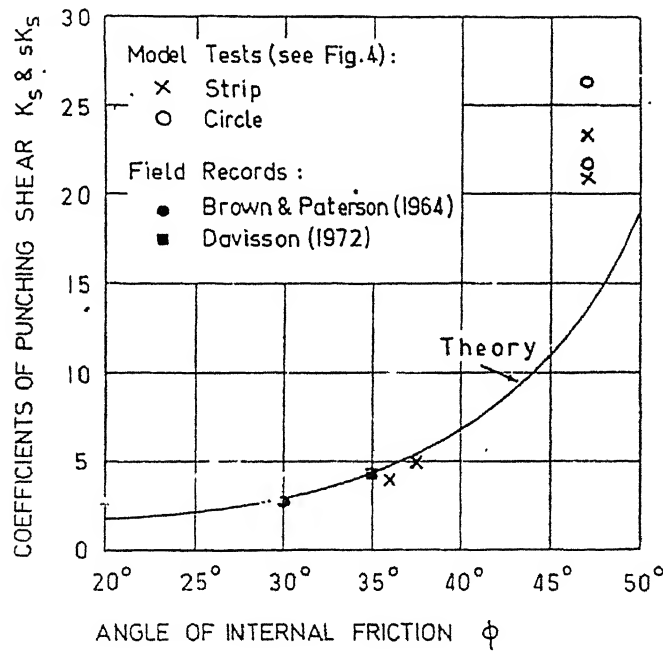


Fig. I.2. Coefficients of Punching Shearing Resistance.

The original shape 'ABCD' of sheet reinforcement is assumed to take the shape 'AEFD' due to punching mode of failure (Fig. I.3).


$$q_{uR} = cN_c + \frac{\gamma H^2}{B} \left( 1 + \frac{2D}{H} \right) K_s \tan \phi + \gamma D + \frac{2T_R}{B} \quad (\text{I.3})$$

In normalized form, equation (I.3) becomes

$$q_{uR}^* = 1 + \lambda(H^*)^2 \left( 1 + \frac{2D^*}{H^*} \right) K_s \tan \phi + \lambda D^* + 2T_R^* \lambda \tan \phi_r (D^* + H^*) (L^* - 1) \quad (\text{I.4})$$

$$\text{where } q^*_{uR} = \frac{q_{uR}}{c_u N_c} \text{ and } T_R^* = \frac{T_R}{\gamma(D+H)(L/B-1)\tan\phi_r}$$

## ***I Inextensible Reinforcement***

The improvement in bearing capacity is estimated for an inextensible reinforcement placed at the interface between the sand and clay deposit.

Model 3 (Chapter 3) based on non linear response of subgrade and non-linear shear-displacement response of the interface and inextensible reinforcement is considered to arrive at the tension developed in the reinforcement (Eqs. 3.66 and 3.67 and Fig. 3.47)

$$T_R^* = f\left(\mu, \eta, \beta, \frac{w_L}{L}\right)$$

$$\text{where } \mu = \frac{1}{2} \frac{k_s}{\gamma} \frac{\left(\frac{L}{B} - 1\right)}{\left(\frac{D}{B} + \frac{H}{B}\right)}$$

$$\eta = \frac{1}{2} \frac{k_r}{\gamma} \frac{\left(\frac{L}{B} - 1\right)}{\left(\frac{D}{B} + \frac{H}{B}\right)} \text{ and}$$

$$\beta = \frac{1}{2} \frac{k_s B}{c N_c} \left(\frac{L}{B} - 1\right)$$

The improvement in bearing capacity for this case is studied for typical values of  $\frac{\gamma B}{c N_c} = 0.35$ ,  $\frac{H}{B} = 0.5$ ,  $\frac{D}{B} = 0.5$ ,  $\frac{L}{B} = 4.0$ ,  $\phi = 35^\circ$  and  $30^\circ$ . The bearing capacity ratio of unreinforced system,  $q_u^*$ , is found to be 2.0. for  $\frac{\gamma B}{c N_c} = 0.35$ ,  $\frac{H}{B} = 0.5$ ,  $\frac{D}{B} = 0.5$ ,  $\frac{L}{B} = 4.0$ ,  $\phi = 35^\circ$  and  $\phi_r = 30^\circ$ .

The variations of bearing capacity ratio of reinforced foundation bed,  $q_{uR}^*$ , with  $\mu$ ,  $\beta$ ,  $\eta$  for the above parameters for  $\frac{w}{B} = 0.015$  is depicted in Figs. I.4, I.5 and I.6.

## II Extensible Reinforcement

The improvement in bearing capacity for an extensible reinforcement placed just above the clay layer is presented in this section.

Model II (chapter 4) based on non-linear subgrade and full shear mobilization is considered) to arrive at the tension developed in the reinforcement (section 4.4.2) .The improvement in bearing capacity for this case is studied for typical values of  $\frac{\gamma B}{c_u N_c} = 0.35$ ,

$\frac{H}{B} = 0.5$ ,  $\frac{D}{B} = 0.5$ ,  $\frac{L}{B} = 4.0$ ,  $\phi = 35^\circ$ , where  $J^* = \frac{J}{\gamma(D+H)(L/B-1)\tan\phi_r}$ , J being the stiffness of reinforcement.

The value of the bearing capacity ratio of unreinforced system,  $q_u^*$ , for the above parameters is found to be 2.0.

The variations of bearing capacity ratio of the reinforced system,  $q_{ur}^*$ , with  $\beta$  and  $J^*$  for  $\frac{w}{B} = 0.015$  considering the above parameters is depicted in Figs. I.7 and I.8.

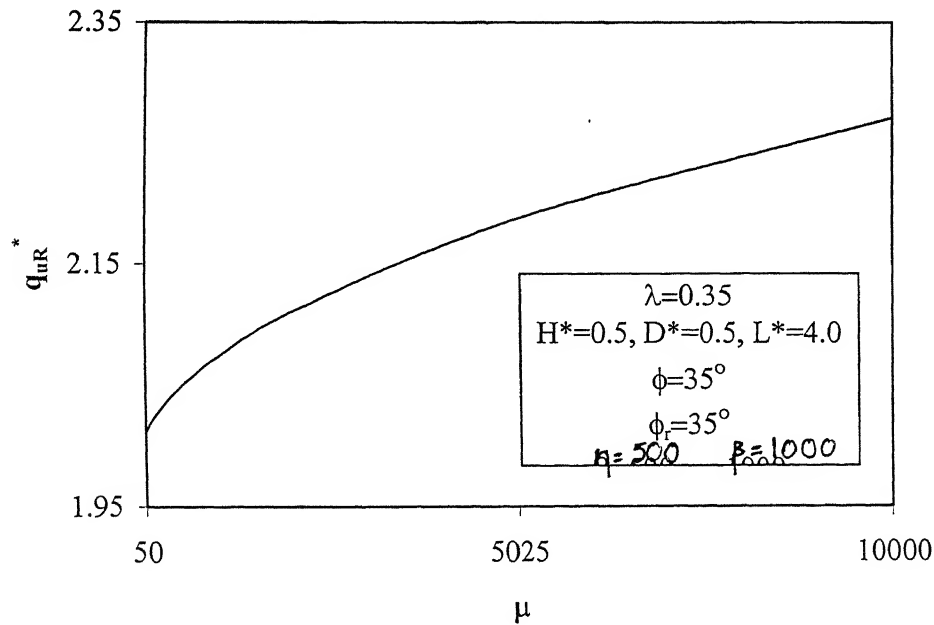


Fig. I.4. Variation of Normalized Bearing Capacity with  $\mu$  with Inextensible Reinforcement

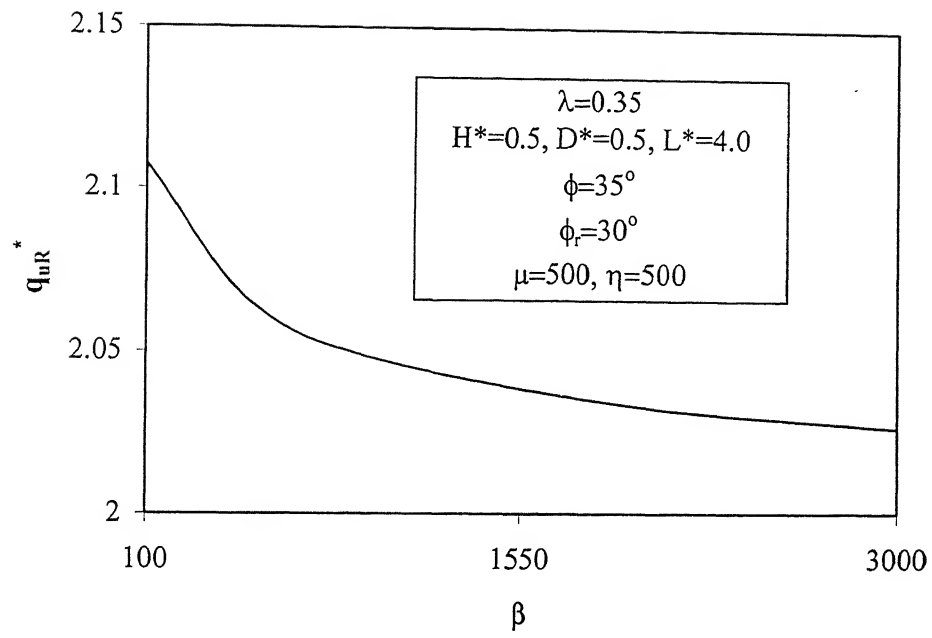


Fig. I.5. Variation of Normalized Bearing Capacity with  $\beta$  with Inextensible Reinforcement

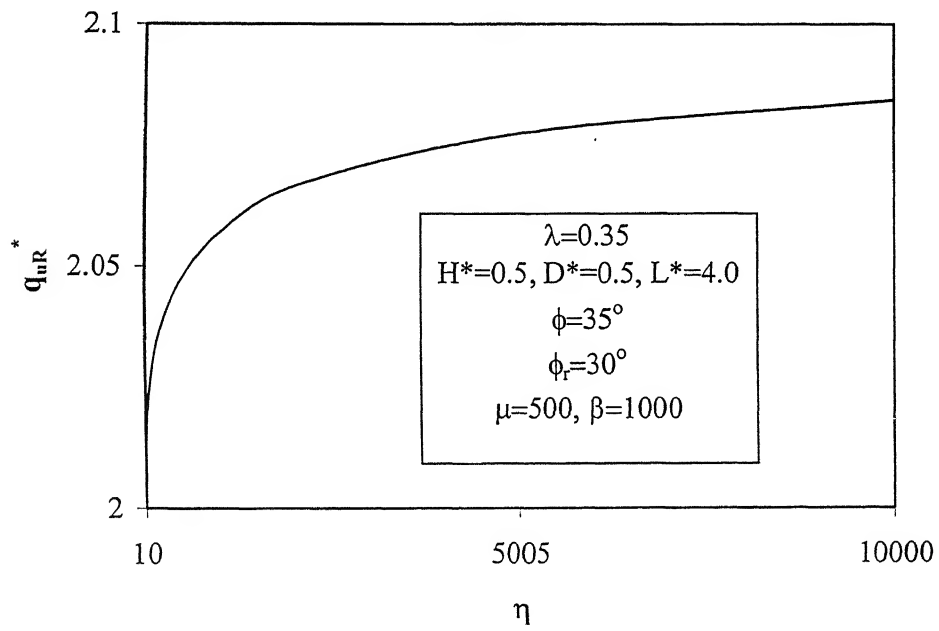


Fig. I.6. Variation of Normalized Bearing Capacity with  $\eta$  with Inextensible Reinforcement

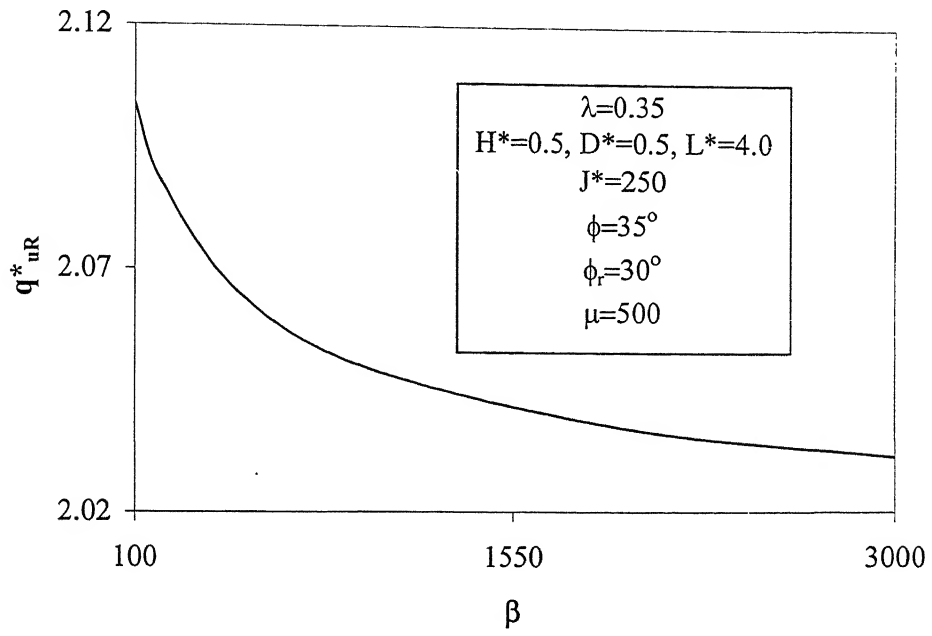


Fig I.7. Variation of Normalized Bearing Capacity with  $\beta$  with Extensible Reinforcement

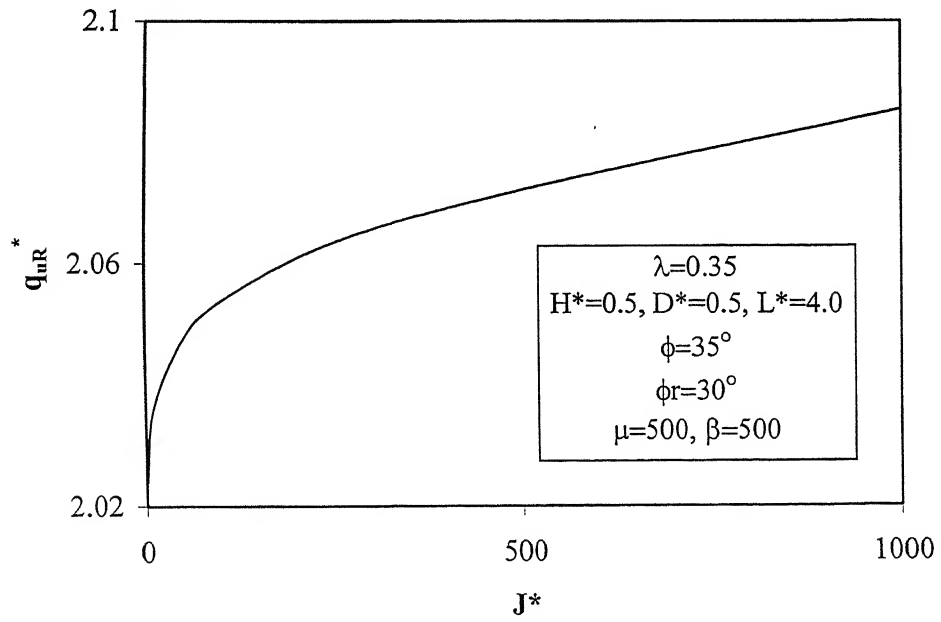


Fig. I.8. Variation of Normalized Bearing Capacity with  $J^*$  Extensible Reinforcement

## References

- Adams, M.T. and Collin, J.G., 1997, "Large Model Spread Footing Load Tests on Geosynthetic Reinforced Soil Foundations", *Journal of Geotechnical and Geoenvironmental Engineering*, Vol. 123, pp. 61-72.
- Akinmusuru, J.O. and Akinbolade, J.A., 1981, "Stability of Loaded Footings on Reinforced Soil," *Journal of Geotechnical Engineering Division, ASCE*, Vol. 107, pp 819-827.
- Alfaro, M.C., Hayashi, S., Miura, N., and Watanabe, K., 1995, "Pullout Interaction Mechanism of Geogrid Strip Reinforcement", *Geosynthetics International*, Vol. 2, No. 4, pp.679-698.
- Athanasopoulos, G.A., 1993, "Effect of Particle Size on the Mechanical Behaviour of Sand-Geotextile Composites", *Geotextiles and Geomembranes*, Vol. 12, pp. 255-273.
- Bergado, D.T. and Chai, J.C., 1994, "Pullout Force/Displacement Relationship of Extensible Grid Reinforcements", *Geotextiles and Geomembranes*, Vol. 13, pp. 295-316.
- Binquet, J. and Lee, K.L., 1975b, "Bearing Capacity Analysis of Reinforced Earth Slabs", *Journal of Geotechnical Engineering Division, ASCE*, Vol. 101, No. GT12, 1257-1276.
- Bourdeau, P.L., Harr, M.L. and Holtz, R.D., 1982, "Soil Fabric Interaction—An Analytical Model", *Proc. 2<sup>nd</sup> Int. Conf. Geotextiles*, Vol. 1, 387-392.
- Brown, B.S. and Poulos, H.G., 1981. "Analysis of Foundations on Reinforced Soil", *Proc. 10<sup>th</sup> Int. Conf. Soil Mech. and Found. Engg.*, Stockholm, Vol. 3, 595-598.
- Burd, H.J., 1995, "Analysis of Membrane Action in Reinforced Unpaved Roads", *Canadian Geotechnical Journal*, Vol. 32, pp.946-956.
- Das, B.M., Omar, M.T., Singh, G. and Shin, E.C., 1996, "Bearing Capacity of Strip Foundation on Geogrid-Reinforced Clay Slope", *Proceedings International Symposium on Earth Reinforcement*, Fukuoka, Japan, Vol. 1, No.4, pp 579-584.
- Degenkamp, G., and Dutta, A., 1989, "Soil Resistance to Embedded Anchor Chain in Soft Clays", *Journal of Geotechnical Engineering, ASCE*, Vol. 115, No.10, pp.1420-1437.
- Farrag, K. Acar. Y.B. and Juran.I., 1993, "Pull-Out Resistance of Geogrid Reinforcements", *Geotextiles and Geomembranes*, Vol. 12, pp. 133-159.

- Fragaszy, R.J. and Lawton, E., 1984. "Bearing Capacity of Reinforced Sand Subgrades", *Journal of Geotechnical Engg. Division.*, ASCE, 110, No. GT-10, 1500-1511.
- Ghosh, C., 1991, "Modelling and Analysis of Reinforced Foundation Beds", Ph.D. Thesis, Dept. of Civil Engineering, Indian Institute of Technology, Kanpur.
- Ghosh.C. and Madhav, M.R., 1994, "Settlement Response of a Reinforced Shallow Earth Bed", *Geotextiles and Geomembranes*, Vol. 13, pp 643-656.
- Giroud, J.P. and Noiray, L., 1981, "Geotextile Reinforced Unpaved Road Design", *Journal of Geotechnical Engg. Division*, ASCE, 107, No. GT-9, 1233-1254.
- Guido, V.A., Chang, D.K. and Sweenay, M.A, 1986, "Comparison of Geogrid and Geotextile Reinforced Earth Slabs", *Canadian Geotechnical Journal*, Vol. 23, pp.435-440.
- Gurung, N., 1999, "Geotechnical Observations, Deformation Analyses and Theoretical Formulations of Pullout Tests for Planar Reinforcements", Ph.D. Thesis, Division of Engineering Systems and Technology, Graduate School of Science and Engineering, Saga University, Japan.
- Gurung, N., 2000, "A Theoretical Model for Anchored Geosynthetics in Pull-Out Tests", *Geosynthetics International*, Vol. 7, No. 3, pp.269-284.
- Halliburton, T.A. and Barron, J.V., 1983, "Optimum Depth Method of Design for Fabric Reinforced Unsurfaced Roads", *Transportation Res. Record*, No. 916, TRB, 26.
- Jewell, R.A., Milligan, G.W.E., Sarsby, R.W. and Dubois, D. 1984, "Interaction Between Soil and Geogrids. Proc. of the Symposium on Polymer Grid Reinforcement in Civil Engineering, London, U.K., pp. 19-29.
- Jewell, R.A. 1990, "Reinforcement Bond Capacity". *Geotechnique*. Vol. 40, No. 3, pp. 513-518.
- Jewell, R.A. 1992, "Keynote Lecture: Links Between the Testing, Modelling and Design of Reinforced Soil". *Proc. International Symposium on Earth Reinforcement Practice*, Fukuoka, Japan, Vol. 2, pp. 755-772.
- Leshchinsky, D., and Boedeker, R.H., 1989, "Geosynthetic Reinforced Soil Structures", *Journal of Geotechnical Engineering*, Vol. 115, No. 10, pp.1459-1478.
- Leshchinsky, D., and Reinschmidt, A.J., 1985, "Stability of Membrane Reinforced Slopes", *Journal of Geotechnical Engineering*, Vol. 111, No. 11, pp.1285-1300.

- Lopes, M.L., and Ladeira, M., 1996, "Role of Specimen Geometry, Soil Height and Sleeve Length on The Pull-Out Behaviour of Geogrids", *Geosynthetics International*, Vol. 3, No. 6, pp.701-719.
- Love, J.P., Burd, H.J., Milligan, G.W.E. and Houlsby, G.T., 1987, "Analytical and Model Studies of Reinforcement of a Layer of Granular Fill on a soft Clay Subgrade", *Canadian Geotechnical Journal*, Vol. 24, 611-622.
- Mandal, J.N. and Shah, H.S., 1992, "Baring Capacity Tests on Geogrid Reinforced Clay", *Geotextiles and Geomembranes*, Vol. 11, pp. 327-333.
- Meyerhof, G.G., 1974, " Ultimate bearing Capacity of footings on Sand Layer overlying Clay", *Canadian Geotechnical Journal*, Vol. 11, No.2, pp 223-229.
- Nishigata, T. and Yamaoka, I., 1992, "Ultimate Bearing Capacity of Unpaved Road Reiforced by Geotextiles", *Symposium on Earth Reinforcement Practice*, Fukuoka, Japan, pp. 659-664.
- Neubecker, S.R., and Randolph, M.F., 1995, "Profile and Frictional Capacity of Embedded Anchor Chains", *Journal of Geotechnical Engineering*, Vol. 121, No. 11, pp.797-803.
- Palmiera, E.M. and Milligan, G.W.E., 1989, "Scale and Other Factors Affecting the Results of Pullout Tests of Grids Buried in Sand. *Geotechnique*, Vol. 39, No. 3, pp. 511-524.
- Peterson, L.M. and Anderson, L.R., 1980, "Pullout resistance of Welded Wire Mats Embedded in Soil". Research Report Submitted to Hilfiker Company, Department of Civil and Environmental Engineering, Utah State University, Utah, U.S.A.
- Sawicki, A., 1983, "Plastic Limit Behaviour of Reinforced Earth", *Jnl. Geotechnical Engg.*, ASCE, Vol. 109, No. 7, 1000-1005.
- Schor, H.J., and Grey, D.H., 1995, "Landform Grading and Slope Evolution", *Journal of Geotechnical Engineering*, Vol. 121, No. 10, pp.729-734.
- Scott, R.F., "Foundation Analysis", 1981, Prentice Hall Inc., Englewood Cliffs, New Jersey,
- Sobhi, S., and Wu, J.T.H., 1996, "An Interface Pullout Formula for Extensible Sheet Reinforcement", *Geosynthetics International*, Vol. 3, No. 5, pp.565-582.
- Shukla, S.K. and Chandra, S., 1995, " Modeling of Geosynthetic- Reinforced Engineered Granular Fill on Soft Soil", *Geosynthetic International*, Vol.11, No.2, pp 603-618.

- Yamanouchi, T., 1979, "A Proposed Practical Formula of Bearing Capacity for Earthwork Method on Soft Clay Ground using a Resinous Mesh", Technology Report of the Kyushu University, Vol. 52, No.3, pp 201-207.
- Yetmoglu, T., Wu, J.T.H. and Saglamer, A., 1994, " Bearing capacity of Rectangular Footings and Geogrid reinforced sand", Journal of Geotechnical Engineering Division, ASCE, Vol. 120, pp. 2083-2099.
- Watari, Y. and Higuchi, Y., 1986, " Field Studies of the Behavior of Geogrids and Very Soft Ground", Third International Conference on Geotextiles, Vienna, Austria.
- Wilson-Fahmy, R.F., Koerner.R.M., and Harpur, W.A., 1995, "Long-Term Pullout Behaviour of Polymeric Geogrids", Journal of Geotechnical Engineering, Vol. 121, No. 10, pp.723-728.